PROTEIN POLYSACCHARIDE COMPLEXES: PERMANENT/NON-PERMANENT INTERACTIONS BETWEEN POLYSACCHARIDES AND POLYPEPTIDES

RICHARD BENJAMIN GILLIS, BSc.

Thesis submitted to the University of Nottingham

for the degree of Doctor of Philosophy

SEPTEMBER 2014

Abstract

This investigation looks at the hydrodynamic characterisation of both covalent and non-covalent protein polysaccharide complexes in the context of novel treatments and healthcare. New techniques were employed and evaluated, such as the MUTLTISIG and SEDFIT-MSTAR algorithms for sedimentation equilibrium analysis, as well as the Extended Fujita Approach for sedimentation velocity. Other characterisation techniques were used such as viscometry, density measurement, Dynamic Light Scattering and Size Exclusion Chromatography coupled to Multi Angle Light Scattering.

Therapeutics for the treatment of Diabetes Mellitus and Coeliac Disease were considered. There is evidence to suggest that a protein-polysaccharide complex extracted from the pulp of pumpkins has a hypoglycaemic effect in human physiology. This extract was assessed in terms of molecular integrity as a precursor to human trial studies. Equally, a novel treatment for Coeliac Disease, gliadin intolerance found in approximately 1% of the population, was assessed in terms of protecting the immune system from gliadin.

Well-established methods, along with newly developed methods, were also used to characterise two glycoproteins relevant to the healthcare and food industries: Human gastric mucin, a natural lubricant found in the human stomach, and gum arabic, a plant extract from the *Acacia* tree. Findings from these investigations were able to add to our current understanding of these two macromolecules.

Acknowledgements

My thanks go to Prof. Stephen Harding, Dr. Gary Adams and Dr. Bettina Wolf for their academic supervision of the project, and David Lafond and Kris Spence from The Kelloggs Company for their industrial sponsorship. I also thank the rest of the NCMH for their support.

I also thank my family and friends, especially my fiancée, for their support and proof-reading.

Abbreviations

AUC	Analytical Ultracentrifugation
c(s)	continuous distribution of sedimentation coefficients
D ($D^0_{20,w}$)	Translational diffusion coefficient, corrected for non-ideality, temperature and buffer conditions ($cm^2\ s^{-1}$)
Da	Daltons
DLS	Dynamic Light Scattering
dn/dc	Refractive index increment (ml/g)
η	Dynamic viscosity (mPa s)
η_r , η_{sp}	Relative, specific viscosity
η_{red} , η_{inh} , $[\eta]$	Reduced, inherent, intrinsic viscosity (ml/g)
GA	Gum arabic
GuHCl	Guanidine hydrochloride
HGM	Human Gastric Mucin
J / j	Fringe concentration corrected for baseline / uncorrected
J(a)	Fringe concentration at the meniscus
k_B	Boltzmann constant (1.381×10^{-16} erg/K)
k_H , k_K	Huggins, Kraemer constant

k_s	Gralén coefficient/concentration dependence of sedimentation coefficient (ml/g)
LBG	Locust bean gum
ls-g*(s)	least square Gaussian apparent fit of sedimentation coefficients
M	Molar concentration (mol/l)
MALS	Multi Angle Light Scattering
MHKS	Mark Houwink Kuhn Sakurada (power law scaling relationships between $M^{a,b,-\varepsilon}$ and $[\eta]$, S and D respectively)
$M_{n,w,z}$	Number average, weight average, Z average molar mass (Daltons)
N_A	Avagadro's constant (6.022×10^{23} mol^{-1})
PBS	Phosphate buffered saline
PTD(G)	Pepsin trypsin digest (Gliadin)
r	Radius (cm)
ρ	Density (g/ml)
$\mathbb{R}$	Gas constant (8.314×10^7 erg/(K mol))
r^2	Coefficient of determination
R_g	Radius of gyration (nm)
r_H	Radius of hydration (nm)
RPM	Revolutions per minute

S ($s^0_{20,w}$)	Sedimentation coefficient, corrected for non-ideality, temperature and buffer conditions (1S = 1 Svedberg =1 x10^{-13} s)
SEC	Size Exclusion Chromatography
$\bar{v}$	Partial specific volume (ml/g)
w/w, v/v, w/v	weight for weight, volume for volume, weight for volume
ω	Angular velocity (rad/s)

Table of Contents

List of Figures

1 Introduction to polysaccharide-polypeptide complexes

1.1 Methodology

Polysaccharides are a diverse and complex class of biomacromolecule. This thesis embodies a series of investigations using hydrodynamics for the study of these molecules and their behaviours in mixtures with proteins and polypeptides. Hydrodynamics involves the study of the movement of molecules through water using a variety of techniques to show different properties of macromolecules. The methods used in these investigations can be classified into three categories: light scattering methods (multi-angle light scattering, dynamic light scattering), hydrodynamic methods (viscometry, sedimentation velocity and equilibrium) and other solution property methods (density measurement, chromatography). Each method, individually, can yield interesting information about a system of macromolecules. Combinations of these techniques can provide complementary and powerful analysis of the overall size and shape and interaction properties (Ortega and García de la Torre, 2007, Aragon, 2011).

One of the major challenges faced with studying polysaccharides is polydispersity (Harding, 2005). Often, techniques will yield an average hydrodynamic value, for example capillary viscometry (yielding a weight-average intrinsic viscometry, used in Chapters 4 and 5) or very limited information on distribution such as dynamic light scattering (hydrodynamic radius, used in Chapters 3 and 5). One method used in Analytical

Ultracentrifugation (AUC) is sedimentation equilibrium which, classically, has been used for the measurement of weight-average molar masses or investigating stoichiometry/dissociation constants of monomer/dimer/n-mer systems of monodisperse proteins (Rowe, 2011). A novel method: MULTISIG (and secondary program MULTISIG-RADIUS) is a data analysis method for sedimentation equilibrium which is capable of analysing polydisperse systems and yielding a range and distribution of molar mass species (Gillis et al., 2013a). This method has been applied in Chapters 4 and 7. Also applied in these chapters is the newly developed SEDFIT-MSTAR package (Schuck et al., 2014) which provides fast analysis of weight average, z-average molar masses and polydispersity indices of sedimentation equilibrium data.

Other techniques are more adept at assessing distributions of macromolecules. The second type of experiment in AUC, specifically sedimentation velocity, can probe macromolecular distributions of sedimentation coefficients which are linked to molar mass through a power law shape factor. This method has been applied in Chapters 3-7, where Chapter 3 takes advantage of this power law relationship to yield molar mass distributions, the basis for the novel Extended Fujita Approach (Harding et al., 2011). Also, SEC-MALS (Size Exclusion Chromatography on-line to Multi Angle Light Scattering) is a very powerful method for distribution analysis (Chapters 3 and 5) due to the ability to separate material based on excluded volume, and then measure the molar mass of elution. Further methods can be linked on-line, for example viscometry, to provide complementary information about shape and conformation.

1.2 Quasi-permanent complexes

In nature, polysaccharides are often found in conjunction with proteins either as quasi-permanently bound complexes or used in non-permanent interactions. The term 'quasi-' is used due the permanence of these interactions under normal conditions. Many can, of course, be broken down under extreme conditions such as high heat, pressure, irradiation or lyase contamination. Mucins are an example of a quasi-permanent protein-polysaccharide complex. They are biologically important macromolecules primarily used as a natural lubricant but also have other functions. For example, in the respiratory system mucus is used to aid the transfer of gases between the atmosphere and blood stream and prevent the epithelium from drying out. They also provide a surface for the immune system to act upon foreign material and pathogens. The mucins of interest in this investigation are from the digestive tract, specifically the stomach. This mucus layer is one of the thickest in the human digestive system and provides a protective barrier for the epithelium against abrasive boluses as well as the harshly acidic and proteolytic environment of the gastric juice. The function of these mucins is linked to their structure. They tend to have a high molar mass with terminal sialic acid residues which provides a 'sticky' and viscous solution. Highly glycosylated regions are bound together end-to-end by disulphide bonds and form large randomly coiled complexes. A major challenge with these biologically important macromolecules is the determination of the molar mass distribution. Chapter 3 showcases a novel method for the determination of a molar mass distribution from sedimentation velocity utilising knowledge of the random-coil nature of this macromolecule.

Protein-polysaccharide complexes are also found naturally in other contexts. Research has shown that the fruit of the *Cucurbita* genus (pumpkins, squashes and gourds) has many health benefits including anti-tumour, anti-bacterial and immunological properties (Adams et al., 2011). In this investigation, the hypogylcaemic qualities of pumpkin (C*ucurbita pepo*) are of interest. What is not clear from studies (Li et al., 2005) is which component of the fruit provides these effects. This investigation looks at the hydrodynamic characterisation of one candidate for this effect: the protein-polysaccharide complex. Chapter 4 outlines the extraction and analysis of this system as a precursor analysis before trials on diabetic patients.

Gum arabic (GA) is an industrially important polysaccharide, which is another example of a protein-polysaccharide complex. The protein content is between 5-10% of the macromolecule, and provides a backbone for mainly arabinose and galactose residues. The exact structure of GA is highly complex and is discussed in more detail in Chapter 5. A full hydrodynamic characterisation is shown for three different sources of GA, at three different ionic strengths, including the use of AUC which has never before been used on this macromolecule in publication. Complementary analyses are used to provide information on size and conformation.

1.3 Non-permanent complexes

Chapters 6 and 7 look at the non-covalent interaction between protein and polysaccharide. The context for these experiments is Coeliac Disease and related gluten intolerance conditions. These conditions affect approximately 1% of the population, and are based on the immune response to gliadin. Although there is currently no cure to this disease, it

has been posited that a potential treatment for this condition is the use of a macromolecular barrier between gliadin and the immune system. Chapter 6 looks at the interaction between gliadin and GA, and gliadin and locust bean gum. Chapter 7 looks at a more biologically-relevant digested form of gliadin (pepsin and trypsin digestion), and a comprehensive approach to finding a potential barrier.

1.4 Aim of investigation

The aim of this investigation is to use hydrodynamics, light scattering and other related techniques to assess the structural/conformational properties of both quasi-permanent and non-permanent protein-polysaccharide complexes. By increasing the level of understanding of these systems one can hope to use this knowledge to develop better healthcare therapies for common diseases.

2 Methods

2.1 Viscometry

2.1.1 Theory

Intrinsic viscosity is a measure of macromolecular size and shape and is determined by measuring the flow times of solutions to yield relative viscosity (η_r) and specific viscosity (η_{sp}):

$$\eta_r = \frac{\eta}{\eta_0} = \left(\frac{t}{t_0}.\frac{\rho}{\rho_0}\right) = \eta_{sp} + 1 \quad \textbf{(2.1)}$$

where (η) is the dynamic viscosity, (t) is the flow time of the solution, (ρ) is the solution density, and the subscript ($_0$) refers to the solvent property. Specific viscosity is described as the change in relative viscosity that the solute has on the solvent (since the relative viscosity of the solvent is 1).

Reduced viscosity (η_{red}) is calculated by dividing specific viscosity by the concentration (c):

$$\eta_{red} = \frac{\eta_{sp}}{c} \quad \textbf{(2.2)}$$

A similarly useful metric, the inherent viscosity (η_{inh}), can be obtained through the natural logarithm of relative viscosity:

$$\eta_{inh} = \frac{\ln(\eta_r)}{c} \quad \textbf{(2.3)}$$

In an ideal system, the reduced viscosity and inherent viscosity would be equal, and directly represent the intrinsic viscosity. However, due to size exclusion (macromolecules cannot superimpose each other in space) and

other effects the reduced and inherent viscosities are dependent on concentration. Plotting reduced viscosity against concentration will yield a linear positive slope (Huggins, 1942), and plotting inherent viscosity against concentration will yield a linear negative slope (Kraemer, 1938), as described by Equation (2.4), where (k_H) or (k_K) are Huggins and Kraemer constants respectively.

$$\eta_{red} = [\eta](1 + [\eta]k_H c) \quad , \quad \eta_{inh} = [\eta](1 - [\eta]k_K c) \tag{2.4}$$

The extrapolation of reduced and inherent viscosities to infinite dilution should converge to the intrinsic viscosity ([η]), as described in Equation (2.5) and illustrated in Figure 2.1. Determination of the Huggins constant can provide information on the solvent properties based on the shape of the macromolecule in question. For example, according to Pamies et al. (2008), for example, the Huggins constant can range between 0.2 and 0.4 for flexible chains in good solvents (surface charges on macromolecule are balanced by ionic strength of the buffered solvent) but closer to 1 for globular/spherical particles.

$$\lim_{c \to 0}(\eta_{red}) = \lim_{c \to 0}(\eta_{inh}) = [\eta] \tag{2.5}$$

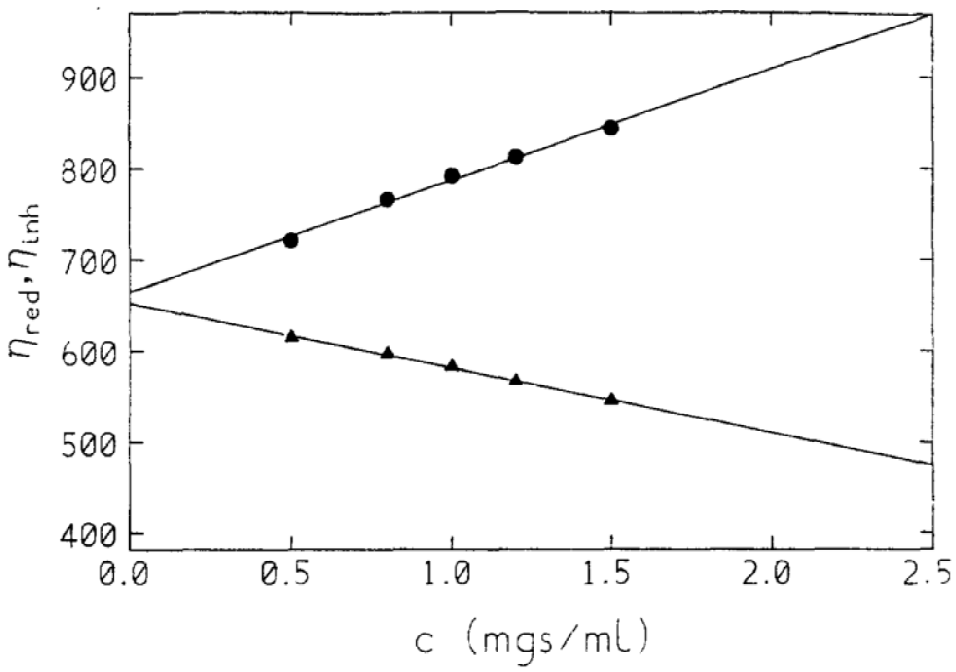

Fig. 2. Huggins and Kraemer extraction methods for intrinsic viscosity. Reduced viscosity η_{red} (ml/g) versus concentration (●) and inherent viscosity η_{inh} $\{=\ln(\eta_{rel})/c\}$ (ml/g) versus concentration (▲) for irradiated (10 kGy) guar in phosphate chloride buffer (pH = 6.8, I = 0.10). The "common" intercept gives $[\eta]$, the slopes are $K_H[\eta]^2$ and $K_K[\eta]^2$. K_H is the Huggins constant and K_K the Kraemer constant, respectively (from Jumel, 1994)

Figure 2.1: Illustration of the extrapolation of reduced and inherent viscosity to converge at the abscissa origin. At infinite dilution, the intrinsic viscosity is yielded (Harding, 1997, Jumel, 1994).

2.1.2 Dependence on size and shape

The intrinsic viscosity of a macromolecule is mainly dictated by its size (molar mass) and shape. This is outlined in the Mark Houwink Kuhn Sakurada (MHKS) equation:

(2.6)

where (k') is a parameter based on solvent conditions, (M) is molar mass and (a) is the shape factor (see for example Harding et al. (1991)). The shape factor refers to specific values to represent macromolecular conformations. For example, for a=0, the shape is a perfect sphere, for

a=0.5-0.8, the shape is a non-draining random coil and for a=1.8, the shape is a rigid rod.

A low intrinsic viscosity (minimum of 2.5ml/g) suggests that the macromolecule is a perfect sphere, independent of size (the 0^{th} power of M is = 1). Although a single intrinsic viscosity value does not convey a large amount of information, larger intrinsic viscosities suggest a less compact conformation and/or larger macromolecule. If it is known that two macromolecules have similar molar masses but significantly different intrinsic viscosities, it can be posited that the smaller intrinsic viscosity implies a more compact macromolecule.

2.1.3 Apparatus

2.1.3.1 Ostwald U-tube capillary

The concept of this viscometer is to measure the flow time of a liquid which is moving under gravity alone (see for example Serdyuk et al. (2007)). The capillary applies a resistance to flow, increasing the flow time to provide more precise results. The flow time of the solution, divided by the flow time of the solvent, is proportional to relative viscosity (Equation (2.1)).

A solution is injected into a reservoir, pumped up to the top of a capillary and the liquid then falls under gravity.

Viscosity is highly dependent on temperature, thus the U-tube is suspended in a temperature-controlled water bath. Temperature was controlled through a Schott-Geräte heater (Schott AG, Germany) and an antagonist cooler (Haake, Thermo Fisher Scientific, MA, USA).

The capillaries used in these experiments were Micro Ostwald viscometers (Schott/SI analytics GmbH, Germany).

2.1.3.2 Large volume Ubbelohde viscometer

While the Ostwald capillary offers the simplicity of just a single reservoir and gravity mechanism, it introduces a limitation that the volume must remain constant to provide reliable results. This is due to air pressure pushing both the solution in the capillary and the solution in the reservoir. To counteract this, a third glass column can be introduced to provide an air pressure balance (refer to Figure 2.2, right). The air pressure will now only affect the liquid in the capillary, not the entire reservoir (See for example Serdyuk et al. (2007)).

This provides the benefit of *in situ* dilution of sample using the sample buffer. This has disadvantages because errors in dilution are multiplied by the number of additions of buffer.

The importance of sample temperature applies for this viscometer also, and was maintained in the same water bath.

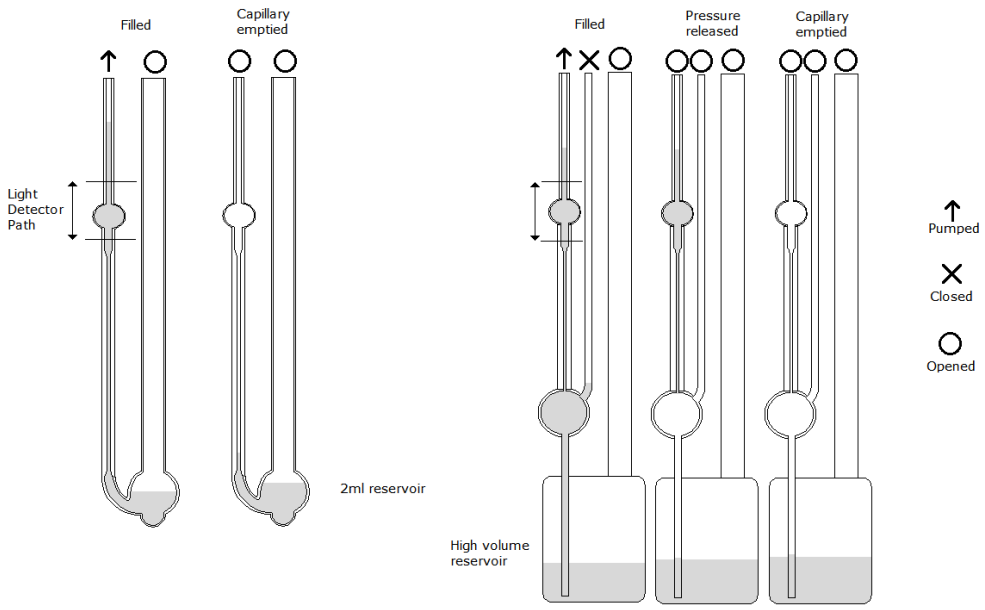

Figure 2.2: Representations of Ostwald (left) and high volume Ubbelohde (right) capillary viscometers.

2.1.3.3 Pressure Imbalance Differential Viscometry

Pressure imbalance created by retaining solvent and solution in two connected channels provides a potential difference which is measured and converted into relative viscosity (Haney, 1985b, Haney, 1985a).

This method is very precise but is prone to blockages, thus occasionally making the apparatus unreliable. This issue can be reduced with the use of a guard column when coupled to Size Exclusion Chromatography (discussed in section 2.2.1). Since the concentration at the point of injection is very low, a combination of the Huggins and Kraemer formulae is used, referred to as the Solomon-Götesmann equation or, sometimes, the Solomon-Ciuta equation (Solomon and Ciuta, 1962):

$$[\eta] \cong \frac{\mathbf{1}}{\boldsymbol{c}}\left(2\left(\eta_{sp}\right) - 2\ln\left(\eta_r\right)\right)^{1/2} \qquad \textbf{(2.7)}$$

The viscometer used in these experiments is the ViscoStar (Wyatt Technology Ltd. Santa Barbara, USA).

2.2 Light scattering techniques

2.2.1 Size Exclusion Chromatography: Multi Angle Light Scattering

2.2.1.1 Static Light Scattering/MALS

Large enough particles in solution will scatter visible light, and the amount of scattering is determined by how large the particle is. Classically, SLS techniques involved measuring the scatter from a solution at a particular angle (usually 90°). This technique is acceptable for spheres but errors are introduced when conformations are even slightly extended. A more advanced SLS technique involves many detectors to account for the shape of the macromolecule – Multi Angle Light Scattering (MALS). Molar mass is obtained from the extrapolation of the Zimm equation, where radius of gyration (R_g) is measured from the angle dependence (Burchard, 1992):

$$\frac{Kc}{\Delta R(\theta, c)} = \frac{1}{M}\left(1 + \frac{q^2 R_g^2}{3}\right) + 2B_2 c \qquad \textbf{(2.8)}$$

where (q) is wave vector, (c) is concentration, (B_2) is the second virial coefficient (a non-ideality term), (K) is described in Equation (2.10) and the ($\Delta R_{(\theta,c)}$) term in Equation (2.11). (q), the wave vector:

$$q = \frac{4\pi\eta_0}{\lambda}\sin\left(\frac{\theta}{2}\right) \qquad \textbf{(2.9)}$$

where (λ) is wavelength of the light and θ is the scatter angle; see for example Serdyuk et al. (2007).

$$K = \frac{4\pi^2 \eta_0^2 \left(\frac{dn}{dc}\right)^2}{N_A \lambda^4} \qquad \textbf{(2.10)}$$

dn/dc is the refractive index increment and N_A is Avagadro's constant.

$$\Delta R(\theta, c) = R_S(\theta) - R_0(\theta) \quad \textbf{(2.11)}$$

$$R_S(\theta) = \frac{I_S(\theta) n_0^2 R_C}{I_C(\theta) n_C^2 N(\theta)} \quad \textbf{(2.12)}$$

($_S$) refers to solute properties, ($_0$) is the solvent, ($_C$) refers to the calibration of the instrument, (I) is intensity, (n) is refractive index, (R_x(x)) is the Rayleigh ratio. (N(θ)) is a normalisation coefficient to 90°. The extrapolation of (ΔR(θ,c)) to infinite dilution and 0° in a 'Zimm plot' provides 1/M and R_g.

As shown in Equation (2.8), MALS requires the measurement of concentration through refractive index measurements. In this investigation the OptiLab rEX (Wyatt Technology) was used. The software ASTRA v4 (Wyatt Technology) was used to calculate number, weight and z-average molar masses and other parameters. The MALS used in this investigation was a DAWN HELIOS II (Wyatt Technology) with 18 angles.

2.2.1.2 SEC

On its own, MALS is a powerful technique for extrapolating weight average molar mass, but for polydisperse and/or heterogeneous systems a separation technique is required. Size Exclusion Chromatography (SEC) separates molecules in terms of their excluded volume (Jumel et al., 1992). Pores of different sizes in a gel matrix allow smaller particles to diffuse within the column so that larger species elute first followed continuously by smaller species. The SEC apparatus used in this investigation was two separation columns (TOSOH Biosciences TSK 3000 and 4000) and a guard column (TSK Guard TWH) maintained at constant temperature of 30°C. Injected samples were pre-filtered at 0.45μm.

2.2.2 Refractive Index

Concentration can be measured using differential refractometry. Macromolecules in solution bend light at different rates, and increasing the concentration increases the amount of bent light. The rate at which a macromolecule bends light is called its refractive index increment (dn/dc). Data for dn/dc parameters were mostly retrieved from Theisen et al. (2000) or from other literature, as reported.

The differential refractometers used in these investigations were the Jencons Atago DD-5 or DD-7 models (apart from the on-line Wyatt rEX system described above). The apparatus was blanked with solvent, approximately 2ml of macromolecule solution injected and a BRIX(% w/v) value yielded. This was converted to mg/ml using the dn/dc of sucrose (0.150ml/g):

$$\boldsymbol{Conc.} = \boldsymbol{BRIX}(\%) * \left(\frac{\left(\boldsymbol{dn}/\boldsymbol{dc}\right)_{\boldsymbol{molecule}}}{\left(\boldsymbol{dn}/\boldsymbol{dc}\right)_{\boldsymbol{sucrose}}} \right) * \mathbf{10}(\boldsymbol{mg}/\boldsymbol{ml}) \qquad \textbf{(2.13)}$$

2.2.3 UV absorbance

Another method of measuring concentration is using the Lambert Beer law:

$$\left(\ln \frac{\boldsymbol{I}}{\boldsymbol{I_0}}\right) = \boldsymbol{\varepsilon_{280nm}}\, \boldsymbol{l}\, \boldsymbol{c} \qquad \textbf{(2.14)}$$

where (I) is light intensity through the solution, (I_0) is light intensity through the solvent, (ε_{280nm}) is the extinction coefficient at 280nm, (l) is path length and (c) is concentration. $\ln(I/I_0)$ is referred to as absorbance, or optical density. Equation (2.14) holds true for absorbance up to 1.4. Another feature of a UV spectrophotometer is to perform a wavelength scan, which measures the absorbance at a range of wavelengths, to

provide information on the presence, or absence, of different chromophores.

Absorbance is based on chromophores present in the macromolecule. In proteins, certain amino acids (Tryptophan, Tyrosine and Phenylalanine) have aromatic groups which absorb light in the ultraviolet spectrum, specifically at 280nm. Other macromolecules absorb at different wavelengths, for example nucleic acids at 260nm. The degree to which a particle absorbs light is expressed in the extinction coefficient, which acts in a similar way to the dn/dc. The extinction coefficient for a protein can be calculated using amino acid sequencing.

Polysaccharides, as a general rule, do not absorb light in the UV spectrum due to a lack of chromophore in the structure. This means that UV spectrophotometry is an unsuitable method for concentration measurements of polysaccharides.

Two UV spectrophotometers were used in this project, a Beckman DU640 wavelength scanning spectrophotometer and an LKB Ultrospec 4050 single wavelength spectrophotometer. Measurements were made using a 1cm pathlength quartz cuvette, which is transparent to UV light.

2.2.4 Dynamic Light Scattering (DLS)

DLS measures the effect of Brownian motion to predict the size of macromolecules in solution. Larger particles move slower than smaller particles. A laser shining through a solution will be blocked and scattered by molecules moving in and out of the path. Thus, if a laser is shone through a solution and the scattering from a molecule takes a relatively long time to cease then the molecule is large. If it takes a relatively short time for the scattering to decrease then the molecule is small. Intensity of

scattered light increases and decreases with different frequencies which gives the different particle sizes. Through this, a couple of time correlation functions $g_x(t)$ are constructed (Burchard, 1992):

$$G_2(t) = \langle i(0)\, i(t)\rangle = A + \left(B g_1(t)\right)^2 \quad \textbf{(2.15)}$$

$$g_1(t) = B\, e^{-\Gamma t} \quad \textbf{(2.16)}$$

Scatter intensity (i) is compared between start (i(0)) and end time (i(t)). (A) and (B) are constants close to 1. (Γ) is the decay constant, described as:

$$\Gamma = q^2 D \quad \textbf{(2.17)}$$

where (q) is the wave vector (Equation (2.9)) and (D) is the translational diffusion coefficient. Translational diffusion coefficients are, therefore, measured as part of correlation functions measured using DLS, and are related to the hydrodynamic radius (r_H) through the Stokes-Einstein equation:

$$D = \frac{\mathbb{R}T}{6\pi\eta_0 r_H N_A} = \frac{k_B T}{f} \quad \textbf{(2.18)}$$

($\mathbb{R}$) is the gas constant, (T) is absolute temperature and (k_B) is the Boltzmann constant. A rearrangement can show that the diffusion coefficient can be described in terms of friction (f). The translational diffusion coefficient can also be applied in the power law equation analogous to the MHKS equation for viscosity (see for example Harding et al. (1991)):

$$D^0 = k''' M^{-\epsilon} \quad \textbf{(2.19)}$$

Thus, the difference in translational diffusion coefficient can be used to interpret size and shape of macromolecules. However, similar to intrinsic viscosity, the translational diffusion coefficient is concentration dependent. That is to say that neighbouring molecules may either slow down localised Brownian motion or increase it through impacts. Thus, the translational

diffusion coefficient is found through a concentration series and extrapolated to infinite dilution. A further extrapolation should be performed for the angle of scatter to remove the effects of rotational diffusion, which have a greater influence with more extended shapes (Burchard, 1992). In this study, the particles under investigation (mucins and gum arabic) were assumed to be near-spherical and were performed at one (higher) angle.

DLS, like all light scattering, is very sensitive to the presence of dust. Significant amounts of large particulates can 'hide' smaller molecules and thus the analysis would not yield a reliable distribution. Therefore samples were injected through 0.45μm (or smaller) filters before measurement.

The DLS used in this investigation was the Malvern Zetasizer NanoZS, with accompanying ZETASIZER SOFTWARE v6.20 (Malvern, UK). Samples were measured at a high (173^{o}) scattering angle and temperature controlled at $(20.00\pm0.01)^{o}C$.

2.3 Analytical Ultracentrifugation

Analytical Ultracentrifugation (AUC) is a membrane-free, macromolecular separation method. Molecules are separated in terms of their size and shape using a strong centrifugal field. Larger molecules will sediment faster than smaller molecules. Furthermore, hydrodynamic shapes, such as spheres or ellipses, will sediment faster than shapes with more friction, such as random coils or rods.

2.3.1 Mechanical systems

2.3.1.1 Analytical Ultracentrifuges

One of two Beckman Optima XL-I analytical ultracentrifuges were used in these investigations (refer to (Furst, 1997)). The ultracentrifuge is powered by an induction drive motor with a top speed of 60k RPM. The chamber is held under vacuum (<0.7 Pa) using a rotary pump and diffusion pump to prevent overheating from air friction. The centrifuge produces a gradient of g-force when the rotor is spun. Temperature is controlled to within 0.1^{o}C of the set temperature. The software used to capture data is ProteomeLab 5.7 (Beckman, Palo Alto, US).

2.3.1.2 Rotors

Titanium rotors with 4 holes (An-60Ti) or 8 holes (An-50Ti) were used to hold 3 or 7 analysis cells respectively and one counterbalance.

2.3.1.3 Cells

Two types of cells were used in these investigations. The first included a 12mm aluminium epoxy resin centrepiece, with sapphire windows. The second are 20mm titanium centrepieces with either sapphire or quartz windows. Both windows are transparent in the UV and visible spectrum.

Windows are contained within aluminium window housings, held in place with protective gaskets. The components are placed into the cell housing and sealed with an aluminium screw ring, tightened to 13.6-15.8 Nm.

Cells were aligned in relation to the centre of rotation. The sectors in the centrepieces are designed such that macromolecules do not push against the sides as they sediment. This leads to a radial dilution effect but is accounted for during analysis.

2.3.2 Optical systems

During rotation, the monochromator and camera perform precisely-timed scans through the cells whilst at high speed. Two optical systems were used in these investigations: Absorbance and Rayleigh Interference.

2.3.2.1 Absorbance

UV absorbance is a useful technique for protein or nucleic acid samples. However, it is ineffective for samples that do not absorb, for example polysaccharides. Scans take a minimum of approximately two minutes, depending on selected resolution, due to the movement of the optical system along the radial length of the cell.

The resolution of data from absorbance is relatively low, as a balance is required between the speed of the scan and the data yielded – species may be sedimenting during the scanning process. Higher resolution will mean that the boundary will move significantly whilst the scan is being completed. This is a problem for sedimentation velocity experiments but not for sedimentation equilibrium.

An ASCII file is created (.RA) with position relative to centre of rotation (cm), Absorbance (Optical Density, OD) and standard error. Absorbance concentration is proportional to mass concentration through the Lambert-Beer Law (Refer to Equation (2.14)).

2.3.2.2 Rayleigh Interference

Monochromatic light, through two slits, produces fringes due to the constructive or destructive superposition of light waves. Passing through transparent media, the light produces straight, horizontal fringes, which are detected by a camera and sent to the computer with no significant scan delay (in comparison to absorbance optics). The software converts these

fringes into one ASCII fringe pattern (.IP) using Fourier Transform (FT) (Furst, 1997). Fringes are displaced when there is a difference in refractive index, such as when a sedimenting boundary is formed. Fringe displacement concentration (ΔJ) is proportional to mass concentration (c) through:

$$\Delta J = c\frac{dn}{dc}\frac{l}{\lambda} \qquad \textbf{(2.20)}$$

Where (dn/dc) is the refractive index increment, (l) is the pathlength of the cell and (λ) is the wavelength of monochromatic light, which for the instrument used in this investigation (Beckman Ultima XL-I) was 675nm.

2.3.3 Sedimentation velocity

2.3.3.1 Theory

This experiment requires samples to be centrifuged at high speed to analyse the boundaries formed during sedimentation. Multiple scans, using either Rayleigh Interference or Absorbance optics, are taken along the length of the solution column in the cell and repeated over an approximate time period of 12 hours, depending on rotor speed, sedimentation coefficient and solvent properties (density and viscosity). The sedimentation coefficient is defined by the Svedberg equation:

$$s = \frac{v}{\omega^2 r} = \frac{M(1-\bar{v}\rho_0)}{N_A f} \qquad \textbf{(2.21)}$$

(s) is the sedimentation coefficient, in Svedberg ($\equiv 10^{-13}$ x sec), (v) is the boundary terminal velocity, (ω) is the angular velocity (in rad/s), (r) is the distance from the centre of rotation ($\omega^2 r$ is the angular acceleration), (M) is the molar mass, ($\bar{v}$) is the partial specific volume, (ρ_0) is the solvent density ($1-\bar{v}\,\rho_0$ is the buoyancy term), (N_A) is Avagadro's constant and (f)

is the friction coefficient. The Svedberg equation complements the Stokes-Einstein equation as such:

$$s = \frac{M(1 - \overline{v}\rho_0)}{N_A f} \quad \textbf{(2.22)}$$

$$D = \frac{k_B T}{f} \quad \textbf{(2.23)}$$

$$s = \frac{M(1 - \overline{v}\rho_0)D}{N_A k_B T} = \frac{M(1 - \overline{v}\rho_0)D}{\mathbb{R}T} \quad \textbf{(2.24)}$$

Avagadro's constant and the Boltzmann constant combine to create the gas constant ($\mathbb{R}$). This equation represents all forces involved in a sedimentation velocity experiment. The centrifugal force causes the sedimentation force (away from centre), with an antagonistic diffusion force (towards centre), the friction force (towards centre) and a buoyancy force (depends on density of macromolecule, but typically away from centre for protein/polysaccharide).

For monodisperse systems, the calculation of the sedimentation coefficient is relatively simple: all the information required is the distance the boundary has travelled in a certain time, knowledge of the rotor speed and radial position. For more complex systems the analysis becomes more complicated. Modern analysis (see for example Schuck (2000)) is based on the Lamm equation (Lamm, 1929), which describes the shape of the boundary formed of a sedimenting system:

$$\frac{dc}{dt} = D\left[\left(\frac{d^2c}{dr^2} + \frac{1}{r}\left(\frac{dc}{dr}\right)\right)\right] - s\omega^2\left[r\left(\frac{dc}{dr}\right) + 2c\right] \quad \textbf{(2.25)}$$

Three dimensional data from the centrifuge - concentration (c), radial position (r) and time (t) - allow computer algorithms to analyse this data. The Lamm equation cannot be solved numerically, thus data is usually iteratively fitted to find an optimum solution to the equation.

Sedimentation coefficients are concentration-dependent, in a similar way to intrinsic viscosity and diffusion coefficient, due to non-ideality. Sedimenting species decrease in velocity due to the self-exclusion of molecules in the boundary. Extrapolating the sedimentation coefficient against concentration yields the Gralén coefficient (k_s) (Gralen, 1944). Combined with the intrinsic viscosity (Wales-van Holde ratio, $k_s/[\eta]$), gives an indication of the shape of the macromolecule (Wales and Van Holde, 1954). $k_s/[\eta]=1.6$ for a perfect sphere or non-draining random coil, and lower values representing asymmetry.

Sedimentation coefficients of macromolecules are usually obtained in a buffered solution to aid their solubility. However, buffer salts affect the solvent viscosity and density, which therefore affect the rate at which the boundary sediments. Sedimentation coefficients are corrected for solvent conditions, as described in Equation (2.26). Sedimentation is also affected by temperature, however all experiments in this study were performed at (20.0±0.1)°C.

$$s_{20,w} = \frac{(1-\overline{v}\rho)_{20,w}}{(1-\overline{v}\rho)_{T,B}} \frac{\eta_{T,B}}{\eta_{20,w}} s_{T,B} \qquad \textbf{(2.26)}$$

($_{T,B}$) refers to the experimental temperature and buffer, and ($_{20,w}$) denotes the conversion to standard conditions. When extrapolated to infinite dilution, there is also a (^{o}). Values were corrected through either SEDNTERP (Hayes et al., 1995) or SEDFIT (Schuck, 2000).

One artefact in sedimentation velocity analysis of polydisperse systems is the self-sharpening, or hypersharpening effect (see for example Dhami et al. (1995)). The macromolecules sediment based on their size, but the largest fraction sediments fastest. However, this fraction encounters a higher concentration of unsedimented solute, thus succumbing to higher self exclusion, non-ideal, effects. The opposite is true for the smaller

fractions, which are slower sedimenting and left behind the weight average, but the reduction in localised concentration increases their sedimentation velocity as there is less self exclusion. The self sharpening effect is only seen with very high molar mass, non-ideal, polydisperse macromolecules.

There are two leading analysis packages in the field of sedimentation profile analysis. UltraScan (Demeler, 2005) is now on its third version. Data is processed through cloud computing to provide sedimentation analysis of discrete 'known' species. SEDFIT (Schuck, 2000), now on version 14 (and sister program SEDPHAT, version 10) uses the host computer's processor(s) to find solutions to the Lamm equation. This requires more time for processing, but there is no need for an internet connection. With UltraScan there is the complication of sending and receiving data to an external supercomputer.

A paper by Mittal et al. (2010) gave a comparison of the functions of these programs, concluding that SEDFIT is good for systems with a single $\bar{v}$, and is superior in removing noise. The downsides were an overcorrection of diffusion coefficients in the c(s) algorithm and systems with more than one $\bar{v}$. UltraScan gave precise sedimentation coefficients, and model independent analysis, but poorly-resolved distributions.

Due to the need for reliable distributions of polydisperse material, all analyses were performed by SEDFIT v12.4 or later. Although many of the systems analysed contained multiple $\bar{v}$ values, the effective difference in $\bar{v}$ of different macromolecules is relatively small, compared to the need for information on the overall distribution of the system.

SEDFIT uses two main procedures for sedimentation velocity analysis. They both rely on superimposing a fitted, discrete stepped model of the

raw (noise-removed) data; the aim being to reduce the difference between fitted and real data (residuals) as much as possible. Two types of noise are removed: Time Invariant (TI) and Radial Invariant (RI). TI noise is removed by searching for patterns which do not change over the course of the run. RI noise is the fringe displacement "jitter" which is an artefact of the Fourier Transformation.

The differential of the fitted data is then plotted as a function of (s) against sedimentation coefficient. If not 'normalised' the distribution will be very 'noisy', so normalisation to 0.683 (standard deviation (1SD)) or 0.95 (2SD) was applied, depending on the requirements of the experiment. Resolution of the graph (distance between fitted steps along sedimentation coefficient axis) was increased or decreased depending on need, but increasing the resolution increased processing time. Data was generally fitted with a resolution of 100-200.

2.3.3.2 Least square Guassian distribution

The first algorithm is based on the Gaussian distribution called ls-g*(s) (least square apparent Gaussian of sedimentation coefficients) against S (Schuck and Rossmanith, 2000). The (*) (apparent) represents independency of the model to diffusion meaning that distributions may not represent a true breadth of sedimentation coefficients. Since diffusion will expand the boundary edges, this is translated into the distribution along the abscissa. For higher friction macromolecules, such as polysaccharides, the diffusion constant is low and can therefore provide a reasonable estimate for the breadth of sedimentation coefficients.

2.3.3.3 Continuous distribution

The second algorithm is called c(s) - continuous distribution of sedimentation coefficients (Schuck, 2000). The fitted data is normalised

using a 'maximum entropy' algorithm. This algorithm has the advantage that it accounts for diffusion, a major shortfall of ls-g*(s). Diffusion is corrected by finding the frictional ratio:

$$f/f_0 = \frac{M(1-\bar{\nu}\rho_0)}{N_A 6\pi\eta_0}\left(\frac{4\pi N_A}{3\bar{\nu}M}\right)^{1/3}\frac{1}{s} \quad \textbf{(2.27)}$$

where (f/f_0) is the frictional ratio and (η_0) is solvent viscosity. Frictional ratio is the ratio of the drag of the macromolecule and the drag of a perfect sphere of equal molar mass. (f/f_0) also relates to the diffusion coefficient:

$$f/f_0 = \frac{k_B T}{6\pi\eta_0}\left(\frac{4\pi N_A}{3\bar{\nu}M}\right)^{1/3}\frac{1}{D} \quad \textbf{(2.28)}$$

Therefore, diffusion can be accounted for and the distribution revised to sharpen peaks.

Knowing these parameters means that SEDFIT can estimate weight average molar mass (Equation (2.24)), and in fact transform the distribution into a c(M) against M plot. This is an accurate technique for single species or with species of the same frictional ratio. If there are species with different frictional ratios then the model may be inappropriate. The algorithm instead fits a weight-averaged frictional ratio and applies it to the whole distribution. SEDFIT does have a built-in model that fits a 3D plot of c(s), s and f/f_0 for multiple species, but is too process-intensive to be used routinely. This is where the ls-g*(s) algorithm becomes useful, since no estimation is made on diffusion and is a much more convenient fit in terms of processing time.

Ls-g*(s) is a good algorithm for large macromolecules which have very small diffusion coefficients, and polydisperse systems such as polysaccharides and glycoproteins. It lacks the ability to sharpen peaks that c(s) does, which was designed for proteins, but does not make

assumptions about the shape of the macromolecules. This project uses both independent algorithms to complement and corroborate the other.

2.3.3.4 Extended Fujita method

A recent variation on the ls-g*(s) algorithm is the extended Fujita model, which converts the sedimentation coefficient distribution into a molar mass distribution (Harding et al., 2011). This uses the MHKS type of relationship, showing that the sedimentation coefficient is proportional to the size and shape (see for example Harding et al. (1991)):

$$s = k'' M^b \tag{2.29}$$

The shape factor (b) ranges between 0.2 (rod) and 0.67 (sphere). A 'random coil' conformation is described as b=0.5, that is to say that the sedimentation coefficient is directly proportional to the square root of the molar mass.

The Fujita method (Fujita, 1962) is a way of transforming a Gaussian distribution of sedimentation coefficients g(s), into a molar mass distribution f(M), through the assumption that the molecule is a random coil: sedimentation coefficients are directly proportional to the square root of molar mass (b=0.5).

$$f(M) = g(s)\left(\frac{ds}{dM}\right) \tag{2.30}$$

$$\frac{ds}{dM} = {k''^2}/{2s} \tag{2.31}$$

The extended Fujita approach does not assume a random coil, and is elaborated to allow for any value of (b):

$$\frac{ds}{dM} = b\, k''^{1/b}\, s^{(b-1)/b} \tag{2.32}$$

This transformation has been included into the SEDFIT package as part of the ls-g*(s) algorithm.

There are certain disadvantages to the extended Fujita method. First, there is still the continued effect of non-ideality that remains from standard sedimentation velocity analysis. This not only means that a concentration series is required, but the 'self sharpening' effect can cause the distribution to be artificially monodisperse.

Second, the b and k" values from Equation (2.29) need to be known, for which there are two options. Either one should know the approximate conformation (compact sphere, rigid rod, random coil: this value can be estimated through other methods such as viscometry or light scattering) and an already known pair of sedimentation coefficient and weight average molar mass; or a series of sedimentation coefficients and molar masses, plotted on a double-logarithmic graph to find the k" and b values. Therefore, this method may not be used for poorly studied macromolecules.

Third, the k" and b values required in Equation (2.32) assumes an average value for all species present, similar to the c(s) assumption of one average f/f_0 value (section 2.3.3.3). Also, in a 'homogeneous' solution, where only the polymer length changes, there may be a conformation change along with a change in length. Examples of this can be seen in inulin/levan (Wolff et al., 2000) where, after a certain molar mass, there is a clear change in conformation.

With these precautions in mind, the advantage of the method is that an indication of the molar mass distribution of a well-studied, polydisperse macromolecule (such as mucin, see Chapter 3) can be achieved quickly with a single sedimentation velocity analysis.

2.3.4 Sedimentation equilibrium

2.3.4.1 Theory

In sedimentation velocity (section 2.3.3), the rotor is accelerated to high speed, approximately 30-50k RPM depending on the size of the macromolecule. Sedimentation equilibrium is where the rotor speed is set much lower to achieve a concentration curve, rather than a complete depletion of concentration to the base, where the macromolecule forms an equilibrium between sedimentation and diffusion forces (buoyancy is also a factor in the shape of the equilibrium signal) (see for example Cole et al. (2008)).

Sedimentation equilibrium analysis is not based on the movement of molecules, therefore the shape of the macromolecule no longer becomes a factor – only the time to reach equilibrium is affected (Van Holde and Baldwin, 1958). Therefore, sedimentation equilibria give reliable weight average molar masses.

Over time, the concentration of the macromolecule depletes at the meniscus and increases at the base. Time-independent noise was removed through taking blank scans at the beginning of the experiment and subtracting from the final scans.

The rotor speed in sedimentation equilibrium is an important factor. If there is too much centrifugal force the macromolecule will sediment completely. If there is not enough centrifugal force the macromolecule will diffuse back to the meniscus. Therefore a small range of rotor speeds is available, which would accurately predict molar mass information. A rotor speed in this range would allow the macromolecule to reach equilibrium and molar mass predicted.

There is, however, a dependence on rotor speed on the weight average molar mass of polydisperse systems. The higher rotor speeds push larger macromolecules to the base, reducing the impact they have on the concentration curve gradient, therefore underestimating the weight average molar mass (Richards et al., 1968).

In terms of protein hydrodynamics, the molar mass of a protein will be determined either through amino acid/nucleic acid sequencing or through gel electrophoresis (SDS-PAGE). Therefore, the use of sedimentation equilibrium by protein chemists has not necessarily been for the determination of molar mass, but more for protein-protein/protein-ligand interactions, kinetics and stoichiometry, analysis for which is typically performed with SEDPHAT. The increasing use of the AUC for polysaccharide analysis has necessitated software for molar mass determination of polydisperse systems (Morris et al., 2014).

2.3.4.2 Curve analysis

As a solution approaches equilibrium, molecules will redistribute so that the concentration will form a natural logarithm gradient in respect to the square of the radius. For an ideal, monodisperse, macromolecular solution the data can be fitted as a linear regression (Van Holde et al., 2006):

$$\frac{d\ln(c)}{dr^2} = \sigma = \frac{\omega^2 M(1-\bar{v}\rho_0)}{2\mathbb{R}T} \qquad \textbf{(2.33)}$$

(σ) is the reduced molar mass, equivalent to A_i in earlier publications (Creeth and Harding, 1982, Rinde, 1928), and takes into account the flotation term, temperature and rotor speed. The gradient is therefore proportional to the molar mass: for a given rotor speed and radial range, the steeper the gradient the higher the molar mass.

For the vast majority of macromolecular solutions this method is not realistic because of non-ideality, which bends the transformed data down towards the base of the cell. Another problem, for polydisperse or heterogeneous solutions, is that this plot will yield an upwards trend towards the base. When both phenomena are present, they may cancel each other out, falsely indicating a monodisperse, ideal system.

One option is to provide a point average, apparent weight average molar mass along the radius, a differentiation of Equation (2.33). This can yield data concerning monomer molar mass, however it yields very little in terms of the overall weight average, especially considering that with real data the meniscus is obscured by error and can be hard to interpret.

2.3.4.3 Analysis: MSTAR

The MSTAR algorithm was developed by Creeth and Harding (1982) as a method for determining the weight-average molar mass along the entire cell. M*(r) is calculated through Equation (2.34) and extrapolated to the base of the cell.

$$M^*(r) = \frac{\big(c(r) - c(a)\big)}{kc(a)(r^2 - a^2) + 2k\int_a^r r\,[c(r) - c(a)dr]} \qquad \textbf{(2.34)}$$

The constant (k) is a conversion from (σ) to molar mass (see Equation (2.33)).

2.3.4.3.1 MSTARA/I

The FORTRAN 77 coded software (Cölfen and Harding, 1997) comes with two subroutines that allow for the two types of optical systems. Absorbance (MSTARA) signal is a relatively simple analysis since the absorbance is proportional to mass concentration and no absorbance means no concentration. Interference optics (MSTARI), however, provides a fringe displacement (section 2.3.2.2). Fringe displacement is

proportional to mass concentration, however there is technically no correlation between absolute fringe values and concentration. In order to match the fringe displacement to mass concentration, the J(a) (fringes at meniscus) is required. MSTARI provides a means of determining the J(a), but is subjective and prone to user error.

2.3.4.3.2 SEDFIT-MSTAR

MSTAR has recently been implemented into the popular AUC analysis suite SEDFIT (Schuck et al., 2014) and released under the name SEDFIT-MSTAR v1.

The problem of J(a) determination has been solved through the application of the c(M) algorithm (as described in section 2.3.3.3), which also provides an estimate for the weight and z-average molar masses (Equation (2.35)).

2.3.4.4 Analysis: MULTISIG/RADIUS

Another approach to the problem of polydispersity is to go back to the principle that a series of macromolecules will produce different concentration gradients, but what is observed is the amalgam, or sum, of these curves.

MULTISIG is a program that allows the fitting of multiple σ terms (Equation (2.33)) onto the raw data. This provides 17 (limited only by processing time) σ terms spaced out logarithmically to provide a tenfold range. The concentration of each σ component is then calculated to provide a continuous distribution of σ. The process is repeated multiple times (five times in this investigation) to provide an average of σ concentrations.

These values can then be plotted in a distribution of c(σ) against σ. Although the algorithm only provides reduced molar mass values, they can be converted to molar mass through SEDNTERP (Hayes et al., 1995).

Three molar mass averages (number, weight and z-; Equation (2.35)) are yielded from the analysis, along with the baseline.

$$M_n = \frac{\sum c_i}{\sum {c_i}/{M_i}} \, , M_w = \frac{\sum c_i M_i}{\sum c_i} \, , M_z = \frac{\sum c_i M_i^2}{\sum c_i M_i} \qquad \textbf{(2.35)}$$

where (i) refers to the i'th species in terms of mass (M_i) and concentration (c_i) (see for example Van Holde et al. (2006)).

Typically, MULTISIG analysis is performed at the 'hinge point', the point where the concentration of the solution does not change during the approach to equilibrium. MULTISIG-RADIUS can be used to perform the c(σ) fit at different points along the curve, producing a plot similar to the differentiation plot described in section 2.3.4.2, however with much smoother results.

Sedimentation equilibrium will never provide the resolution that sedimentation velocity is capable of, due to the simple fact that one dataset is used as opposed to multiple (e.g. 100), with errors being reduced through time-independent noise reduction techniques. However, this distribution from sedimentation equilibrium does allow the interpretation of heterogeneous systems, for example two distinct peaks which would otherwise be interpreted with a weight average between the two true molar masses in algorithms such as MSTAR.

The disadvantage of this method is the processing time required. MULTISIG is currently programmed into ProFit (QuantumSoft, Zurich), and running on a Mac Mini using an Intel Core i7. One series of iterations of 17 sigma terms, on the current computer running the software, required approximately two minutes. Once an iterative series was completed, the parameters were randomised (this is user defined, although 7% randomisation was used in these investigations) and the process can start

again. Five repeats took approximately 10 minutes, although the processing speed occasionally reduced after the first fit due to the smaller percentage error put onto the original fitted parameters. MULTISIG is therefore limited by the current limits of computing power, however could be implemented into a server-based application such as MatLab (or equivalent).

3 Mucins – application of the Extended Fujita Approach

3.1 Introduction

Mucins are the principal macromolecular component of mucus and are heterogeneous glycoproteins found in many different species and in different forms. Mucus has many functions but in the human gastro-intestinal (GI) tract acts mostly as a protective layer against abrasion. One of the thickest layers in the GI tract is in the stomach, along with rectum (Jordan et al., 1998, Pullan et al., 1994).

The mucins produced from the stomach (fundus) epithelium are coded from the MUC5B and MUC5AC genes (Audie et al., 1993) meaning that the protein backbone (apomucin) is relatively standardised and monodisperse. Apomucins are linked end-to-end with disulphide bonds from cysteine groups along the peptide. Most of the peptide backbone is glycosylated, having O-glycosidic bonds to threonine and serine residues, which account for approximately half of residues in the polypeptide. There are also regions of naked polypeptides vulnerable to protease digestion. The enzyme-controlled production of the glycosylation gives the mucins great polydispersity. Mucins range in molar mass (0.5-20MDa) depending on source, species as well as length of time undergoing proteolytic hydrolysis (Bansil and Turner, 2006, Strous and Dekker, 1992). The glycosylation consists of 50-80% of the mass of mucins with different sugar residues such as fucose, galactose, N-acetyl glucosamine (NAGs) and N-acetyl

neuraminic acid (sialic acid). The combination of sialic acid, a negatively charged residue, and fucose, a methylated residue, results in a strongly cohesive infrastructure and accounts for the rheological and surface properties of mucus. These residues are also responsible for interactions with other biomacromolecules, such as chitosan (Deacon et al., 2000, Fiebrig et al., 1995), glycosaminoglycans (Xu et al., 1996) and some bacterial surface macromolecules (Levine et al., 1978, Schuler et al., 2012). Human gastric mucin (HGM) is an important group of macromolecules and highly relevant to studies of the effects of mucus on drug delivery, diagnosis and general understanding of the workings of the GI tract. Although purification methods for mucins from various sources are well established (Creeth et al., 1977), mucins still suffer greatly from proteolytic degradation and storage in 6M guanidine hydrochloride (GuHCl) is recommended. Analysis of purified mucin often includes gel electrophoresis (SDS-PAGE), light scattering, viscometry, sedimentation equilibrium and sedimentation velocity. Light scattering, both dynamic and static, and sedimentation velocity were employed in this particular study.

3.2 Materials

Human gastric mucin was donated from University College London, and was aspirated from a healthy patient code-named YAN.

0.1M phosphate buffered saline (PBS) was produced using sodium chloride (0.05M), dihydrogen potassium orthophosphate and sodium dihydrogen dodecahydrate (0.05M combined) from Fisher Scientific, UK. EDTA and guanidine hydrochloride was from Sigma Aldrich, UK. Sodium azide and caesium chloride was from Fisher Scientific, UK. All compounds were analytical grade.

3.3 Methodology

HGM was purified using ultrafiltration and isopycnic density gradient ultracentrifugation as outlined by Creeth et al. (1977).

3.3.1 Purification

3.3.1.1 Ultrafiltration

After extensive dialysis against water, the mucus preparation was put under high pressure with nitrogen gas. Excess water was pushed through a filter leaving a brown, concentrated solution of crude mucin.

3.3.1.2 Sedimentation velocity

Before further purification work was carried out, the preparation was analysed for macromolecular content with sedimentation velocity. Serial dilutions were made of the stock solution, and deionised water was used as a reference buffer. Interference optics were used on all cells, and absorbance optics were used on the 1/8 and 1/64 dilutions. Results are shown in section 3.4.1.

3.3.1.3 Isopycnic Density Gradient Ultracentrifugation

Density gradient centrifugation was carried out at Bristol Royal Infirmary with help from Dr. Anthony Corfield and Dr. Monica Berry.

The freeze dried impure mucin sample was dissolved in PBS pH7 with 4M guanidine hydrochloride (GuHCl) and adjusted to density of 1.4g/ml with caesium chloride. Samples were centrifuged at 58k RPM at 10^{o}C for 24 hours. 0.5ml aliquots were taken from the centrifuge tubes from the top (low density) to bottom (high density). Samples were tested with an antibody dot blot test for high HGM concentrations (method adapted from

Antibodies: a laboratory manual, Harlow and Lane (1988)). The mucin-rich fractions were pooled and the process was repeated at 0.5M GuHCl for 48 hours. Antibody dot blot tests used anti-MUC5AC CLH2 mouse monoclonal IgG1 (unconjugated) and anti-mouse monoclonal IgG1, (horseradish peroxidise (HRP) conjugated). Diaminobenzidine (DAB) was used to assay for antibody concentration.

Results from the second dot blot are shown in Figure 3.1. The red squares show the density values for each fraction and the black squares the corresponding optical density, registering HRP-oxidised hydrogen peroxide (proportional to anti-MUC5AC antibody binding). The lowest fractions (numbers 0 to 9) were not collected as the density values correspond to protein impurity. The top fractions (from 23 to 25) had high concentrations of mucins however were not pooled to remove the possibility of nucleic acid contamination and thus maintain a pure sample. Fractions 11 to 22 however correspond to the macromolecular mucin, and split into two groups of density, termed "lower density mucin" (fractions 11 to 15) and "higher density mucin" (fractions 16 to 22). These pools are indicated in Figure 3.1.

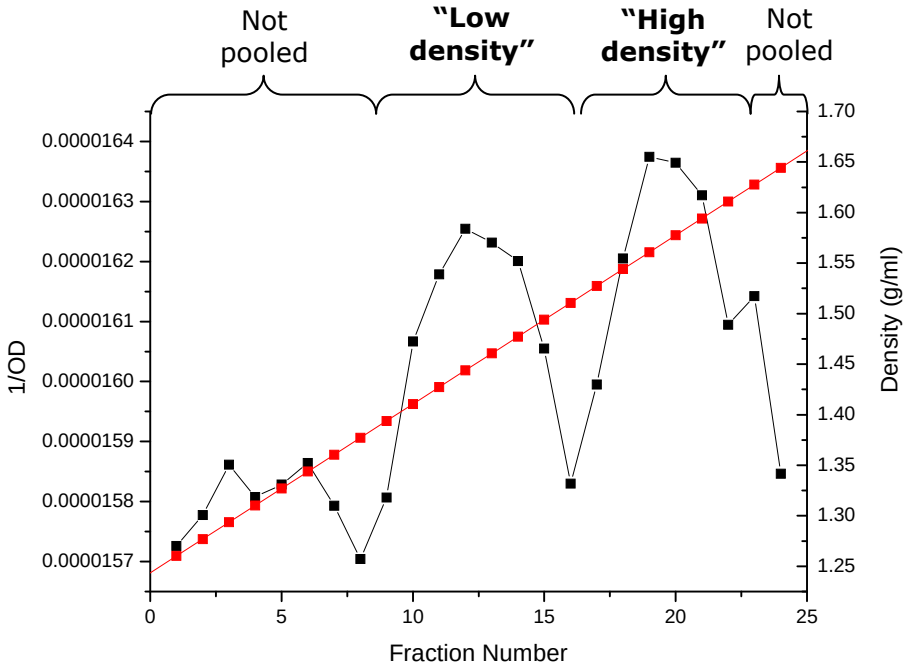

Figure 3.1: Dot-blot test of second density gradient ultracentrifugation. Two peaks are clearly seen at fractions 11 to 15 and 16 to 21. Higher density fractions were not pooled as there was a possibility of nucleic acid contamination.

Two 3ml aliquots, one from each pool, were dialysed twice into PBS, at ionic strength 0.1M and pH 7, with additives to prevent degradation of the mucins (1mM sodium azide and 1mM EDTA). An aliquot was also dialysed once into $PBS_{azide,EDTA}$ and once into 6M GuHCl to completely preserve the samples (14kDa cut off, BioDesignDialysis Tubing D006, Fisher Scientific, UK).

The rest of the sample was frozen to -40°C and freeze dried for two days. There was a mechanical failure of the freezer drier in the first attempt to dry the samples, leading to an unavoidable freeze-thaw cycle. The other density fractions were stored at -20°C.

3.3.2 Sedimentation velocity

The sedimentation coefficient profiles (ls-g*(s)) were obtained for the high density and low density pools of HGM in $PBS_{Azide,EDTA}$. Seven serial dilutions were prepared from stock (half, quarter, eighth, 1/16, 1/32, 1/64). The centrifuge was set to (20.0±0.1)^{o}C at 40k RPM.

The high density pool was also analysed in the presence of 6M guanidine hydrochloride. Three concentrations were prepared from stock (half and quarter). The centrifuge was set to (20.0±0.1)^{o}C at 45k RPM, the higher rotor speed to account for the increased viscosity of the guanidine hydrochloride in the solvent.

3.3.3 Extended Fujita method

The Mark Houwink Kuhn Sakurada (MHKS) parameters were obtained through a literature search of relevant material based on sedimentation velocity and molar mass of mucins. Due to the lack of information from this specific mucin (human, gastric) different species, sources and ionic conditions were selected. Appendix 1 shows collated data from the literature search, highlighting potential issues with the data analysis, for example the sedimentation coefficient may not have been extrapolated to infinite dilution. Some values were found to be corrected to $s_{25,w}$, so these values were corrected to 20^{o}C through the software SEDNTERP.

As mentioned in Section 2.3.3.4, a double logarithmic plot of these values yield k" and b values from the MHKS equation: (2.29).

Figure 3.2 shows all the data collected from the literature search. These plots are split into all data (top), ideal and buffer corrected data (middle) and guanidine hydrochloride data (bottom). The k" and b parameters were

yielded from linear regressions of these data and are summarised in Table 3.1.

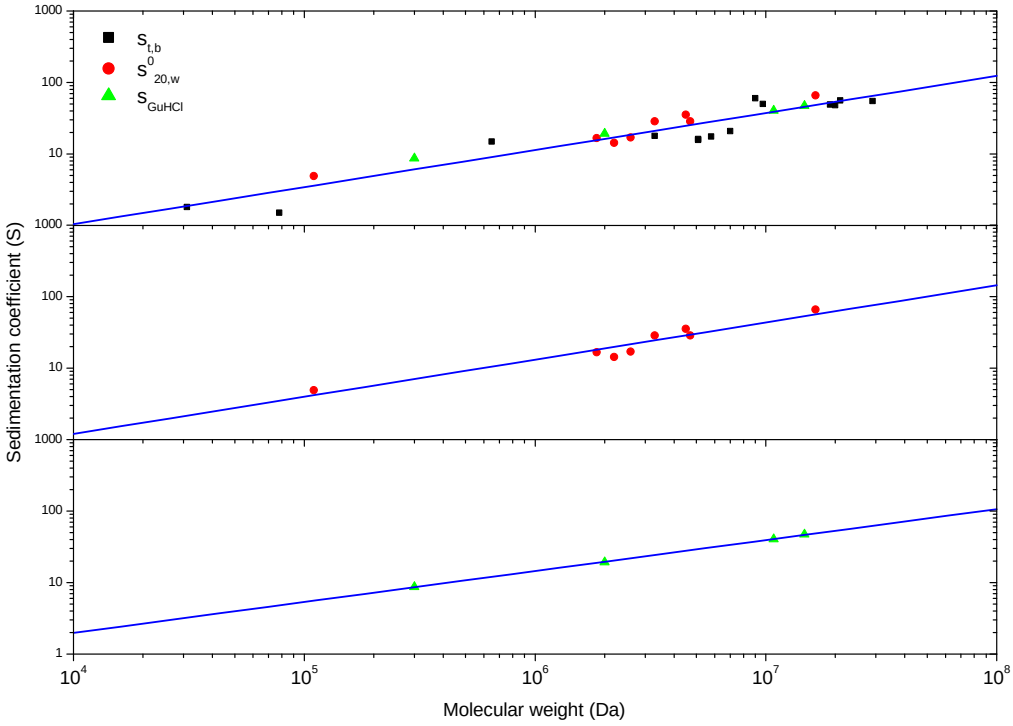

Figure 3.2: Double logarithmic s vs. M_w plots of mucins from literature data. Top: All data obtained through literature search. Middle: Only data for $s^0_{20,w}$ (red). Bottom: Guanidine hydrochloride conditions (green).

Table 3.1: Regression analysis of Figure 3.2 to yield the (b) and (k") of mucin.

Data	Data points (n)	k"	±	b	±
All data	26	0.0088	0.0038	0.519	0.037
$s^0_{20,w}$	8	0.0100	0.0058	0.520	0.059
GuHCl	4	0.0366	0.0032	0.433	0.006

3.3.4 DLS

Dynamic Light Scattering analysis was performed as per section 2.2.4. Single concentrations of mucins were filtered through 0.45µm Wattman filters and analysed using a 173^{o} scattering angle, appropriate as mucins have an expanded, random coil conformation with low overall asymmetry (hence rotational diffusion effects are small). Measurements of samples were repeated five times to aid reliability.

3.3.5 SEC-MALS

SEC-MALS was carried out as described in section 2.2.1, with MALS and dRI detectors coupled to two SEC columns. Temperature through MALS and dRI were 20.0^{o}C. A dn/dc of 0.172ml/g was used (Carlstedt et al., 1983).

3.4 Results

3.4.1 Sedimentation velocity

3.4.1.1 Crude preparation

To confirm the presence of macromolecular content, a sedimentation velocity experiment was performed on the crude mucin preparation (Figure 3.3).

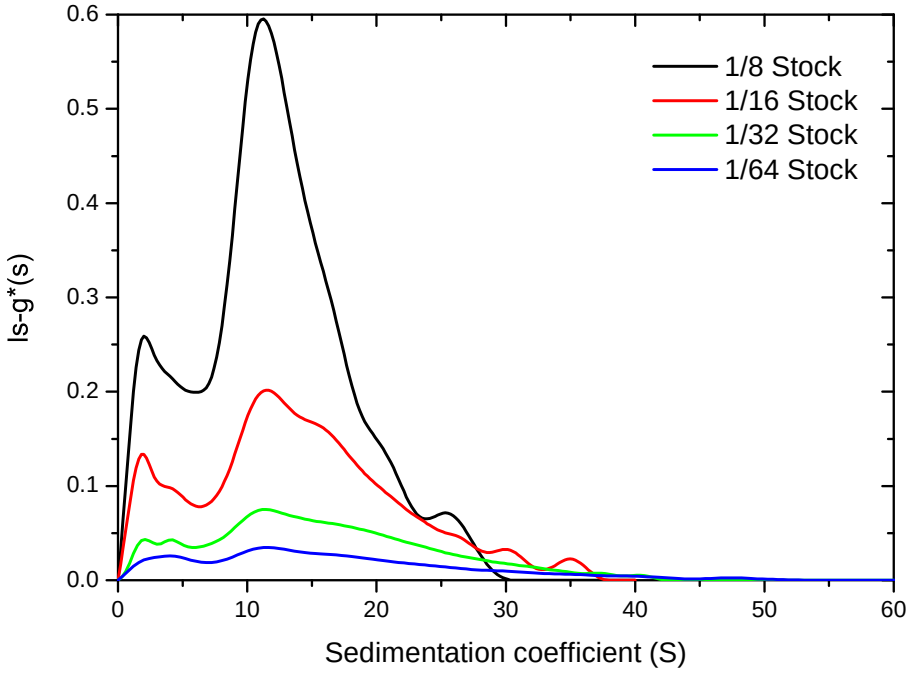

Figure 3.3: ls-g*(s) profile of crude mucin after dialysis and ultrafiltration. Reference medium was deionised water.

This profile was converted to a f(M) distribution, using k" (0.0100) and b (0.520) values from Table 3.1, to provide an indication of the molar mass distribution of the preparation (Figure 3.4).

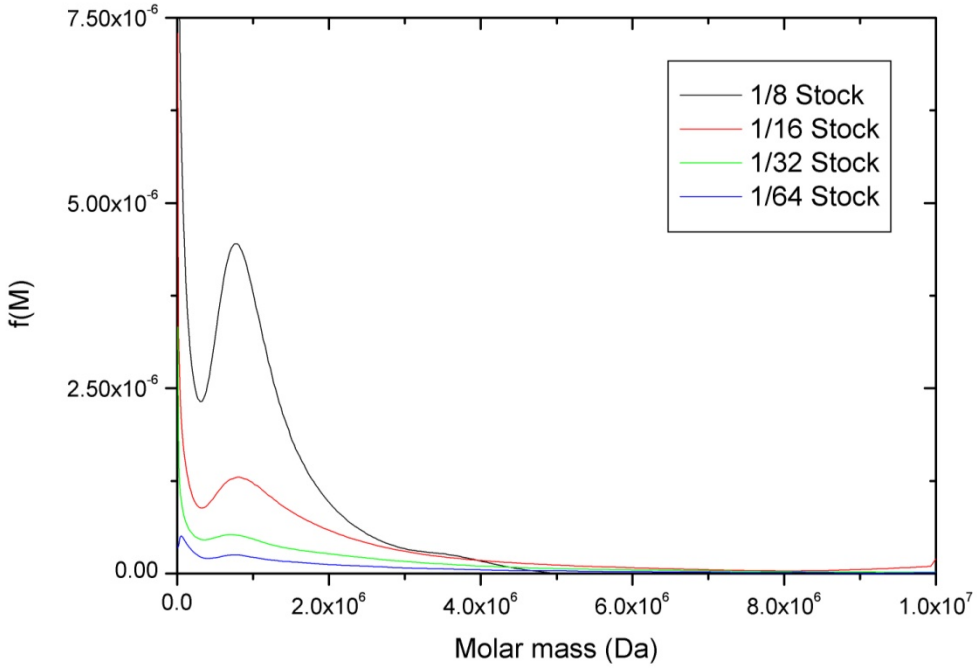

Figure 3.4: f(M) profile of crude mucin after dialysis and ultrafiltration. Reference medium was deionised water.

3.4.1.2 High density pool

Sedimentation profiles from SEDFIT were exported into Origin and plotted simultaneously. They show that the profiles match in basic shape, except for their height on the ls-g*(s) axis. From the sedimentation profiles shown in Figure 3.5, two peaks were identified. For the stock concentration, the first peak lies between 5 and 25S, and the second peak between 25 and 30S. The second peak acts in a non-ideal way as it shifts further along the scale at lower concentration.

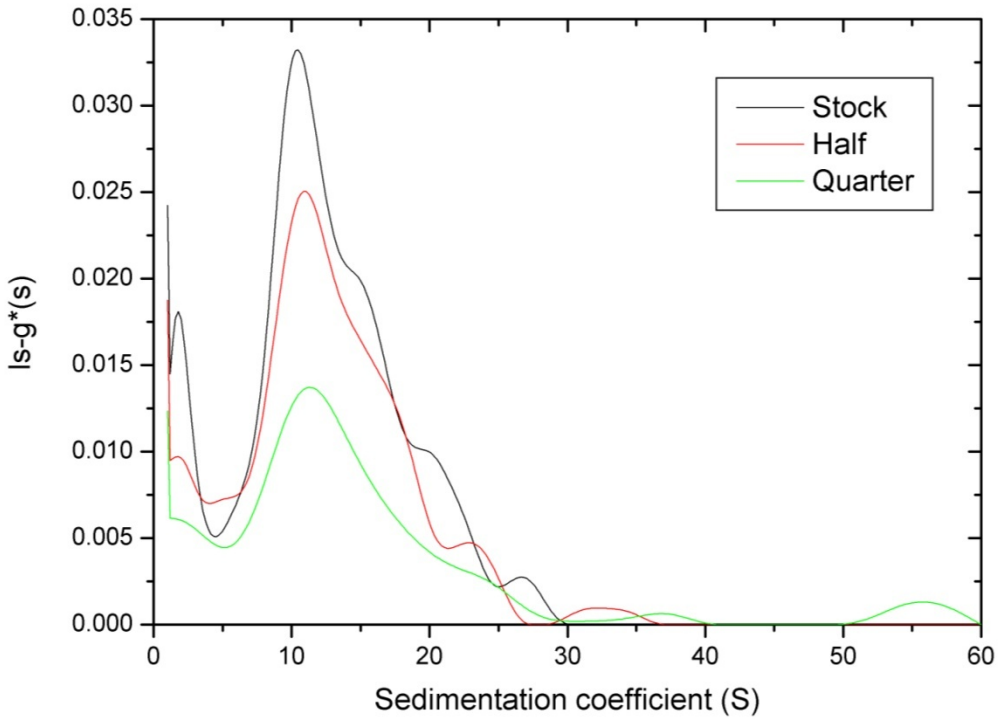

Figure 3.5: ls-g*(s) profile of high density pooled HGM in $PBS_{Azide,EDTA}$, at 20°C, pH7, centrifuged at 40k RPM.

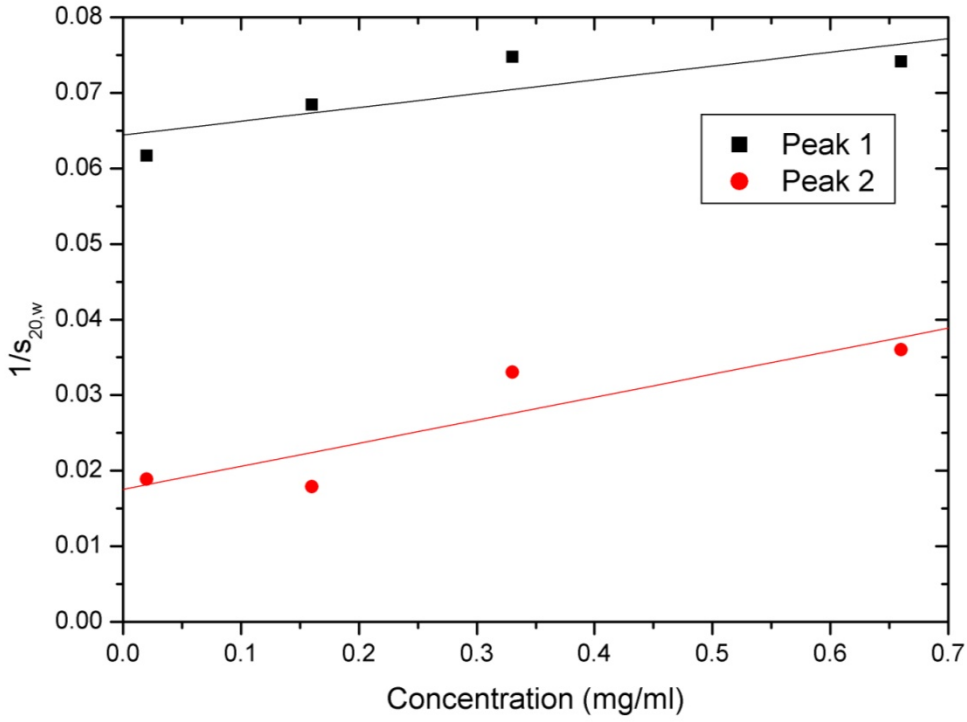

Figure 3.6: Reciprocal $s_{20,w}$ against concentration of two peaks of high density pooled HGM.

By plotting the integrated sedimentation coefficients of the peaks, against concentration, an $s^0_{20,w}$ can be obtained:

$$\frac{1}{s_{20,w}} = \frac{1}{s^0_{20,w}}(1 + k_s c) \qquad \textbf{(3.1)}$$

Figure 3.6 shows the reciprocal of the sedimentation coefficients plotted against concentration.

The ls-g*(s) distribution in Figure 3.5 was converted into the f(M) distribution in SEDFIT. The parameters obtained from Figure 3.2 (middle plot) were used. This distribution is shown in Figure 3.7.

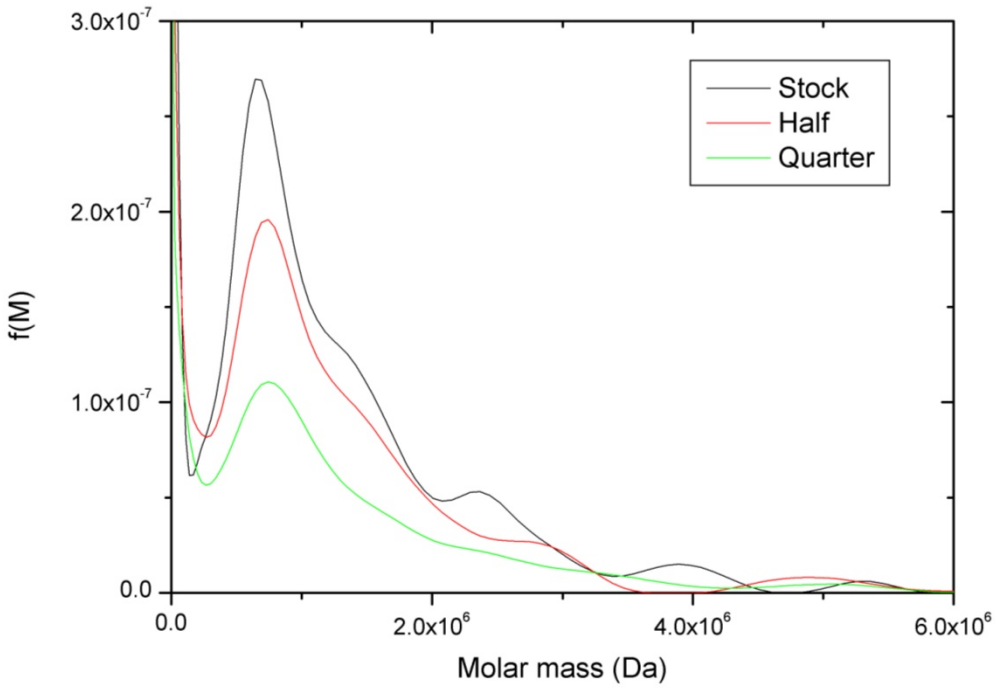

Figure 3.7: f(M) distribution of high density pooled HGM in $PBS_{Azide,EDTA}$, at 20.0°C centrifuged at 40k RPM.

3.4.1.3 Low density pool

Figure 3.8 shows three concentrations of the ls-g*(s) distribution of the low density pooled HGM. The distribution appears to be similar to that of the high density equivalent (Figure 3.5). They both approximately share a 12S peak, there is a shoulder on this peak at 14S however there appears not to be an obvious second peak around 25-30S. Closer examination of some of the concentrations yielded a small peak, which was compiled in Figure 3.9.

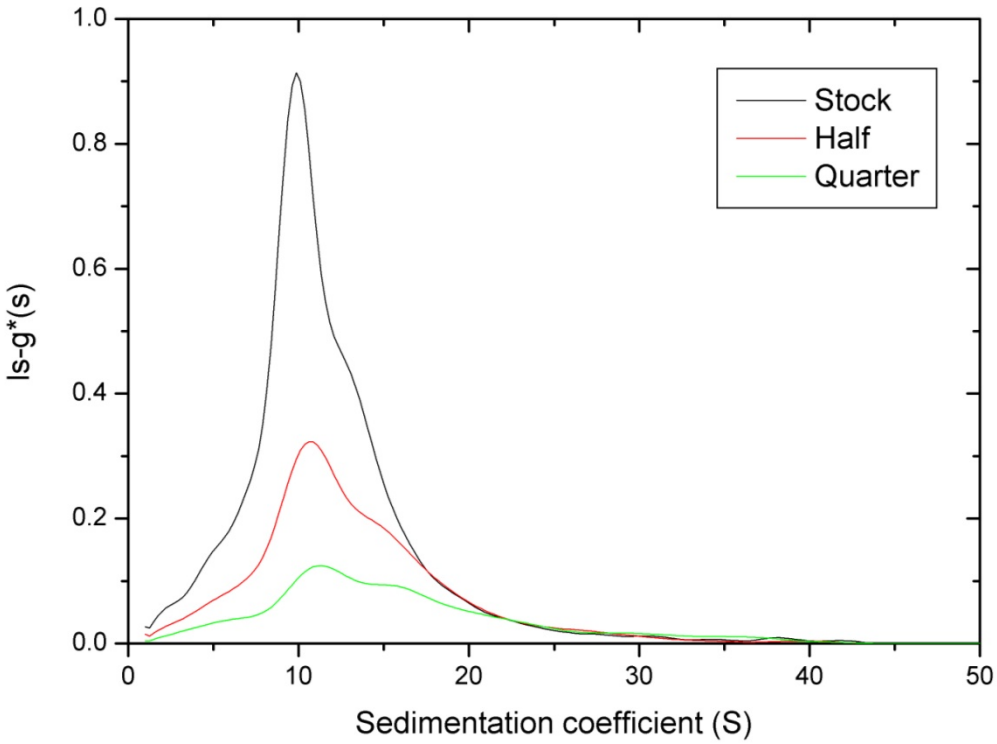

Figure 3.8: ls-g*(s) profile of low density pooled HGM in $PBS_{Azide,EDTA}$, at 20.0°C centrifuged at 40k RPM.

Figure 3.9 shows the plotted reciprocal integrated sedimentation coefficients of low density pooled HGM. 'Peak 2' refers to the occasional appearance in the distributions of peaks similar to those found in high density pools.

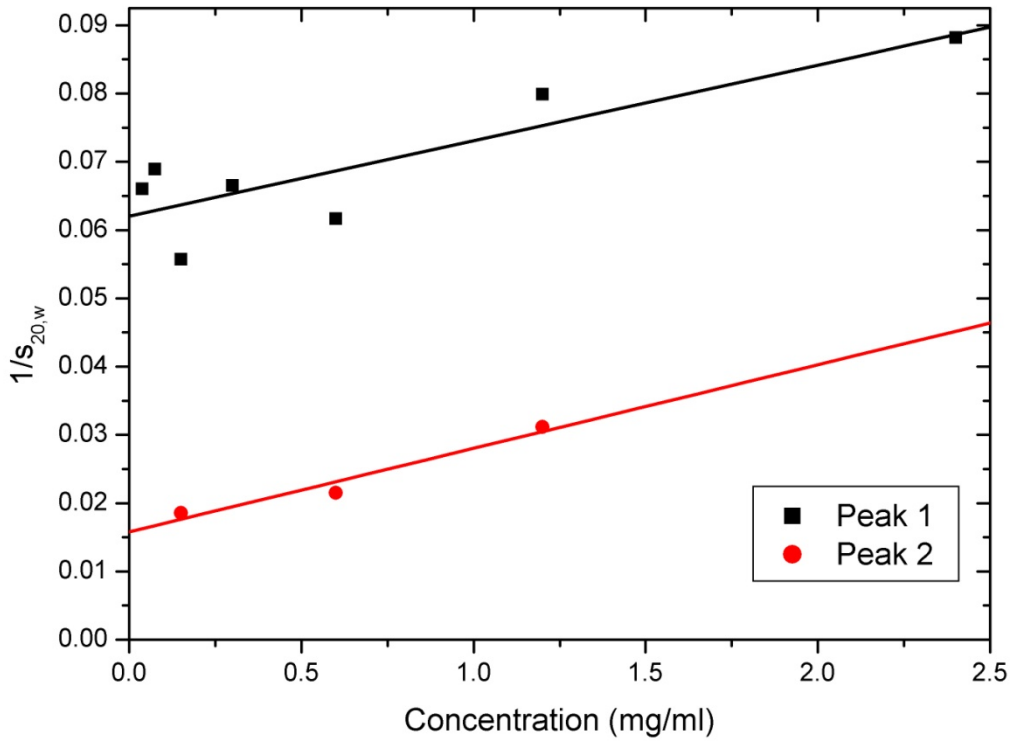

Figure 3.9: A reciprocal plot of $s_{20,w}$ against concentration from ls-g*(s) plots shown in Figure 3.8.

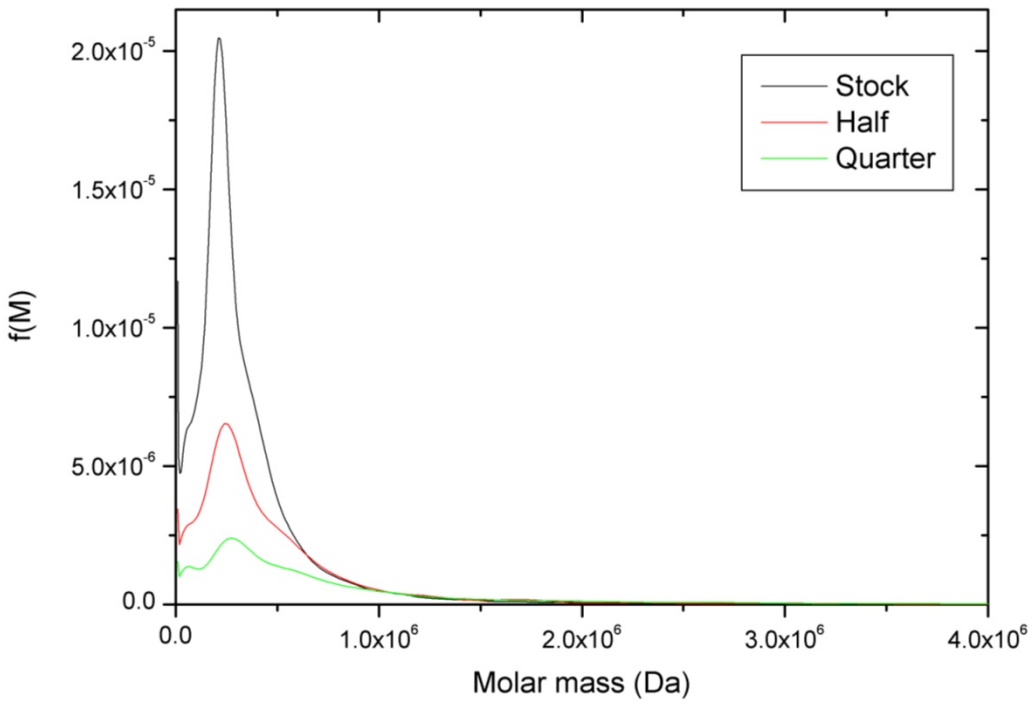

Figure 3.10: A f(M) profile of low density pooled HGM in $PBS_{Azide,EDTA}$, at 20.0°C centrifuged at 40k RPM.

Figure 3.10 shows the molar mass distribution of the data from Figure 3.8. Compared to Figure 3.7, which used the same MHKS parameters, they both have peaks just before 1MDa however, again, there does not appear to be a second peak around 3MDa.

3.4.1.4 Guanidine hydrochloride

Figure 3.11 shows a sedimentation coefficient plot of the high density pool HGM sample in guanidine hydrochloride. Out of three concentrations set up, only two were capable of being analysed by SEDFIT.

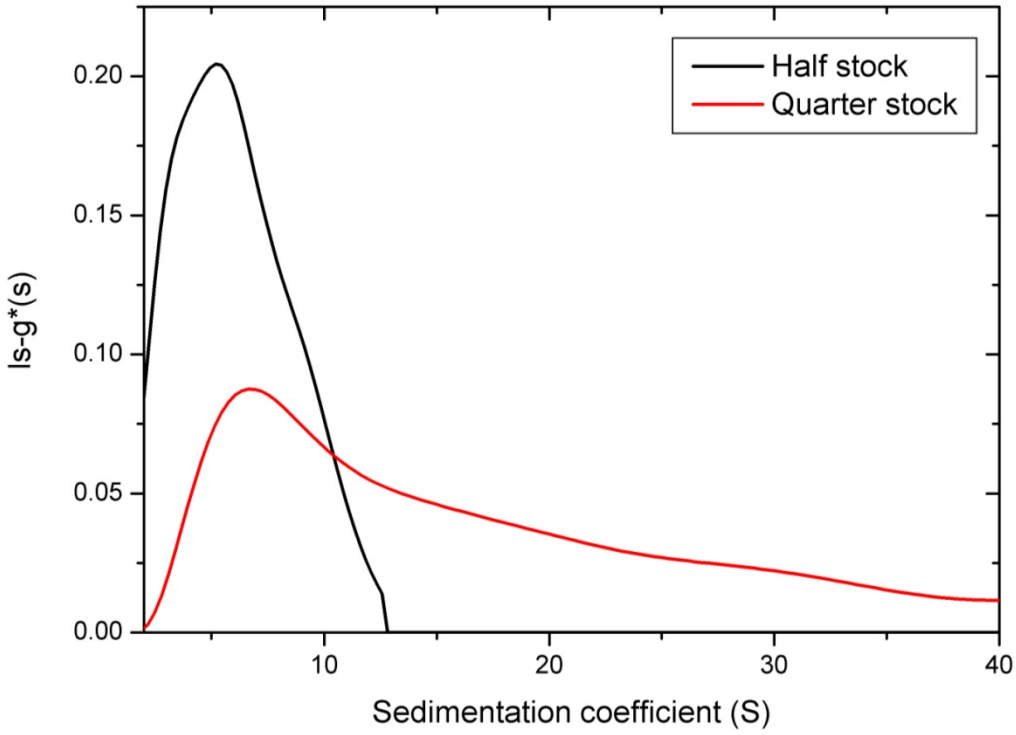

Figure 3.11: A ls-g*(s) profile of high density pooled HGM in 6M GuHCl at 20.0°C centrifuged at 45k RPM.

A reliable s^0 was not feasible with only two values measured. However, the two concentrations do concur with each other and show non-ideal behaviour. The lower-concentration distribution is comparable with the $PBS_{azide,EDTA}$ sample which spans between 5 and 30S.

Different MHKS values were used to analyse the GuHCl sample, as shown in Figure 3.12, however they both show similar distributions in terms of peak values. They are also similar to, but higher molar mass than, the distributions found from the sample in $PBS_{azide,EDTA}$ which lies between 500 to 4000 kDa.

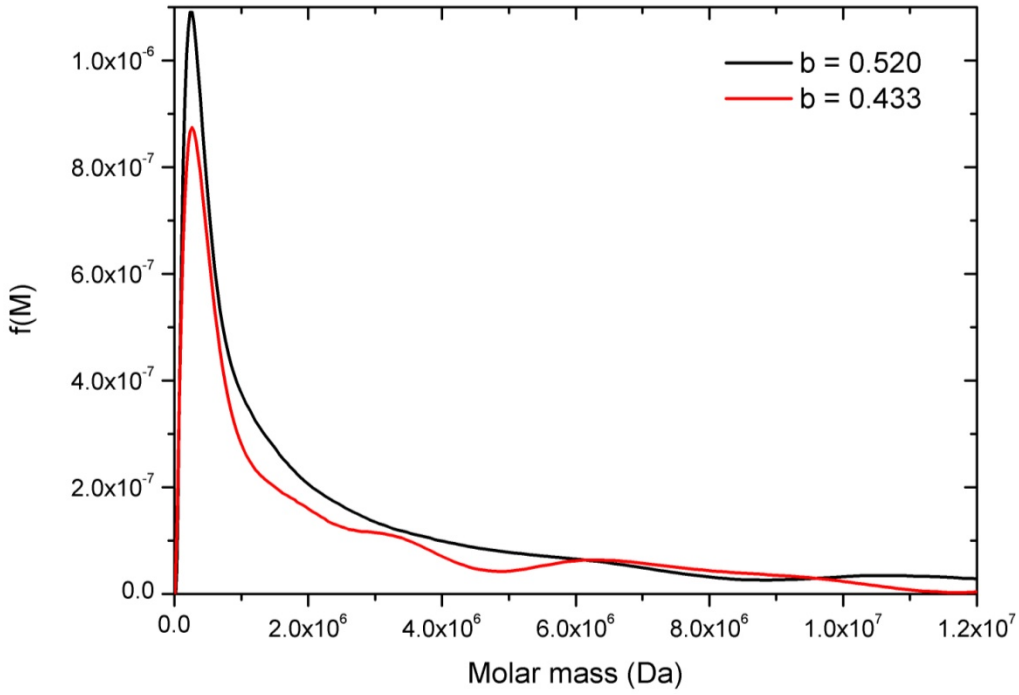

Figure 3.12: A f(M) profile of quarter stock high density pooled HGM in GuHCl at 20.0°C and centrifuged at 45k RPM, using two different MHKS values.

3.4.2 DLS

Figure 3.13 shows size distributions converted into diffusion coefficient distributions against intensity. The sharp peak at very low diffusion (<0.1x10^{-7} cm^2 s^{-1}) is an anomaly due to a proportion of component too large for the software to analyse.

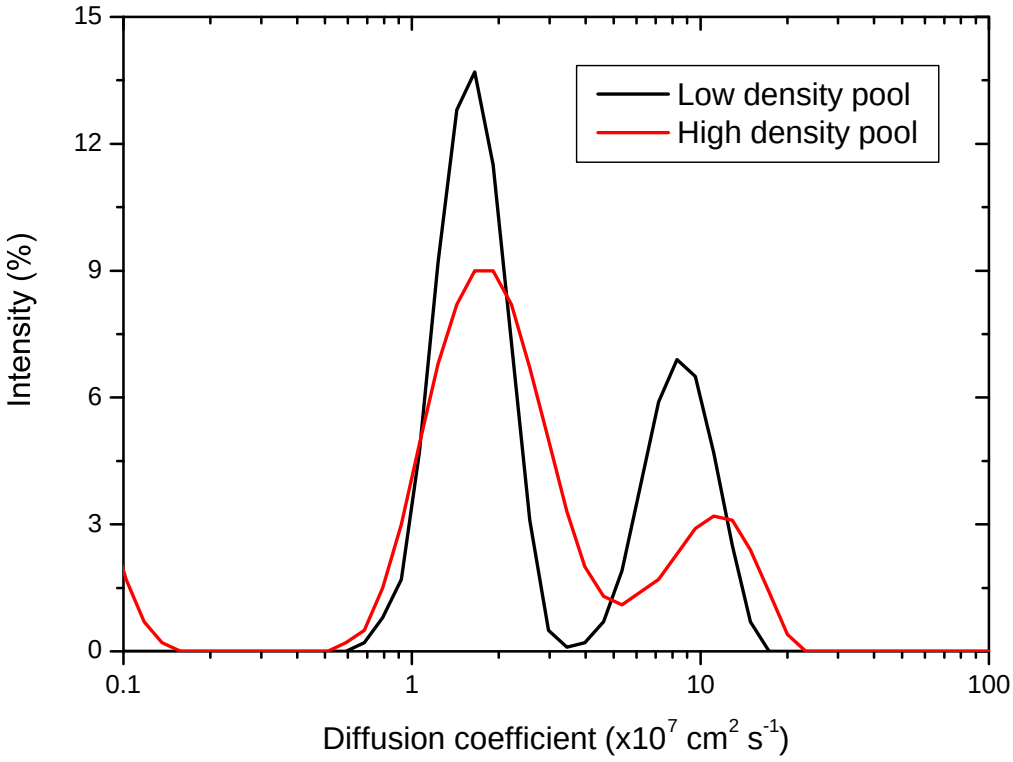

Figure 3.13: Diffusion coefficient distribution of high density (red) pooled HGM at 0.66mg/ml and low density (black) pooled HGM at 0.60mg/ml.

Both plots clearly show two peaks, with the high density fraction at 2 and 11 x10^{-7} cm^2 s^{-1} and the low density fraction at 2 and 9 x10^{-7} cm^2 s^{-1}. The low density pool has more resolved peaks than the high density pool. This could be due to experimental error, and the presence of the low diffusion coefficient species unresolved by the software.

The summary of hydrodynamic properties of high and low density fractions for HGM is shown in Table 3.2. Weight average molar mass was determined using Equation (2.24), with a partial specific volume assumed to be 0.65ml/g.

Table 3.2: Sedimentation and diffusion coefficient information on HGM from high and low density pools. Data has been combined to provide weight average molar mass estimations from the Svedberg equation (2.24).

HGM	Peak	$s^0_{20,w}$ ($x10^{13}$s)	D ($x10^7$ cm^2 s^{-1})	$M_{S,D}$ (MDa)
High	1	15.5	11	0.10
	2	57.0	2.0	2.0
Low	1	16.1	9.0	0.13
	2	62.5	2.0	2.2

3.4.3 SEC-MALS

Table 3.3 shows the molar mass data of the high and low density samples, followed by a plot of the scattering intensity versus elution time from the MALS. Molar masse average (number, weight, z-; M_n, M_w, M_z respectively) are in Daltons, with standard error as percentages in parentheses. Polydispersities (unitless) are also shown. There was no data collected for undegraded low density HGM. Figure 3.14 shows the elution intensities of the mucin samples.

Table 3.3: Molar mass (Da) comparisons between the three samples run through SEC-MALS (standard error estimates in parentheses).

	High density undegraded	High density degraded	Low density degraded
$\mathbf{M_n}$	1.318×10^6 (12%)	7.093×10^3 (25%)	4.851×10^5 (2%)
$\mathbf{M_w}$	1.727×10^6 (23%)	4.347×10^4 (10%)	7.702×10^5 (1%)
$\mathbf{M_z}$	2.520×10^6 (74%)	8.060×10^4 (18%)	1.192×10^6 (3%)
$\mathbf{M_w/M_n}$	1.310 (26%)	6.129 (27%)	1.588 (2%)
$\mathbf{M_z/M_n}$	1.912 (75%)	11.363 (31%)	2.456 (3%)

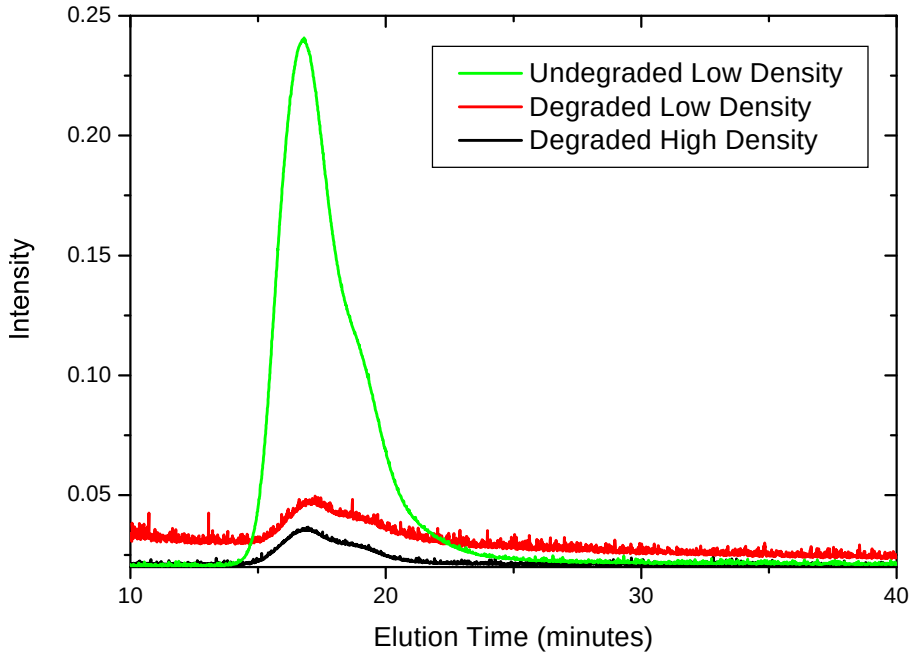

Figure 3.14: Elution time distribution of high and low density pooled degraded HGM, and undegraded high density HGM from size exclusion chromatography. Y axis represents intensity of scattered light (detector 11 shown).

3.5 Discussion

3.5.1 Purification

The isopycnic density gradient (Figure 3.1) produced two peaks of mucins. Subsequently, two sets of fractions were pooled as high and low density mucins. This result is different to other studies (Davies et al., 1996, Carlstedt et al., 1983) who found a single peak. However this distribution is similar to results found by Sheehan & Carlstedt on Human Cervical Mucin, who isolated a third pool of mucin (Sheehan and Carlstedt, 1987). Because the components of this pool might have contained protein, it was

decided not to use this in the investigation. Equally, the highest density fractions were not used to eliminate the presence of nucleic acids.

There was an increase in weight average molar mass by isopycnic density gradient ultracentrifugation (Table 3.4). This was probably due to the removal of low molar mass proteins, thus increasing the weight average of the overall solution. There was therefore probably a low level of nucleic acid content.

3.5.2 Conversion from g(s) to f(M)

3.5.2.1 Practicalities of the algorithm

The conversion of data from g(s) to f(M) was performed by SEDFIT (Schuck, 2000). There seemed to be few differences in analysis time between the two fits.

The main drawback for this method is obtaining MHKS parameters. Most hydrodynamic characterisation investigations do not state both the k" and b values, often quoting just b which is related to its shape. For example, when the method was attempted for konjac glucomannan samples, papers were available giving the conventional hydrodynamic properties but did not give a k" value (Kök et al., 2009). With a value for 'b' and a single pairing of s-M values, an estimation of k" can be calculated. For mucins, no MHKS parameters were given, although rough estimations have been made previously (Sheehan and Carlstedt, 1984), thus it was necessary to perform the literature search for corresponding sedimentation coefficients and weight average molar masses.

The method was also flawed when analysing heterogeneous systems. The f(M) plot produced from sedimentation velocity data from before the final purification (Figure 3.4) gave three general peaks, however the molar

masses of the peaks will be inaccurate since the MHKS parameters used were just for mucin and not for the protein/nucleic acid impurities. The distribution therefore does not represent the presence of protein and nucleic acid.

3.5.2.2 Effect of guanidine hydrochloride

Guanidine hydrochloride was shown to have an effect on mucin conformation. According to Table 3.1, the b shape factor for mucins in standard aqueous conditions was 0.520, and in guanidine hydrochloride it was 0.433. This suggests that guanidine hydrochloride is extending the macromolecule, which is usually more compact without this salt. This is consistent with what is known of the denaturing effect of guanidine hydrochloride (Qasim and Taha, 2013).

3.5.3 Size distribution

3.5.3.1 Profile

The f(M) data shows that the molar mass profiles of the mucins (Figure 3.7, Figure 3.10) are similar to the profiles from SEC-MALS (Figure 3.14). The DLS data (Figure 3.13, Table 3.2) corroborate the profiles to a degree, however there seem to be two well defined peaks which are not so defined in the SEC-MALS or f(M).

The difference between DLS and SEC-MALS in terms of sizing is that the ability for DLS to detect smaller particles is greatly affected by the presence of larger particles, since larger particles scatter more light than smaller ones. Ideally, some sort of chromatographic method would be required to measure the diffusion coefficients of elutions. The SEC-MALS was not able to fully resolve the peaks, due to insufficient elution resolution, so the distribution is measured over the entire elution.

3.5.3.2 Molar mass averages

The following table (Table 3.4) is a comparison between weight average molar mass measurements. Crude mucin was only analysed using sedimentation velocity under standard ionic conditions. For the low density pool, there was no definitive measurement for the weight average molar mass from SEC-MALS so the degraded molar mass has been shown. Guanidine hydrochloride was only used for the high density pool. The Svedberg equation was applied to two peaks from each pool.

Overall, the values obtained are consistent with the range of molar mass found in the literature, referring to the collective data from Figure 3.2 and Appendix 1.

There is good agreement between f(M) and MALS, especially with the high density pool. The Svedberg equation yields two different weight average molar masses, which are either side of the averages from the f(M) method. The overall weight average molar mass was higher for the high density pool compared to the low density pool, as observed with SEC-MALS and f(M). Contrary to this, the Svedberg equation yielded a higher weight average molar mass for the low density pool. This might be explained by the fact that these systems are polydisperse. The Svedberg equation is well suited for monodisperse systems and the values will change significantly in the presence of polydispersity. This is especially true for the determination of diffusion coefficients using dynamic light scattering, which is prone to under representing smaller components (higher diffusion coefficients).

Table 3.4: Weight average molar masses from three different methods for the high and low density pooled HGM in two different buffers. All values are in millions of Daltons with polydispersity indices (z/w) in parentheses. All samples were measured at 20°C. M^0 refers to an extrapolation of data to infinite dilution. * refers to degraded sample.

HGM	SEC-MALS (PBS)	f(M) (PBS, M^0)	f(M) (GuHCl)	Svedberg (PBS)
Crude	N/D	1.17	N/D	N/D
High Density	1.73 (1.46)	1.87 (1.34)	2.77	0.10 2.00
Low Density	*0.70 (1.55)	1.13 (1.69)	N/D	0.13 2.20

3.5.4 Degradation

The guanidine hydrochloride study not only shows the properties of HGM in that medium, but also allows a degradation study to be performed. The effect of guanidine hydrochloride as a denaturant/preservative has been applied to mucin preparations for decades (Spragg et al., 1969). It is also known that azide and EDTA have antiseptic properties (Lantz and Eisenberg, 1978, Mucci et al., 1963) however these additives were only used to maintain the stability of the mucins for reasonable experimental periods.

Observations from SEC-MALS $PBS_{azide,EDTA}$ experiments showed the weight average molar mass of the high density HGM fell significantly after two months of storage at +4°C from 1.7 MDa to 43 kDa and increased in

polydispersity from 1.3 to 6.1 (refer to Table 3.3). Unfortunately it was not possible to run GuHCl through the SEC-MALS to make a more direct comparison, to prevent possible degradation of the column medium, however from Table 3.4 it can be seen that the weight average molar mass of mucins in 6M GuHCl is significantly higher than the $PBS_{azide,EDTA}$ sample (2.77 and 1.87 MDa respectively).

So in respect to the AUC study, it can be seen that the sample has not degraded after three months. In fact the weight average molar mass from the GuHCl run is higher than that of the $PBS_{azide,EDTA}$ experiments, suggesting that degradation had occurred in the short time between purification and preparation.

3.6 Conclusions

The two pools, separated based on their densities were not the same in terms of molar mass distribution but both tested positive for presence of MUC5AC.

The Extended Fujita approach is a novel method for showing the molar mass distribution of homogeneous, polydisperse systems. These experiments have shown that it accurately and precisely predicts molar mass distributions of mucin samples from this purification process.

This investigation also showed the effect that guanidine hydrochloride had on the mucin preparations, such that the weight average molar mass was higher, and the macromolecule is more extended as expected through knowledge of the denaturation properties of this salt. Guanidine hydrochloride provided more protection than the combination of EDTA and azide at the concentrations presented in this investigation.

4 Hydrodynamic characterisation of *Cucurbita* extract

4.1 Introduction

Diabetes Mellitus types I and II (DM-I, DM-II) are diseases which affect the body's ability to self-regulate blood-glucose levels to 4-7mmol/L (Berg et al., 2012). DM-I is an autoimmune disease, usually onset from a young age, where the body is incapable of producing insulin in high enough quantities to effect a hypoglycaemic response. As a result, current treatment is the injection of supplementary insulin either in native human form or as an analogue. DM-II is a disease associated with metabolic syndrome and develops later in life. It is where the insulin produced by the pancreas is less effective than normal. Treatment for DM-II includes behavioural change, pharmaceutical intervention such as Metformin (Knowler et al., 2002) but it can also be to manually regulate the blood-sugar level by using insulin (Wallia and Molitch, 2014). Both diseases are prevalent throughout the world and cause serious health problems in patients. There is, therefore, a drive to find preventative and/or alternative treatment options other than invasive insulin injections.

Pumpkin (*Cucurbita pepo*) has been seen as a beneficially healthy food for quite some time (Adams et al., 2011), presenting antibacterial, anticancer, and immunomodulatory properties. It also shows anti-metabolic syndrome properties such as hypocholesterolaemic and hypoglycaemic effects on human physiology. There have been numerous studies looking at different

components of pumpkin and related *Cucurbita* sp. For example, pumpkin seeds, a source of dietary fibre, vitamins, minerals, essential fatty acids and phytosterols (Nishimura et al., 2014, Gossell-Williams et al., 2008, Yadav et al., 2010), were tested for their hypoglycaemic effect (Adams et al., 2012a, Adams et al., 2014) and shown to reduce blood glucose levels in rats when orally delivered.

Another study (Li et al., 2005) indicated that, in rats, the intake of protein bound polysaccharide from pumpkin pulp reduced the effective toxicity of Alloxan, a drug used to cause diabetes in rats (Lenzen, 2008), on pancreatic β-islet cells. This study did not clarify whether it was the protein, the polysaccharide or the complex of the two which caused the desired effect. Later, the same research group suggested that it may have been the polysaccharide component which was active in reducing blood glucose levels (Fu et al., 2006).

The aim of this study is to characterise the protein-polysaccharide extract from pumpkin pulp which may be the contributing component towards pumpkin's hypoglycaemic effect. Hydrodynamic methods such as viscometry, density measurement, sedimentation velocity and sedimentation equilibrium will be used to identify the components of pumpkin extract.

4.2 Materials and Methods

4.2.1 Extraction and Purification

Extraction and purification was performed as per methods outlined in Li et al. (2005). One ~5Kg pumpkin (*Cucurbita pepo* L. var. *pepo*) was peeled, deseeded, chopped into small ~1cm^3 pieces and dried in an oven at 53^{o}C

(range 43-56^{o}C, sampled 10 times) for 55 hours. There was no significant change in temperature over time (from Analysis of Variance - ANOVA, $F_{(1,8)}$=0.44, P=0.525, no significance). The pieces were continually agitated to aid drying, during which the sample was inspected for significant Maillard browning (none observed).

The dried pieces were ground into a powder. The particulate size was not precisely determined, however the ground powder was sifted through a 250μm sieve - particle size was therefore <250μm.

The powder was suspended in deionised water 5% w/v (10.2g in 200ml) and allowed to dissolve for 5 hours with constant stirring. The suspension was centrifuged at 2600 x g for 25 minutes at 4^{o}C. ~180ml of supernatant was recovered from centrifuge tubes. The supernatant was concentrated in a water bath at 45^{o}C, covered with a 250μm sieve to reduce dust contamination, for two days.

The volume of the concentrate was 80ml which was reduced to 75ml after vacuum filtration through a Whatman grade 1 paper filter (11μm).

25ml of 95% v/v chilled ethanol (Fisher Scientific, UK; analytical grade) was added to the solution and centrifuged at 2600 x g for 25 min at 4^{o}C.

Pelletted material was washed with absolute ethanol. The material was freeze dried (Edwards Super Modulyo) at -80^{o}C, 35Pa for 4 days. The recovered powder, labelled Protein-Bound Polysaccharide from Pumpkin (PBPP), totalled approximately 300mg providing a yield of 3% from original ground powder.

4.2.2 Sample preparation

Freeze dried PBPP powder was dissolved in deionised water (0.0767g + 3.825ml) by mixing for six hours at 17°C at low shear. The sample was contained in an 8kDa cut off dialysis bag (BioDesignDialysis Tubing D106, Fisher Scientific, UK) and dialysed with deionised water (4ml in 500ml) at 4°C for approximately 12 hours to remove low molar mass sugars and salts. The dialysis bag was transferred to 1 litre 0.1M pH 6.8 Phosphate Buffered Saline (PBS) for 12 hours. The volume increased to ~7.5ml during dialysis.

Concentration was measured using differential refractometry with a dn/dc of 0.155ml/g (Theisen et al., 2000) on the assumption that the majority of the sample will be similar to pectin (Košťálová et al., 2010).

4.2.3 Hydrodynamic analysis

4.2.3.1 Density & Viscosity

Density measurement was carried out with a concentration series using the Anton Paar DMA5000 oscillating capillary density meter at 20°C. Densities were measured to 7 significant figures and temperature was maintained to 3 decimal points (±.0005°C).

Intrinsic viscosity was measured using an Ostwald capillary viscometer suspended in a water bath at 20.0°C and an automatic timer. Density measurements from the DMA5000 were used for the calculation of relative viscosity.

4.2.3.2 Sedimentation velocity

Sedimentation velocity was carried out at 40k RPM in the Beckman XL-I using Rayleigh Interference (all samples) and 280nm Absorbance optics (lower concentrations).

400µl of PBPP, in a concentration range between 0.5-3.5mg/ml, and corresponding dialysate were injected into standard centrifuge cells. They were constructed with 12mm aluminium epoxy resin centrepieces and sapphire windows (refer to section 2.3.1.3).

Data were analysed using the SEDFIT ls-g*(s) vs s algorithm (refer to section 2.3.3.2).

4.2.3.3 Sedimentation equilibrium

Sedimentation equilibrium was carried out in the same ultracentrifuge with Rayleigh Interference optics. Long path-length cells were constructed with 20mm titanium centrepieces and sapphire windows, and injected with 100µl volumes of sample and reference buffer (~0.2cm radial range). Samples were centrifuged at 6000 RPM for 3 days. The sample concentration was 0.3mg/ml to reduce the effects of non-ideality.

Data were analysed using SEDFIT-MSTAR v1 (Schuck et al., 2014) and MULTISIG (Gillis et al., 2013a) incorporated into the ProFit package (refer to sections 2.3.4.3 and 2.3.4.4).

4.3 Results & Discussion

4.3.1 Density measurement & Viscometry

The partial specific volume was obtained using Equation (4.1) and the linear regression from density measurements against concentration (Figure 4.1). This was calculated to be 0.647ml/g (±8.5%). The value is consistent with the theory that polysaccharides tend to be ~0.60ml/g and protein ~0.73ml/g, thus a mixture of the two macromolecule types would yield a partial specific volume between these two values.

$$\overline{v} = \frac{1}{\rho_0}\left(1 - \frac{d\rho}{dc}\right) \quad \textbf{(4.1)}$$

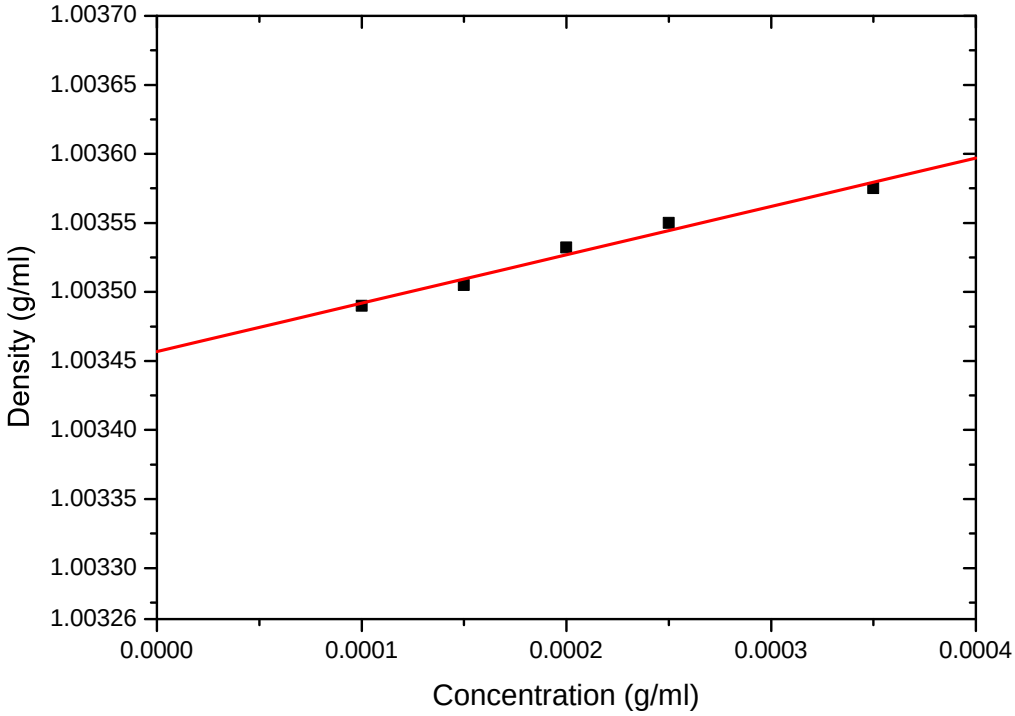

Figure 4.1: Determination of partial specific volume of PBPP using density measurement in PBS at 20°C.

Intrinsic viscosity was yielded from Figure 4.2 at 80ml/g (12%). This value is lower than findings from Ptitchkina et al. (1994) and Yoo et al. (2012)

who found the intrinsic viscosity of the pectin/polysaccharide component to be 337ml/g and 500-950ml/g (respectively) in 0.1M NaCl. The reason for the large difference is likely to be due to the protein component which would have a low intrinsic viscosity (BSA has an intrinsic viscosity of ~5ml/g) and therefore reduce the weight average value presented in this study.

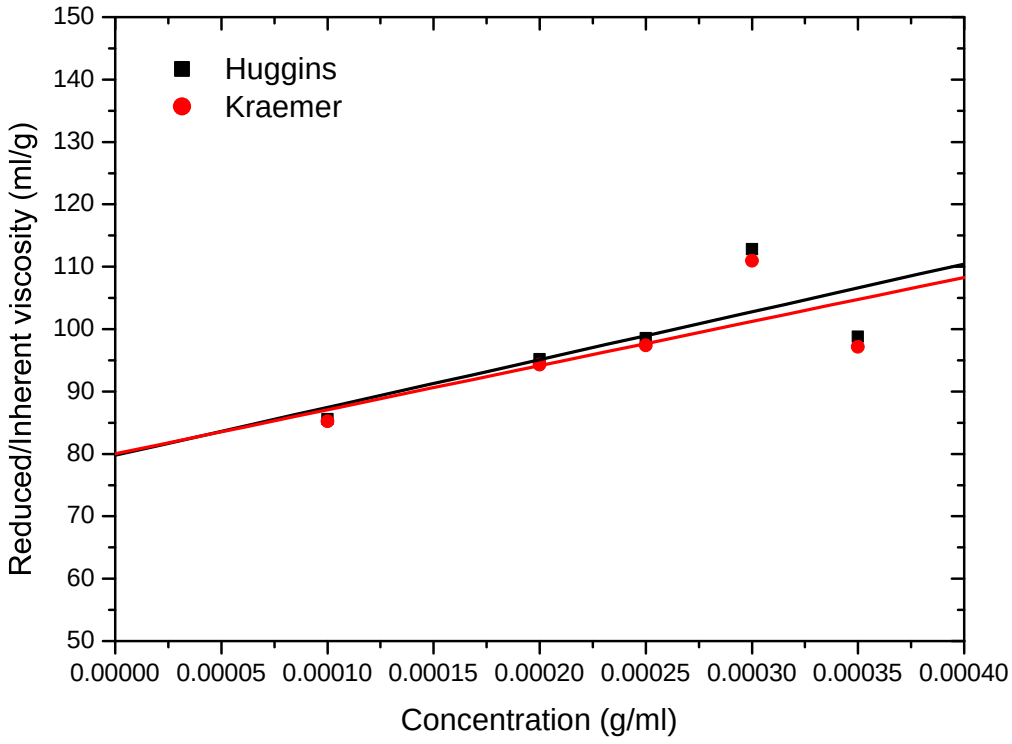

Figure 4.2: Extrapolation of reduced and inherent viscosity of PBPP in PBS at 20°C to infinite dilution to determine intrinsic viscosity.

Both Huggins and Kraemer regressions show positive slopes whereas Ptitchkina et al. yielded negative Kraemer plots. This may be explained by incomplete solubility of PBPP or the heterogeneity of the sample. The error in extrapolation may have affected the intrinsic viscosity value measured.

4.3.2 Sedimentation velocity

Figure 4.3 shows three plots related to PBPP in terms of sedimentation velocity analysis. Top left is a concentration series analysed using ls-g*(s) vs. s analysis. The distribution appears heterogeneous and polydisperse. There are three regions: Peak 1 which ranges between 0-2S, Peak 2 ranging between 2-5S and a range of higher molar mass material from 5S upwards.

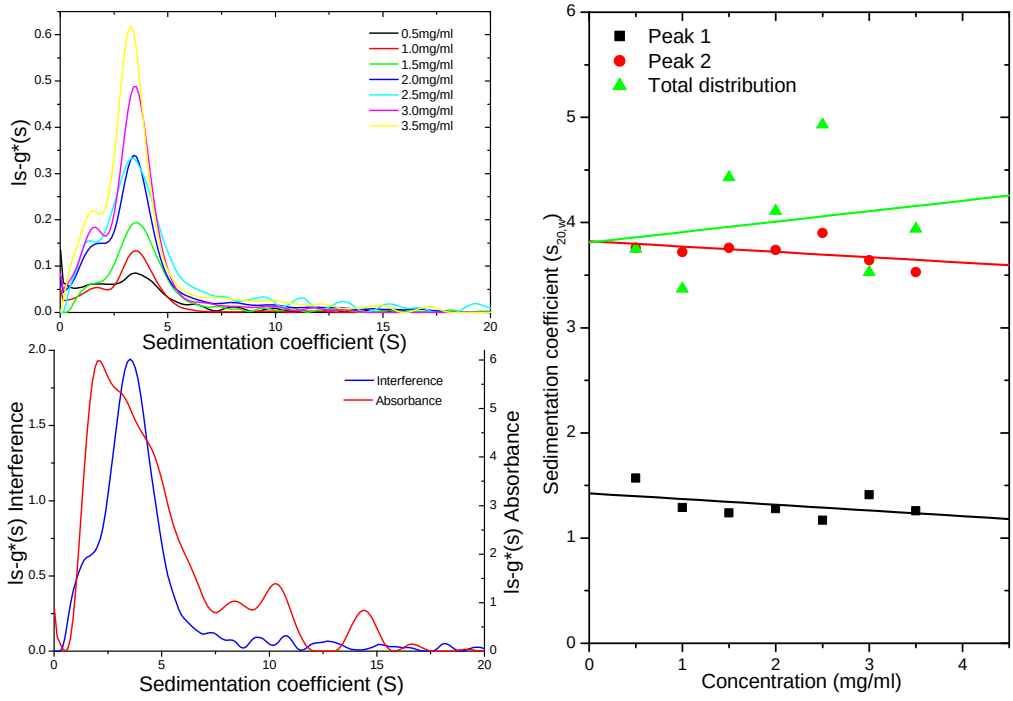

Figure 4.3: Summary of sedimentation velocity analysis. Top left: concentration series ls-g*(s) of interference optics; Bottom left: Comparison of interference and absorbance (280nm) optics at 1.5mg/ml; Right: Extrapolation of corrected sedimentation coefficients to infinite dilution.

Bottom left is a single concentration (1.5mg/ml) with a comparison between interference and absorbance optics. Absorbance scans were performed at 280nm wavelength to detect for protein content, whereas the interference scans detect any macromolecular material. 'Peak 1' has a

high absorbance and slightly lower for 'Peak 2'. The remainder of the distribution contains various absorbing and non-absorbing material.

The approximate percentage of material was obtained through integrating the interference peaks in SEDFIT and averaged (no observable trend). 'Peak 1' represents (18±2.4)% and 'Peak 2' represents (74±1.4)%. 'Peak 1', having a high absorbance concentration, is likely to be a protein-rich component. 'Peak 2' is likely to be a protein-polysaccharide complex due to the slightly lower absorbance concentration and higher fringe concentration. These approximate percentages for protein/polysaccharide components are consistent with information provided from the literature. The wet-weight protein percentage is 4.91%, dry-weight 5.4%, and wet weight carbohydrate content is 74.11%, dry-weight 81% (Aziah and Komathi, 2009). Assuming that these components will not be discrete species, as they are covalently linked protein and polysaccharide, these values corroborate the peak percentage concentrations.

The plot on the right (Figure 4.3) is the extrapolation of integrated peaks to infinite dilution, as described in Equation (4.2).

$$s_{20,w} = s^0_{20,w}(1 - k_s c) \qquad \textbf{(4.2)}$$

Both 'Peak 1' and 'Peak 2' follow typical concentration dependence based on non-interacting species. They extrapolate to 1.43S (7.7%) and 3.82S (2.4%). The 'Total distribution' is the integration of the entire distribution, and does not closely follow a linear regression, however this was not unexpected since it includes the heterogeneous material from 5S upwards. This data extrapolated to 3.81S (13%). Estimates for k_s are 38 and 13ml/g for Peak 1 and 2 respectively, however these values are unreliable due to the overall heterogeneity of the system and would be affected by the Johnston-Ogston effect (Johnston and Ogston, 1946) where larger

species are distorted in their apparent sedimentation velocity and concentration by the presence of smaller components.

4.3.3 Sedimentation equilibrium

4.3.3.1 SEDFIT-MSTAR

The c(M) algorithm within SEDFIT yielded the baseline and concentration at the meniscus. This information was used to find the ln(J) vs. r^2, $d\ln(J)/dr^2$ vs. r or J and M* vs. r plots. Results are summarised in Table 4.2, with outputted plots in Figure 4.4. Plot (a) shows the raw data transformed into a natural logarithm plot against radius squared. The linear regression (red line) can yield a weight average molar mass from the slope, however is not representative of the distribution as it does not fit the raw data. The data appears to bend upwards, suggesting a polydisperse system. Plots (c) and (d) show a differentiation (smoothed using Savitzky–Golay) to show the slope at each point in plot (a). These slopes are both positive, also suggesting a polydisperse system with little non-ideality. Plot (b) is the M* plot which extrapolates to the base of the cell (~7.095cm). The extrapolation (red plot) was 249.7kDa.

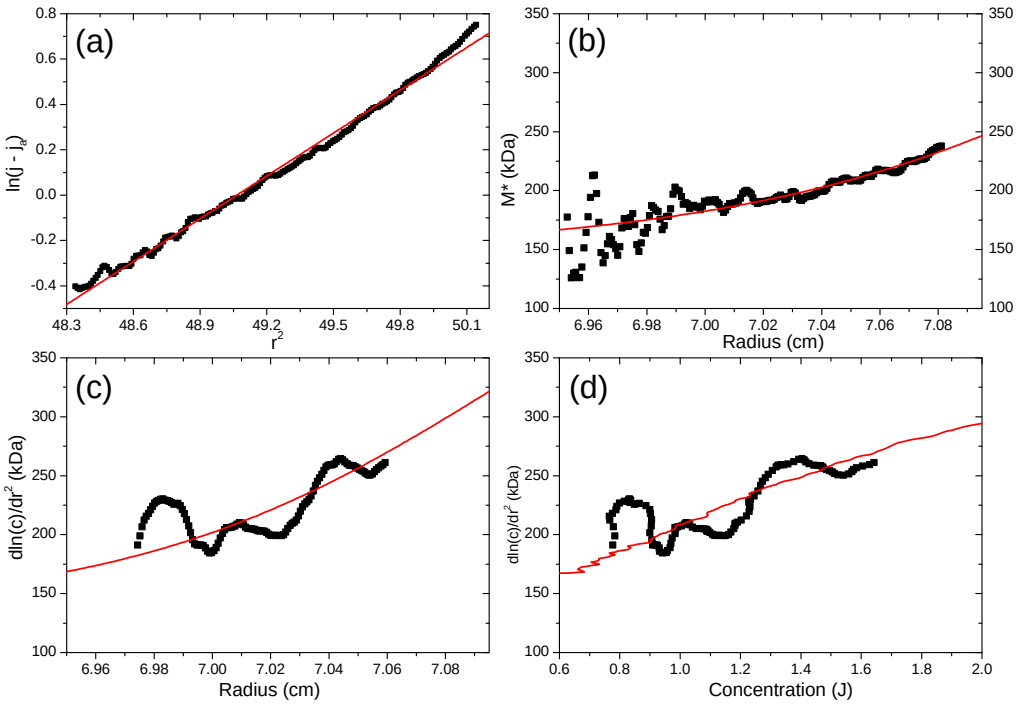

Figure 4.4: SEDFIT-MSTAR output for PBPP. (a): natural logarithm concentration against radius squared; (b): M* against radius; (c): differentiation of plot (a) against radius; (d): as (c), against concentration.

The c(M) algorithm was also able to estimate the weight average and z-average molar mass at 249.7 and 375.7kDa respectively.

The hinge point value is a measure of checking for the presence of non-ideality, however it is generally a less accurate measure of weight average molar mass. In this case, the hinge measurement coincides with the MSTAR and c(M) very closely, thus the non-ideality is not a significant factor in this system at the low concentration measured.

4.3.3.2 MULTISIG/RADIUS

Average molar mass data is presented in Table 4.2 in terms of number, weight, z average and polydispersity indices yielded from the MULTISIG algorithm. MULTISIG was also capable of providing a distribution of reduced molar mass in terms of fringe concentration. This was plotted and

presented in Figure 4.5. Table 4.1 represents the peak analysis of PBPP from c(sigma). 'Peak 1' is at approximately 135kDa, 'Peak 2' is at 205kDa and 'Peak 3' is at the 820kDa mark, however it is likely that MULTISIG was not able to resolve heterogeneous material and summarised all high-sigma material in the final 'peak'.

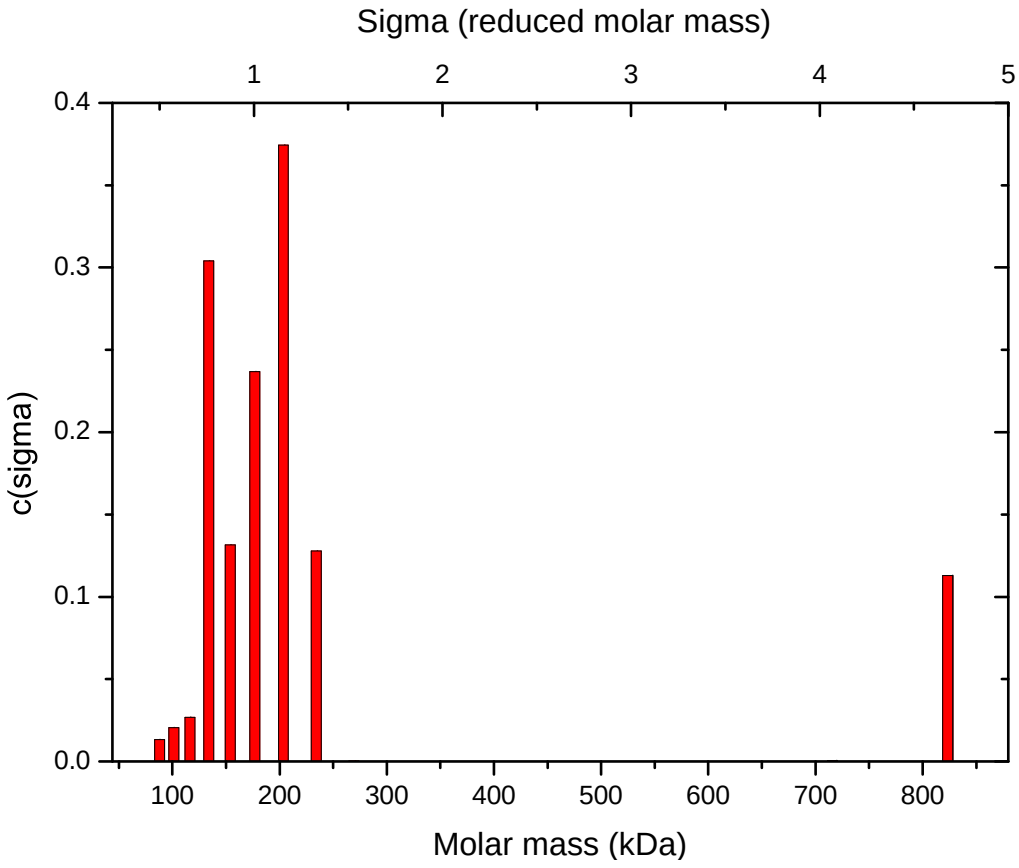

Figure 4.5: Continuous distribution of molar mass and reduced molar mass of PBPP.

The peaks match closely to the distribution in Figure 4.3, including the number of peaks and approximate percentage content.

Table 4.1: Peak analysis of MULTISIG analysis of PBPP.

	Molar mass (kDa)	Concentration (fringes)	Content (%)
Peak 1	135	0.365	27
Peak 2	205	0.871	65
Peak 3	820	0.113	8.4
Total (weight average)	230	1.349	100

Figure 4.6 shows an equivalent plot to Figure 4.4c and d (which represents the apparent weight average molar mass alone). The MULTISIG-RADIUS weight average ranges between approximately 200-300kDa, similar to the SEDFIT-MSTAR analysis. The extrapolation to approximately 200kDa may represent the lower portion of the distribution, as the higher molar mass material would have distributed towards the bottom of the cell.

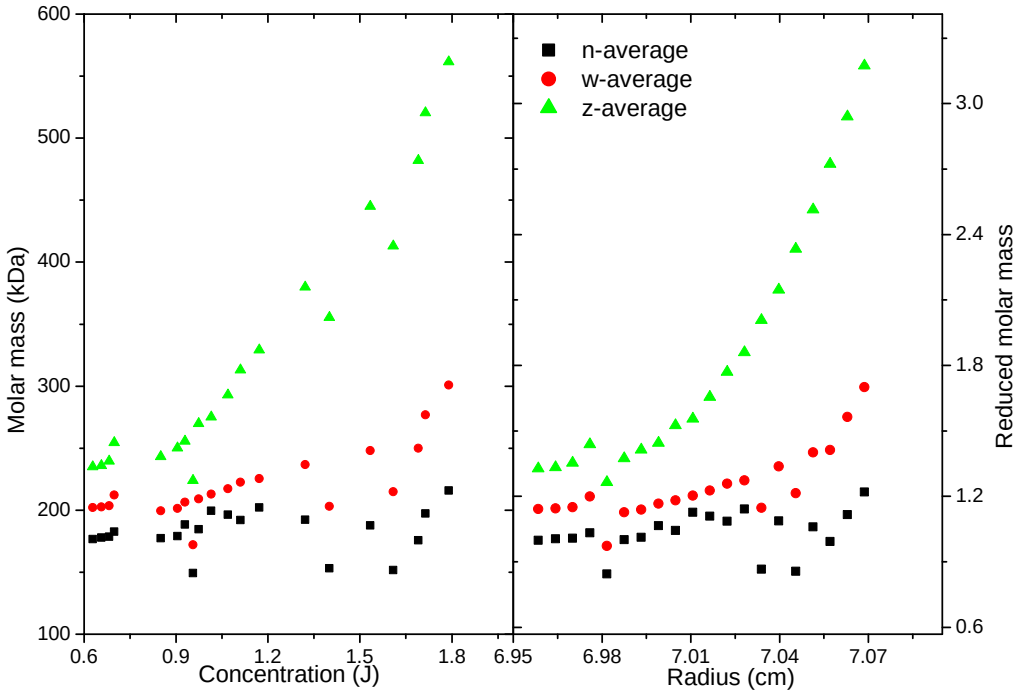

Figure 4.6: Apparent molar mass and reduced molar mass against fringe concentration (left) and radius (right).

Figure 4.7 represents the distribution of polydispersity indices spread across the cell in terms of radial position and concentration. The higher part of the cell (lower concentration) shows a polydispersity index of approximately 1.17/8, depending on whether calculated through z/w averages or w/n averages. As the concentration increases the polydispersity increases up to approximately 1.9 (1.4 w/n). Referring to Figure 4.5, the heavier section of the distribution 'Peak 3' would be nearly depleted close to the meniscus. Thus it can be concluded that the polydispersity values from 1.17 to 1.7 (z/w) represents 'Peak 1' and 'Peak 2', and values of 1.7 to 2.0 (z/w) represent 'Peak 3'.

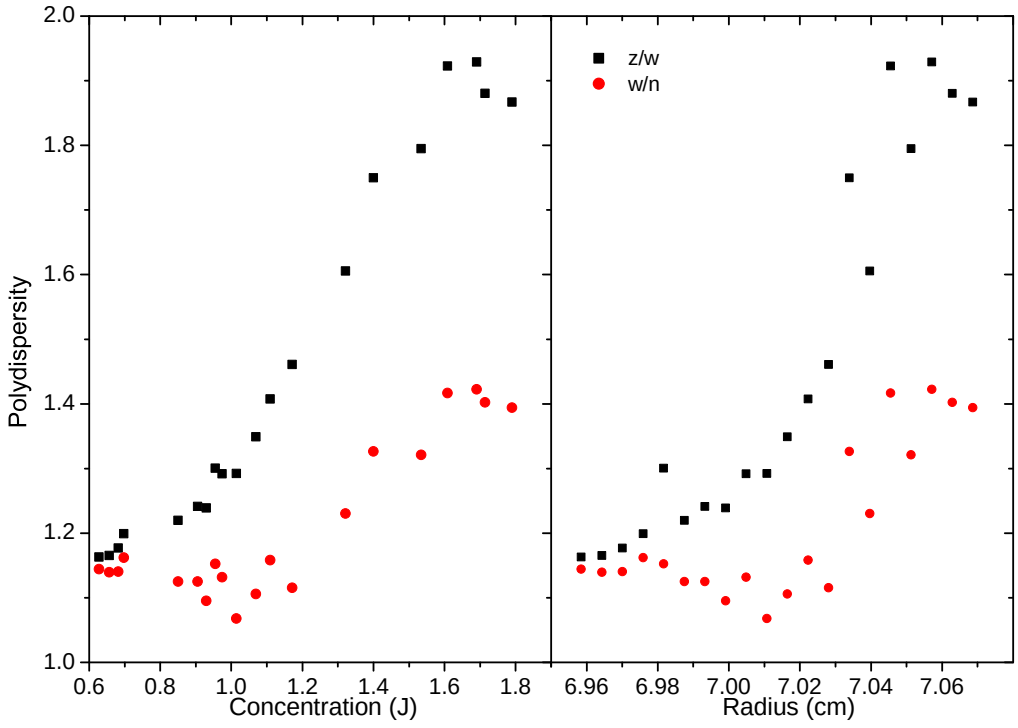

Figure 4.7: Polydispersity indices of PBPP from MULTISIG-RADIUS.

4.3.3.3 Summary of molar mass results

Table 4.2: Summary of sedimentation equilibrium analysis, using SEDFIT-MSTAR and MULTISIG.

Method	Number average (kDa)	Weight average (kDa)	Z-average (kDa)	M_z/M_w	M_w/M_n
MSTAR	-	249.7	-	-	-
c(M)	-	249.7	375.7	1.505	-
Hinge	-	248.2	-	-	-
MULTISIG	182.1	230.4	375.5	1.630	1.265

The weight average molar mass was measured using SEDFIT-MSTAR (MSTAR, c(M) and Hinge point analysis) and MULTISIG. The MSTAR analyses are all complementary to each other with the weight average at 249.7kDa and the hinge point (less accurate but non-ideality independent) slightly lower. The agreement suggests that the system does not have a significant level of non-ideality at the concentrations analysed.

MULTISIG weight average results are lower than SEDFIT-MSTAR, although the z-average matches very closely to the c(M) analysis. The weight average molar masses are not representative of the distribution as it takes into account the high molar mass heterogeneous component and not the main components.

This value is similar to weight average molar masses obtained by Yoo et al. (2012) through a microwave extraction method (430kDa), however their sample extracted by strong acid instead provided a higher weight average molar mass of 850kDa. In addition, they found polydispersity to be ~1.6 which is consistent with the findings from this investigation. Polydispersity in the present study was found to be between 1.25 and 1.63, although this

is not representative of the distribution as the smaller components probably have polydispersity indices of ~1.2 and larger components with ~1.9.

4.4 Conclusions

A hydrodynamic characterisation study was carried out on the protein-polysaccharide complex isolated from pumpkin extracts. Viscometry, density measurement, sedimentation velocity and equilibrium were used to provide a basic component analysis of the system in terms of percentage content of components and hydrodynamic properties (Table 4.3). It was shown that the main component was a protein-polysaccharide complex of approximately 70% weighted concentration at 4S and 200kDa, 20% protein/high protein content component at 1.5S and 135kDa and an unresolved higher molar mass fraction at 10% content. Although MULTISIG estimated 820kDa for this component, the likely value is a range between 0.3 to beyond 1MDa.

Table 4.3: Summary of composition, hydrodynamic parameters and molar mass properties of PBPP. Standard error (%) presented in parentheses.

	Peak 1	Peak 2	Peak 3	Overall (weight average)
Percentage composition	18% (±13%)	74% (±2.0%)	8%	100%
Macromolecular composition	Protein	Protein polysacch.	Unknown	Mixture
$\bar{v}$ (ml/g)	-	-	-	0.647
[η] (ml/g)	-	-	-	80 (±12%)
$s^0_{20,w}$ (S)	1.4 (±7.7%)	3.8 (±2.4%)	-	3.8 (±13%)
MSTAR (kDa)	-	-	-	250
MULTISIG (kDa)	135	205	820	230

The link between structure and function is of critical importance in novel therapy development. The information provided from hydrodynamic characterisation goes towards our full understanding of the structure of this extract. Once this is understood it will aid in our understanding of the function for a novel treatment for Diabetes Mellitus.

5 Determination of size and shape of gum arabic using hydrodynamic techniques

5.1 Introduction

Gum arabic, or acacia gum, is a glycoprotein with multiple applications in the food and pharmaceutical industries. It is able to form viscous solutions, emulsify suspensions and bind with other macromolecules. These factors account for its widespread use (Verbeken et al., 2003).

5.1.1 Composition

The primary structures of both the sugar and protein fragments have been well studied (Nie et al., 2013a). The polysaccharide component represents approximately 95% of the macromolecule and consists of a very complicated, heavily branched β (1→3) D-galactopyranose backbone with a high proportion of arabinofuranose and rhamnopyranose residues (Nie et al., 2013b) and terminal glucuronic acids. The protein component consists of a 250 amino acid chain, with regions of polysaccharide covalently O-linked to hydroxyproline and serine residues (Mahendran et al., 2008). This is often referred to as the wattle blossom model (Ali et al., 2009).

5.1.2 Conformation/structure

The overall hydrodynamic structure has been well studied typically either with light scattering techniques or with chromatographic methods or both (see for example Mahendran et al. (2008)). The wattle blossom model is

the commonly agreed standard, with the idea that the molecule is close spherical. There was also a suggestion of a 'hairy rope' model by Qi et al. (1991) using TEM to image the glycoprotein fragment however the wattle blossom model is more commonly accepted in terms of solution properties.

It is generally agreed that the weight average molar mass lies between $3x10^5$ and $2x10^6$ Da with high degree of polydispersity (Andres-Brull et al., 2013), which is typical for an unfractionated polysaccharide. It is also tightly bound with Stokes radii between 5-30nm (Alftrén et al., 2012, Goycoolea et al., 1995) and an intrinsic viscosity between 10-30ml/g.

Analytical Ultracentrifugation (AUC), as a separation and analytical technique, has the benefit of no columns or membranes for macromolecules to interact with, which particularly for charged polysaccharides like gum arabic (Funami et al., 2008), may cause complications. It is therefore surprising that AUC has previously not been used for this polysaccharide in publication. Our current investigation uses AUC, specifically the sedimentation velocity technique, to probe the hydrodynamic characteristics of gum arabic. Both a comparison, and a complementary analysis, will be performed on three sources of gum arabic and three differing ionic strength buffers.

5.2 Materials and Methods

5.2.1 Gum arabic samples

Gum arabic was obtained through three sources: Arthur Branwell (Essex, UK), Glycomix (Reading, UK) and Sigma Aldrich (Dorset, UK). All samples were purified from the *Acacia senegal* crop and prepared into buffered

solutions from spray-dried powder. Samples were undialysed due to little evidence of salt impurities.

Samples were dissolved in a pH 7.0 phosphate buffered saline made up to 0.1, 0.3 or 0.5M ionic strength. 0.05M of the buffer was disodium hydrogen orthophosphate dodecahydrate and potassium dihydrogen orthophosphate (Fisher Scientific, UK). Further ionic strength was made up with sodium chloride (Fisher Scientific, UK). Table 5.1 shows the mass of salts added to buffer made up to 2 litres.

Table 5.1: Salts added to buffer, made up to 2 litres with deionised water. Main values are calculated masses required, bracketed figures were actual weighed masses.

Ionic strength (M)	NaCl (g)	$Na_2HPO_4.12H_20$ (g)	KH_2PO_4 (g)
0.1	5.845 (5.8459)	9.190 (9.1902)	3.122 (3.1217)
0.3	29.230 (29.2281)	9.190 (9.1896)	3.122 (3.1224)
0.5	52.614 (52.6147)	9.190 (9.1892)	3.122 (3.1223)

The refractive index increment used was 0.145ml/g (Huglin et al., 1989) at 0.1M ionic strength. For higher ionic strengths, no information was available for dn/dc and was therefore assumed at 0.150ml/g.

Samples were assigned codes denoting source and buffer conditions, for example GAs0.1 represents gum arabic from Sigma in 0.1M ionic strength PBS.

5.2.2 Methods

5.2.2.1 Density measurement

The concentration dependence of gum arabic upon density was used to find the partial specific volume, and provide supplementary density information for viscometry.

5.2.2.2 Viscometry

A large volume Ubbelohde viscometer was suspended at 20.0^{o}C. Buffer flow times were obtained with 15ml of solvent, then removed and replaced with 15ml of solution, and subsequent aliquots of solvent added (2, 4, 8ml…) to serially dilute the sample. Data were analysed using Huggins, Kraemer and Solomon-Ciuta (S-C) equations (Refer to section 2.1).

5.2.2.3 Dynamic Light Scattering

Samples of gum arabic at 0.1M ionic strength were filtered through 0.2µm Minisart single use sterile filters (Sartorius, Surrey, UK) and measured in the Zetasizer NanoS (Malvern, UK) using capped, plastic, disposable cuvettes. 173^{o} backscatter was used in the determination of the diffusion coefficients and hydrodynamic radii of the concentration series (refer to section 2.2.4). The reasonable assumption was made (refer to section 3.3.4) that rotation diffusion effects were negligible due to low asymmetry of the macromolecule.

5.2.2.4 Sedimentation velocity

Experiments were performed in cells constructed with aluminium epoxy resin 12mm 2 channel centrepieces, sapphire windows in aluminium window holders. 400µl of sample and corresponding buffer were injected

into the cells, sealed and balanced. The XL-I was set to 30k RPM, with scans taken every minute.

The stock gum arabic solutions were diluted to 1-7mg/ml. Data analysis was performed with the SEDFIT ls-g*(s) algorithm. Apparent sedimentation coefficients, fringe concentration, and percentage content were taken by integrating the main peak.

Sedimentation coefficients were corrected for buffer conditions and percentage content. Fringe concentration was converted to mass concentration and corrected for radial dilution.

5.2.2.5 SEC-MALS

The system was equilibrated with the appropriate buffer for at least 10 hours prior to injection of 100µl of sample. Three gum arabic samples were injected at three concentrations at three ionic strengths. The system is described in section 2.2.1, using MALS, viscometer, dRI and UV detectors.

Since the procurement of signal was unreliable only one concentration from each gum arabic, at each ionic strength, was analysed.

5.2.2.6 Statistical analysis

Linear regressions for partial specific volume, intrinsic viscosity and sedimentation coefficients were tested for significance using Analysis of CoVariance (ANCOVA) in GenStat v15 (VSN International). F values are the ratio of regression sum of squares over mean square error. The critical level of significance was set to $p \leq 0.05$.

5.3 Results and discussion

5.3.1 Density measurement

Partial specific volumes were calculated using Equation (4.1), with parameters obtained from linear regression analyses of Figure 5.1. Results are shown in Table 5.3.

The partial specific volume of the three gum arabic samples ranged between 0.61-0.64ml/g depending on ionic strength. ANCOVA did not show a correlation between the partial specific volume and ionic strength for GAb, GAg or GAs ($F_{2,26}$=0.94, P=0.403; $F_{2,21}$=1.01, P=0.382; $F_{2,23}$=0.25, P=0.778 respectively).

The average value for partial specific volume was 0.629ml/g, with a standard deviation of 0.012. Typical values for partial specific volume are approximately 0.6ml/g for polysaccharides and 0.73ml/g for proteins. Results in between these two values, slightly higher than 0.6ml/g, correlates with the known composition of gum arabic, which is generally 5% protein.

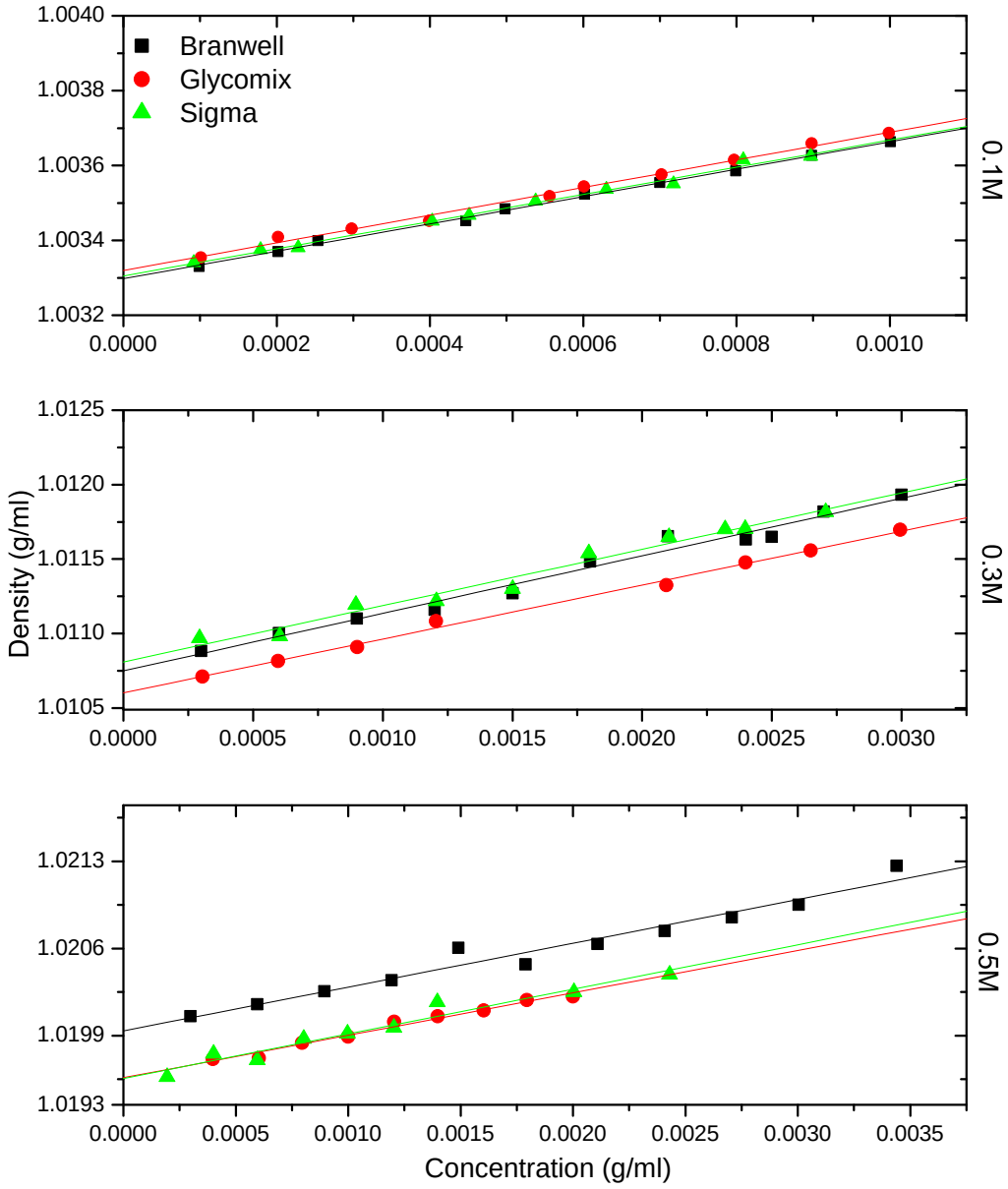

Figure 5.1: Summarised density measurement results at 20°C for gum arabic at three ionic strengths. The density of the buffer was used as the origin of the y axis.

5.3.2 Viscometry

Figure 5.2 shows the Huggins, Kraemer and S-C analysis of the viscometry data. Extrapolated intrinsic viscosities (from S-C) are summarised in Table 5.3. All nine plots show a good agreement between Huggins, Kraemer and S-C, with very good fitted regressions.

The Huggins plots show typical positive slope behaviour for all nine samples. Linear regression typically yielded a gradient of ~300ml^{2}g^{-2}, and a Huggins constant (Equation (2.4)) of ~0.8, which is consistent with literature values (Pamies et al., 2008). Kraemer plots all yielded a positive slope, except for GAb0.1 which is negative. This is atypical behaviour for the Kraemer plot, which is usually negative. However, previous studies (Goycoolea et al., 1995) have also shown a positive Kraemer plot. The Solomon-Ciuta plot offers an 'average' of the other two, and therefore should be close to horizontal. In this case, the Solomon-Ciuta plot does show a regression in between the Huggins and Kraemer plots but, due to the positive slope of the Kraemer data, the Solomon-Ciuta is positive too.

Statistical analysis revealed that there was a significant dependence ($P<0.05$) of concentration on Solomon-Ciuta intrinsic viscosity for all nine samples (Table 5.2). There was also a significant difference of the ionic strength on the extrapolation to infinite dilution; but the ionic strength did not significantly affect the concentration dependence of the intrinsic viscosity. Of note, however, is the similarity between statistical values obtained for the Glycomix and Sigma samples on analysis of the ionic strength on gradient (concentration dependence).

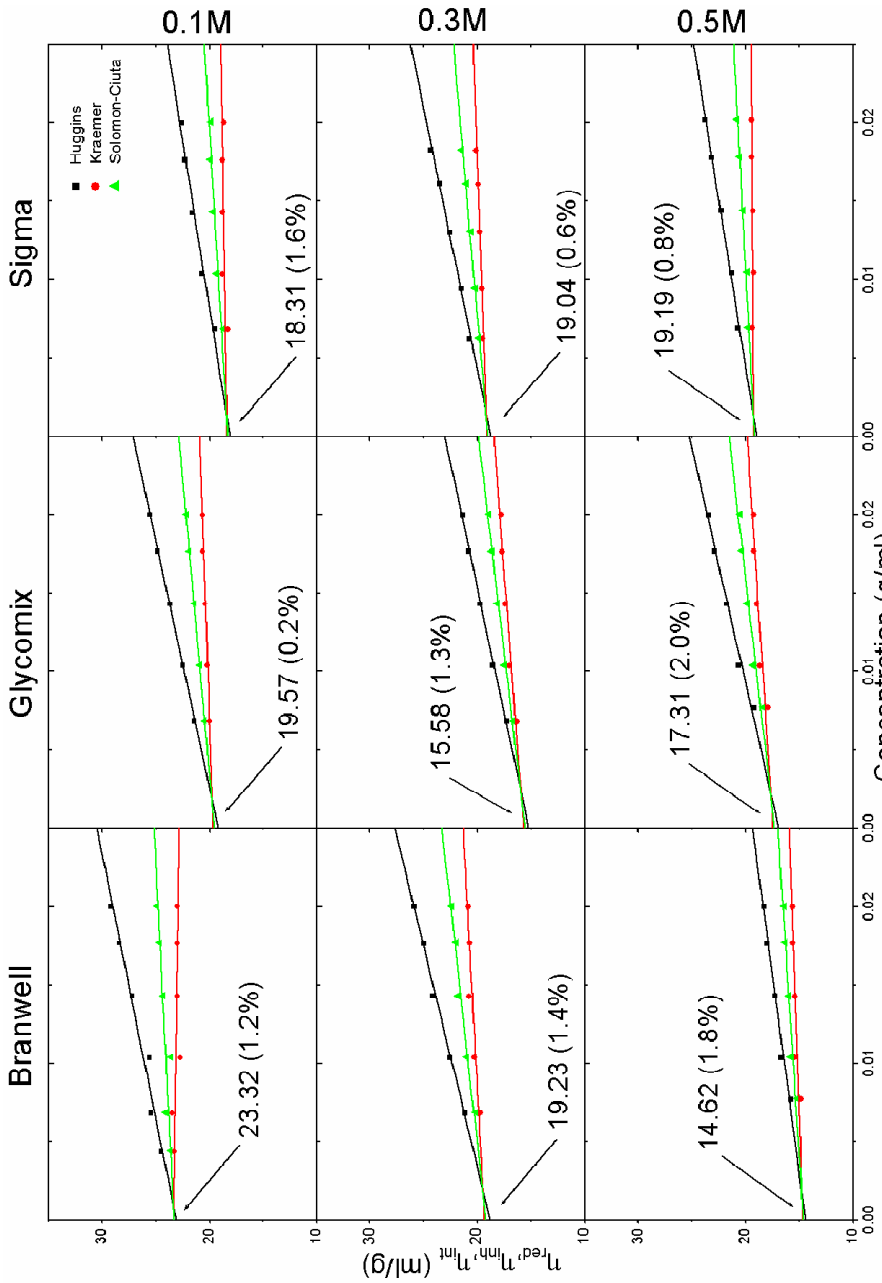

Figure 5.2: Huggins (black), Kraemer (red) and Solomon-Ciuta (green) analysis of gum arabic samples at three ionic strengths and 20°C.

Table 5.2: Statistical analysis (ANCOVA) for intrinsic viscosity results of gum arabic. Degrees of Freedom expressed in brackets.

Sample		η_{red} vs. c gradient ($ml^2\ g^{-2}$)	Concentration dependence (S-C)		Ionic strength on intercept		Ionic strength on gradient	
			F	P	F	P	F	P
GAb	0.1	236	12.76 (1,4)	0.023	28.32 (2,10)	<0.001	1.89 (2,10)	0.201
	0.3	300	79.50 (1,3)	0.003				
	0.5	233	28.33 (1,3)	0.013				
GAg	0.1	333	5619 (1,3)	<0.001	420.4 (2,9)	<0.001	3.89 (2,9)	0.061
	0.3	313	151.4 (1,3)	0.001				
	0.5	317	46.42 (1,3)	0.006				
GAs	0.1	197	19.19 (1,3)	0.022	92.05 (2,9)	<0.001	3.47 (2,9)	0.076
	0.3	354	203.5 (1,3)	<0.001				
	0.5	296	58.67 (1,3)	0.005				

5.3.3 Dynamic Light Scattering

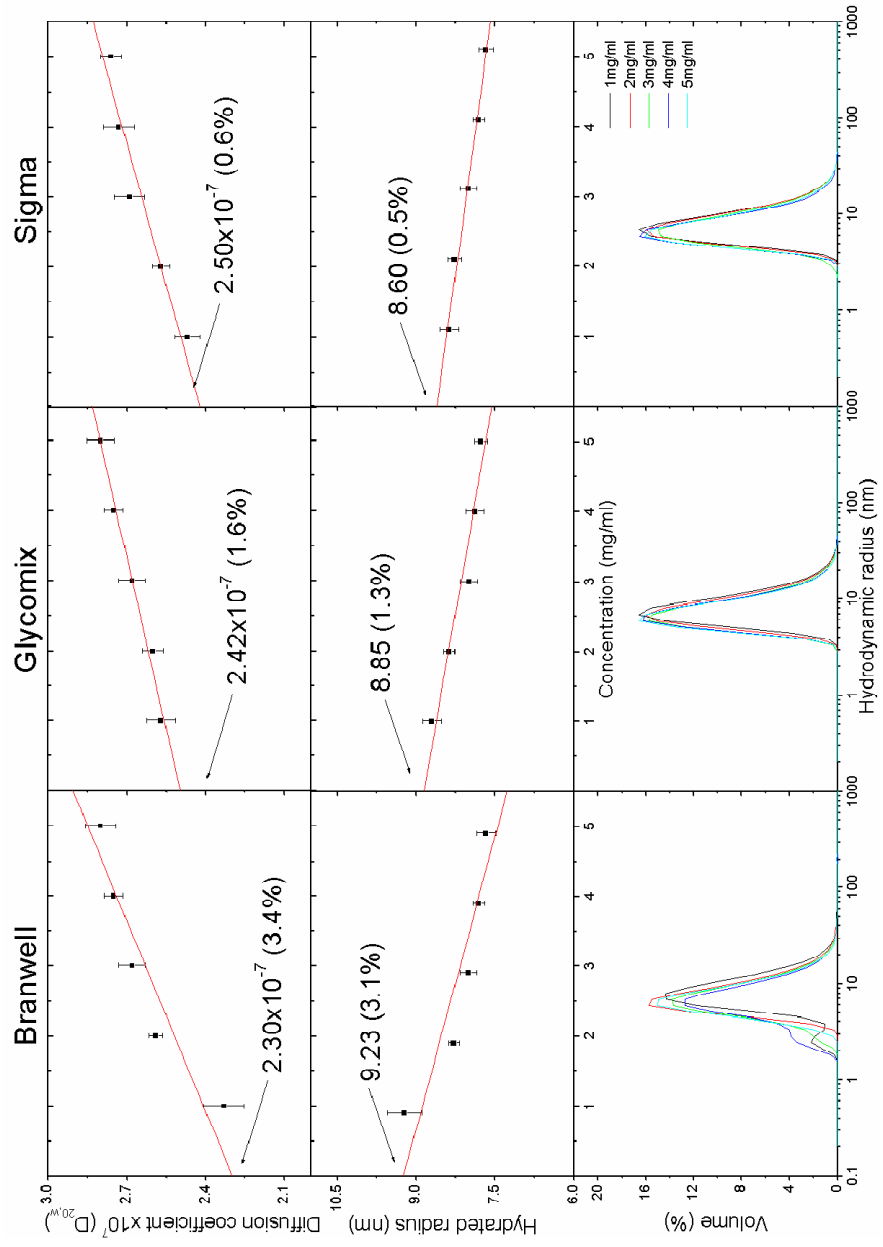

Figure 5.3: Results from DLS, yielding hydrated radius, diffusion coefficient and volume distribution at a single ionic strength (0.1M) at 20°C.

Figure 5.3 shows plots of diffusion coefficients and hydrodynamic radii against concentration at 0.1M PBS only. A weak concentration dependence can be observed, thus the extrapolated values are summarised in Table 5.3. The gradient of these plots, i.e. the concentration dependence of diffusion coefficients (and consequently hydrated radius), can be either positive or negative, but not usually very large. The data fits the regression very well, except for Branwell, which shows a slightly lower diffusion coefficient for the lowest concentration. This can be explained by the distribution plot which shows a shoulder around 2.5nm for 1 and 4mg/ml. The other samples show a single, fairly polydisperse distribution, from approximately 2-40nm.

Table 5.3: Summary of hydrodynamic parameters obtained from density measurement, capillary viscometry and dynamic light scattering. Percentage in brackets represents standard error.

Sample	Ionic Strength (M)	$\bar{v}$ (ml/g)	[η] (ml/g)	k_H	$x10^7\ D^0_{20,w}$ (cm^2/s)	r_H^0 (nm)
GAb	0.1	0.633	23.32 (1.2%)	0.43	2.30 (3.4%)	9.23 (3.1%)
	0.3	0.607	19.23 (1.4%)	0.81	N/D	N/D
	0.5	0.636	14.62 (1.8%)	1.09	N/D	N/D
GAg	0.1	0.629	19.57 (0.2%)	0.87	2.42 (1.6%)	8.85 (1.3%)
	0.3	0.631	15.58 (1.3%)	1.29	N/D	N/D
	0.5	0.647	17.31 (2.0%)	1.06	N/D	N/D
GAs	0.1	0.635	18.31 (1.6%)	0.59	2.50 (0.6%)	8.60 (0.5%)
	0.3	0.615	19.04 (0.6%)	0.98	N/D	N/D
	0.5	0.630	19.19 (0.8%)	0.80	N/D	N/D

5.3.4 Sedimentation velocity

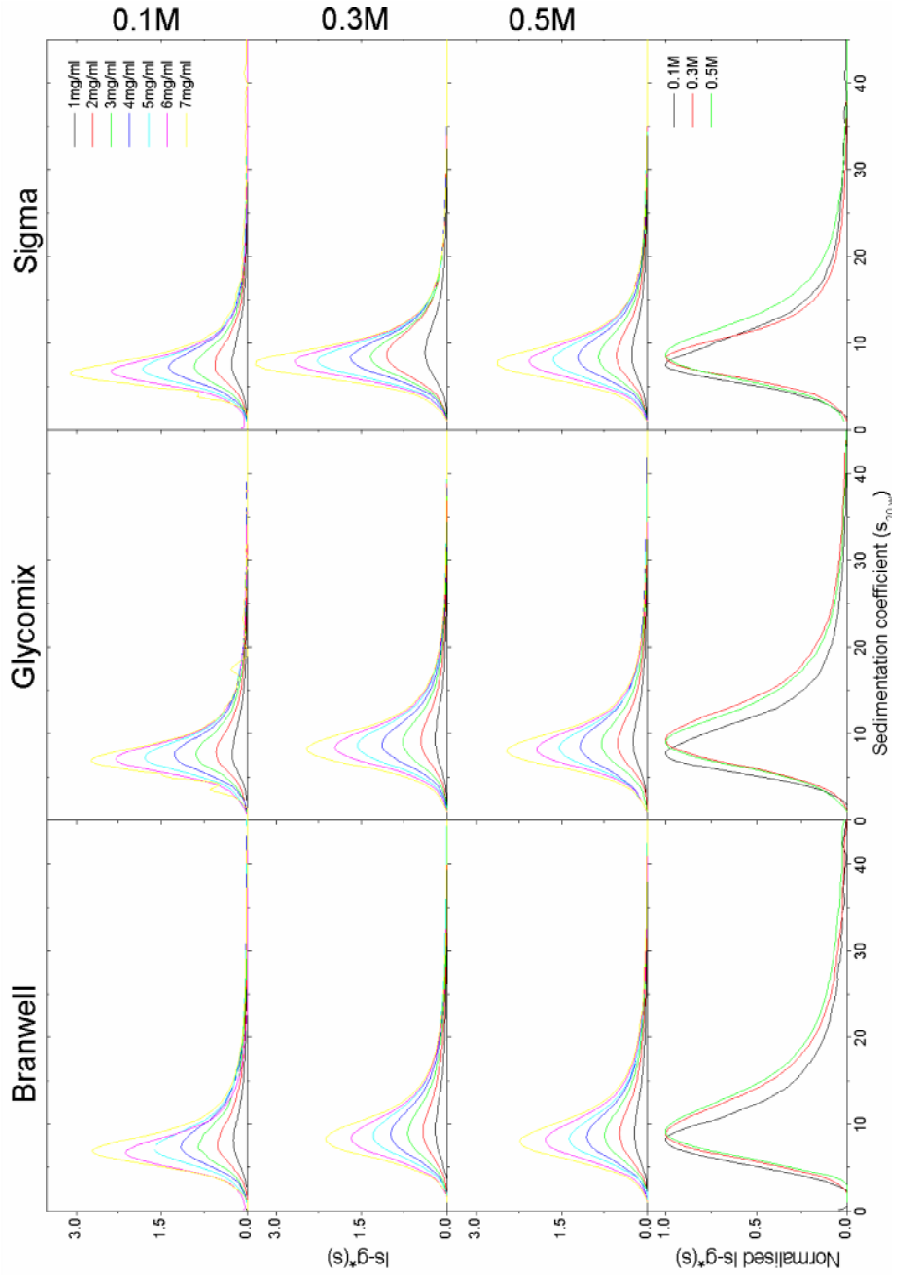

Figure 5.4: Least Square Gaussian analysis of gum arabic. The lower row shows a normalised distribution at lowest concentration comparing ionic strengths.

The gum arabic samples were analysed using a ls-g*(s) fit, as shown in Figure 5.4. The first nine plots show a single distribution, peaking at approximately 8S, with a distribution between ~2 and ~30S and very little, or no, contamination with smaller or larger material.

The plots also show very little concentration dependence, for all three ionic strengths. Significant concentration dependence would show, with decreased concentration, increased sedimentation coefficient and broader distribution as predicted by non-ideality.

The bottom row compares the lowest concentration of each sample, normalised to equal height. For Branwell and Glycomix, there is a definite difference between the 0.1M and higher ionic strengths, although not for 0.3 and 0.5M. For Sigma, the difference is not as pronounced.

With reference to Figure 5.5, the lowest concentrations for Branwell and Glycomix for all three ionic strengths are quite similar in their respective group. However, the lowest concentrations of Sigma samples are slightly different, with 0.3M being slightly more concentrated than the other two. Due to non-ideality, this would push the distribution to the left of what is expected. This may explain the discrepancy in Figure 5.4, where the Sigma ionic strength comparison plot shows the red (0.3M) plot slightly left of 0.5M.

5.3.5 Concentration dependence of sedimentation velocity

Concentration dependency was measured in two ways using Equations (4.2) and (3.1). Each equation relates to slope and constant of a linear regression analysis, results of which are shown in Table 5.4.

In general, it was found that the 'normal' sedimentation coefficient extrapolation (Equation (4.2)) had a lower standard error than the reciprocal plot for both the intercept and the slope. Thus these values were used later on in subsequent hydrodynamic analysis. Plots of these equations are shown in Figure 5.5.

The statistical analysis showed a significant difference between the concentration dependence of sedimentation coefficients and ionic strength for GAb ($F_{2,14}$=5.57, P=0.017). There was also a significant difference between $s^0_{20,w}$ for 0.3 and 0.5M ionic strength ($F_{1,10}$=11.50, P=0.007).

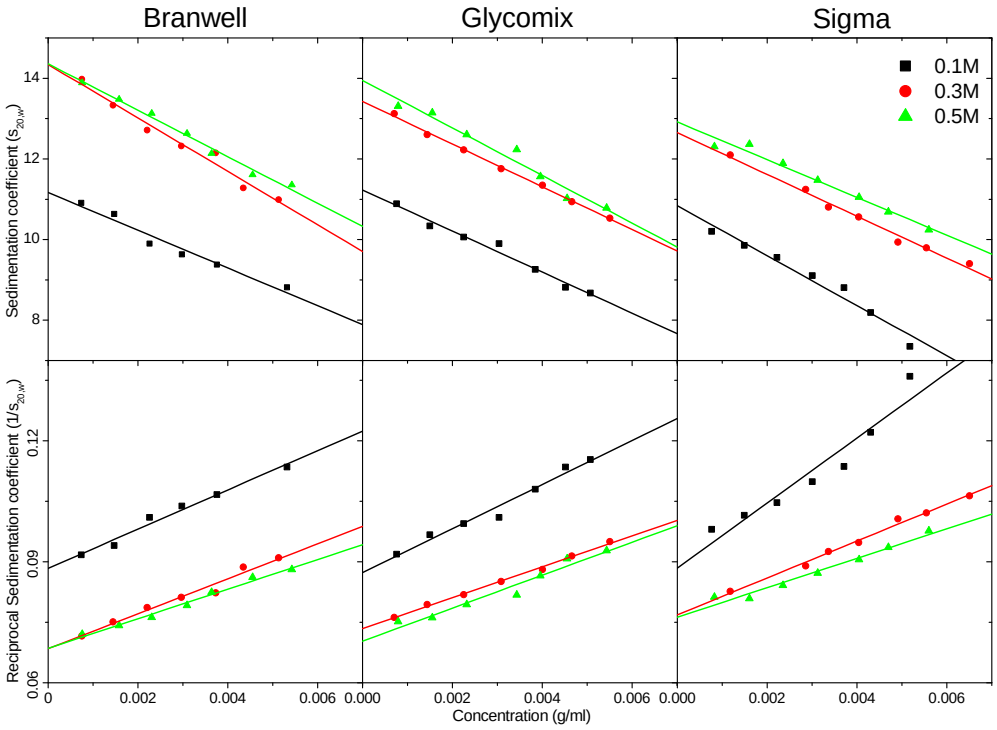

Figure 5.5: Implementation of Equations (4.2) (above) and (3.1) (below) on gum arabic at three ionic strengths.

For GAg and GAs, although there was a significant dependence between extrapolated sedimentation coefficients for different ionic strengths ($F_{2,15}$=669, P<0.001; $F_{2,14}$=679, P<0.001), there was no significant difference on the concentration dependence ($F_{2,15}$=1.54, P=0.246;

$F_{2,14}$=1.20, P=0.331). There were also significant differences between $s^0_{20,w}$ values for 0.3 and 0.5M ($F_{1,10}$=18, P=0.002; $F_{1,10}$=41, P<.001).

Bearing in mind that for GAb the concentration dependence seems to be dependent on ionic strength, and the other two have no significant dependence, it is possible that GAb results are an anomaly.

This information can be combined with intrinsic viscosity data to provide information about the shape/symmetry of the macromolecule. The Wales-Van Holde ratio (Wales and Van Holde, 1954) is the ratio between k_s and [η] and provides a hydration-independent shape factor. Table 5.5 shows $k_s/[\eta]$ values for the gum arabic samples, with intrinsic viscosity values taken from both Ubbelohde capillary and pressure imbalance results from SEC-MALS.

Table 5.4: Linear regression analysis from sedimentation coefficients against concentration (standard error in parentheses).

Sample		s vs. c		1/s vs. c	
		s^0	k_s (ml/g)	s^0	k_s (ml/g)
GAb	0.1	11.17 (1.3%)	41.87 (11%)	11.31 (1.2%)	55.02 (8.6%)
	0.3	14.34 (1.1%)	46.20 (8.3%)	14.61 (1.5%)	63.38 (9.2%)
	0.5	14.36 (0.7%)	40.14 (5.6%)	14.58 (0.9%)	53.46 (6.2%)
GAg	0.1	11.23 (1.0%)	45.34 (7.4%)	11.45 (1.5%)	62.37 (9.2%)
	0.3	13.43 (0.3%)	39.44 (2.6%)	13.62 (0.5%)	52.21 (3.1%)
	0.5	13.95 (1.2%)	42.30 (9.6%)	14.22 (1.9%)	58.07 (12%)
GAs	0.1	10.84 (1.6%)	57.17 (10%)	11.31 (3.8%)	91.17 (18%)
	0.3	12.65 (0.9%)	40.97 (5.8%)	13.01 (1.1%)	59.63 (5.2%)
	0.5	13.15 (0.3%)	39.78 (2.5%)	13.47 (0.4%)	55.66 (2.3%)

Table 5.5: Wales-Van Holde ratios of gum arabic with standard errors from intrinsic viscosities either from capillary measurements or SEC-Viscostar analysis.

Sample		$k_s/[\eta]$ (capillary)		$k_s/[\eta]$ (SEC-Viscostar)	
GAb	0.1	1.80	(11%)	1.34	(12%)
	0.3	2.40	(8.4%)	1.64	(8.7%)
	0.5	2.75	(5.9%)	1.41	(6.0%)
GAg	0.1	2.32	(7.4%)	1.62	(8.0%)
	0.3	2.53	(2.9%)	1.57	(3.8%)
	0.5	2.44	(9.8%)	1.68	(11%)
GAs	0.1	3.12	(10%)	2.13	(10%)
	0.3	2.15	(5.8%)	ND	-
	0.5	2.07	(2.6%)	1.59	(4.4%)

According to Table 5.5 the average of the capillary derived $k_s/[\eta]$ values was 2.40±0.39, while SEC-MALS derived data was 1.62 ±0.24. It is commonly accepted that the maximum theoretical $k_s/[\eta]$ value for any macromolecule is ~1.6 (Rowe, 1992). The results from capillary viscometry do not correlate well with this, while the SEC-Viscostar data is within an acceptable range accounting for experimental error. The only possible doubt would be GAs0.1 with a value of 2.13, however in this case the intrinsic viscosity was within the expected range of values (Table 5.6) but the k_s was not (Table 5.4). Looking at the plotted data (Figure 5.5) the highest concentration for GAs0.1 is affecting the slope more than other points, almost to a degree that the slope could be interpreted as polynomial. However, this is not replicated in the other two samples, so this is likely to be an anomaly.

5.3.6 SEC-MALS-Viscostar

Figure 5.6 shows elution times for the three gum arabic samples. The data has been normalised for detector voltage to aid comparison. The molar mass data yielded from this data acquisition is shown in Table 5.6.

The data shows that all nine samples eluted at approximately the same time, at ~8 minutes. What can also be seen from the zoomed section is the 0.1M elution indicating a secondary peak at around 14-18 minutes, not present in 0.3 and 0.5M ionic strengths.

For Sigma 0.3M, the elution is very noisy. There is no explanation why however when the data was being collected, the sigma 0.3M sample was repeated in triplicate, with poor signal for each elution. This was the best/cleanest elution plot of the three. Unfortunately, the online viscometer did not pick up notable amounts of signal, thus the intrinsic

viscosity was not determined (Table 5.6), and the standard error for the molar mass parameters was the poorest.

Weight average molar mass of GAb was determined between 861kDa and 960kDa. For GAg, the weight average molar mass was between 535 and 561kDa. For GAs, the range is between 405 and 524kDa, however the lowest value was for 0.3M, which provided poor signal.

The polydispersity for GAb was the highest, at around 1.6, with GAg and GAs having similar values around 1.3 (ignoring GAs0.3).

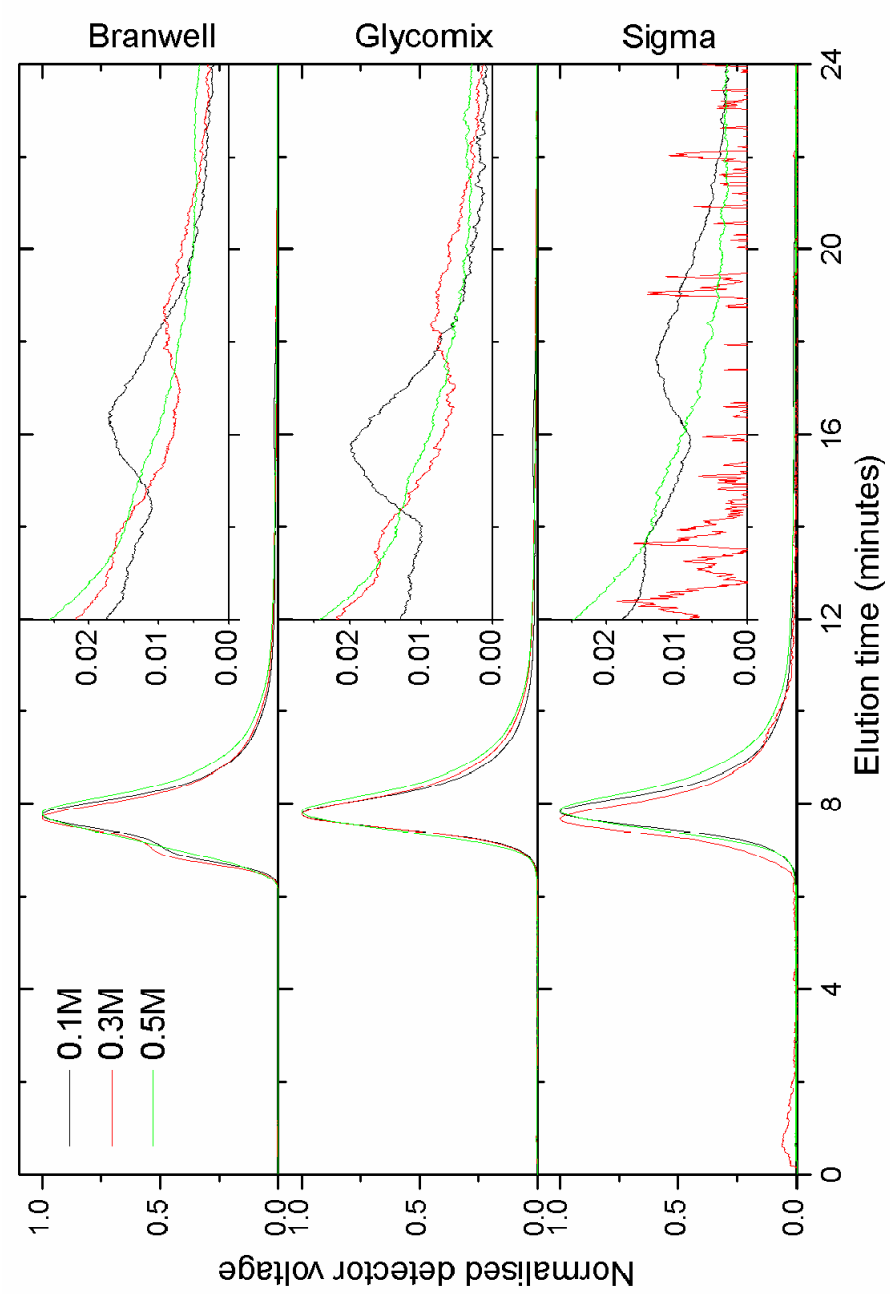

Figure 5.6: Elution plots of gum arabic at different ionic strengths, with normalised scatter signal. Elution from 12-24 minutes is enlarged and shown to the right of the main peak (equal elution axis, expanded detection axis).

Table 5.6: Summary of data yielded from SEC-MALS from three gum arabic samples at three ionic strengths (M). Standard error is shown in parentheses. Results for GAs0.3 have high error due to noisy elution data.

Sample		M_w ($x10^{-5}$ Da)	M_n ($x10^{-5}$ Da)	$M_w/_n$	[η] (ml/g)	r_H ($x10^{7}$ cm)	R_g ($x10^{7}$ cm)
GAb	0.1	9.512 (1.3%)	5.988 (0.8%)	1.588 (1.6%)	31.25 (1.3%)	15.52 (0.6%)	29.1 (3.0%)
	0.3	9.595 (1.4%)	5.763 (0.9%)	1.665 (1.7%)	28.24 (3.4%)	14.96 (0.9%)	28.4 (3.4%)
	0.5	8.609 (1.2%)	5.482 (0.9%)	1.570 (1.5%)	28.41 (2.9%)	14.70 (1.0%)	29.4 (3.1%)
GAg	0.1	5.606 (0.9%)	4.556 (1.2%)	1.231 (1.5%)	27.92 (5.6%)	13.16 (1.8%)	19.9 (7.6%)
	0.3	5.472 (0.8%)	4.210 (1.1%)	1.300 (1.4%)	25.12 (5.4%)	12.58 (1.9%)	18.4 (8.5%)
	0.5	5.355 (0.8%)	4.240 (1.0%)	1.263 (1.3%)	25.13 (17%)	12.52 (5.1%)	19.3 (7.0%)
GAs	0.1	5.235 (0.8%)	4.231 (0.9%)	1.237 (1.2%)	26.84 (1.5%)	12.68 (0.6%)	20.6 (6.1%)
	0.3	4.053 (4.8%)	1.750 (31%)	2.316 (32%)	14.91 (128%)	9.11 (44%)	19.4 (106%)
	0.5	5.133 (0.7%)	4.014 (0.7%)	1.279 (1.0%)	25.08 (11%)	12.31 (3.8%)	18.7 (5.8%)

The intrinsic viscosity obtained through the online pressure imbalance viscometer shows that for GAb, the value ranged between 28.2 and 31.3ml/g. For GAg, this range is lower, between 25.1 and 27.9ml/g. GAs is similar, between 25.08 and 26.84ml/g. All three GA samples consistently show a reduction in intrinsic viscosity with an increase in ionic strength from 0.1M to 0.3M and above. Compared to the results from capillary viscometry (Table 5.3), the values from SEC-MALS were consistently higher, and show more of a trend in ionic strength.

The hydrated radius was calculated as a function of intrinsic viscosity and weight average molar mass. Values for GAb were between 14.7-15.5nm, GAg were between 12.5-13.2nm and GAs between 12.3-12.6nm (excluding anomalous result for 0.3M ionic strength). This is consistent with both the molar mass and intrinsic viscosity measurements that the GAb is the largest sample, and GAg and GAs are equivalent in size. The DLS results yielded lower hydrated radii by a factor of ~1.5, but are consistent with SEC-MALS in that GAb is the largest, with GAg and GAs being equivalent in size. Although the hydrated radius increased with ionic strength, the change is not significant taking into account the standard error. This is especially appropriate considering the intrinsic viscosity and molar mass results do not follow the same pattern.

Radius of gyration was calculated through the angle dependence of scattered light. Values ranged between 28 and 29.5nm (GAb), 18-20nm (GAg), 18.5-20.5nm (GAs). These values are consistent with the hydrated radius values in that they are similar in range; however this hydrodynamic parameter is not reliable for light scattering from smaller macromolecules (Harding and Jumel, 1998). The wavelength of light used by the Dawn Helios was 658nm, with an approximate law that the cut-off for reliable radii of gyration being $\lambda/20$ due to the effect of Rayleigh scattering and the

reliability of the measurement of angular dependence (see for example van Holde et al. (2006)). In this case, the cut-off should be ~33nm. These values are therefore at the borderline of what could be considered valid for this method, as is indicated by the standard error increasing with smaller radii of gyration.

5.3.7 Molar mass from the Sedimentation coefficient

It is possible to estimate molar mass from combinations of sedimentation coefficient and diffusion coefficient, and from sedimentation coefficient and Gralén coefficient (k_s). Both methods involve approximations, as discussed below. The feasibility of these methods was investigated by a comparison with SEC-MALS.

5.3.7.1 Sedimentation and Diffusion

Using the Svedberg equation (2.24), the molar mass can be derived from the sedimentation coefficient, the diffusion coefficient and the buoyancy factor. Diffusion coefficients (translational) were obtained through DLS and were uncorrected for rotational effects based on an assumption of low-asymmetry. Combining data obtained above, the molar mass was calculated and is presented in Table 5.7.

5.3.7.2 Sedimentation and concentration dependence

Molar mass (M) can be estimated through the combination of data from sedimentation velocity data. This method requires an assumption on the hydration (δ) of gum arabic, hence a value of 4g/g (Phillips et al., 1996) was used to calculate the V_s (swollen specific volume) term in Equation (5.1). Recent research has suggested that the hydration term is between 4.4-8.9g/g (Masuelli, 2013) depending on the temperature of the solution, however 4g/g was used as a more conservative estimate. Equation (5.2)

used the swollen volume and other sedimentation data to provide an estimate for the weight average molar mass. Results of this calculation are presented in Table 5.7.

Although one parameter (hydration) required an estimation, the effect of the error due to this estimation of molar mass will be reduced, as the hydration parameter is part of a square root term (Rowe, 1992).

$$\delta = \rho_0(V_s - \overline{v}) \quad \textbf{(5.1)}$$

$$M = N_A\left(\frac{6\pi\eta_0 s^0}{(1-\overline{v}\rho_0)}\right)^{3/2}\left(\frac{3\overline{v}}{4\pi}\left(\frac{k_s}{2\overline{v}}-\frac{V_s}{\overline{v}}\right)\right)^{1/2} \quad \textbf{(5.2)}$$

Table 5.7: Comparison of approximate molar mass determination estimated from sedimentation velocity and dynamic light scattering with molar mass from SEC-MALS. Standard error is shown in parentheses.

Sample		$M_{s,D}$ (Da x10^{-5})	$M_{s,ks}$ (Da x10^{-5})	M_{MALS} (Da x10^{-5})
GAb	0.1	3.2	5.2	9.51 (1.3%)
	0.3	N/D	7.4	9.60 (1.4%)
	0.5	N/D	7.8	8.61 (1.2%)
GAg	0.1	3.1	5.4	5.61 (0.9%)
	0.3	N/D	6.7	5.47 (0.8%)
	0.5	N/D	8.1	5.36 (0.8%)
GAs	0.1	2.8	6.1	5.24 (0.8%)
	0.3	N/D	5.9	4.05 (4.8%)
	0.5	N/D	6.6	5.13 (0.7%)

The MALS data shows good agreement within the sample set, with limited effect of ionic strength. Equally the concentration dependence calculation shows agreement within each sample set, although these figures rise with ionic strength. This could be due to errors in density and partial specific volume measurement.

To compare the molar mass obtained through sedimentation methods, the sedimentation-diffusion calculation provided a rough estimation of the weight average molar masses, within the same $x10^5$ Daltons, but underestimated by a factor of either 2 or 3 compared to determination by SEC-MALS. The difference may be due to breakdown in the hydration or asymmetry assumptions in Diffusion coefficient determination. Concentration dependence and sedimentation coefficients provided much closer estimates to SEC-MALS, slightly underestimating for GAb and overestimating for GAg and GAs. Small differences may be accounted for by experimental error in measurement.

5.3.8 Conformational analysis

5.3.8.1 Hydrodynamic radius (r_h) and radius of gyration (R_g)

The ratio of R_g and r_h provides information on macromolecular conformation. Equation (5.3) shows the relationship between these two parameters for a perfect sphere (see for example Van Holde et al. (2006)). As the conformation becomes more extended, the ratio increases.

$$\frac{R_g}{r_h} = \sqrt{\frac{3}{5}} \qquad \textbf{(5.3)}$$

Data from Table 5.6 show the R_g data from SEC-MALS. A conformational analysis was performed using the ratio of gyration/hydration radii, as shown in Table 5.8. For GAb, the ratio is approximately 1.9, GAg approximately 1.5 and GAs approximately 1.6. As mentioned in section 5.3.6, the values for radii of gyration are on the borderline of reliability for this technique, however these values are consistent with Alftrén et al. (2012) who found a value of 1.6 for the ratio for gum arabic of weight

average molar mass 690kDa. Although this value would indicate a random coil/rod conformation (Brewer and Striegel, 2009), this ratio increases with polydispersity, and may represent a more compact random coil (Burchard, 1992, Burchard et al., 1980).

Table 5.8: Ratio of radii of gyration over hydration for gum arabic samples. Standard error is shown in parentheses.

Sample		R_g (nm)	r_h (nm)	R_g/r_h
GAb	0.1	29.1 (3.0%)	15.52 (0.6%)	1.88 (3.1%)
	0.3	28.4 (3.4%)	14.96 (0.9%)	1.90 (3.5%)
	0.5	29.4 (3.1%)	14.70 (1.0%)	2.00 (3.3%)
GAg	0.1	19.9 (7.6%)	13.16 (1.8%)	1.51 (7.8%)
	0.3	18.4 (8.5%)	12.58 (1.9%)	1.46 (8.7%)
	0.5	19.3 (7.0%)	12.52 (5.1%)	1.54 (8.7%)
GAs	0.1	20.6 (6.1%)	12.68 (0.6%)	1.62 (6.1%)
	0.3	19.4 (106%)	9.11 (44%)	2.13 (115%)
	0.5	18.7 (5.8%)	12.31 (3.8%)	1.52 (6.9%)

5.3.8.2 MHKS power law analysis

Data from SEC-MALS were analysed for the comparison of molar mass and intrinsic viscosity. The double logarithmic relationship between the two hydrodynamic parameters is used as a measure of the conformation of the macromolecule. Figure 5.7 shows the plots for all nine samples, whilst regression data is summarised in Table 5.9. Data were cleared of significant amounts of noise, and reduced to an appropriate range of molar mass, as predicted from Table 5.6.

The GAs0.3 sample shows little correlation between molar mass and intrinsic viscosity especially in context of other samples with positive slopes. This is accounted for by the poor signal obtained from the elution signal. Equally, very little data was obtained from GAg0.1, so although the r^2 shows a very good fit, there are only 10 data points to analyse, whist the others have over 50. This is also observed from the very low constant obtained from the intercept with 0 molar mass.

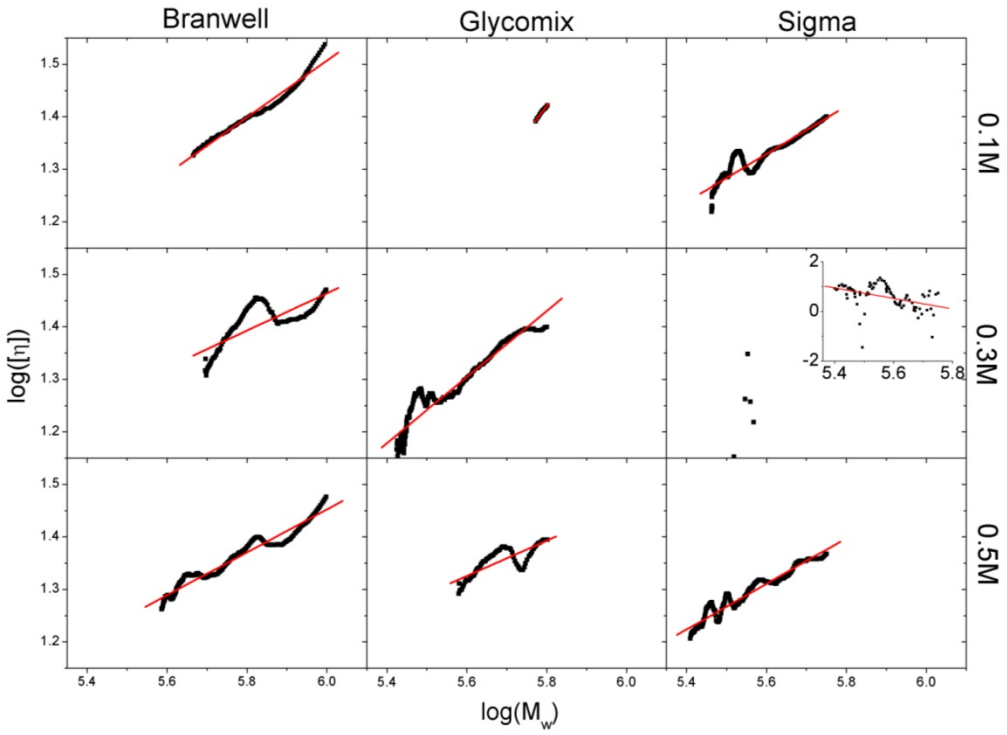

Figure 5.7: MHKS power law plots for gum arabic. GAs0.3 inset represents the full, anomalous dataset.

Apart from these two datasets, the standard error of the fitted slope is generally very good, being <10%. The intercept consistently had poor error due to the reverse logarithm required to obtain the constant, but this is consistent with other findings (Gillis et al., 2013b) and does not greatly affect the reliability of the gradient as the main conformational probe.

There appeared to be no reliable trend for the shape factor and the ionic strength, thus the slopes were averaged and presented in Table 5.9. Average values between 0.43 and 0.48 represent a conformation between a compact sphere (≈0) and a random coil (≈0.5-0.8), although closer to random coil.

The values obtained through SEC-MALS are consistent with those found in other gum arabic GPC studies in similar conditions, such as Renard et al.

who found a=0.45 (2014) and 0.35 (2012), Sanchez et al. (2008) found 0.46 and Idris et al. (1998) found a=0.47.

Table 5.9: MHKS power law parameters for gum arabic. Standard error is shown in parentheses. *Not considered for the average.

Sample		r^2	k'	a	$\bar{a}$
GAb	0.1	0.97	0.019 (>100%)	0.540 (1.7%)	0.434
	0.3	0.60	0.218 (83%)	0.354 (8.8%)	
	0.5	0.95	0.100 (43%)	0.409 (1.7%)	
GAg	0.1	0.99	4.45×10^{-5} (>100%)	0.995* (3.8%)	0.483
	0.3	0.89	0.006 (>100%)	0.629 (2.3%)	
	0.5	0.65	0.275 (62%)	0.337 (8.9%)	
GAs	0.1	0.86	0.060 (>100%)	0.456 (3.1%)	0.446
	0.3	0.17	2.31×10^{12} (<0.01%)	-2.11* (25%)	
	0.5	0.93	0.075 (67%)	0.435 (2.1%)	

5.3.8.3 Ellipsoid modelling

Data from sedimentation velocity and SEC-MALS were used to determine the molecular dimension and axial ratio of the gum arabic samples using SingleHydFit v3 (Ortega and García de la Torre, 2007). An assumption of 4g/g hydration was made to yield a hydrodynamic volume, as used for Equation (5.2). The axial ratios yielded from the fit fell below 1, which represent an oblate ellipsoid structure. The graphical output from SingleHydFit, transformed in terms of classical axial ratios (reciprocal of HydFit output) in Figure 5.8. A summary of the fitted parameters are shown in Table 5.10 including estimations for the error of the model.

Table 5.10: Summary of dimensional analysis from SingleHydFit for gum arabic at various ionic strengths. Standard error shown in parentheses.

		d (nm)	Axial ratio	Oblate axial ratio	Model Standard Error (%)
GAb	0.1	2.1 (0.1)	0.07 (0.01)	14	19.6
	0.3	2.4 (0.2)	0.09 (0.01)	11	13.2
	0.5	2.7 (0.2)	0.11 (0.01)	9.1	4.9
GAg	0.1	2.3 (0.1)	0.11 (0.01)	9.1	7.7
	0.3	3.0 (0.1)	0.17 (0.01)	5.9	0.3
	0.5	3.8 (0.3)	0.25 (0.03)	4.0	6.6
GAs	0.1	2.8 (0.2)	0.15 (0.01)	6.7	0.0
	0.3	-	-	-	-
	0.5	3.2 (0.3)	0.20 (0.02)	5.0	3.3
Average	-	2.8	0.14	8.1	-

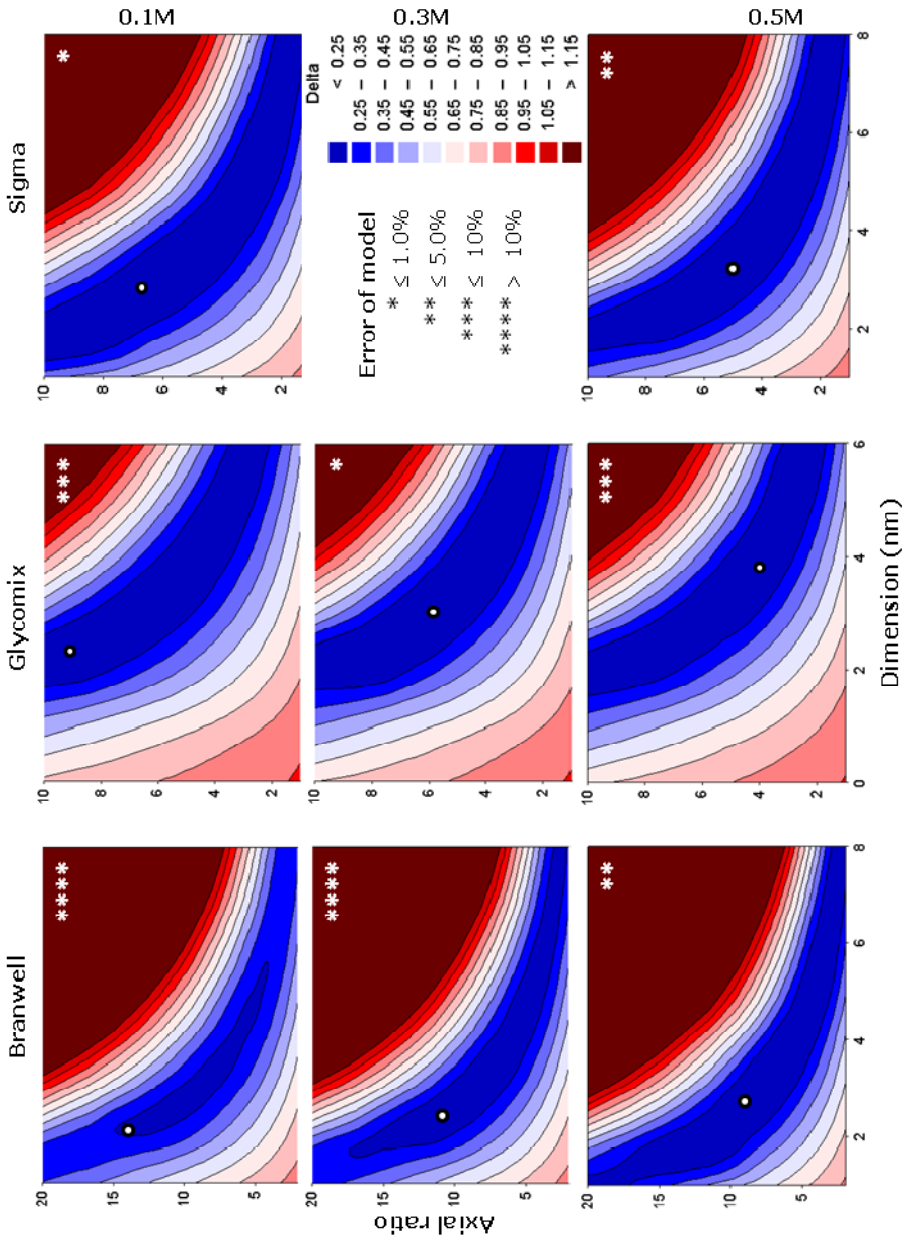

Figure 5.8 SingleHydFit output contour plots of gum arabic (left to right: Branwell, Glycomix and Sigma; top to bottom: 0.1M, 0.3M and 0.5M ionic strength). No results obtained for Sigma 0.3M.

From this data, an ellipsoid was modelled using the program ELLIPS (Harding et al., 1997), specifically the ELLIPSDRAW module. These are depicted in Figure 5.9. These estimates are similar to structures represented by Sanchez et al. (2008) produced by the DAMMIN model. This group published expected values of hydrodynamic properties based on this model, including a sedimentation coefficient of 0.24S. They were not able to verify this value experimentally and it is appreciably different to results obtained in this investigation.

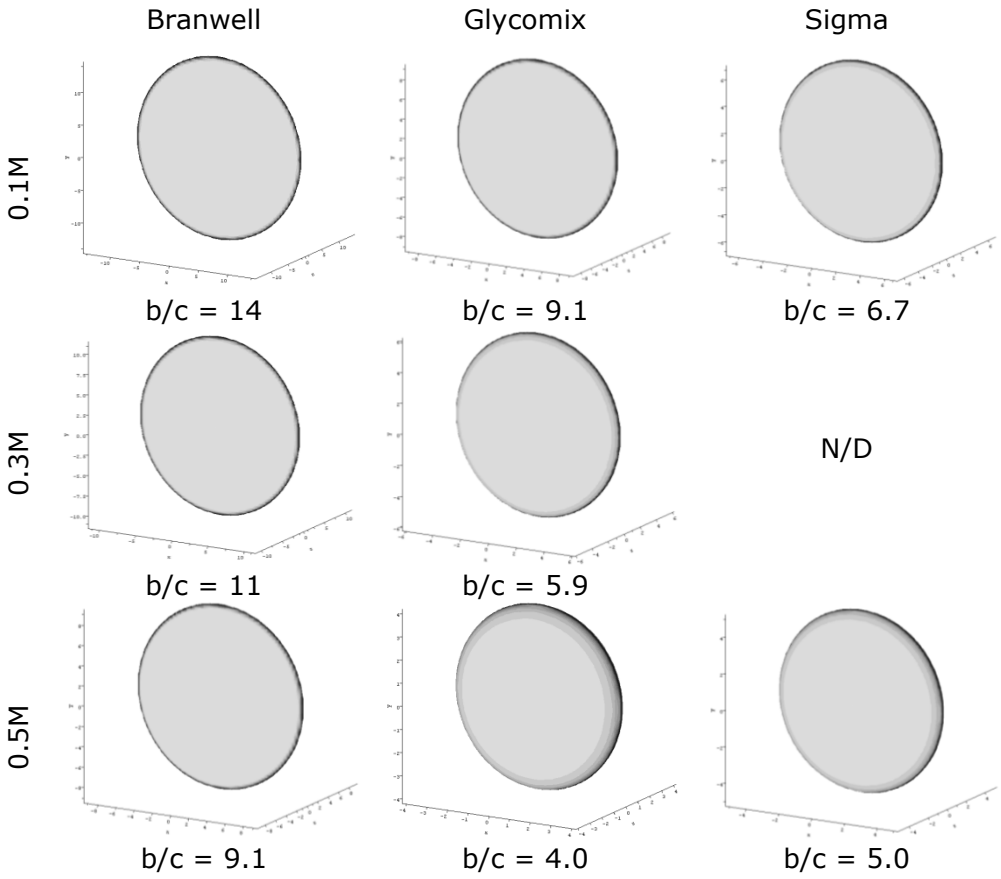

Figure 5.9: Oblate ellipsoid models of the gum arabic samples as predicted by HydFit and modelled by ELLIPS.

The data for GAb 0.1 and 0.3M have high percentage errors which appear to have led to a higher-than-average axial ratio. The 0.5M result has a better standard error of <5%.

A trend can be seen that the increase in ionic strength consistently decreased the axial ratio and increased the dimension. Although this cannot be confirmed definitively with statistical analysis, this trend is consistent for all three samples.

Taking an average of the complete dataset leaves a dimension of 2.8nm and an axial ratio of 8.1. If the two 'outliers' of GAb01,03 are taken out of the average, the axial ratio is 6.63, which is most similar to GAs01, which gave a value for standard error of less than 0.05%. It could therefore be concluded that the most likely oblate structure for gum arabic is represented in Figure 5.9 as Sigma 0.1M. However, what is more likely is a distribution of axial ratio/dimension as seen from the bluest contours in Figure 5.8. For example, the Branwell samples showed a higher axial ratio than the other samples, possibly because of the higher weight average molar mass. What this would suggest is an arrangement that the polysaccharide collapses in on itself as the charge density builds. Increasing the ionic strength suppresses these charges and the macromolecule relaxes into a slightly more spherical shape.

5.4 Conclusions

Gum arabic is a commercially important non-dietary fibre with a wide range of applications. Three sources were characterised using complementary hydrodynamic techniques including AUC (sedimentation velocity), SEC-MALS, DLS, viscometry and density measurement. Light scattering techniques yielded similar results found in previous research. Compiled results obtained through these hydrodynamic techniques were able to yield an estimate for the ellipsoid structure of gum arabic using SingleHydFit, in the form of an oblate ellipsoid with an average axial ratio of 8.1. The ionic

strength range in this investigation appeared to make the macromolecule reduce in axial ratio with increased ionic strength, although with most hydrodynamic properties this difference was not observed. The MHKS plot corroborated the observations made from SingleHydFit that the macromolecule has a conformation between a sphere and a random coil ($a \approx 0.45$). Data from capillary viscometry, specifically the Huggins constant, yielded values of approximately 0.8, which if the assumption is made of a conformation between sphere and random coil is consistent with being in good solvent conditions for all three ionic strengths. The R_g/r_h parameter, although unreliable due to limitations of the wavelength of light used and the general rule that the size of the particles should be greater than $\lambda/20$ for reliable estimates of R_g (Van Holde et al., 2006), produced a ratio of approximately 1.6. This value is in agreement with the literature and suggests a polydisperse, branched or star-shaped, tightly-bound coil.

6 Gliadin interactions with non-digestible polysaccharides

6.1 Introduction

6.1.1 Gliadins

Gluten occurs naturally as a storage protein in wheat, barley and rye, between 7-20% of the endosperm, and is an important component in bread, pasta and many other products prevalent in a western diet. Gliadins are the ethanol-soluble component of gluten. It was previously thought that gliadins consisted of four types: α, β, γ and ω (Woychik et al., 1961) based on results from electrophoretic mobility as shown in Figure 6.2. The range observed in Figure 6.2 shows bands of protein suggested to be α, β, and γ fractions, however it is now known that α and β are actually different sub-fractions of the same type. From genetic sequencing, α and β types are structurally similar with molar mass ranging between 30-34kDa (Ang et al., 2010). γ-gliadins appear to range between 26-36kDa and ω-type range between 50-60kDa. Prolate ellipsoid models for α, γ, ω_{fast} and ω_{slow}, based on axial ratio obtained from hydrodynamic techniques, are shown in Figure 6.1.

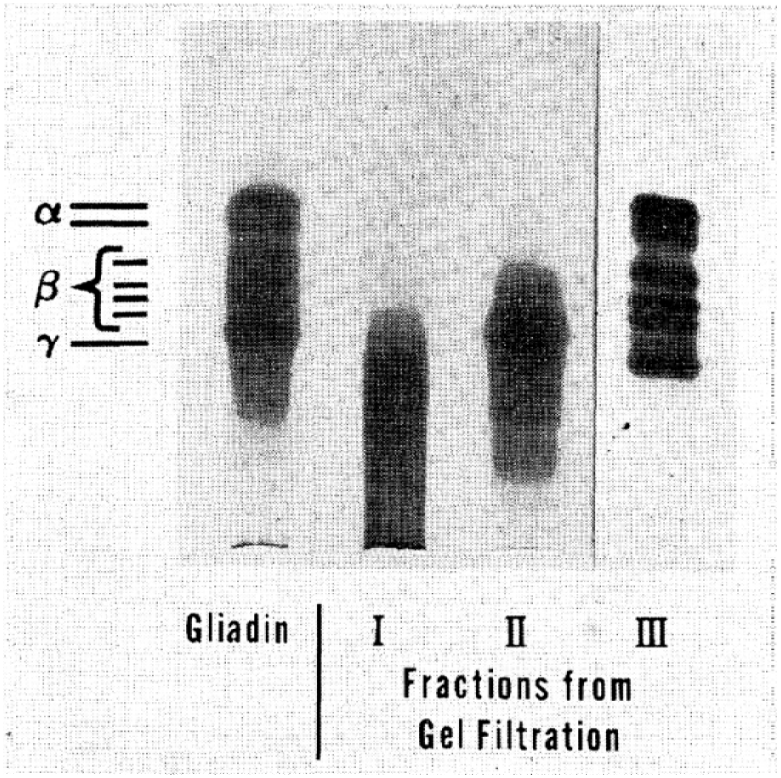

Figure 6.2: Starch gel electrophoresis of whole and fractioned (Sephadex) gliadins. Different groups of gliadins are indicated on the left (Beckwith et al., 1966).

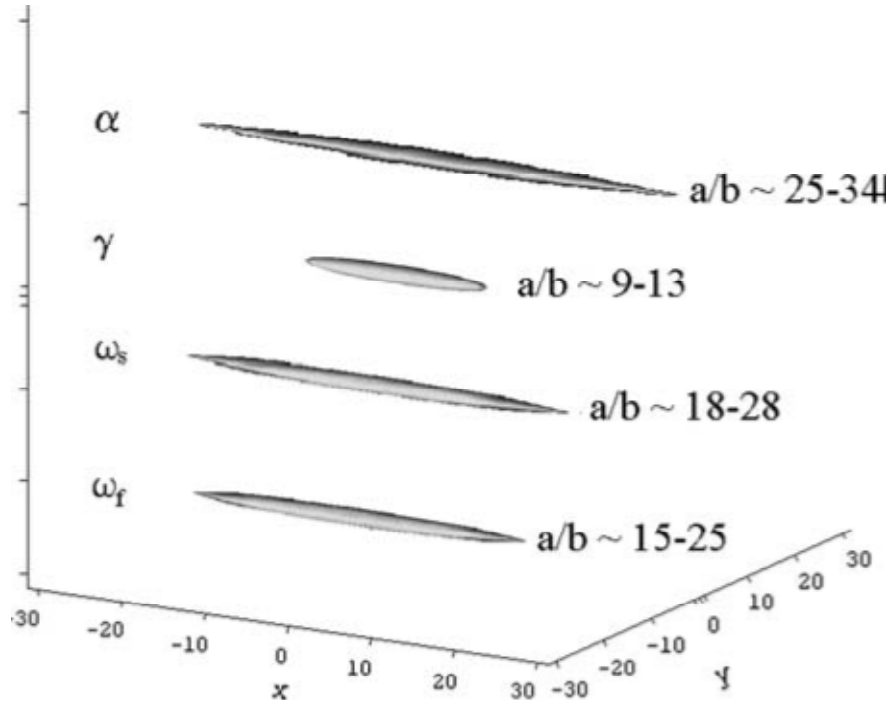

Figure 6.1: The four subtypes of gliadin shown in terms of axial ratio (a/b) obtained through sedimentation velocity (Ang et al., 2010).

6.1.2 Coeliac Disease

Coeliac Disease is an intolerance to gliadin affecting approximately 1% of the population of England and North America (West et al., 2003, Katz et al., 2011). The disease is twice as common in women as in men, but it is not known why (Green and Cellier, 2007). It has been reported that Coeliac Disease is linked with Diabetes Mellitus. It is suggested that there is a genetic link, since prevalence of Coeliac Disease in diabetic patients is 5-7 times higher than healthy patients (Szaflarska-Popławska, 2014).

Coeliac patients express the Human Leukocyte Antigen (HLA)-DQ2 (95% of patients) or –DQ8 (5%) (Wieser et al., 2012) on the intestinal epithelia (CACO-2 cells) that interacts with specific sequences of digested gliadin and causes the inflammatory response. Symptoms of Coeliac Disease are mostly abdominal pain, however can be asymptomatic (Alaedini and Green, 2005).

The biological process of Coeliac Disease is represented in Figure 6.3 (Green and Cellier, 2007). Partially digested gliadin is deamidated by transglutaminase, which happens in both healthy and Coeliac patients. Deamidated gliadin is treated as an antigen and presented to the CD4 T cell. Cytokines released from T cells cause inflammation and the destruction of epithelial villi. B cells are also activated to produce antibodies against gliadins and the body's own transglutaminase proteins, which is often used as a diagnostic tool (Nadeem, 2013).

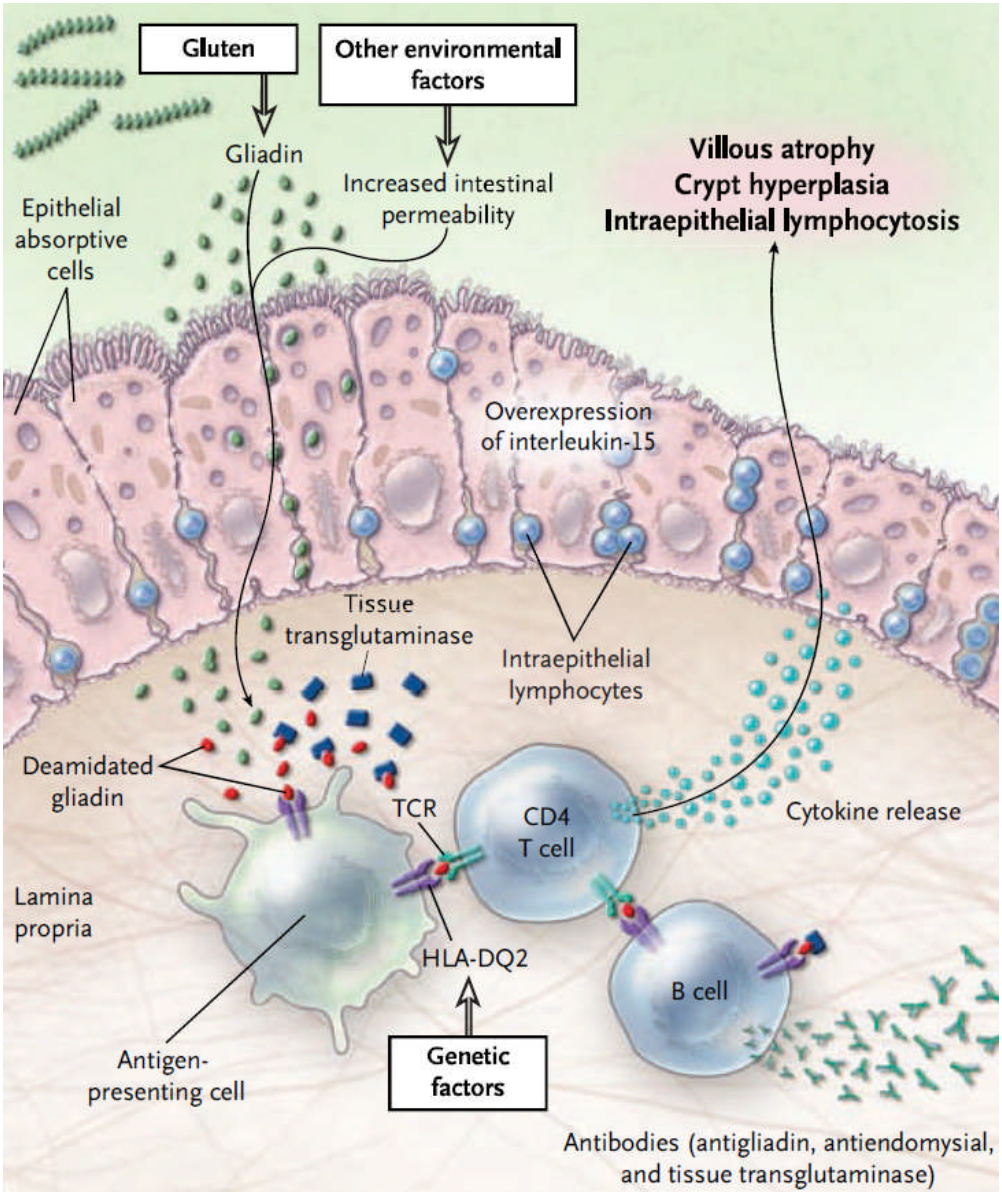

Figure 6.3: Diagram summarising the reaction of a Coeliac immune system in the presence of gliadin (Green and Cellier, 2007).

Figure 6.4 shows an example of epithelial tissue in the duodenum damaged by the autoimmune response compared to a healthy individual (Green and Cellier, 2007). The reduced surface area of the villi, due to the constant destruction and scarring of the epithelium, can clearly be seen in the Coeliac histology.

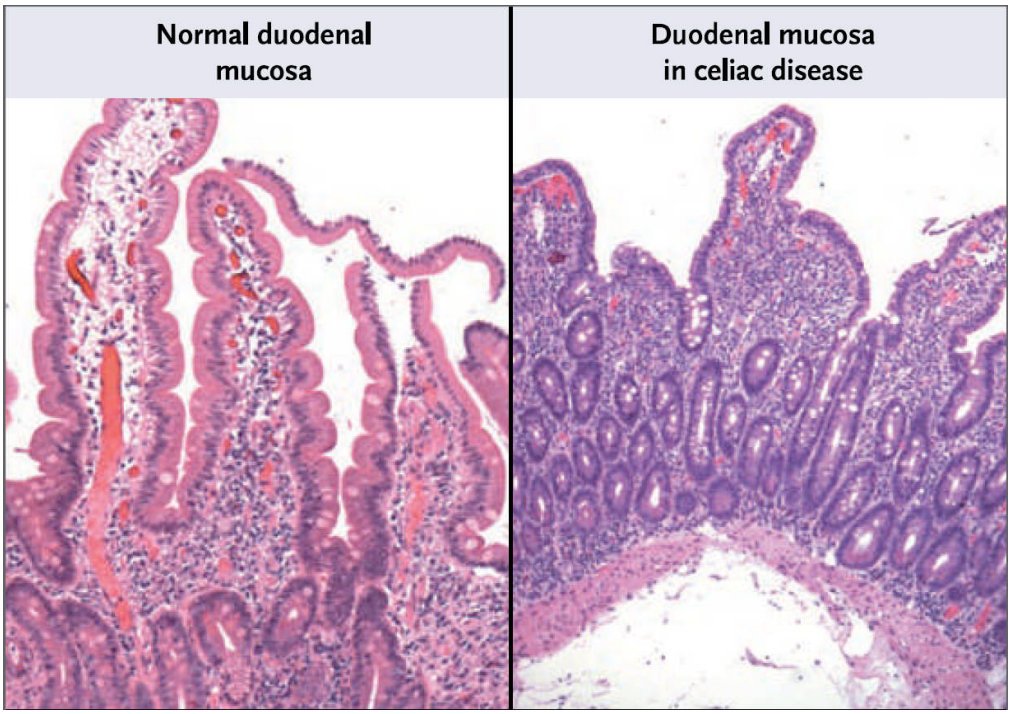

Figure 6.4: Histological micrographs of healthy (left) and Coeliac (right) duodenum (Green and Cellier, 2007).

6.1.3 Treatment

At present, there is no cure for Coeliac Disease. Patients have very limited options in terms of maintaining a healthy lifestyle. The principal method is to avoid eating gluten-containing products, commonly referred to as the Gluten Free Diet (GFD). This provides a challenge to maintain since gluten is prevalent in many foods in a western diet and is often an active and critical component of food structure (Ryan and Grossman, 2011).

Alternative treatment methods include ingestion of proteolytic enzymes (to aid digestion of immunogenic gliadin peptides) or inhibiting key pathway proteins in the small intestine (tissue transglutaminase, HLA-DQ, leukocyte adhesion inhibitors) however these therapies can yield side effects (Sollid and Khosla, 2005, Schuppan et al., 2009). There has been research into the protective benefits of breastfeeding on Coeliac patients, however

mechanism and long-term benefits are still under debate (Szajewska et al., 2012, Pozo-Rubio et al., 2013).

If the patient does not comply with GFD, damage to the epithelium, due to the intake of gluten, causes nutritional malabsorption. If the patient does choose to adhere to GFD their dietary choice is significantly reduced and nutritional deficiencies may arise due to a lack of variety. These deficiencies can include vitamin $B_{6,12}$, vitamin D, vitamin K (Wierdsma et al., 2013, Mager et al., 2012) and iron (Kavimandan et al., 2014). This variety problem is a common reason for non-adherence. Another problem is sociological effects of younger age-groups and social/emotional factors (Sainsbury et al., 2012, Olsson et al., 2008) i.e. not wanting to 'stand out' as someone with dietary needs.

Coeliac Disease has been associated with type I diabetes, low bone density, osteoporosis (Mager et al., 2012), Down's syndrome, Turner's syndrome, Williams syndrome, auto-immune thyroid disease, (Newton and Singer, 2012) infertility (Sebastian Lasa et al., 2014) and a possible genetic link with Primary Lactase Deficiency (Basso et al., 2012).

The UK Food Standards Agency (FSA) have recognised the necessity of gluten labelling for Coeliac patients and have put in place legislation to control the advertisement of 'very low gluten (<100ppm)' and 'gluten-free (<20ppm)' foods, (FSA, 2011). The US Food and Drug Administration (FDA) use the same measure of <20ppm for allowing the use of 'gluten-free' and similar labels (FDA, 2013).

Efforts have been made to reproduce the plasticising effect of gluten using other biopolymers (Hager et al., 2012, Gallagher et al., 2004, Sanchez et al., 2002). These food products are marketed as part of 'gluten free' ranges. When heated, gluten polymerises into a network that keeps the

structure in foods. This effect can sometimes be imitated by polysaccharide additives such as xanthan gum. There are sometimes issues with matching the quality of the original product, although research is still ongoing.

6.1.4 Macromolecular barriers

This investigation looks at the interaction between gliadin and non-digestible fibres, as macromolecular barriers, for the potential treatment of gluten intolerance/Coeliac Disease. Recent research has shown promising results in binding gliadins with polymers to reduce inflammatory response. Work by Liang et al. (2009) has shown a link between polymers with sulphonated groups with whole α-gliadin *in vitro*. The study used Circular Dichroism, Fourier Transform Infrared Spectroscopy (FT/IR), Turbidity, Steady State Fluorescence and Dynamic Light Scattering (DLS) to assay the interaction. Their copolymer, hydroxyethyl methacrylate (HEMA) and sodium 4-styrene sulphonate (SS), was incubated with gliadins for 2-3 hours at room temperature and showed a conformational change of gliadin at pH 1.2 and 6.8.

The same group later released a paper (Liang et al., 2010) with similar work on polymers of only SS and random copolymers previously described from Liang et al. (2009). Zeta potential was also measured, confirming the binding of the polymers to gliadins. The study showed that binding affinity depended on the frequency of the SS groups on the polymer and that there was an optimum concentration of SS in the polymer which allowed binding (29% SS as reported). It was therefore concluded that a polyanionic chain was required for effective binding to α-gliadin.

The same research group showed *in situ* that pHEMA-co-SS helped to reduce the immune response on CACO-2 cells from humans (Pinier et al.,

2009). Pinier et al. (2012) then showed that the same model worked *in vivo* with murine HLA-HCD4/DQ8.

The INSERM research group (France) has looked into interactions between gliadin and gum arabic (GA) (Ducel et al., 2008, Ducel et al., 2005b, Ducel et al., 2004b, Ducel et al., 2005a, Ducel et al., 2004a, Chourpa et al., 2006). The interaction was verified using different methods: NMR, Light Scattering (MALS, DLS), Turbidity and Zeta Potential as well as Light microscopy to view the micelle formations. The study focussed on the use of the complex as an oil droplet stabiliser and not necessarily on the mechanism of the interaction between the two macromolecules. It was suggested that gliadin, as for most proteins, is a foam and emulsion stabiliser and used GA to yield larger complexes. Nevertheless, the GA-gliadin complex could be a potential candidate for the treatment of gluten intolerance.

The same research group also suggested that sodium alginate, pectin and carboxymethylcellulose bind to gliadins. Mohsen et al. (2010) concurred that these three polysaccharides may bind to gliadins, although their findings were in relation to bread quality.

Elofsson et al. (2000) reported an interaction between arabinogalactan and gliadin. The arabinogalactan in their investigation was very similar to GA, including the ~10% protein content. An interaction of arabinoxylan with gliadin has also been reported in the same research group.

Results from a polysaccharide interaction study with gluten (Linlaud et al., 2011) agreed with the previous findings. This study was also in relation to bread quality, since it took into account the presence of starch. The focus of this study was on the availability and movement of water within the dough using Differential Scanning Calorimetry and Raman assay.

In addition, studies were conducted on mixtures between gliadin and methyl cellulose (Song et al., 2010). With a very concentrated mixture of gliadin in 70% (v/v) ethanol and methyl cellulose, the rheological properties of the solution significantly changed. Gliadins reduced the pseudoplastic effect of methyl cellulose. The reported explanation for this interaction was the glutamine residues hydrogen-bonding with modified cellulose. Song et al. (2010) did not conduct the interaction in physiological conditions, therefore it is possible that reduced ethanol content would reduce incidents of interaction.

Interactions between starch/dextrin and gliadin were studied using ATR-FT/IR (Guerrieri et al., 2004, Secundo and Guerrieri, 2005). The study does show interactions between the macromolecules, however this combination is inappropriate for this study since the presence of both macromolecules are already in wheat products and would therefore not hide the gliadin from the immune system. This investigation is also about the use of non-digestible fibres and, since starch is digestible in human physiology, the polysaccharide may not reach the duodenum intact.

The National Centre for Macromolecular Hydrodynamics, Nottingham UK, has been actively researching gliadin interactions since 1995 (Adams et al., 2012b, Kök et al., 2012, Ang, 2009, Seifert et al., 1995). Seifert et al. (1995) described an interaction between locust bean gum (LBG) and both whole and pepsin-trypsin digested gliadins (PTDG). Components of the interaction were all dissolved in PBS pH 6.5. The LBG dissolved at 80^{o}C but the intact gliadin proved difficult to hydrate. The mixtures were incubated for three hours at 37^{o}C, however all experiments were performed at 20^{o}C. Results showed that LBG bound to both the whole and PTDG. Their sedimentation velocity experiments were observed using Schlieren optics, which only showed one boundary as it sedimented away from the

meniscus. This paper also suggested it was galactomannan, as a group of polysaccharides, which interacted with gliadin. This investigation aims to use the same sedimentation velocity technique, although different optical systems, to verify these findings.

6.2 Materials and Methods

6.2.1 Gliadin

Gliadin preparation was performed by Arthur Tatham and colleagues at Cardiff Metropolitan University. White wheat flour (*Triticum aestivum* cv. Chinese Spring) was defatted with chloroform (twice, 10:1 (v/w), solvent:flour), filtered and air-dried. Non-prolamins were extracted by stirring with 0.5M NaCl (twice, 10:1 (v/w), solvent:flour) at room temperature for 2 hours. After centrifugation the supernatant was discarded and the flour washed twice with deionised water to remove residual salt. Gliadin was extracted with 70% (v/v) aqueous ethanol (twice, 10:1 (v/w), solvent:flour) for 2 hours at 4^{o}C. Supernatant was dialysed against 1% (v/v) acetic acid and freeze-dried.

Lyophilised gliadin was dissolved into deionised water at an approximate concentration of 5mg/ml. The resulting preparation was a translucent slurry containing undissolved gliadin. This portion was filtered out at 0.45µm to leave a mostly clear solution. The concentration was accurately measured using refractometry (Atago DD-7) with a dn/dc of 0.160ml/g (Robertson and Greaves, 1911).

Samples were dialysed into various buffers, depending on the experimental method (refer to Table 6.1), using 14kDa molar mass cut-off (BioDesignDialysis Tubing D006, Fisher Scientific, UK).

6.2.2 Polysaccharides

6.2.2.1 Locust bean gum

Locust bean gum, for which the structure is shown in Figure 6.5, was prepared by heating a solution to 80°C for 30 minutes and lyophilising the product. The sample was dissolved in deionised water at an approximate concentration of 5mg/ml. An accurate concentration was measured using refractometry and a dn/dc of 0.150ml/g (Kapoor et al., 1994).

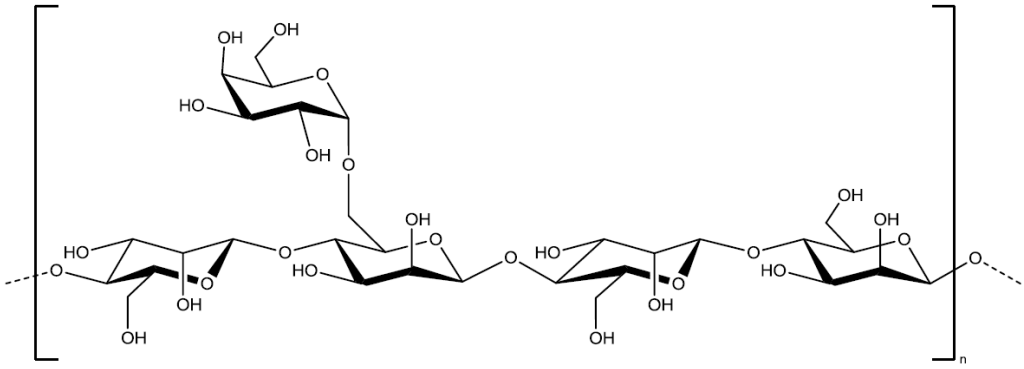

Figure 6.5: Repeating structure of locust bean gum galactomannan (Winkworth-Smith and Foster, 2013).

6.2.2.2 Gum arabic

Gum arabic (see Chapter 5) has a backbone structure of poly β (1→3) D-galactan. Branches contain many arabinofuranose and rhamnopyranose residues and often terminate with glucuronic acid. These polysaccharides are branches which make up ~90% of the overall complex. There is a protein core which covalently links polysaccharide chains to the serine and hydroxyproline residues (Funami et al., 2008, Nie et al., 2013b). The result appears to be a high-molar mass and very compact glycoprotein.

GA from Glycomix (analytical grade), was dissolved in deionised water at approximately 5mg/ml. Depending on further experimental design, samples were either dialysed in appropriate buffer or used directly in the

experiments. Concentration was checked using refractometry and a dn/dc of 0.145ml/g (Huglin et al., 1989).

6.2.3 Qualitative interaction study

Experiments were performed according to the original method from Seifert et al. (1995). The mixture samples were incubated at 37°C for 3 hours. The samples in the original study were dissolved in Phosphate Buffered Saline (PBS), however, in an attempt to induce stronger macromolecular interactions, deionised water was used. Mixtures were assessed using sedimentation velocity methods with both UV absorbance (280nm) and Rayleigh Interference optics. Scans were analysed using ls-g*(s) in SEDFIT.

6.2.4 Quantitative interaction study under ideal conditions

The proportion of polysaccharide to gliadin in deionised water was assessed using sedimentation velocity and ls-g*(s) analysis. Peaks were integrated to find concentrations of unbound polysaccharide, unbound gliadin and bound complex. This yielded an interaction index (percentage of gliadin removed from system). The samples were centrifuged at 50k RPM and scanned with interference optics, approximately one hour after being mixed and kept at room temperature.

6.2.5 Interaction under physiological conditions

Introduction of physiological conditions allows the analysis of any complexes formed to be put into *in situ* context. Interactions were assayed in the presence of PBS and Gastric Fluid Analogue (GFA). PBS was

prepared as per Table 6.1. All salts were from Sigma Aldrich and were of analytical grade.

Gastric Fluid Analogue was made to a consensus formula from Dare et al. (1972) and Stefaniak et al. (2010), summarised in Table 6.1. Dry powders of sodium, calcium and potassium chlorides (Sigma Aldrich, analytical grades) were weighed and dissolved into 400ml of deionised water. The pH was measured and titrated down to pH 1.5 (17.0^{o}C) with approximately 25ml of 1M hydrochloric acid (Fisher Scientific, analytical grade). The volume was corrected to 500ml with deionised water. The pH did not change significantly upon this dilution.

Table 6.1: Summary of components of aqueous solvents used to assay gliadin interaction studies.

Component	PBS		GFA	
	Molarity (M)	Added (g/L)	Molarity (M)	Added (g/0.5L)
NaCl	0.05	2.9225	0.05	1.4609
$Na_2HPO_4.12H_20$	0.025	4.5951	-	-
KH_2PO_4	0.025	1.5622	-	-
$CaCl_2$	-	-	0.002	0.1117
KCl	-	-	0.01	0.3728
HCl	-	-	0.1	25(ml)
Total molarity	0.1		0.162	
Total ionic strength	0.1		0.174	

6.3 Results and Discussion

6.3.1 Gliadin solubility

Solubility of the gliadin preparation in deionised water was probed using a scanning spectrophotometer, the results of which are shown in Figure 6.6. The plot shows a peak at approximately 280nm which was expected for a protein preparation. The large amount of absorption below 220nm was

also expected as this represents the region where absorption from the solvent takes effect. What was also evident was a tail from 300-400nm. This was attributed to incomplete solubility and the formation of clusters of undissolved gliadin, which scattered the light.

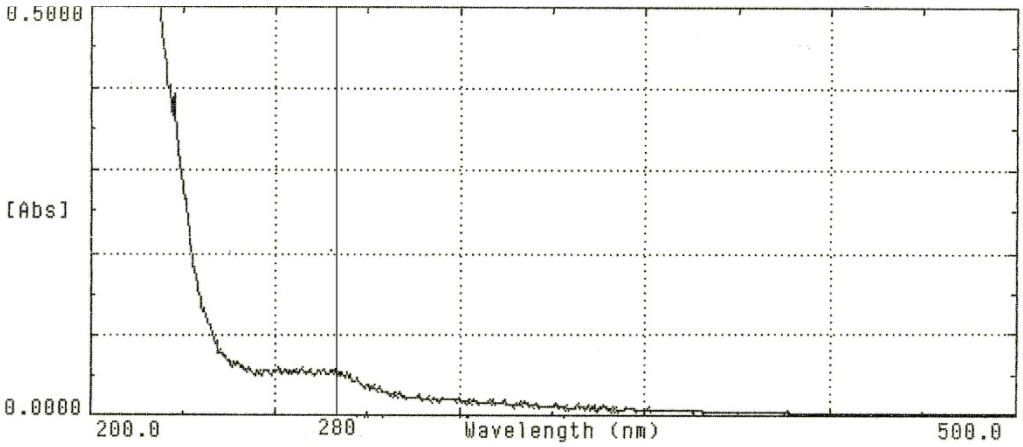

Figure 6.6: Wavelength scan of gliadin preparation, dialysed against distilled water, at an estimated concentration of 0.5mg/ml.

6.3.2 Locust bean gum

6.3.2.1 Qualitative results

Figure 6.7 shows the ls-g*(s) analysis of locust bean gum mixed with native gliadin in deionised water. The concentration of locust bean gum increases from top to bottom plot. The gliadin concentration was kept the same. The gliadin peak (black plot) can be observed at approximately 2S and is typically at a height of 0.5 on the g(s) scale. The locust bean gum (red plot) is the peak between 2 and 8S. As the concentration increased, the sedimentation coefficient of the locust bean gum decreased, as would be expected from typical non-ideal behaviour.

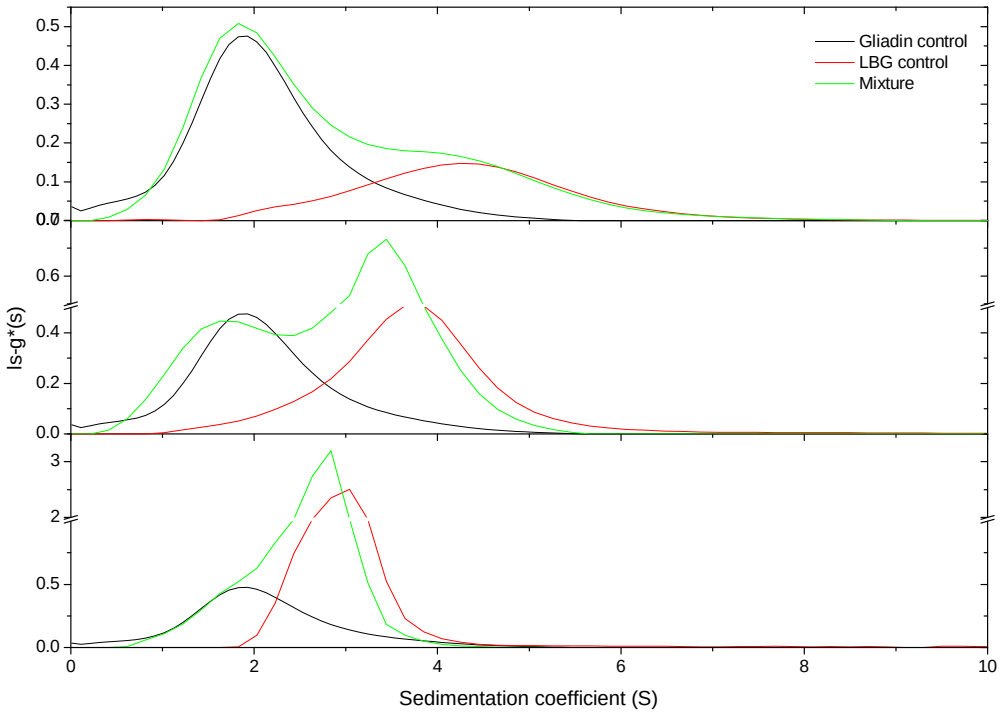

Figure 6.7: Least square Gaussian distribution plot of locust bean gum (LBG) mixed with native gliadin at three ratios in water using interference optics. Top: 2:1 gli:LBG; Middle: 1:1 gli:LBG; Bottom: 1:2 gli:LBG.

The green plot represents a system where both components are present as opposed to the black and red controls. The green plot traces both black and red plots with little deviation along the sedimentation coefficient axis. Because of this, it can be concluded that there is no significant interaction between these two macromolecules in deionised water. This is in contrast with findings presented by Seifert et al. (1995) who used the same technique of sedimentation velocity but with a different optical system (Schlieren optics). Schlieren optics do not provide as high a resolution as Rayleigh Interference thus the details of the individual peaks may have been missed. This is especially true for the bottom plot of Figure 6.7, performed at a mass ratio of 1:2 gliadin:LBG, where the gliadin peak only appears as a shoulder. Seifert et al. also performed their interaction

studies in PBS. Even though interactions are more likely to occur in deionised water than a buffered solution, there were still no indications of interaction in Figure 6.7.

6.3.3 Gum arabic

6.3.3.1 Initial interpretation of results

Figure 6.8 shows initial ls-g*(s) results from the test for interaction between gum arabic and native gliadin in deionised water. The black plot represents the gliadin control and is at approximately 2S. This is similar to what was observed in Figure 6.7, although the sedimentation coefficient axis has been extended to accommodate the gum arabic distribution. The red peak represents the gum arabic control and loading concentration increases from top to bottom plots. The distribution ranges between 2-25S. There is a slight indication of concentration dependence as the peak moves further to the origin as the concentration increases, however this is not as pronounced as per the results from locust bean gum and is consistent with the findings from section 5.3.5.

The green plot represents the mixture between gliadin and gum arabic. The gliadin peak can be observed to be much smaller than the control at the same loading concentration. The size of the peak reduces with increased concentration of gum arabic. Equally, the gum arabic peak is larger and higher in sedimentation coefficient, compared to the control of the same loading concentration. This suggests an increase in mass. These findings show that there is a significant interaction between gliadin and gum arabic under these conditions. This is supportive of evidence found by Ducel et al (2004b).

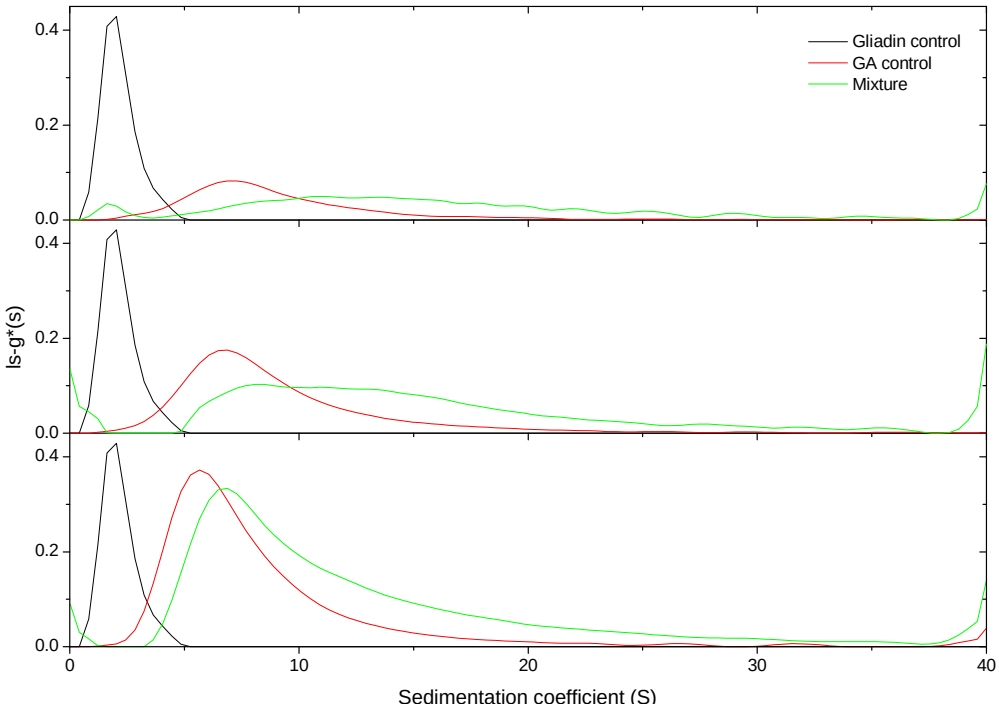

Figure 6.8: Least square Gaussian distribution plot of gum arabic (GA) mixed with native gliadin at three ratios in water using interference optics. Top: 2:1 gli:GA; Middle: 1:1 gli:GA; Bottom: 1:2 gli:GA.

6.3.3.2 Quantitative results

Once the interaction was confirmed, multiple sedimentation velocity experiments were carried out at varying mass ratios to quantify the interaction. This was performed in:

- Deionised water, as per the qualitative study.
- Phosphate buffered saline (PBS), to closer match physiological conditions.
- Gastric fluid analogue (GFA) to replicate the conditions inside the stomach.

A summary of binding index percentage is summarised in Table 6.2. The binding index percentage is a measure of 'free' gliadin removed from the

system: 100% represents complete removal of unbound gliadin, 0% is completely unbound gliadin.

Table 6.2: Percentage of gliadin removed from system in response to the addition of gum arabic. Removal was calculated by division of integrated peak concentration of gliadin with and without gum arabic.

Ratio gli:GA (g/g)	Gliadin binding index (%)		
	dH_2O	PBS	GFA
10	64	N/D	8
9.5	59	15	N/D
9	53	92	24
8.5	N/D	34	N/D
8	64	80	-28
7.5	66	N/D	N/D
7	75	N/D	2
6	80	61	9
5	88	N/D	-12
4	91	N/D	N/D
2	94	N/D	N/D
1	87	N/D	N/D
0.5	97	N/D	N/D

The deionised water results show a general increasing trend of gliadin binding with a decreasing ratio of gliadin to gum arabic. This was expected, since the availability of binding sites on the gum arabic macromolecule would decrease as a higher amount of gliadin was available. This data is presented in Figure 6.9 with a sigmoid fit. It shows that the upper limit is (92±2.3)%, the lower limit is (58±3.5)%, the central point is (6.65±0.35)%, a spread of (0.82±0.32)% with an r^2 (coefficient of determination) of 0.94. Several observations are of interest within this figure. The first is that the results of the lowest concentrations of gliadin still do not reach levels of 100% binding. An argument could be made to introduce an artificial data point so that a ratio of 0w/w gliadin:GA would be 100% removal, however there appears to be a plateau occurring

from 4:1 and smaller. This suggests a form of reversible interaction between gum arabic and gliadin.

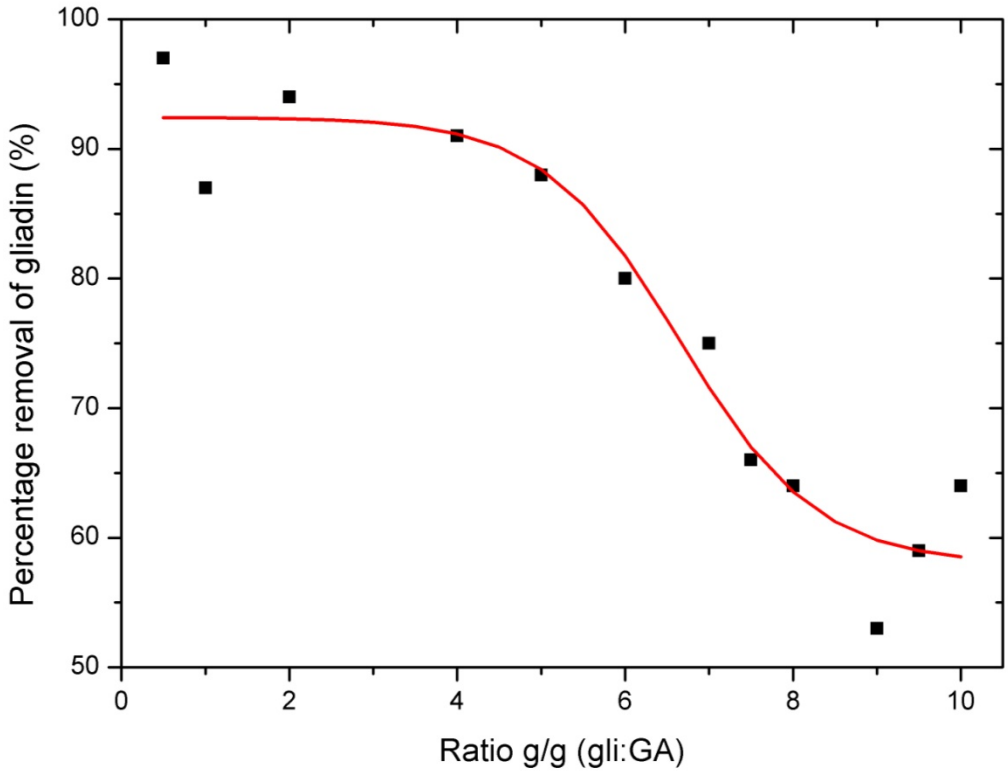

Figure 6.9: Quantitative analysis of the interaction between gum arabic and native gliadin in unbuffered deionised water.

Another point to note is the appearance that the data plateaus from 8:1 ratio onwards. It could be that the data point at 10:1 is an anomaly, thus the fit should continue further towards 0%. Unfortunately further data points would be difficult to obtain, since the limited solubility of gliadin in water would limit the increase in ratio. Equally, a decrease in gum arabic concentration would be difficult to achieve since the optical systems may not be sensitive enough to register the change.

In PBS (0.1M, pH 7), there appears to be some binding with an average of (56±32)% (standard deviation, ±56% change), however does not consistently change with concentration as it does in deionised water. For the GFA conditions (low pH, high salt), there is no trend and averages at

(1±18)% binding (standard deviation, ±3330% change). Consequently, it can be concluded that the interaction between gliadin and gum arabic is completely suppressed under these conditions. The data also suggests that this interaction is ionic due to the suppression of the interaction in high ionic strength and low pH conditions.

Interpretation of the association/dissociation constant and stoichiometry is difficult from this data. It could be posited that the large surface area of the gum arabic molecule, with a M_w of ~550kDa and R_g ~20nm (Chapter 5), would attract more than one molecule of gliadin with a M_w ~25-60kDa (Ang et al., 2010) and R_g ~13nm (Zhao et al., 2012). Although the molar masses differ greatly, the radius of gyration does not. Thus it is possible that the stoichiometry is closer to 1:1.

6.4 Conclusions

The findings from this investigation have ruled out the possibility of an interaction between native gliadin and locust bean gum using sedimentation velocity. The same technique, however, was able to confirm a clear interaction between gliadin and gum arabic. For the purpose of a macromolecular barrier, for the prevention of the Coeliac response, this interaction may not however be suitable. Reasons for this include the incomplete binding of the entire gliadin population, and the complete inhibition of the interaction in the presence of stomach conditions.

7 Digested gliadin interactions with non-digestible polysaccharides

7.1 Introduction

7.1.1 Gliadin-polysaccharide interaction

Coeliac Disease (described in detail in section 6.1.2) is an autoimmune disease, presented as intolerance to gluten. Once chewed, the bolus of food is swallowed and enters the stomach. Here, food undergoes proteolytic hydrolysis by pepsin, an endopeptidase, for approximately 2 hours. The resulting chyme is passed through to the duodenum. Trypsin, an exopeptidase, is introduced to the digestant from the pancreas. It is at this point in the digestive system that the Coeliac response occurs.

According to Shan et al. (2002) it is a 33 amino acid peptide region, in the α-gliadin, which is the major antigen for Coeliac Disease. Caputo et al. (2010) have suggested that there are two significant series of peptides responsible: p31-43 and p57-68. P31-43 triggers the release of IL-15 leading to an immune response from T-cells and p57-68 presents itself as an antigen on HLA.

A group in Rome, Italy, has been working on the protective effects of two polysaccharides in relation to the physical protection of the CACO-2 cells. Silano et al. (2004) found that a modified chitosan was able to reduce the effect that pepsin-trypsin-digested gliadins had on the cells. Vincentini et al. (2005) also suggested mannan as an option for the same treatment.

These studies show potential for the treatment of Coeliac Disease, however they did not report on the mechanism for such an interaction, nor do they take into account the presence of intestinal mucins, normally coating the CACO-2 cells *in situ*. This is of significant importance for the modified chitosan findings since massive complexes are formed when these two components are mixed (Fiebrig et al., 1995, Deacon et al., 1999).

The aim of this chapter is to assess the possibility of using non-digestible fibres as a macromolecular barrier for the treatment of Coeliac disease. Differing from Chapter 6, interactions were assessed between a physiologically relevant sample of gliadin, digested using pepsin and trypsin, and a plethora of non-digestible fibres from plant, animal and bacterial sources, natural and synthetic production and different anionic/cationic properties.

7.2 Materials

7.2.1 Gliadin

7.2.1.1 Source

Gliadin preparation was performed by Arthur Tatham and colleagues at Cardiff Metropolitan University. Gliadins were purified from wheat (*Triticum aestivum* cv. Chinese Spring) as described in section 6.2.1.

Tryptic-peptic digests were prepared according to the method of Seifert et al. (1995). Gliadin (2g) was incubated in 100ml 0.02M HCl, with 25K units of pepsin-agarose (Sigma Aldrich, UK) for 4 hours at 37^{o}C, with gentle stirring. The pH was adjusted manually every 15 minutes to 1.9-2.0. The mixture was centrifuged (10 minutes 10,000 x g) and the peptic digest

adjusted to pH 8.0 with 2M ammonium hydroxide solution. 150 units of trypsin-agarose (Sigma-Aldrich, UK) was added and digested for 4 hours at 37^{o}C, with gentle stirring. The trypsin beads were removed by centrifugation (10 minutes 10,000 x g), the mixture boiled for 1 minute then re-centrifuged (10 minutes 10,000 x g). The supernatant was freeze-dried and termed pepsin-trypsin digested gliadin (PTDG). The recovery was approximately 40%.

7.2.1.2 Preparation

Concentrations of PTDG were measured using UV spectrophotometry and the Lambert-Beer law. An extinction coefficient of 600 ml.g^{-1}.cm^{-1} was used, based on the cDNA protein sequence of α-gliadin (Kasarda et al., 1984) and entered into the PERKINS software v1.0 (Perkins, 1986).

7.2.2 Polysaccharides

In total, 26 polysaccharides were tested for an interaction with PTDG (Table 7.1). Amino-modified celluloses and xylan sulphates were kind gifts from the laboratory of Dr.Thomas Heinze, University of Jena, Germany. Arabinoxylan and 4-O-Methyl Glucuronoxylan were kind gifts from the laboratory of Dr. Zdenka Hromádková, Bratislava, Slovak Republic. Flax and Inulin samples were kind gifts from David Lafond, Kelloggs company, Battlecreek, USA.

Polysaccharides were dissolved in deionised water at a relatively high stock concentration (~5mg/ml). Concentrations were measured using an Atago DD-7 differential refractive index meter calibrated to 0.150ml/g (sucrose). BRIX percentage concentrations were corrected to mg/ml using a respective dn/dc presented in Table 7.2. Polysaccharide stock solutions were mixed with PTDG in a 1:1 (w/w) ratio with PTDG. The exceptions to

this methodology were the two amino-modified celluloses which were dissolved in phosphate buffered saline, pH6.8 and I=0.1M, to aid solubility (Table 7.2).

Table 7.1: List of polysaccharides tested for interaction with digested gliadin. The source for each polysaccharide is listed as well as an assigned three letter code.

Polysaccharide	Code	Source
Alginate	ALG	Glycomix, UK
Amino cellulose EDA-1	AC1	Prof. Thomas Heinze
Amino cellulose TAEA	AC2	Prof. Thomas Heinze
Arabinoxylan	ARX	Dr. Zdenka Hromadkova et al.
k-Carrageenan	KCG	Sigma Aldrich, UK
i-Carrageenan	ICG	Sigma Aldrich, UK
l-Carrageenan	LCG	Glycomix, UK
Chitosan	CHI	Archimedes, UK (SeaCure)
Flax	FLX	Kelloggs, USA
Gellan	GEL	CPKelco, UK (Kelcogel)
Guar gum	GUG	Meyhall, Switzerland (M30)
Gum arabic	GAR	Glycomix, UK
Heparin	HEP	Sigma Aldrich, UK
Hyaluronic acid	HUA	Sigma Aldrich, UK
Hydroxypropyl methylcellulose	HPM	Dow Chemical Company, USA (Methocel)
Agave Inulin	AGI	Kelloggs, USA
Chicory root Inulin	CRI	Kelloggs, USA (Beneo ST)
Konjac glucomannan	KGM	Glycomix, UK
Locust bean gum	LBG	Sigma Aldrich, UK
4-O-Methyl Glucuronoxylan	MGX	Dr. Zdenka Hromadkova
Pectin	PEC	Danisco, DuPont, USA
Xanthan	XTN	Glycomix, UK
Xylan Sulphate low DS	XSL	Prof. Thomas Heinze
Xylan Sulphate med DS	XSM	Prof. Thomas Heinze
Xylan Sulphate high DS	XSH	Prof. Thomas Heinze
Xyloglucan	XGL	Danisco, DuPont, USA

Table 7.2: List of refractive index increments associated with each polysaccharide.

Code	dn/dc (ml/g)	Reference	Comments
ALG	0.165	(Buchner et al., 1961)	
AC1	0.150	assumed	In PBS
AC2	0.150	assumed	In PBS
ARX	0.150	assumed	
KCG	0.126	(Wittgren et al., 1998)	
ICG	0.126	assumed	
LCG	0.126	assumed	
CHI	0.163	(Rinaudo et al., 1993)	
FLX	0.146	(Theisen et al., 2000)	
GEL	0.150	assumed	
GUG	0.150	(Kapoor et al., 1994)	
GAR	0.145	(Huglin et al., 1989)	
HEP	0.150	(Peitzsch et al., 1992)	
HUA	0.176	(Huglin et al., 1989)	
HPM	0.150	assumed	
AGI	0.140	(Nikolić et al., 2001)	
CRI	0.140	(Nikolić et al., 2001)	
KGM	0.150	assumed	
LBG	0.150	(Kapoor et al., 1994)	
MGX	0.150	assumed	
PEC	0.146	(Theisen et al., 2000)	High methoxy, hairy
XTN	0.155	(Milas et al., 1996)	
XSL	0.150	assumed	DS = 0.35
XSM	0.150	assumed	DS = 1.33
XSH	0.150	assumed	DS = 1.80
XGL	0.150	assumed	

7.3 Methodology

7.3.1 PTDG characterisation

7.3.1.1 Sedimentation velocity

Sedimentation velocity of PTDG was carried out simultaneously with polysaccharides being tested, as a control, during experimental runs. Analysis carried out with c(s) and ls-g*(s), with both interference and absorbance optics, can be observed in top plots of Figure 7.4 onwards.

7.3.1.2 Sedimentation equilibrium

Sedimentation equilibrium was carried out on a single concentration of PTDG at 50k RPM, 20.0°C. Data were analysed using SEDFIT-MSTAR (Schuck et al., 2014) and MULTISIG (Gillis et al., 2013a).

7.3.2 Interaction studies

7.3.2.1 Sedimentation velocity

Samples were prepared by diluting stock concentrations directly into an eppendorf and diluted up to 1ml with solute. Seven eppendorfs were used per experimental batch, comprising a PTDG control, three polysaccharide controls and three mixtures. This provided seven cells, plus counterbalance, to be aligned in an 8-hole rotor. The rotor speed was set to between 40-50k RPM to allow the low molar mass, low sedimentation coefficient, PTDG to sediment. ~100 scans were taken every 14 minutes with both interference and absorbance optics.

7.3.2.2 Analysis

Approximately 100 scans from each cell were loaded into SEDFIT (Schuck, 2000). Both ls-g*(s) and c(s) analyses were performed, yielding four distributions: g(s)-Interference, g(s)-Absorbance, c(s)-Interference, c(s)-Absorbance. The four distributions from individual cells were plotted on the same graph for comparison. Blue plots represent interference, red plots represent absorbance, darker colour represents c(s), lighter colour represents g(s).

7.4 Results

7.4.1 Pepsin-Trypsin digested gliadin characterisation

7.4.1.1 Sedimentation velocity

All distributions are in general agreement, although some sedimentation coefficient axes may differ depending on the size of the polysaccharide tested.

Resolvable peaks were generally observed at 0.5 and 1.0S using c(s) analysis, particularly visible in Figure 7.12, with boundary spreading to approximately 2S according to ls-g*(s) analysis.

7.4.1.2 Sedimentation equilibrium

The concentration of PTDG in the centrifuge cell was measured at approximately 0.5 mg/ml (1.5 fringes) using the c(M) algorithm in SEDFIT-MSTAR. Figure 7.1 shows the MSTAR analysis. The black points represent the raw, or transform, data points. The red line shows the c(M) fit performed by SEDFIT-MSTAR. The green lines are linear regressions performed on the raw data points.

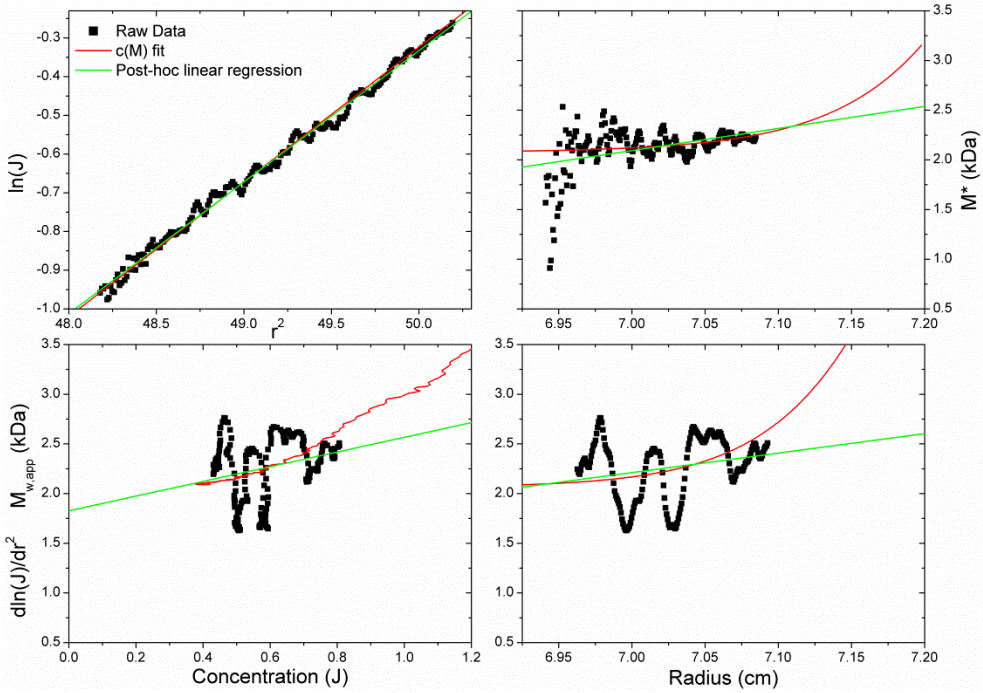

Figure 7.1: SEDFIT-MSTAR analysis of PTDG sedimentation equilibrium data at 0.5mg/ml. Anti-clockwise from top left: ln(J) vs. r^2, differential of previous plot vs. J, same as previous plot vs. radius, M* function extrapolated to base.

The $dln(J)/dr^2$ plots both show a slight positive slope, indicative of a polydisperse system, although this upwards trend is less evident in the ln(J) vs. r^2 plot. The green linear regression on the differential plot shows an extrapolation to the meniscus/infinite dilution between 1.7-2.1kDa, corroborated by the c(M) red trend line on the bottom right. The M* extrapolation to the base of the cell, estimated by c(M), shows a weight average molar mass of 3.2kDa, whereas the linear regression provides a lower estimate of 2.54kDa. This is due to long extrapolation where c(M) estimates a curvature upwards. The c(M) analysis also yielded a z-average molar mass of 5.9kDa, giving a polydispersity index (z/w) of 1.8.

MULTISIG analysis yielded number, weight and z-average reduced molar masses (converted to molar mass using SEDNTERP). These were 1.83

(±5.3%), 2.55 (±1.8%) and 3.40 (±1.4%) kDa respectively. The polydispersity indices (z/w, w/n) were 1.33 and 1.39 respectively.

These values are inconsistent with the c(M) SEDFIT-MSTAR values. Weight average molar mass differed by 25%, z-average differed by 74% and polydispersity differed by 29%. The linear regression for M*, on the other hand, provides a very similar value to the MULTISIG analysis, differing by just 0.3%. It is likely that the c(M) overestimation of the weight average had a large effect on the z-average also.

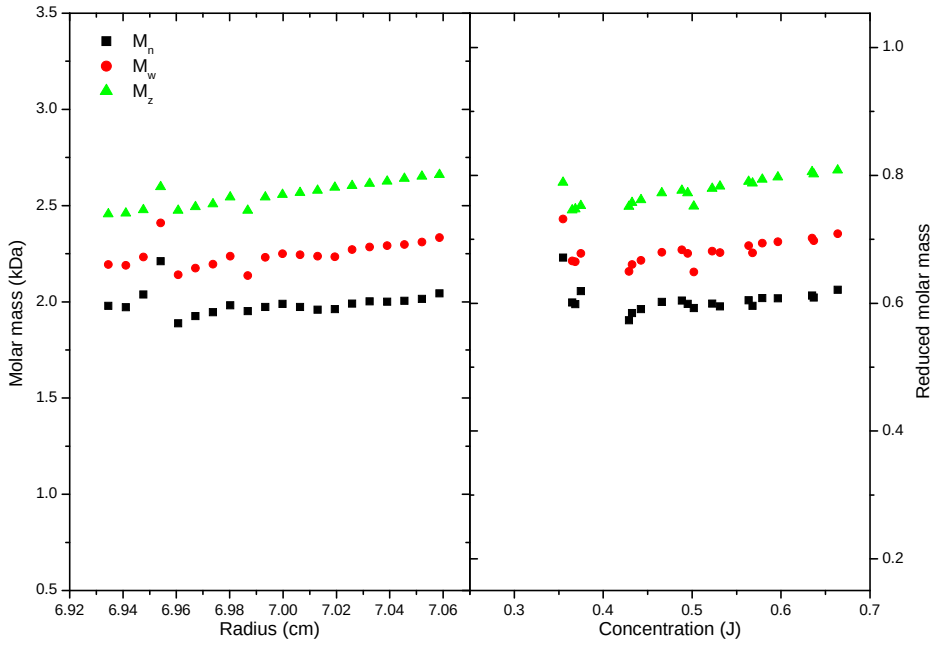

Figure 7.2: MULTISIG-RADIUS output of number, weight and z-average molar mass values of PTDG at 0.5mg/ml.

The MULTISIG-RADIUS algorithm was performed on the data, to yield the number, weight and z-average across the cell (Figure 7.2) and c(σ) against radius, concentration and molar mass (Figure 7.3). Although minor errors were calculated at 6.950, 6.985 and 7.020cm, the data across the cell is consistent that peak 1 is at 2kDa and peak 2 is at 4kDa, increasing in

concentration as towards the base. Extrapolated values yielded a weight average of ~2.25kDa, which is 12% lower than the MULTISIG results. The difference between the two algorithms is that the repetitions are repeated either at the hinge point five times or across the cell in 20 radial positions.

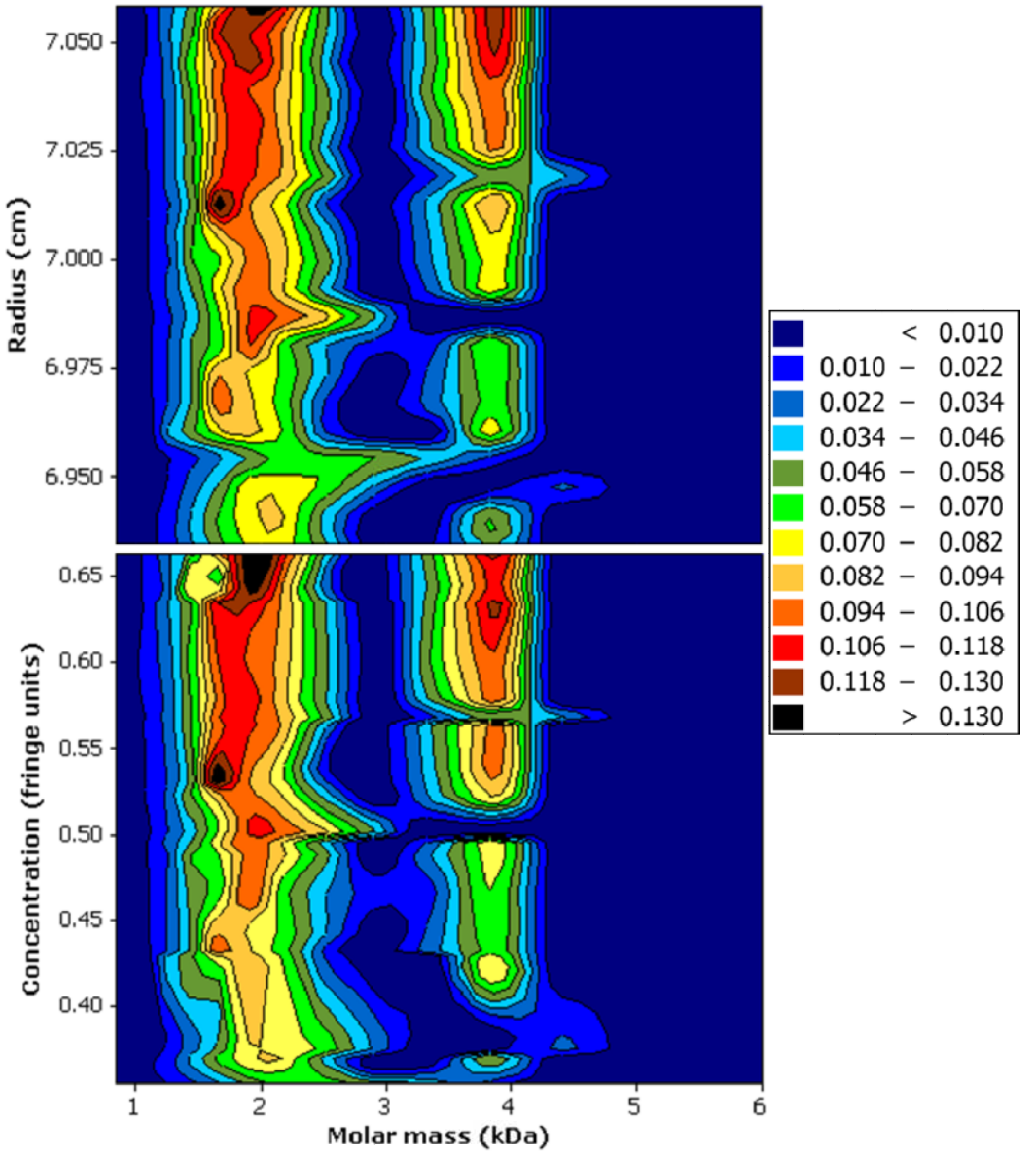

Figure 7.3: MULTISIG-RADIUS c(σ) output for PTDG sedimentation equilibrium data at 0.5mg/ml against radius and concentration.

7.4.2 Natural plant polysaccharides

7.4.2.1 Arabinoxylan

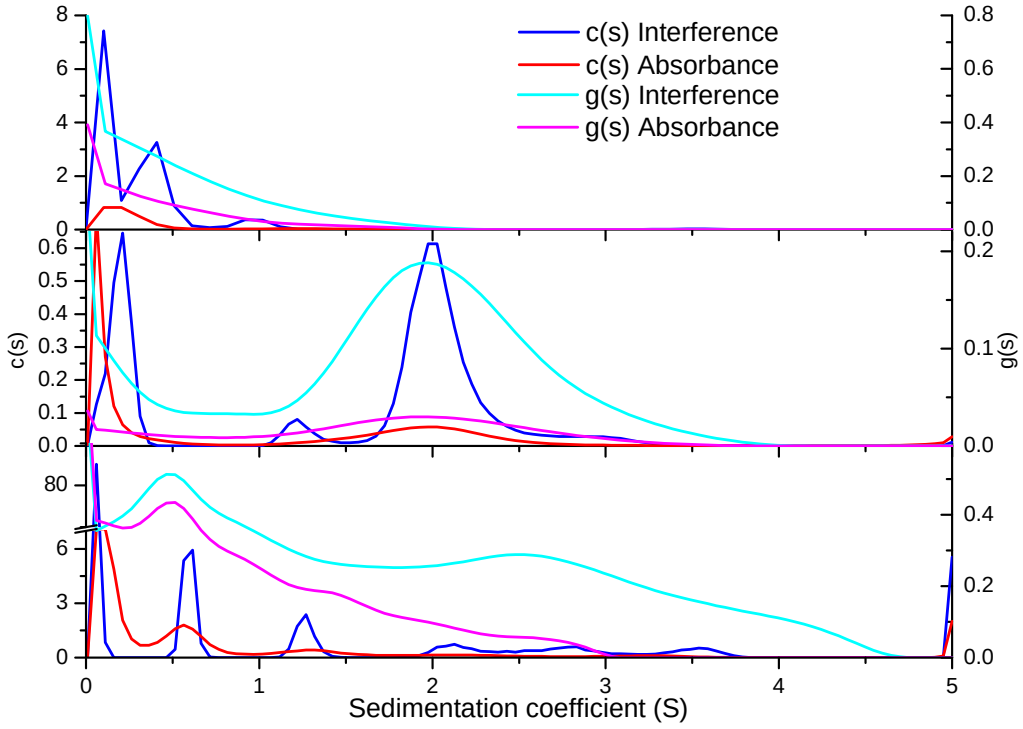

Figure 7.4: Arabinoxylan (ARX) with PTDG. Top: PTDG control, middle: ARX control, bottom: 1:1 mixture.

Figure 7.4 shows the mixture between a low protein content arabinoxylan (ARX) and pepsin-trypsin digested gliadin (PTDG). The PTDG plot shows a peak around 0.4 and 0.9S for c(s) interference, with definite absorption taking place. The ARX plot shows a major peak at 2S, with the c(s) resolving two minor peaks at 1.2 and 3S. All peaks are absorbing to some extent, suggesting that there was not a complete removal of protein during purification. For the mixture the PTDG and ARX peaks are visible, with no significant species indicating an interaction. Absorption was present in ARX before and after mixture with PTDG.

7.4.2.2 Flax

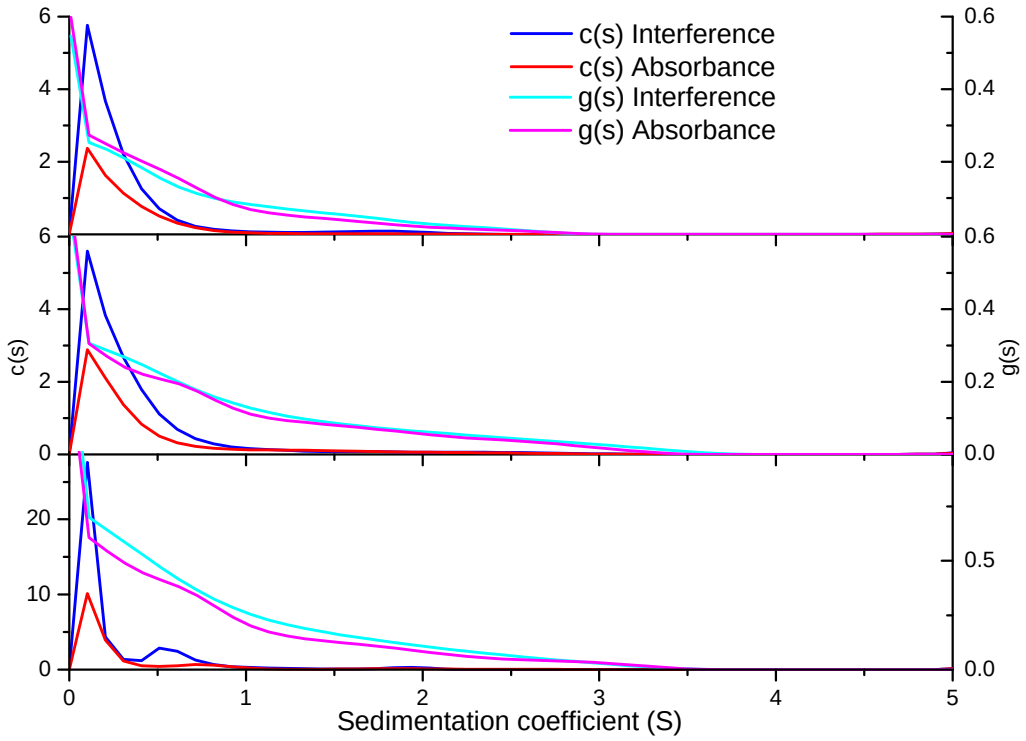

Figure 7.5: Flax (FLX) combined with PTDG. Top: PTDG control, middle: FLX control, bottom: 1:1 mixture.

The PTDG plot in Figure 7.5 does not resolve any clear peaks, except a species at 2S. Equally, the FLX plot shows a general distribution between 0 and 3S. In the mixture plot, we can see the peak at 2S, but there is a resolved peak at 0.7S, which is consistent with other PTDG figures.

7.4.2.3 Galacto/glucomannan

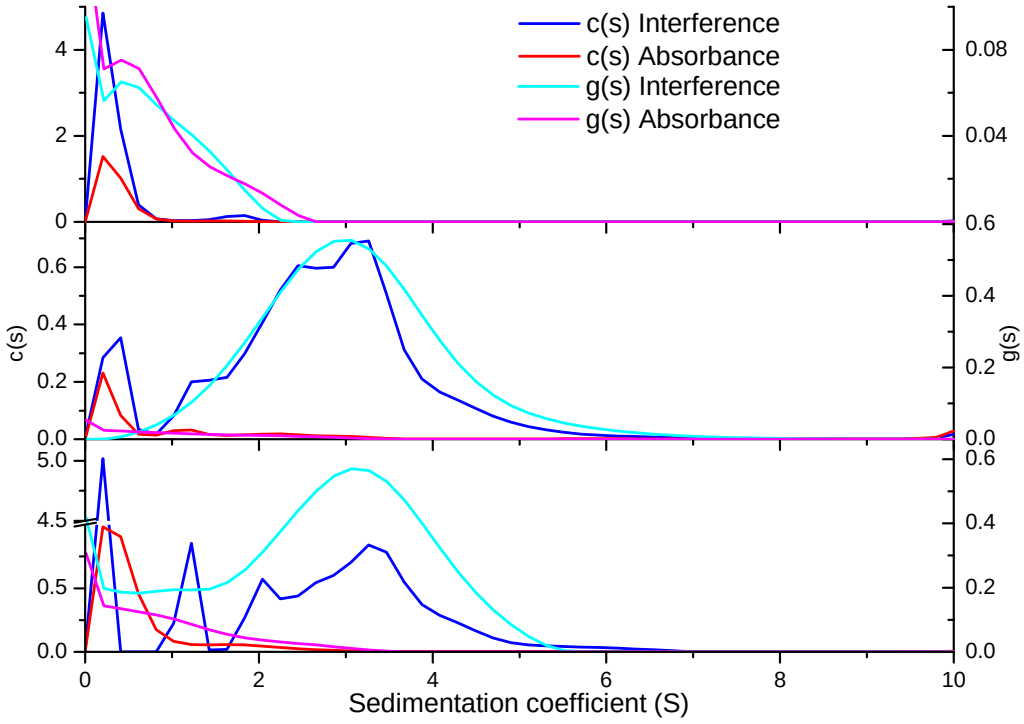

Figure 7.6: Galactomannan from guar gum (GUG) mixed with PTDG. Top: PTDG control, middle: GUG control, bottom: 1:1 mixture.

Figure 7.6 shows a PTDG plot with peaks at approximately 0.5 and 2S. The GUG control shows a large peak at 3.5S, with a shoulder at 3S. The same peak can be seen in the combined sample plot. There is also little change in absorbance profile between the two controls and the mixture.

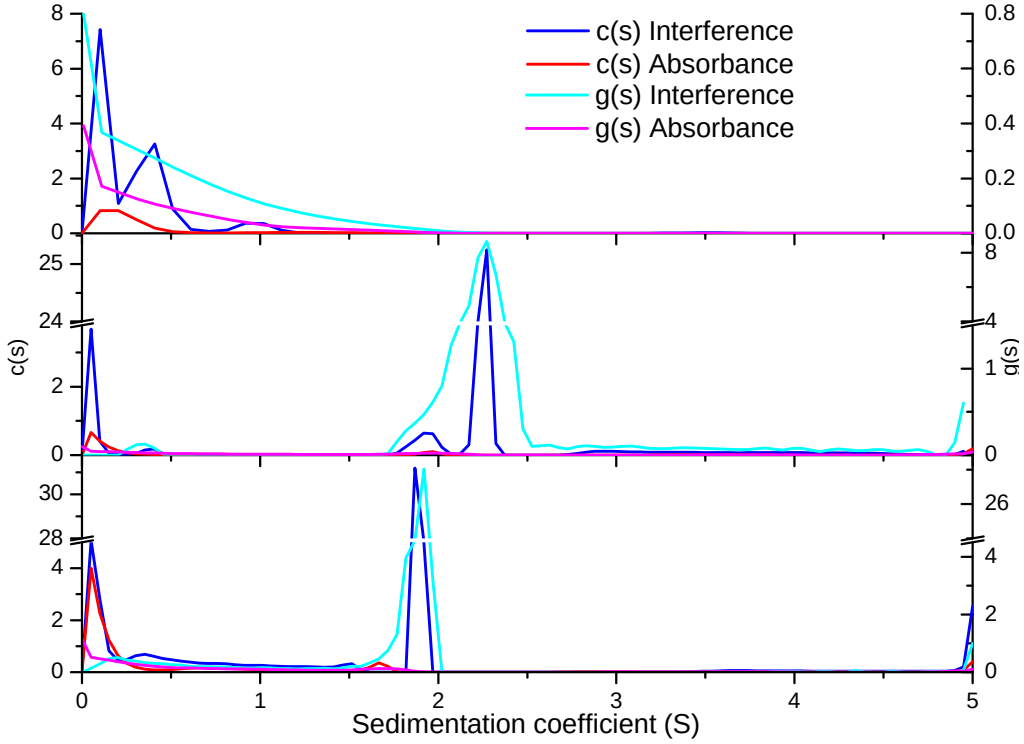

Figure 7.7: Glucomannan from konjac (KGM) mixed with PTDG. Top: PTDG control, middle: KGM control, bottom: 1:1 mixture.

The KGM control in Figure 7.7 shows a single narrow peak at 2S, with limited absorbance. As compared to the mixture plot, the distribution has not changed, equally there is comparable absorbance compared to what is present in the PTDG control plot.

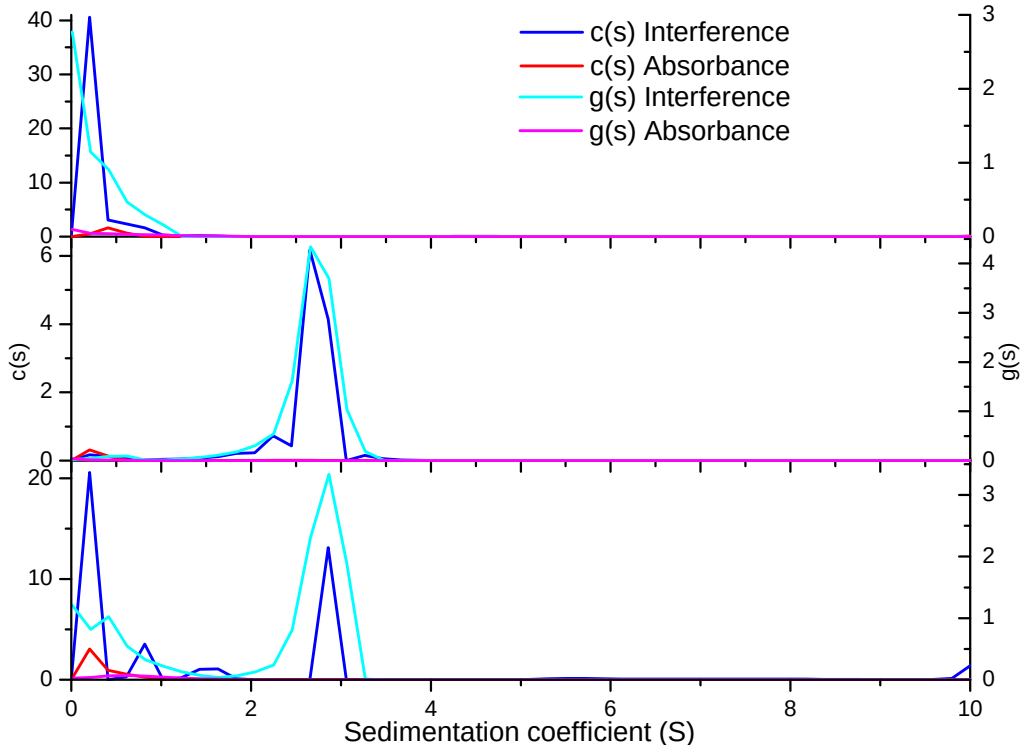

Figure 7.8: Galactomannan from locust bean gum (LBG) mixed with PTDG. Top: PTDG control, middle: LBG control, bottom: 1:1 mixture.

LBG (Figure 7.8) shows a similar distribution to KGM (Figure 7.7) with an equally low absorbance profile. The mixture, however, shows a new peak at around 6S in the c(s) distribution, however this is not corroborated by the g(s) analysis and is likely to be an artefact. There also seems to be no change between the PTDG control and the mixture.

7.4.2.4 Gum arabic

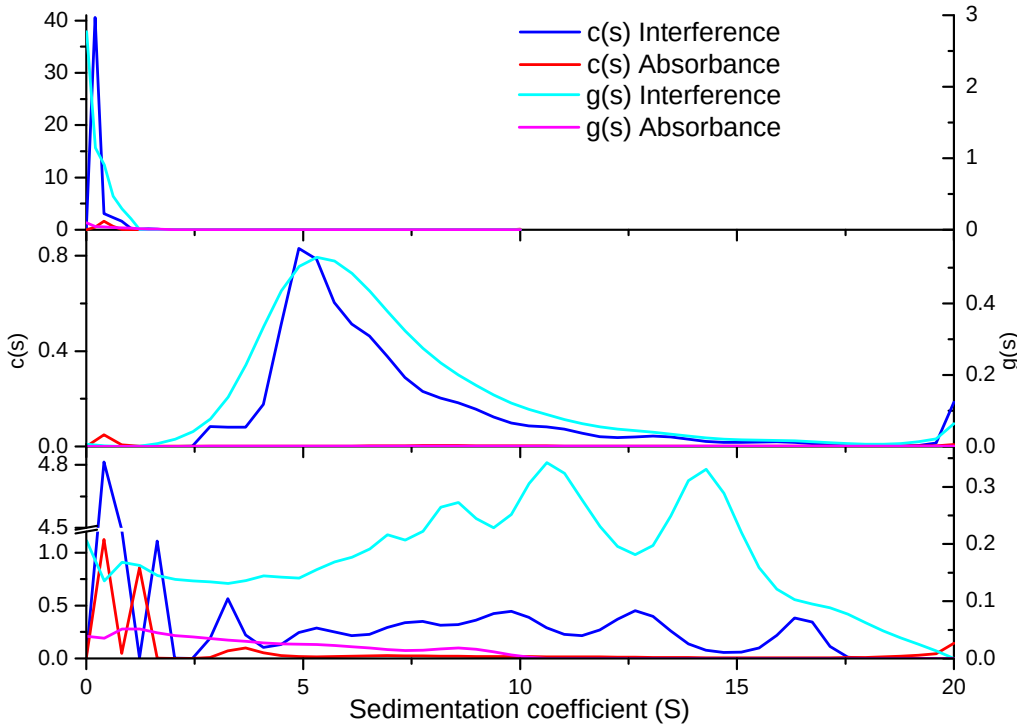

Figure 7.9: Mixture between gum arabic (GAR) and PTDG. Top: PTDG control, middle: GA control, bottom: 1:1 mixture.

PTDG control plot shows a compact peak distribution, difficult to evaluate completely, but shows that species are below 2S. GAR control shows a peak ranging from 2.5 to 17.5S peaking at 6S. No absorbance is shown in the polysaccharide control. The mixture plot shows an extended interference plot up to 20S. Absorbance peaks range up to 10S in g(s) and show peaks at 3 and 7S. The shape of the distribution changes from smooth to rough, especially between 8-15S.

7.4.2.5 Inulin

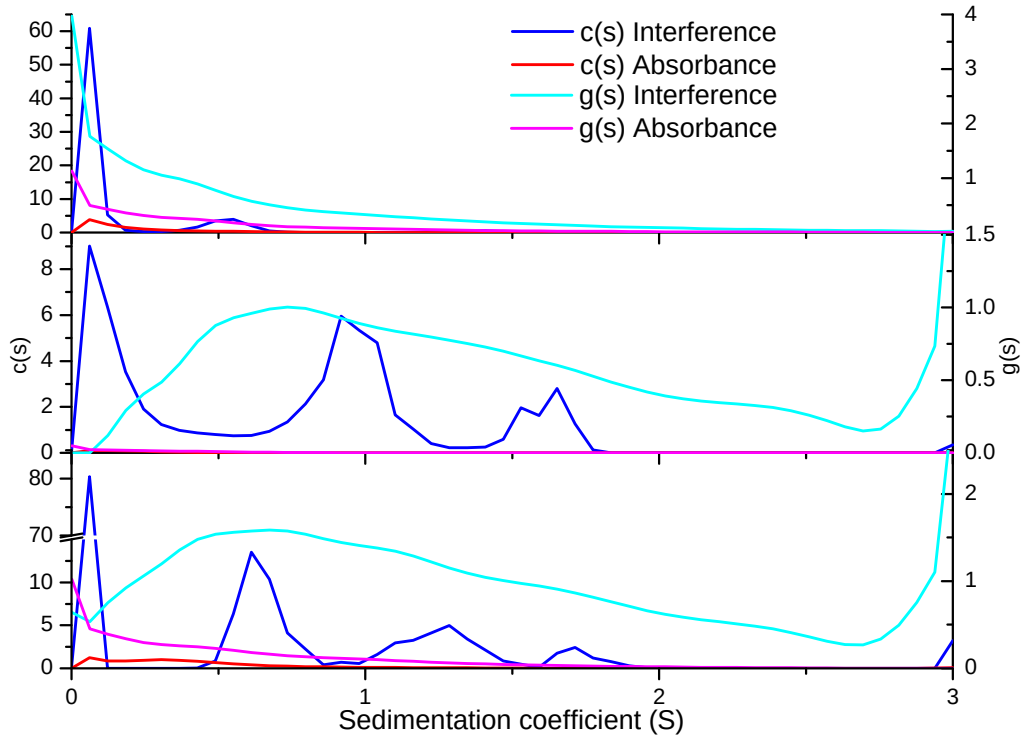

Figure 7.10: Inulin, sourced from Agave (AGI), mixed with PTDG. Top: PTDG control, middle: AGI control, bottom: 1:1 mixture.

The PTDG plot shows a similar distribution to Figure 7.4 with peaks at 0.5 and 1.4S. AGI alone shows no absorbance signal and a peak at 0.9 and 1.7S. The mixture shows no significant difference between the solo combined c(s) peaks (expected 0.5, 1.0, 1.5) and the experimental mixture. There is also no change in the absorption profile from PTDG.

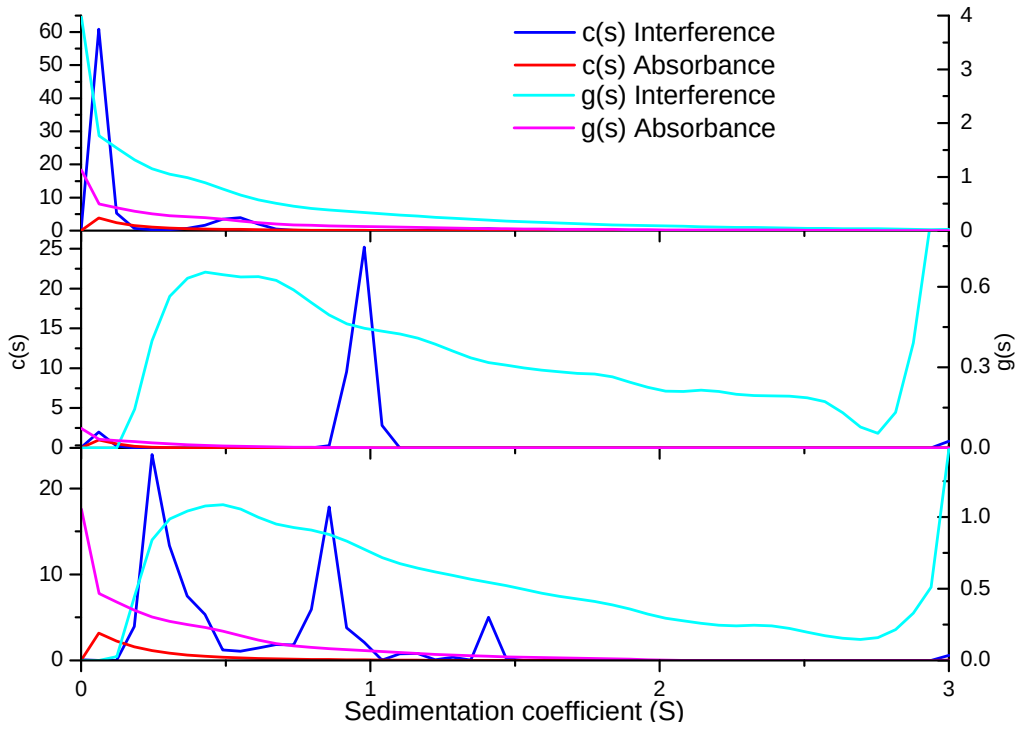

Figure 7.11: Inulin, sourced from Chicory root (CRI), mixed with PTDG. Top: PTDG control, middle: CRI control, bottom: 1:1 mixture.

The PTDG plot in Figure 7.11 is the same as for Figure 7.10, repeated here as reference only. The CRI control shows a single c(s) peak at 1S, although a broader distribution in the g(s) analysis. No absorbance was detected for the polysaccharide. The mixture shows no difference in absorption signal from PTDG, and c(s) peaks are as expected, with no significant changes.

7.4.2.6 4-O-Methylglucuronoxylan

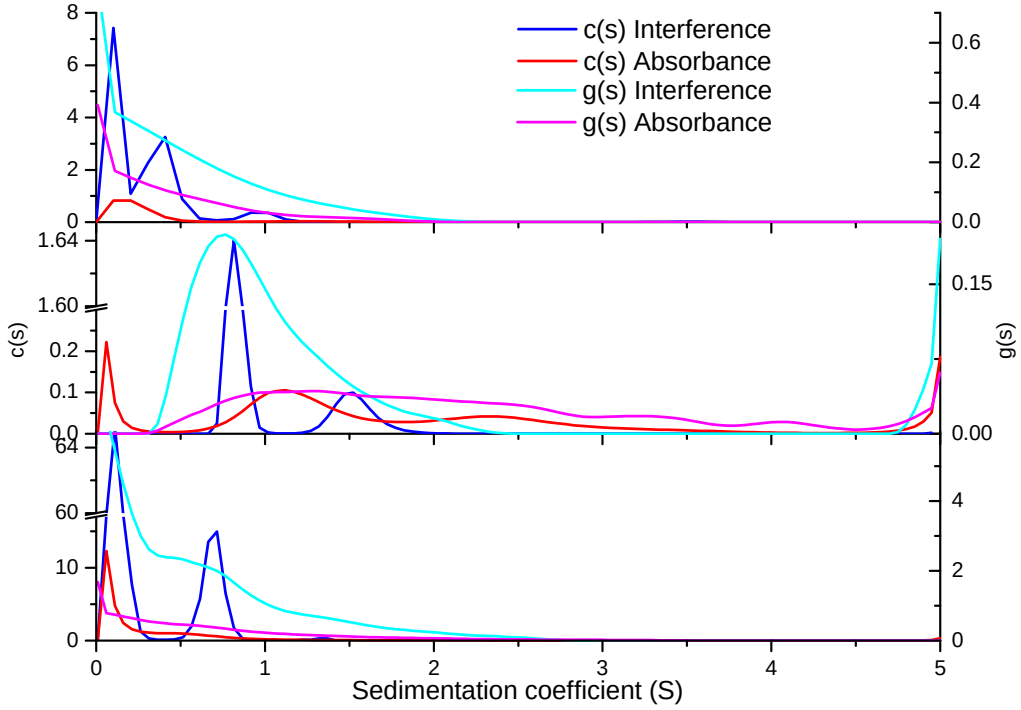

Figure 7.12: Mixture between 4-O-Methyl Glucuronoxylan (MGX) and PTDG. Top: PTDG control, middle: MGX control, bottom: 1:1 mixture.

The PTDG and MGX samples in Figure 7.12 show similarly sized distributions at below 1S. The absorbance for MGX appears to be high for a polysaccharide, suggesting that the sample may not have been purified of all protein components. The mixture shows no additional peaks expected from an interaction between the two species. Equally, the absorbance profile still remains in the smaller part of the distribution.

7.4.2.7 Pectin

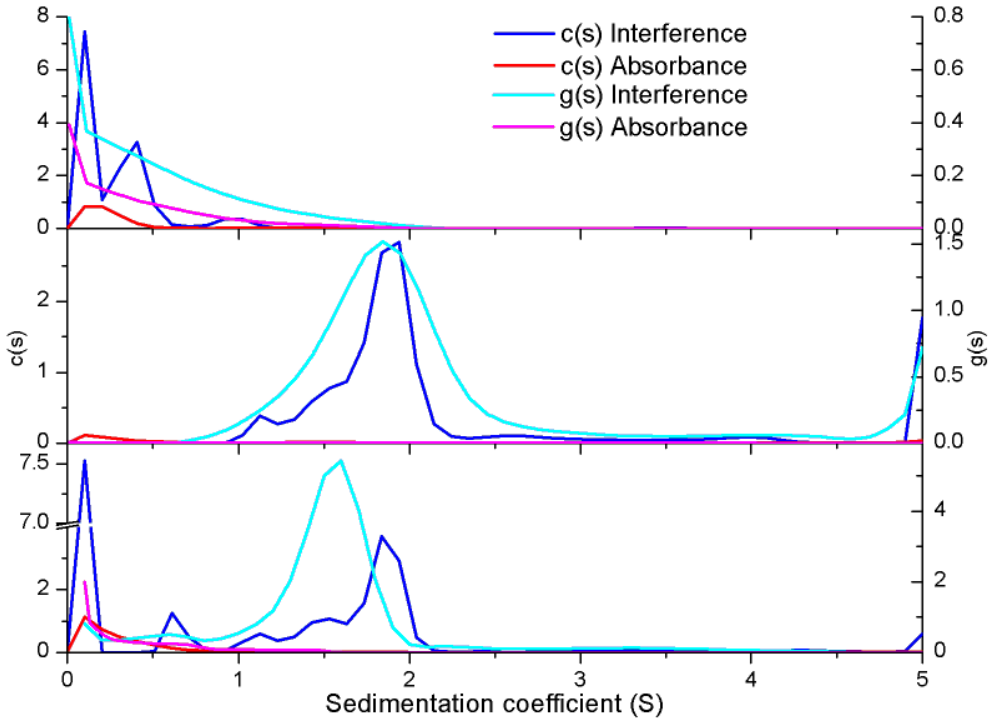

Figure 7.13: High methoxy pectin (PEC) mixed with PTDG. Top: PTDG control, middle: PEC control, bottom: 1:1 mixture.

Figure 7.13 shows the PTDG component in the top and bottom plots in approximately the same position. There appears to be a small amount of absorbing material in the middle, polysaccharide only, plot which is also present in the mixture. The g(s) distribution appears to be slightly shifted to the left (lower sedimentation), however this is likely to be an anomaly as the c(s) is in a similar position to the polysaccharide control.

7.4.2.8 Xyloglucan

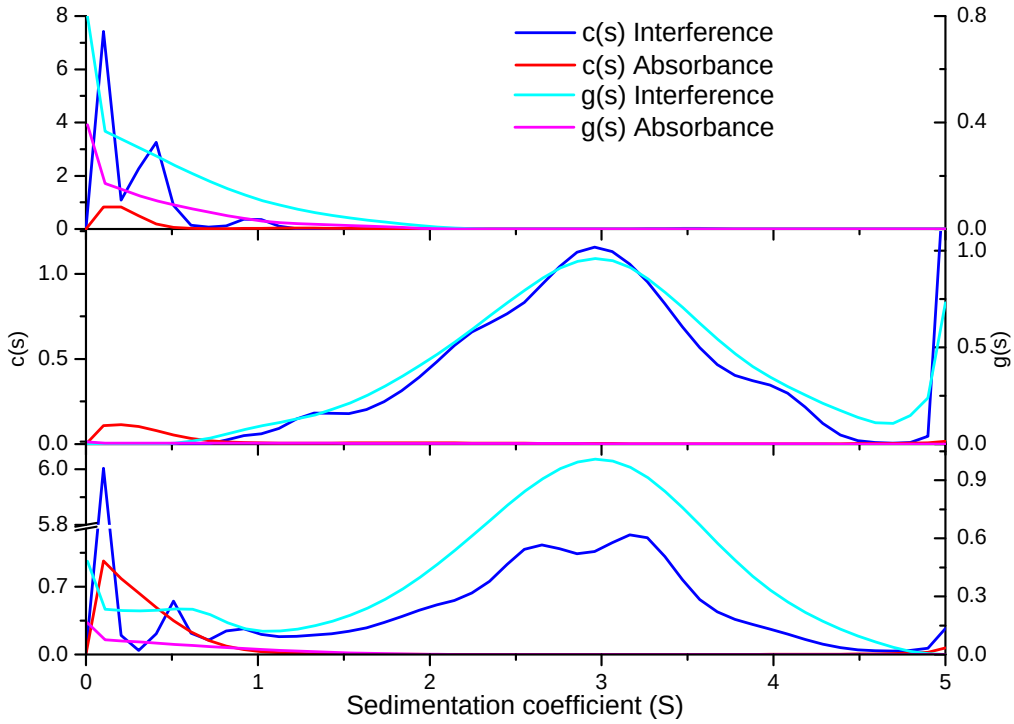

Figure 7.14: Xyloglucan (XGL) mixed with PTDG. Top: PTDG control, middle: XGL control, bottom: 1:1 mixture.

The XGL control and mixture in Figure 7.14 do not differ significantly in terms of the c(s) and g(s) interference trace. The c(s) resolved three peaks at 2, 3 and 4S for the control, but two peaks at 2.5 and 3.5S for the mixture. This is unlikely to be a significant difference due to the active peak-narrowing method used by c(s). Absorbance traces do not appear to change significantly between the top and bottom plots.

7.4.3 Synthetic plant polysaccharides

7.4.3.1 Amino cellulose

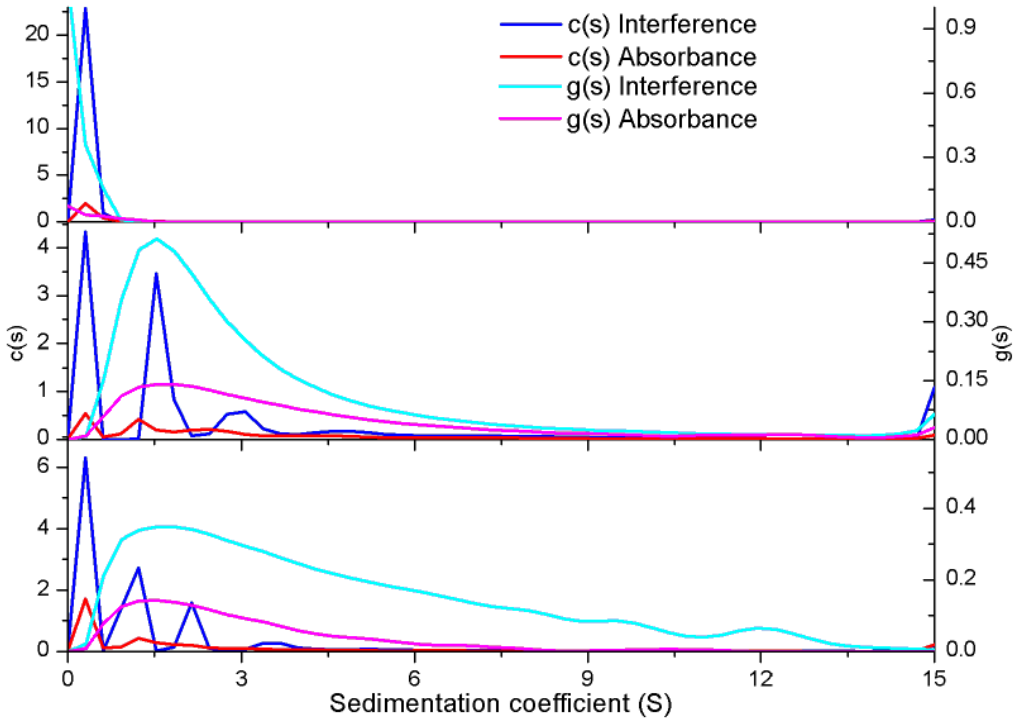

Figure 7.15: Aminocellulose (AC1) mixed with PTDG. Top: PTDG control, middle: AC1 control, bottom: 1:1 mixture.

Figure 7.15 shows the comparison between PTDG and the AC1. The PTDG shows a peak approximately 0.5S, although the resolution in this figure is lower than others due to the larger size of AC1. Peaks of AC1 are observed at ~1.5, 3, 4.5S. The mixture plot shows no significant change in distribution. AC1 peaks move to ~1, 2, 3.5S, but this would be expected if the PTDG is increasing the viscosity of the system and slowing larger macromolecules down. The absorbance plots also do not change with the addition of PTDG, however this polysaccharide does absorb at 280nm, thus making a conclusion from this evidence more difficult.

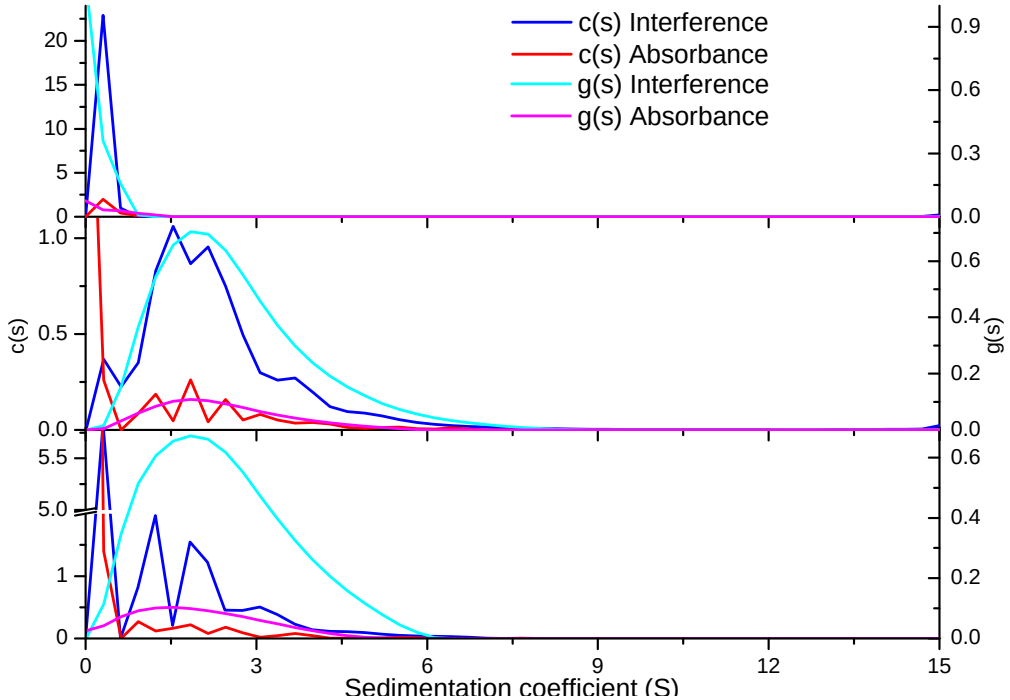

Figure 7.16: Aminocellulose (AC2) mixed with PTDG. Top: PTDG control, middle: AC2 control, bottom: 1:1 mixture.

The PTDG peak in Figure 7.16 is similar to that of the AC2 results. The AC2 distribution also shows a similar distribution to the AC1 results, however the peaks are closer together at ~2, 3.5, 5, 6S. With the addition of PTDG the distribution does not change greatly, with similar c(s) peak positions and similar absorbance signal.

7.4.3.2 Hydroxy propyl methyl cellulose

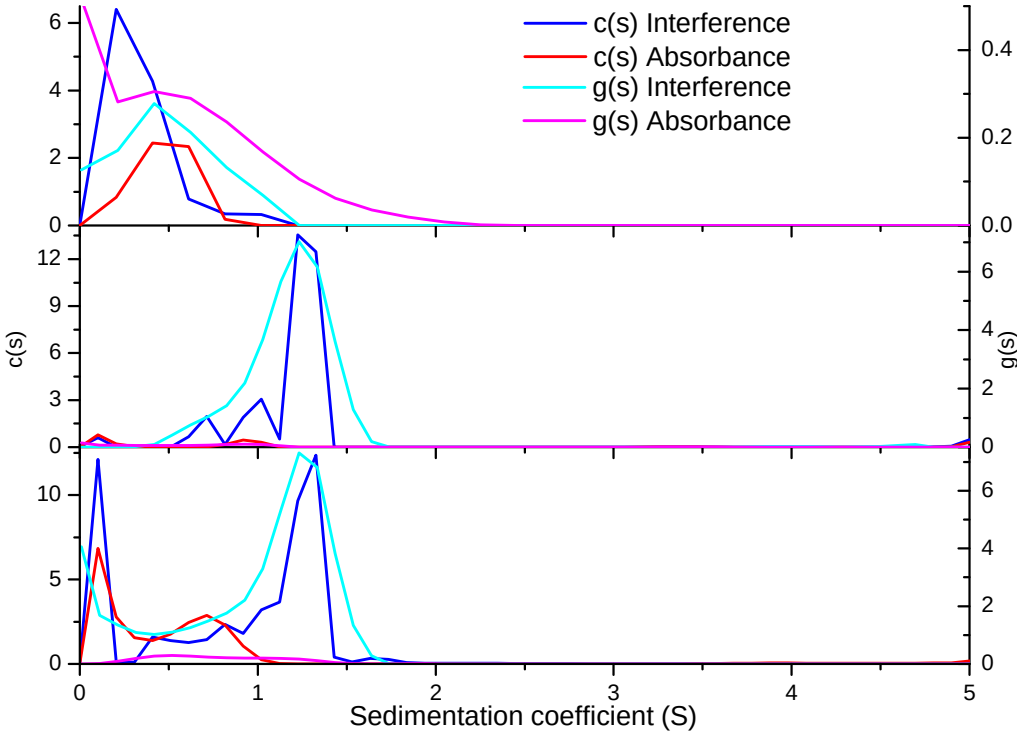

Figure 7.17: Hydroxy propyl methyl cellulose (HPM) mixed with PTDG. Top: PTDG control, middle: HPM control, bottom: 1:1 mixture.

The HPM plot in Figure 7.17 shows a peak at approximately 1.3S. There are also smaller peaks at 0.7 and 1S, and the plot shows very little absorbance except in the 1S peak. The PTDG shows a distribution less than 1S, as shown in previous results. The mixture of the two again shows the main peak at 1.3S with, now unresolved, shoulders between 0.5-1S. There is a strong absorbance signal in c(s) at 0.7S, however this is consistent with the findings from the PTDG control. A larger peak was also resolved at 1.6S using c(s), however this may be an artefact as the g(s) algorithm was unable to include this information.

7.4.3.3 Xylan sulphate

Xylan sulphate, assayed at three different degrees of sulphation (DS), shows the PTDG plot with peaks at 0.5 and 0.7S, generally the distribution being less than 1S. The lowest DS (XSL, Figure 7.18) shows a peak at 0.5S, resolved using c(s). The g(s) analysis shows a broad distribution up to 3S, with a shoulder at 2.5S, however this is not well represented by the c(s) analysis. When mixed with PTDG, the c(s) algorithm resolved a second peak at 1S, however the g(s) reduced in peak breadth to 1.5S.

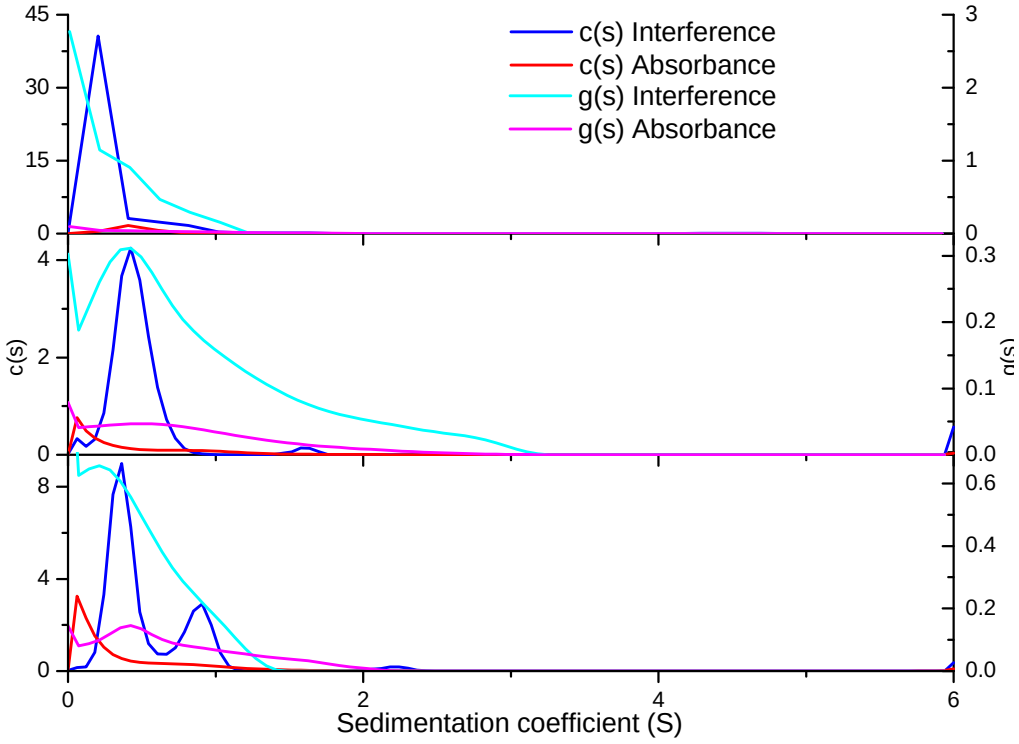

Figure 7.18: Xylan sulphate (XSL, low DS) mixed with PTDG. Top: PTDG control, middle: XSL control, bottom: 1:1 mixture.

The medium DS xylan sulphate (XSM, Figure 7.19) shows peaks at 0.5 and 1S, suggesting that the c(s) analysis in the XSM control in Figure 7.18 may not have been able to resolve this peak. The g(s) for XSM also shows a peak at 2.5S, but is not corroborated with c(s) and is possibly an artefact. The mixture with PTDG appeared to sharpen the c(s) peaks, but with

generally a similar peak position as before. c(s) was able to resolve a peak at 2.1S, and an artefact at 5S.

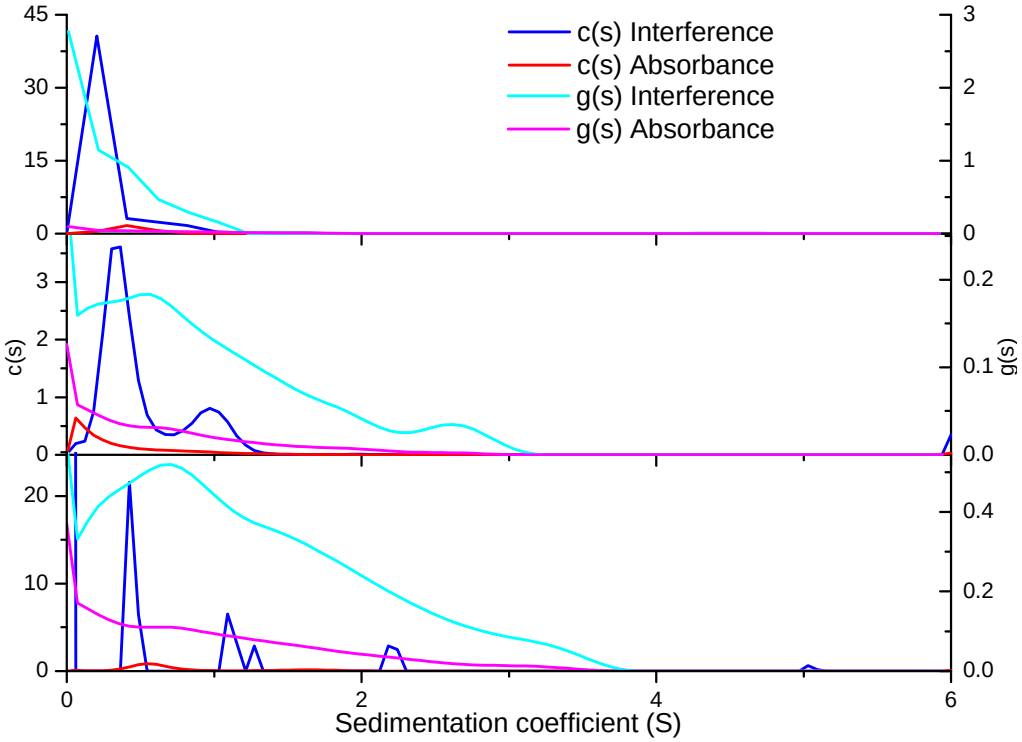

Figure 7.19: Xylan sulphate (XSM, medium DS) mixed with PTDG. Top: PTDG control, middle: XSM control, bottom: 1:1 mixture.

The highest DS xylan sulphate (XSH, Figure 7.20) shows a similar peak distribution to XSL and XSM, although larger at 1 and 2.1S. Upon mixture with PTDG, c(s) attempted to resolve an extra peak at 1.9S, however this is likely to be an artefact of the split of the 2.1S peak in the control. The g(s) analysis does not change significantly between control and mixture.

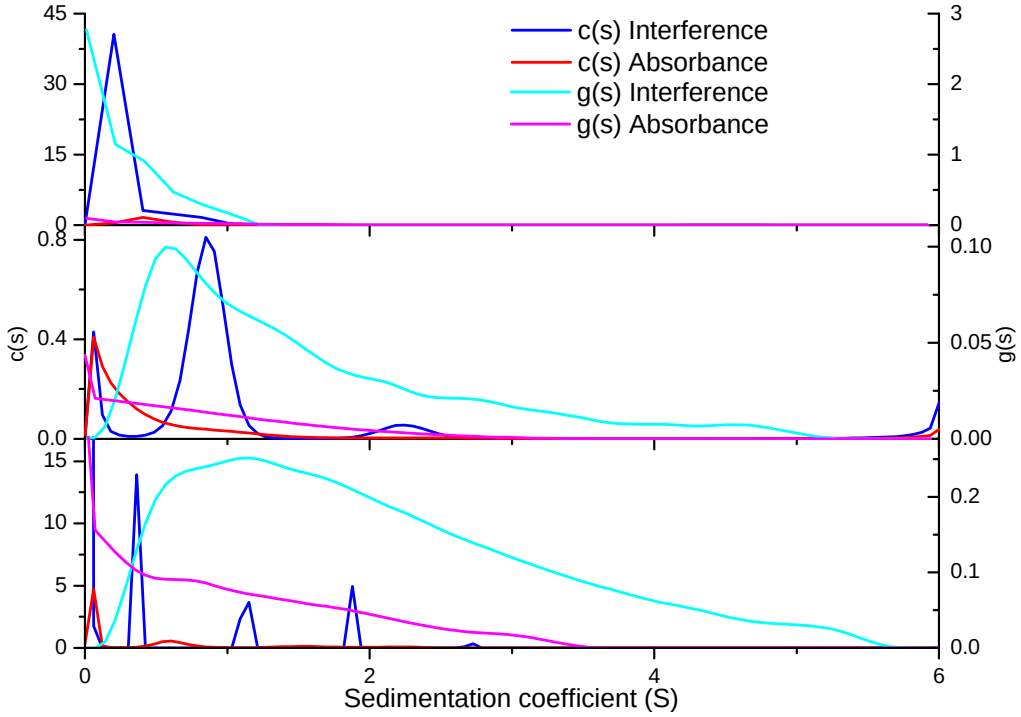

Figure 7.20: Xylan sulphate (XSH, high DS) mixed with PTDG. Top: PTDG control, middle: XSH control, bottom: 1:1 mixture.

7.4.4 Seaweed polysaccharides

7.4.4.1 Alginate

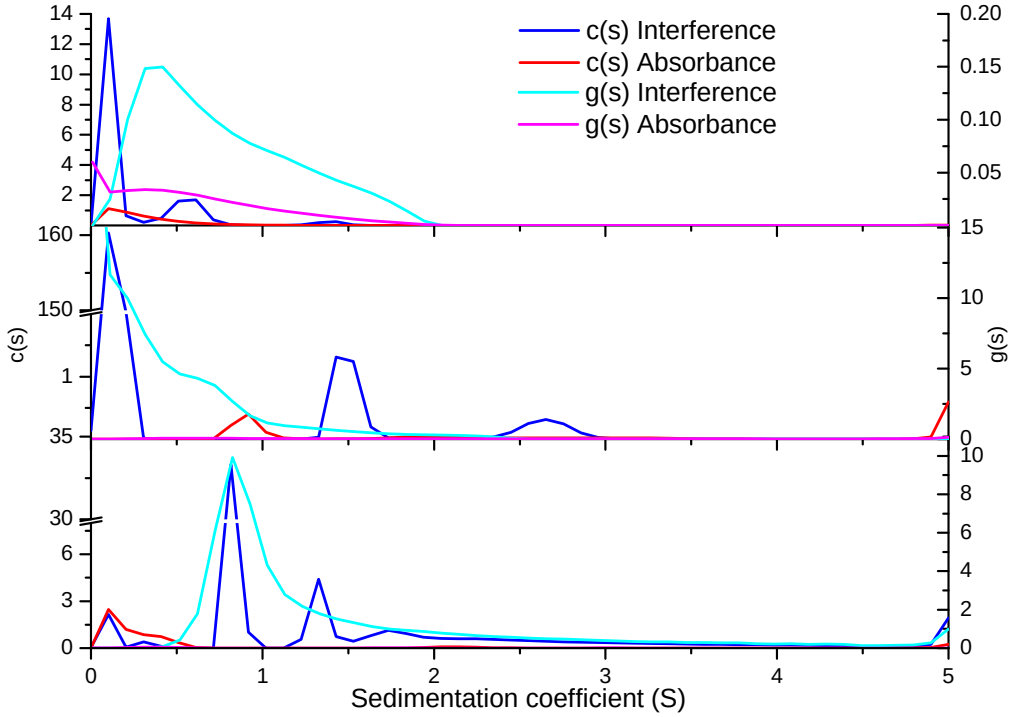

Figure 7.21: Alginate (ALG) mixed with PTDG. Top: PTDG control, middle: ALG control, bottom: 1:1 mixture.

ALG (Figure 7.21) shows peaks at 1.5 and 2.8S according to c(s) interference analysis, although this is not the case for g(s) which only suggests a peak at 0.8S. Absorbance shows peaks at 1 and 2S for c(s). The mixture shows a major peak at 0.9S, which concurs with the g(s) profile from the polysaccharide control. However, the overall shape of the distribution has changed in terms of breadth and position along the abscissa.

7.4.4.2 Carrageenan

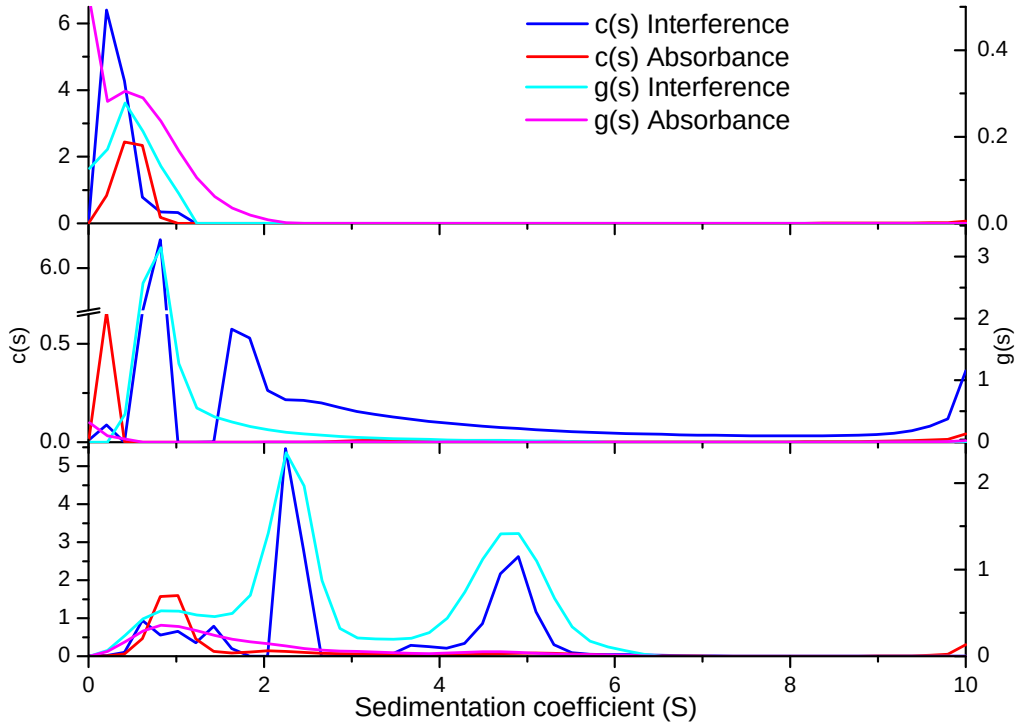

Figure 7.22: Carrageenan (KCG, low DS) mixed with PTDG. Top: PTDG control, middle: KCG control, bottom: 1:1 mixture.

Figure 7.22 shows KCG with a g(s) interference peak at 1S, although c(s) shows a very broad distribution extending beyond 10S. Absorbance signal is limited to species smaller than 0.5S and a small amount of signal at 3S. The mixture shows the PTDG in approximately the same sedimentation position as in the control. The KCG sample has narrowed to two discrete peaks at 2.5 and 5S, with limited evidence of the peak at 1S. Absorbance signal expands up to 5S, however this may be part of the 3S signal observed in the polysaccharide control.

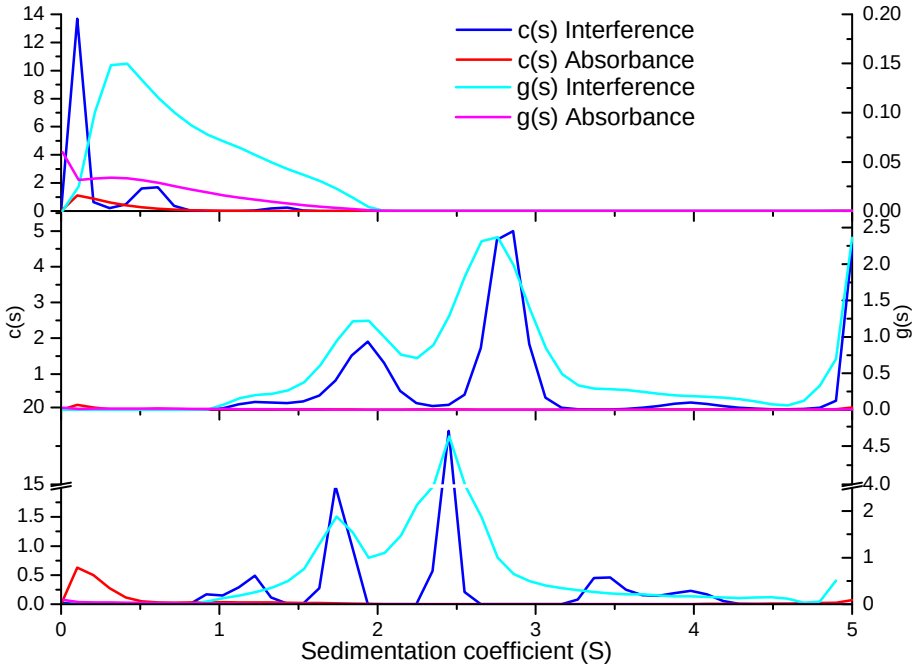

Figure 7.23: Carrageenan (ICG, moderate DS) mixed with PTDG. Top: PTDG control, middle: ICG control, bottom: 1:1 mixture.

ICG (Figure 7.23) presents two main peaks at 2 and 3S, with a larger, minor peak at 4S. These peaks do not change in shape upon the addition of PTDG, but do shift to lower sedimentation coefficients of 1.8, 2.5 and 3.4S respectively. Absorbance signal is minimal throughout the polysaccharide distribution in both control and mixture.

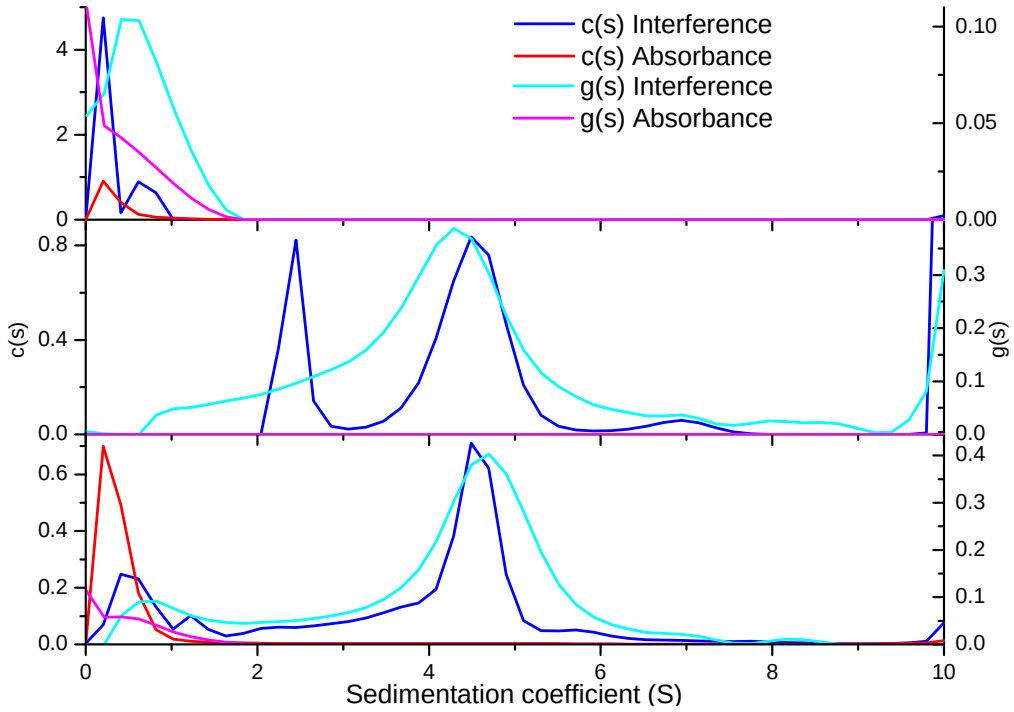

Figure 7.24: Carrageenan (LCG, high DS) mixed with PTDG. Top: PTDG control, middle: LCG control, bottom: 1:1 mixture.

LCG (Figure 7.24) presents a control distribution of three peaks: 2.5, 4.5 and 7S, with evidence of larger components above 10S. The 2.5S peak is present only in the c(s) analysis, which is smoothed over in g(s). The mixture plot shows the same 4.5S peak, but smaller 6S peak, and non-existent 2.5S peak, now presented as shoulders. Absorbance signal is only present, in the mixture plot, as associated with the PTDG region matching closely with the control.

7.4.5 Animal polysaccharides

7.4.5.1 Chitosan

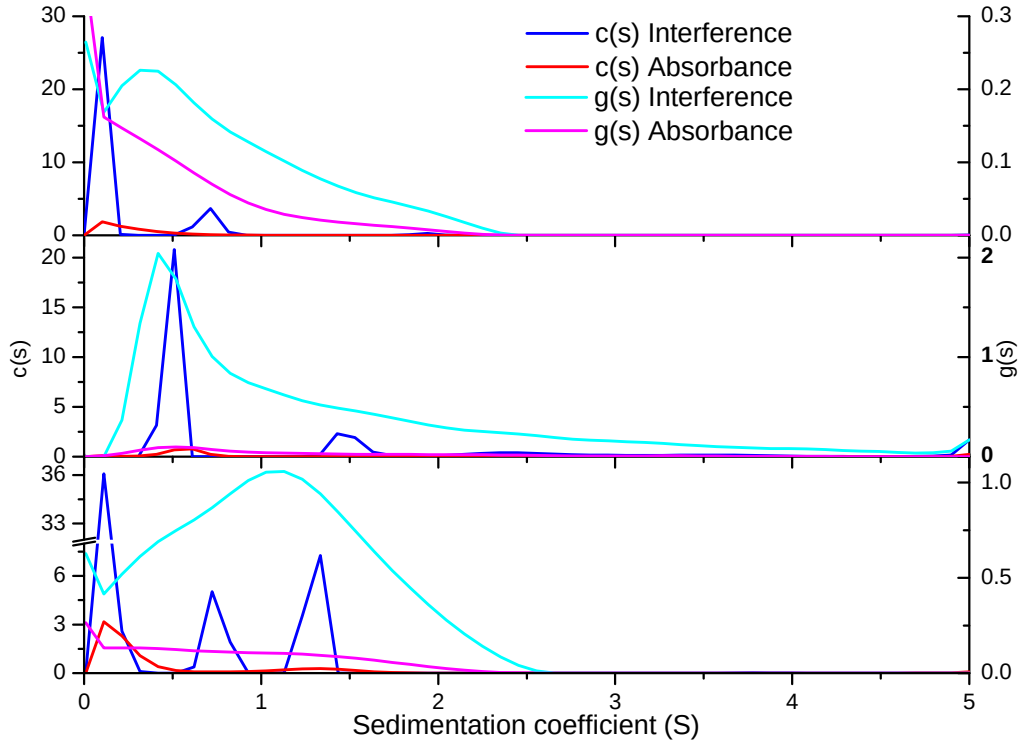

Figure 7.25: Chitosan (CHI) mixed with PTDG. Top: PTDG control, middle: CHI control, bottom: 1:1 mixture.

CHI (Figure 7.25) presents a similar sedimentation coefficient range to PTDG. PTDG acts similarly to previous distributions with g(s) ranging between 0 and 2S. CHI presents the major peak at 0.5S, with a polydisperse tail up to 5S. There is also a limited absorbance signal at the 0.5S peak. The mixture is therefore difficult to interpret in terms of an interaction, since both species are similar in sedimentation coefficient, however there is no evidence of any larger complex being formed beyond 2S.

7.4.5.2 Heparin

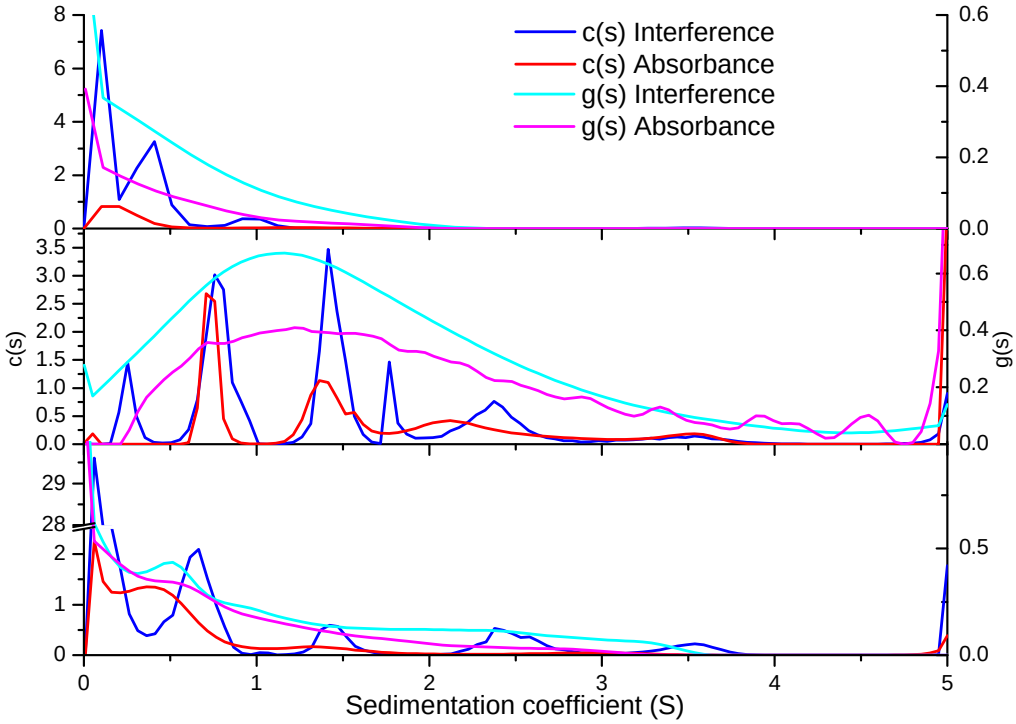

Figure 7.26: Heparin (HEP) mixed with PTDG. Top: PTDG control, middle: HEP control, bottom: 1:1 mixture.

Figure 7.26 shows HEP as a highly polydisperse polysaccharide between 0 and 5S. c(s) attempted to resolve individual peaks at 0.8, 1.5, 2 and 3.5S with both interference and absorbance optics. g(s) interpreted the signal as a broad distribution and is a more likely prediction for the macromolecular composition. When mixed with PTDG, similar peaks are resolved through c(s): 0.5, 1.5, 2.5 and 3.5S. Absorbance signal is present at the 0.5S region as expected with PTDG, but spreads further along with the HEP signal.

7.4.5.3 Hyaluronic acid

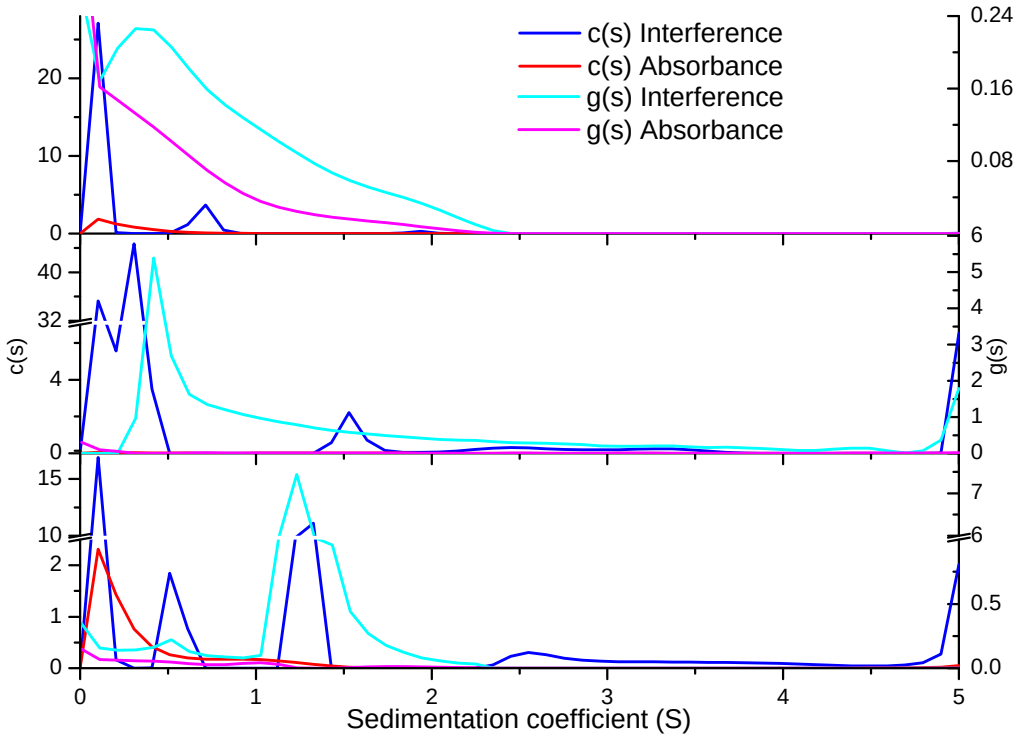

Figure 7.27: Hyaluronic acid (HUA) mixed with PTDG. Top: PTDG control, middle: HUA control, bottom: 1:1 mixture.

HUA (Figure 7.27) presents as a broad distribution with a peak at 0.5S and spreading along the abscissa to 4S. The c(s) algorithm attempted to resolve peaks at 1.5, 2.5 and 3.4S but these are likely to be over-resolved peaks. There is no absorbance present in the HUA control. When mixed with PTDG, the main polysaccharide peak shifts to 1.3S but maintains its breadth of sedimentation coefficients. Absorbance signal remains below 1.5S, consistent only with the PTDG control.

7.4.6 Bacterial polysaccharides

7.4.6.1 Gellan

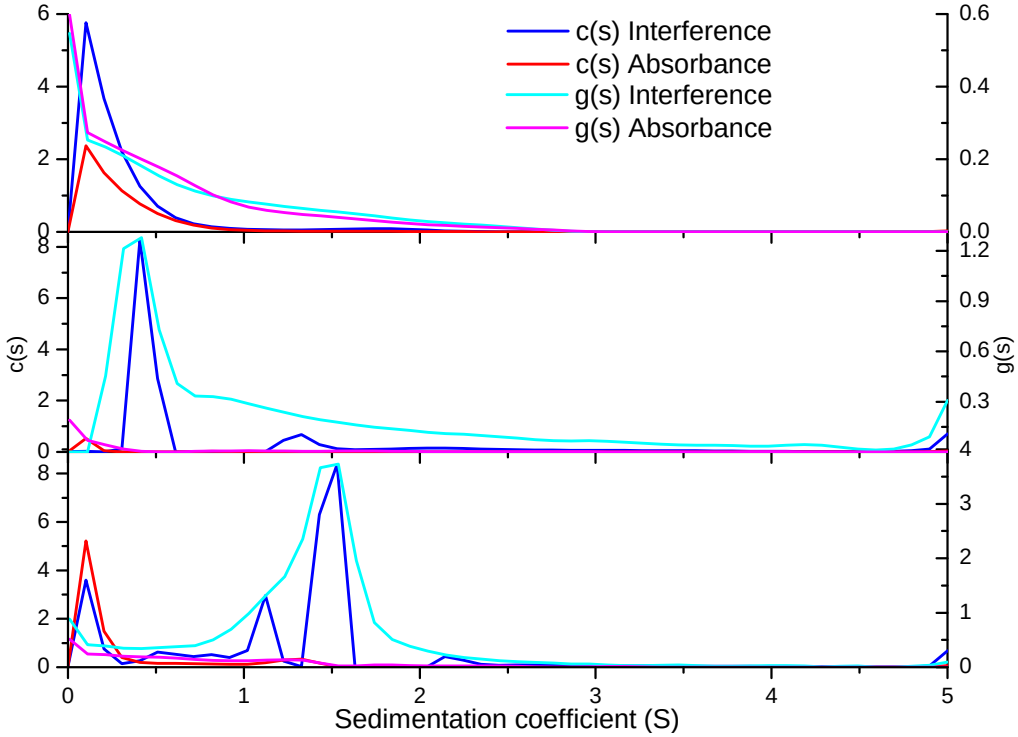

Figure 7.28: Gellan (GEL) mixed with PTDG. Top: PTDG control, middle: GEL control, bottom: 1:1 mixture.

Figure 7.28 shows the mixture between GEL and PTDG. The GEL control has a main peak at 0.5S with a tail extending to 4S. c(s) resolves an extra peak at 1.4S but this is likely to be part of the over-resolved tail. With the addition of PTDG, the main peak shifts to 1.5S and accompanying absorbance signal.

7.4.6.2 Xanthan Gum

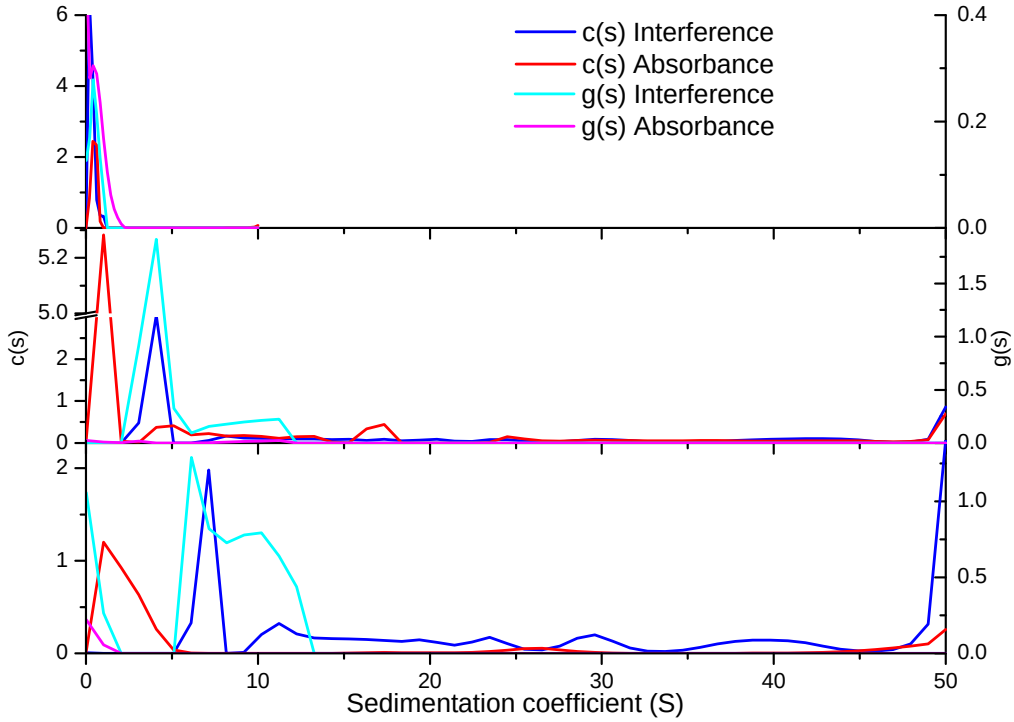

Figure 7.29: Xanthan (XTN) mixed with PTDG. Top: PTDG control, middle: XTN control, bottom: 1:1 mixture.

XTN (Figure 7.29) shows a very large sedimentation coefficient profile, but equally noisy. Peaks from g(s) are at 5 and 10S, and c(s) at 5 (interference) and 17S (absorbance). The reliability of the peak at 17S is limited since the interference optics do not correlate with this peak. The main peak position does not change significantly with addition of PTDG. Absorbance signal is stronger below 5S, which is expected from the PTDG control plot, and noisy above 20S.

7.5 Discussion

7.5.1 PTDG characterisation

A partial characterisation was performed on the pepsin-trypsin digested gliadin (PTDG) sample in terms of molar mass and sedimentation coefficients. Sedimentation velocity c(s) profiles yielded two peaks at 0.5 and 1S. MULTISIG-RADIUS yielded molar masses of these two peaks as 2 and 4kDa respectively. Both methods were able to determine that there was a higher concentration of the smaller component compared to the larger component. Since the MULTISIG-RADIUS output (Figure 7.3) showed no change in the proportion of each component, with increasing concentration, it is unlikely that the two species are related: for example as a monomer-dimer system. This model would also be evident from Figure 7.2 where extrapolated values for the three averages would converge to the same point at infinite dilution.

Previous studies have shown a higher molar mass distribution than has been presented in this investigation. De Ritis et al. (1979) had previously performed size exclusion chromatography on variously digested gliadins. Pepsin-trypsin digested form eluted between 63 and 1kDa, suggesting an incomplete digestion of some of the gliadin in solution. Paganuzzi et al. (1985) reported that their preparation of PT-digest was prepared such that oligomers of 2kDa and smaller were removed through ultrafiltration leaving a range between 2-12kDa. Another study on PT digested gliadins (Bolte et al., 1996) used silver-stained electrophoresis gels yielding a molar mass range of 31-14kDa. These ranges are larger than found in section 7.4.1.2.

It can be concluded that the preparation in this investigation was devoid of any high molar mass/undigested gliadins, based on the absence of high

sedimentation coefficient material in sedimentation velocity analysis and from the low weight average molar mass provided from sedimentation equilibrium.

7.5.2 Amine residue polysaccharides

7.5.2.1 Amino cellulose

Cellulose, a linear polysaccharide made up of β (1→4) linked D-glucopyranose, was modified with amine groups, and a certain number of tosyl groups (Zemljič et al., 2011, Nikolajski et al., 2012). Two samples were tested for interactions with gliadin, labelled "EDA-T1" and "TAEA", the base structure for which shown in Figure 7.30 with varying degrees of R' side groups. Samples were synthesised by Dr. Melanie Nikolajski. The result is a polymer with side-chains that closely resemble amino acid residues, in particular arginine, lysine and phenyl alanine.

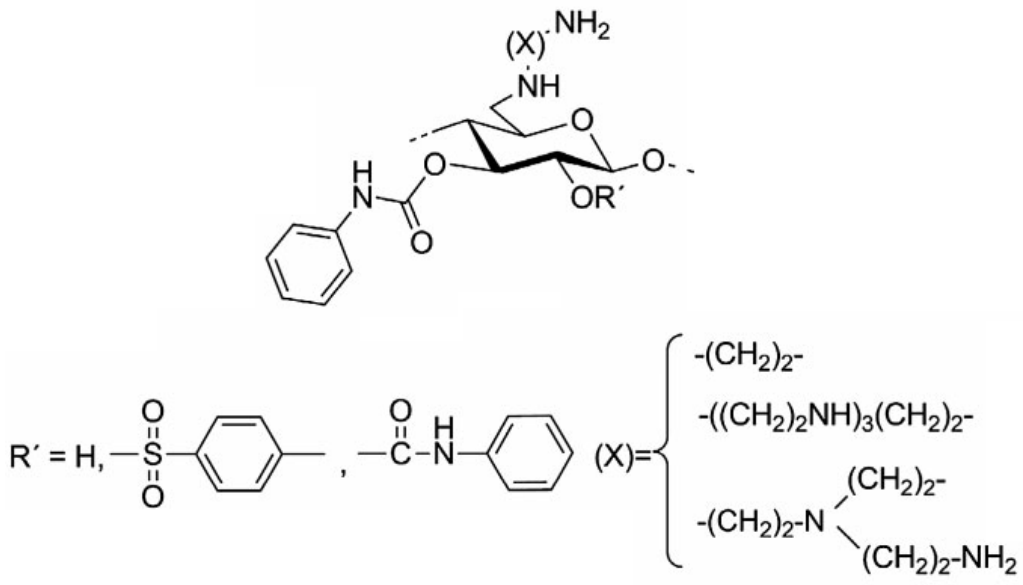

Figure 7.30: Structure of aminocellulose modified with amine groups. Figure adapted from Nikolajski et al. (2012)

Figure 7.15 and Figure 7.16 show mixtures of amino-modified celluloses and PTDG. The peak distributions of the controls are consistent with findings from Nikolajski et al. (2014). Neither mixture plot indicates any interaction with PTDG. One of the properties of these aminocelluloses is the self-association which creates the multiple c(s) peaks (Heinze et al., 2011). The association with its own species has not been replicated with the PTDG.

7.5.2.2 Chitosan

Chitosan is a unique polysaccharide, in that it is positively charged. It is a poly-D-glucosamine and is produced by the deacetylation of insoluble chitin, a structural polysaccharide found in the shells of crustaceans.

The polysaccharide control plot in Figure 7.25 shows two peaks, with the main peak indicating a small amount of absorbance signal. Upon mixture with PTDG the second peak becomes much more significant and there is a shift in the g(s) distribution also. This indicates a possible interaction, although the existence of the absorption signal in the polysaccharide control plot casts some doubt on this conclusion.

7.5.3 Neutral residue polysaccharides

7.5.3.1 Arabinoxylan

Arabinoxylan was purified by Dr. Zdenka Hromádková et al. (2012, 2008). They have a poly β (1→4) D-xylopyranose backbone with α (2→1), (3→1) or (2,3→1) L-arabinofuranose side chains (Mazumder and York, 2010). It is found in plant cell walls, and arabinoxylan in this investigation was purified from wheat (*Triticum aestivum*).

Arabinoxylan was shown to absorb at 280nm (Figure 7.4) which could make a determination of an interaction difficult to conclude. In fact, the

distribution appears to change dramatically when PTDG is added. However, observing the axes shows that the distribution for AX-1 does not change significantly, still reaching an approximate c(s) height of 0.6. The change in number of peaks is likely to be over-resolved c(s) analysis, as evidence by the g(s) analysis.

Arabinoxylans have been labelled as a potential functional food in terms of their pro-immunity and antioxidant qualities (Hromádková et al., 2012). However, in the context of a treatment for Coeliac Disease, it must be remembered that this product primarily comes from wheat which is also the source of gliadin.

7.5.3.2 Galacto/glucomannan

Gum mannan fibres are types of hemicelluoses. Guar gum consists of poly β (1→4) D-mannopyranose with α (1→6) D-galactopyranose branches and has a mannose:galactose ratio of approximately 2:1. Figure 7.6 shows the mixture between GUG and PTDG. Absorbance signal was shown to stay within the PTDG sedimentation coefficient range, and not extend to the GUG peak. Therefore these macromolecules did not interact.

Konjac glucomannan is another hemicellulose similar in rheological behaviour to guar gum but a β (1→4) backbone of both D-mannopyranose and glucopyranose (Williams et al., 2000). Although there is no repeating pattern, the mannose:galactose ratio is between 1.4:1 and 1.6:1 (Bewley and Reid, 1985). This fibre showed no interaction with PTDG. The control peak (Figure 7.7) presented at ~2.3S, which shifted to ~1.9S when mixed with PTDG, however no significant level of absorbance was observed on this peak. It would also be expected that the peak gets faster/heavier rather than slower/lighter.

Locust bean gum (refer to 6.2.2 and Figure 6.5 for structural information) has a mannose:galactose ratio of approximately 4:1. Previous evidence has shown that this polysaccharide interacts with PTDG (Seifert et al., 1995). Figure 7.8 shows that the distribution does not change significantly, and that there is still absorbance signal below 2S but not at the LBG peak. It can therefore be concluded from this experiment that these two macromolecules do not interact. This investigation provided optimum conditions to induce more interactions since the experiment was performed in deionised water, rather than in PBS as per the 1995 results.

7.5.3.3 Hydroxypropyl methylcellulose

HPMC is cellulose which has been modified with organic groups to aid solubility (Figure 7.31). The groups provide steric hindrance to prevent aggregation of cellulose polymers.

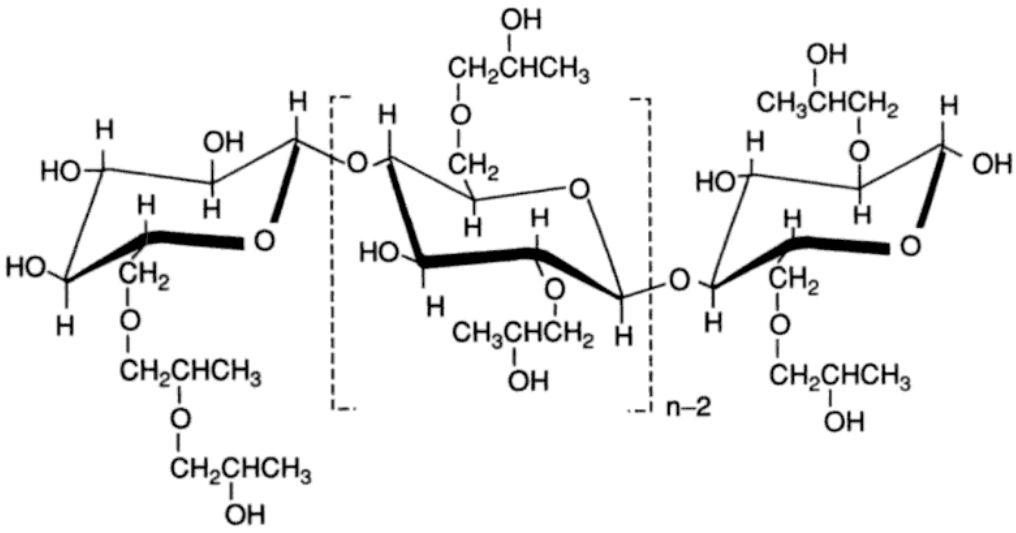

Figure 7.31: Structure of hydroxypropyl methylcellulose backbone (Stephen et al., 2006).

The results from Figure 7.17 show no change in distribution from the control HPMC and added PTDG. Any absorbance is attributed to the PTDG

region for less than 2S. There was therefore no interaction that took place between HPMC and PTDG.

7.5.3.4 Inulin

Inulin is an oligosaccharide comprising β (2→1) linked fructofuranose and usually a terminal glucose. It is found in a range of plants including onion, agave, chicory root, dahlia and Jerusalem artichoke. Two inulins were tested in this investigation: a straight chain polyfructose from agave and a branched polyfructose from chicory root. The two distributions showed different control similar g(s) distributions, both within the range of 0-3S (Figure 7.10 and Figure 7.11). Chicory root inulin showed a single c(s) peak, whereas agave showed two peaks. When PTDG was added to the agave inulin, there was a slight shift of distribution to the right, making room for the PTDG peak. Chicory root c(s) introduced a second peak when PTDG was added, however this is probably an anomaly occurring for the c(s) algorithm. Neither g(s) interference peak changed visibly, and absorbance was the same for the PTDG control and mixture plots. The conclusion is that neither agave (straight chain) nor chicory root (branched) interacted with PTDG.

7.5.3.5 Xyloglucan

Xyloglucan is another type of hemicellulose. The backbone is based on cellulose (poly β-D-glucopyranose) with xylose branches. Xyloglucan results (Figure 7.14) did not show an interaction with PTDG due to the fact that the xyloglucan control did not absorb at 280nm, and neither did the xyloglucan peak in the mixture plot. Any change in the surface of the c(s) interference profile is likely to be due to slight differences in noise levels and c(s) peak normalisation.

7.5.4 Sulphated residue polysaccharides

7.5.4.1 Carrageenan

Carrageenan is a polygalactose found in red seaweed. It is rare within the polysaccharide industry for naturally containing sulphate groups. Different degrees of sulphation give different classes of carrageenan. For example λ-carrageenan is heavily sulphated, κ-carrageenan has little sulphation and ι-carrageenan is in between the two (Sangha et al., 2011). Exact levels of sulphation were not determined. A dn/dc of 0.126ml/g was assumed for all three carrageenans. Although the exact dn/dc of different carrageenans may have varied, the resulting difference in concentration would have been insignificant in reference to the presence of an observable interaction.

From Figure 7.23 (iota) and Figure 7.24 (lambda) it can be observed that, although the addition PTDG changed the peak positions of carrageenan slightly to the left (smaller sedimentation coefficient), there was little evidence of interaction due to the lack of absorbance on the polysaccharide peak. Figure 7.22 (kappa), on the other hand, shows a new well-resolved peak at 5S, with some absorption. However, there is also a small degree of absorption observed on the κ-carrageenan control, so the results of this experiment are inconclusive since the absorbance signal in the mixture could be contributions from either carrageenan or gliadin.

7.5.4.2 Heparin

Heparin is a highly sulphated glycosaminoglycan. It commonly consists of repeating units of α (1→4) 2-O-sulphated L-iduronic acid and β (1→4) 6-O-sulphated, N-sulphated glucosamine.

The mixture of heparin and PTDG (Figure 7.26) shows a change of profile upon the addition of PTDG, however the number of peaks, and peak positions, do not vary greatly. The heparin sample absorbed at 280nm so

identification of an interaction is difficult. No further peaks were produced from the mixture.

7.5.4.3 Xylan sulphate

Xylan sulphate was synthesised from beechwood xylan by Daus et al. (2011). Xylan is similar in structure to cellulose: a poly β (1→4) D-xylopyranose and is normally insoluble in water, however their modification with sulphate groups allows aqueous solutions.

These modified xylans had three degrees of sulphation: DS = 0.35, 1.33 and 1.80, where DS was calculated as 60/(32*[%C/%S]) (Daus et al., 2011). All three xylan sulphate samples appeared to absorb at 280nm, which made a definitive interaction hard to identify, however little difference is observed in any of the three samples between xylan sulphate controls and mixtures (Figure 7.18, Figure 7.19, Figure 7.20).

7.5.5 Uronic residue polysaccharides

7.5.5.1 Alginate

Sodium alginate is polysaccharide from brown seaweed made up of (1→4) linked α-L-glucuronic acid (G) and β-D-mannuronic acid (M) residues, in different combinations. The sequence of this batch of sodium alginate was not determined, but should not contribute greatly to the qualitative presence/absence of an interaction with gliadin.

Alginate is highly non-ideal due to its negative charges and size (Horton et al. 1991). Sodium salt is required to balance out the charges to reduce this effect on non-ideality (Cohen and Priel, 1989). The lack of buffering ions increased the self exclusion effect and this phenomenon caused problems in these experiments. Upon the addition of PTDG (Figure 7.21), the Zwitter-ionic effect of oligopeptides may have increased the buffering

capacity of the system. The lack of ions balancing charges on the extremity of the macromolecule will have maximised the chance of interaction yet no significant change in sedimentation coefficient distribution was observed.

7.5.5.2 Pectin

Pectin is primarily a rhamnogalacturonan with a complex side-branching structure. It has a very complex structure, and can be generalised into High Methoxy and Low Methoxy classes (Morris et al., 2010). The pectin used in this investigation was a highly branched, high methoxy pectin.

Pectin showed no evidence of interaction with PTDG. The absorbance signal did not change from the PTDG control (Figure 7.13) and no larger species formed in the mixture profile.

7.5.5.3 Flax

Flax is considered to be structurally similar to pectin (Naran et al., 2008) with high galactose and rhamnose content (Chernova et al., 2007). Polysaccharide and PTDG plots (Figure 7.5) show similar distributions in terms of sedimentation coefficients, with no larger complexes formed in the mixture plot. It can therefore be concluded that no interaction takes place between the two macromolecules.

7.5.5.4 Gellan

Gellan is a polysaccharide from *Sphingomonas elodea*. It is a polymer of the pattern β (1→4) D-glucopyranose, β (1→4) D-glucuronic acid, β (1→ 4) D-glucopyranose, α (1→3) L-rhamnose. Gellan was tested for an interaction with PTDG, results of which are presented in Figure 7.28. The middle plot shows a main peak at 0.5S, which shifts to 1.5S upon the addition of PTDG. It is possible that these macromolecules interacted considering there is also an increase in absorption signal around this peak.

This is similar to the range found for the PTDG control and therefore may be a false-positive result.

7.5.5.5 Gum arabic

From the Acacia tree, gum arabic is a very complex, branched arabinogalactan (structure described in section 6.2.2.2). The previous investigation in Chapter 6 presented results showing that a reversible interaction exists between gum arabic and whole/native gliadin in deionised water conditions. Figure 7.9 presents the same mixture, but with a digested form of gliadin. The control plot for gum arabic shows a peak at approximately 6S and breadth up to 17S. This is consistent with findings from section 5.3.4, although the key difference is that the characterisation of gum arabic was performed in PBS ionic strength 0.1-0.5M. The mixture plot from Figure 7.9 suggests that the gum arabic component has increased considerably in both the shape of the distribution and size. Further absorbance is also shown up to 10S, suggesting that the PTDG has bound to the gum arabic. However, there still exists a large amount of absorption below 2S, meaning the PTDG has not been completely removed from the system.

7.5.5.6 Hyaluronic acid

Hyaluronic acid is another glycosaminoglycan consisting of repeating sugar units of glucuronic acid and N-acetyl glucosamine, alternating between β (1→3) and β (1→4) linkages. Figure 7.27 shows a shift in sedimentation coefficient of hyaluronic acid towards heavier material when mixed with PTDG. This may be an indication of interaction since there is absorption signal up to the main polysaccharide peak. It is possibly a similar effect to the sodium alginate experiment where PTDG acted as a buffering agent, since the absorbance signal does not shift from the PTDG control. These

results are similar to gellan, in that an interaction is possible, but the absorbance peak is too similar to the PTDG control to be confirmed.

7.5.5.7 4-O-Methylglucuronoxylan

4-O-Methyl glucuronoxylan was purified by Dr. Zdenka Hromádková et al. as per methods described by her publication: (Hromádková et al., 2005). It consists of a xylose backbone with methylated glucuronic acid branching. There was limited evidence of an interaction between 4-O-Methylglucuronoxylan and PTDG (Figure 7.12). Although the distribution did change on the addition of PTDG, there were no larger components created from the mixture and little change in the absorption signal suggesting this either.

7.5.5.8 Xanthan

Xanthan gum is a bacterial polysaccharide from *Xanthomonas campestris*. Its structure is very complex and varies in terms of acetylation and pyruvylation. Its main structure is a cellulose (poly β (1→4) glucopyranose) backbone with β (3→1) D-mannopyranose, β (2→1) D-glucuronic acid, and β (4→1) D-mannopyranose trisaccharide branches. The terminal mannose is often pyruvylated on C4 and C6 although there is variation in pyruvate and acetate content among different sources (Tavallaie et al., 2011).

The mixture between xanthan and PTDG did not present any evidence of an interaction (Figure 7.29) since the absorbance signal did not change greatly upon mixing.

7.5.6 Polysaccharide interaction summary

The results from this chapter are summarised in Table 7.3. Interactions are classed as positive (+), negative (-) or inconclusive (+-).

+- designations were assigned to those polysaccharides where either there was a weak interaction or where it was not possible to determine whether there was an interaction or not. Polysaccharides are grouped by source (natural plant, modified plant, seaweed, animal and bacterial), then alphabetical, with a 1 letter designation to their functional residue composition (A: amine, N: neutral, S: sulphated, U: uronic acid).

All polysaccharides were mixed with gliadin in deionised water, except for the two amino-celluloses, which were tested in PBS 0.1M pH6.8, to aid solubility.

Four amine polysaccharides were tested: chitosan, heparin, hyaluronic acid and amino-modified cellulose. Heparin and hyaluronic acid are classed as glycosaminoglycans and also contain uronic acid groups. Hyaluronic acid and chitosan were both classed as possible/inconclusive interactants whereas heparin and aminocellulose conclusively did not interact.

Table 7.3: Summary of interactions of non-dietary fibres with PTDG. (+) positive interaction; (+-) inconclusive or possible interaction; (-) negative interaction. Residue types: A (amine) N (neutral) S (sulphated) U (uronic acid).

Source	Polysaccharide	Residue	Interact
Natural plant	Arabinoxylan	N	-
	Flax	U	-
	Guar gum	N	-
	Konjac	N	-
	Locust bean gum	N	-
	Gum arabic	U	+
	Agave inulin	N	-
	Chicory inulin	N	-
	4-O-Methyl glucuronoxylan	U	-
	Pectin	U	-
	Xyloglucan	N	-
Modified plant	EDA-T1	A	-
	TAEA	A	-
	HPMC	N	-
	XS035	S	-
	XS133	S	-
	XS180	S	-
Seaweed	Alginate	U	-
	κ-carrageenan	S	+-
	ι-carrageenan	S	-
	λ-carrageenan	S	-
Animal	Chitosan	A	+-
	Heparin	ASU	-
	Hyaluronic acid	AU	+-
Bacterial	Gellan	U	+-
	Xanthan	U	-

None of the eight neutral polysaccharides interacted with PTDG. Evidence from Seifert et al. (1995) suggested that galactomannan, as a group of polysaccharides, might be capable of interacting to some degree with both whole gliadin and PTDG based on concentration dependence of the sedimentation coefficient for the LBG-PTDG mixture. Using the more detailed procedure here these interactions were not found to be significant not only for LBG but also for guar gum and konjac glucomannan.

Three sulphated polysaccharides were also tested including carrageenan, heparin and sulphate-modified xylan. The theory behind the selection of

sulphated polysaccharides was based on the research by Liang et al. (2009), who used pHEMA-co-SS with different degrees of SS content. Carrageenan and xylan sulphate were both tested at three degrees of sulphation. The only possible candidate, from this group of polysaccharides, was kappa carrageenan which has a very low degree of sulphation. Even so, this interaction was not definitive, and failed to remove the gliadin completely from the system. The other polysaccharides did not show any signs of interaction.

Uronic acid polysaccharides were the most promising class of polysaccharide in this investigation for interacting with PTDG. Gum arabic showed a potential interaction with PTDG, which supports the findings from Chapter 6. There was a strong trend for the PTDG to significantly change the profile of the polysaccharide. For example, sodium alginate, hyaluronic acid and gellan changed in distribution upon the addition of PTDG, posited to be through a Zwitter-ionic effect balancing surface charges on the polysaccharides. For hyaluronic acid and gellan, the results were inconclusive due to the presence of absorbance signal at the polysaccharide peak and coinciding with the PTDG control absorbance profile. A higher affinity on behalf of uronic group polysaccharides is surprising since it has been shown that sulphated polysaccharides interact more strongly with proteins than uronic acids (Doublier et al., 2000).

The use of gum arabic for a macromolecular barrier was also discussed previously (section 6.3.3), although this was in the context of undigested gliadin. The purpose of assaying a pepsin-trypsin digested form was to show a more physiologically relevant form of gliadin, as it would present itself in the small intestine. Although there is evidence of an interaction from this investigation, it was not a complete removal of gliadin from the

system. It is also likely to be a reversible interaction as was found for the undigested gliadin results (section 6.3.3.2).

The mechanism of the whole-gliadin interaction was shown to be ionic (section 6.3.3.2) but has not been clarified in terms of exact functional groups on the gum arabic macromolecule. Uronic acid groups were a potential candidate for the existence of this interaction; however other polysaccharides, with uronic acid groups, were tested with no evidence of interaction. Gliadin contains a high proportion of glutamine (~35%) with the protein consisting of nearly 50% non-polar hydrophilic amino acids. Hydrophobic residues make up 30%, and proline makes up approximately 14% of the peptide structure (Kasarda et al., 1984). Thus, a uronic residue interaction would probably coincide with the glutamine residues.

7.6 Conclusion

A range of polysaccharides, varying in sugar residue composition (amine, neutral, sulphonated and uronic acid) and source (natural/synthetic plant, seaweed, animal, bacterial), were tested for interaction with a pepsin-trypsin digested gliadin. Of the 26 polysaccharides tested, only one was shown to interact significantly with PTDG: gum arabic, a densely-packed, high molar mass, uronic acid polysaccharide. This interaction is consistent with results from the previous chapter. Other polysaccharides which showed potential interactions, or inconclusive results, were kappa carrageenan, chitosan, gellan and hyaluronic acid.

The scope of this investigation did not include an exact mechanism for the interaction and is, thus, undetermined. Gum arabic, gellan and hyaluronic acid are all uronic acid polysaccharides, but there were five other examples

of uronic acid polysaccharides which did not interact. These polysaccharides also ranged in macromolecular conformation.

None of these interactions showed a complete removal of gliadin from the system, even gum arabic. This would suggest that these polymers would not act as an effective macromolecular barrier against the immune system. A complete removal would have been shown by faster-sedimenting, absorbing species being formed and no/little absorbance signal remaining between 0 and 1S.

Further research could be conducted on the conditions required to attain a complete, and permanent, interaction between gum arabic and PTDG. The study could focus on specific parts of the gum arabic molecule and regions of immunogenic gliadin polypeptides.

8 Conclusions and suggestions for future work

In the series of investigations which form the various parts of this thesis hydrodynamics, light scattering and other related techniques have been utilised to characterise quasi-permanent protein-polysaccharide complexes (Chapters 3-5) and assess non-permanent interactions between polysaccharides and protein/polypeptide (Chapters 6-7). Advancements in methodology, primarily in analytical ultracentrifugation, for both sedimentation velocity and equilibrium, were developed and applied. Below describes the conclusions made from these investigations and an outline of possibilities for future work.

8.1 Methodology

8.1.1 Sedimentation velocity

Sedimentation velocity was performed in all results chapters of this investigation. It was critical in the characterisation of protein-polysaccharide complexes and in the observations of non-permanent interactions between protein and polysaccharide. The use of dual-optical systems (280nm absorbance and Rayleigh Interference) provided information on the presence/interaction of proteins (absorbing) and polysaccharides (non-absorbing).

The advantage of this method is the high resolution output of distributions of sedimentation coefficients, with a general rule that larger Svedberg

components are larger in size. However, especially concerning the difference between protein and polysaccharide, the shape has a large effect on the sedimentation coefficient of a macromolecule. The Extended Fujita Approach was utilised to convert sedimentation coefficient distributions into molar mass distributions by using information about shape and size of macromolecules. The major disadvantage to this method is prior knowledge of the macromolecule in question. Either the macromolecule needs to be fully characterised, with a large amount of published data concerning molar masses and sedimentation coefficients (as was found for mucin, see chapter 3), or assumptions need to be made about a single molar mass-sedimentation coefficient pairing and the shape factor. For example, a different Mark Houwink Kuhn Sakurada (MHKS) shape parameter (obtained through intrinsic viscosity, diffusion coefficient or radius of gyration information) could be used to estimate the sedimentation shape factor.

For newly characterised macromolecules this method may be inappropriate, but for well-characterised macromolecules this method provides a fast and reliable molar mass distribution determination.

8.1.2 Sedimentation equilibrium

Many advances were made in the field of sedimentation equilibrium analysis during these investigations. SEDFIT-MSTAR is a modern incorporation of the MSTAR algorithm into the popular SEDFIT package. Combined with the c(M) algorithm, it allowed a fast and reliable evaluation of sedimentation equilibrium data for the determination of weight average molar masses of polydisperse systems. It also performs a basic quantitative evaluation of the polydispersity index, through the c(M)

algorithm, and a qualitative check on the non-ideality of the system with the hinge-point method.

SEDFIT-MSTAR is a significantly faster program, but is less resolving, compared to MULTISIG. With the latter, processing time is reliant on the simultaneous fitting of 17 discrete species. However, this processing time cost is balanced by the larger amount of information provided by MULTISIG. A distribution of molar masses can be obtained, which is particularly useful for multi-modal distributions, along with z-, weight and number averages. MULTISIG-RADIUS provides extra information by performing this fitting multiple times across the column providing molar mass vs. radius/concentration plots.

Both algorithms are useful in their own respects: MULTISIG/RADIUS provides comprehensive information about the system at significant cost to processing time and assumes thermodynamic ideality; whereas SEDFIT-MSTAR is much faster, takes account of non-ideality but is more basic in its analysis. In the future, MULTISIG will benefit from faster processors and/or multi-threading, both decreasing analysis time and increasing resolution of molar masses.

8.2 Mucin characterisation

Human Gastric Mucin, a well characterised macromolecule, was purified and assessed for molecular integrity using the newly published Extended Fujita Method.

Ultrafiltration and isopycnic density-gradient ultracentrifugation were used to purify mucins from gastric aspirate from a healthy patient. An antibody dot blot test (HRP-anti MUC5AC) confirmed the presence of two species of

mucin and pooled separately. These preparations were preserved primarily in 6M guanidine hydrochloride (GuHCl), a common denaturing preservative for mucins. They were also dissolved in phosphate buffered saline (PBS) with low concentration preservatives: EDTA (a chelator) and sodium azide (a potent antiseptic).

Weight average molar mass was assessed using SEC-MALS and sedimentation velocity analysed using the Extended Fujita Approach. A literature search was performed (refer to Appendix 1) to find weight average molar mass-sedimentation coefficient pairs of mucins. A double-logarithmic plot yielded the MHKS parameters which were used for the Extended Fujita data analysis. The data provided the opportunity to assess the shape factor difference between mucins in GuHCl and in PBS. The shape factor was lower (more extended) in GuHCl which is consistent with the denaturation properties of the salt. It was also found that GuHCl conditions yielded much higher molar masses than PBS with low concentration preservatives. Therefore GuHCl provided more protection than these additives but at the cost of a change in macromolecular conformation.

Weight average molar mass was found to be similar between the two methods. The Extended Fujita Approach was capable of providing a high resolution molar mass distribution. In a complex solvent, such as high molar GuHCl which would not normally go through chromatographic columns at the risk of destruction of the column, the Extended Fujita Approach was still able to provide molar mass information.

Future work

SEC-MALS analysis was performed without an on-line pressure imbalance differential viscometer, due to technical reasons at the time of the

investigation. Further work could include this apparatus and cover the MHKS parameters yielded from combined intrinsic viscosity and molar mass data ([η]-M pairings) as was found in Chapter 5 with gum arabic. It would be predicted to corroborate with literature search s-M pairings. Sedimentation equilibrium could also be performed, with the new analysis techniques, to further corroborate the findings from velocity and MALS, especially for difficult solvent conditions (GuHCl).

8.3 Pumpkin protein-polysaccharide complex extract

It was posited that extracts from *Cucurbita* sp. provided anti-diabetic properties on human physiology. Diabetes Mellitus, a highly prevalent disease, is the inability of the body to regulate its own glucose levels. Current treatment is based on injecting insulin and there has been a drive to find alternative, preventative and less invasive treatments.

Protein-polysaccharide complex (PBPP) was purified from pumpkin powder. Hydrodynamic techniques, such as density measurement, viscometry, sedimentation and equilibrium (SV and SE), were used to assess the molecular integrity of this component.

Intrinsic viscosity and partial specific volume verified the presence of a mixture between protein and polysaccharide. Proportions of protein and polysaccharide were consistent with literature values thus verifying that the method used was appropriate for extraction of PBPP. SV and SE, used to probe the distributions of sedimentation coefficients and molar masses, found a main peak, a smaller protein-rich peak and an unidentified high molar mass, highly polydisperse component.

Future work

This information is useful for the research into alternative treatments for Diabetes Mellitus. The use of any new therapeutic requires a good understanding of the molecular structure, as well as function. Future work would include fractionation of peaks indentified by SV and SE in order to individually characterise them. As it stands, the information on partial specific volume and intrinsic viscosity are weight averages of the entire distribution. It would also be beneficial to use light scattering techniques, such as SEC-MALS and DLS. Light scattering has a disadvantage that polydisperse and heterogeneous systems are not easily analysable. Separation techniques (either fractionation or SEC) would aid the use of these techniques. Once these components are fully characterised, they can be assessed for their anti-diabetic function within cell cultures and animal studies.

From a culinary perspective, pumpkin is usually heated/cooked before ingestion. Although this purification did involve heat treatment to 50^{o}C this temperature is not necessarily high enough for macromolecules to undergo significant bioprocessing. Thus it would be ideal to characterise the components after heat treatment. This could be performed in a controlled fashion via autoclaving (121^{o}C) or boiling (100^{o}C) for specific time periods. The efficacy of these components on anti-diabetic effects could be compared before and after heat processing.

8.4 Gum arabic

Gum arabic is an arabinogalactan extracted from the Acacia tree. In this investigation its macromolecular conformation was assessed, using hydrodynamic techniques, in three varying ionic strength buffers. This

investigation uses analytical ultracentrifugation, specifically sedimentation velocity, to assess gum arabic for the first time.

Data from DLS, viscometry, density measurement, SV and SEC-MALLS were used to show that the macromolecule is a high molar mass, fairly compact glycoprotein. SingleHydFit was used to combine these techniques to find an ellipsoid structure: an oblate (axial ratio = 4-14). In general increasing ionic strength decreased the axial ratio and increasing molar mass increased axial ratio.

SEC-MALS was able to yield a large amount of information including molar mass averages and intrinsic viscosity. The angular dependence of scatter is theoretically capable of measuring the radius of gyration, but for visible light scattering techniques there is a limit of approximately 30nm. The values found in this investigation were 20-30nm and are thus borderline within range. The ratio of radii of gyration and hydration provides limited information on the conformation, but is complicated by the polydispersity.

Future work

Radius of gyration could be confirmed using Small Angle X-ray Scattering (SAXS). This has been performed by other groups but recent advances in the technique, such as SEC-SAXS, could provide more information on this polydisperse material. If fractionated by SEC-MALS/SAXS, the gyration/hydration ratio could be observed over a range of molar masses.

8.5 Interaction between polysaccharides and gliadin

Gliadin is a prevalent protein used in western cuisine, but also causes an inflammatory response in approximately 1% of the population. It was posited that gliadins could be hidden from the immune system by an interaction with a non-digestible fibre.

Two sets of experiments were performed: whole/native/undigested gliadin (Chapter 6) and pepsin-trypsin digested gliadin (Chapter 7) were assayed against various polysaccharides using sedimentation velocity. Chapter 6 focussed on two polysaccharides which, according to the literature, were shown to interact with gliadin: locust bean gum, a neutral galactomannan, and gum arabic, described earlier in Chapter 5. Locust bean gum was ruled out as an interacting species. Gum arabic showed a promising interaction with whole gliadin. In deionised water conditions, a reversible interact was observed, but was slightly suppressed in PBS and completely suppressed in a Gastric Fluid Analogue.

Chapter 7 took a more comprehensive approach by assaying gliadin, in a more physiologically-relevant, digested form (PTDG), against 26 polysaccharides ranging in composition and active groups. They included amino, sulphated, neutral and uronic polysaccharides. Sedimentation velocity with dual optical systems was used to assess whether a polysaccharide peak gained a significant level of absorbance upon mixing with PTDG. Many of the polysaccharides conclusively did not interact and four were either a weak or inconclusive interaction. Gum arabic showed an interaction, similar to the interaction observed in Chapter 6. Although the exact mechanism for this interaction was not assessed in this investigation

suppression of all interactions under high ionic strength and acidity suggested an electrostatic attraction.

Future work

The main problem with this interaction is its reversibility. An increase in gum arabic proportion was not able to show a complete removal of free gliadin from the system, thus presenting equilibrium. Further studies may elucidate the kinetics of this interaction, for example with the use of Isothermal Titration Calorimetry, but without information on the stoichiometry of the interactants it would be difficult to yield accurate dissociation constants. Molecular dynamics could also be used; but there are complications that there is no crystal structure for gliadin, nor precise structure for gum arabic from electron microscopy (at time of writing).

With reversibility comes the problem of the inability of the polysaccharide to completely hide gliadin from the immune system. Future work could include researching how to make the interaction permanent. This could be through heating which would replicate a real-life application of this treatment, i.e. adding gum arabic to bread dough before baking. The resulting mixture would need to be tested whether:

1) The interaction is still present after heating;
2) The interaction becomes permanent after heating;
3) The resulting complex is resistant to human digestive processes (enzymes, bile salts, mucins etc.);
4) The complex hides the gliadin from the immune system.

In regard to point 4), the work presented in Chapters 6 and 7, on *in vitro* interactions between gliadin and a macromolecular barrier, did not take into account *in situ* conditions. There has been a large amount of research on CACO-2 cell lines, epithelial cells from the small intestines, where

polysaccharides have been added to the surface and the immune response has been reduced. This suggests that an interaction may not need to take place between the gliadin and polysaccharide *per se* but in fact may be effective if polysaccharides can bind to the epithelia and repel gliadin. Furthermore, if a polysaccharide-gliadin complex were to bind to mucins, it may actually aid the adsorption of immunogenic gliadin sequences.

References

ADAMS, G. G., IMRAN, S., WANG, S., MOHAMMAD, A., KOK, M. S., GRAY, D. A., CHANNELL, G. A. & HARDING, S. E. 2014. The Hypoglycemic Effect of Pumpkin Seeds, Trigonelline (TRG), Nicotinic Acid (NA), and D-Chiro-inositol (DCI) in Controlling Glycemic Levels in Diabetes Mellitus. *Critical Reviews in Food Science and Nutrition,* 54**,** 1322-1329.

ADAMS, G. G., IMRAN, S., WANG, S., MOHAMMAD, A., KÖK, M. S., GRAY, D. A., CHANNELL, G. A., MORRIS, G. A. & HARDING, S. E. 2011. The hypoglycaemic effect of pumpkins as anti-diabetic and functional medicines. *Food Research International,* 44**,** 862-867.

ADAMS, G. G., IMRAN, S., WANG, S., MOHAMMAD, A., SAMIL KOK, M., GRAY, D. A., CHANNELL, G. A. & HARDING, S. E. 2012a. Extraction, isolation and characterisation of oil bodies from pumpkin seeds for therapeutic use. *Food Chemistry,* 134**,** 1919-1925.

ADAMS, G. G., KÖK, M. S., IMRAN, S., HARDING, S. E., ILYAS, M. & TATHAM, A. S. 2012b. The interaction of dietary fibres with disulphide bonds (SS) and a potential strategy to reduce the toxicity of the gluten proteins in coeliac disease. *Biotechnology & Genetic Engineering Reviews,* 28**,** 115.

ALAEDINI, A. & GREEN, P. H. R. 2005. Narrative review: Celiac Disease: Understanding a Complex Autoimmune Disorder. *Annals of Internal Medicine,* 142**,** 289-298.

ALFTRÉN, J., PEÑARRIETA, J. M., BERGENSTÅHL, B. & NILSSON, L. 2012. Comparison of molecular and emulsifying properties of gum arabic and mesquite gum using asymmetrical flow field-flow fractionation. *Food Hydrocolloids,* 26**,** 54-62.

ALI, B. H., ZIADA, A. & BLUNDEN, G. 2009. Biological effects of gum arabic: a review of some recent research. *Food and Chemical Toxicology,* 47**,** 1-8.

ANDRES-BRULL, M., AL-ASSAF, S., PHILLIPS, G. O. & JACKSON, K. 2013. Optimisation of asymmetrical flow-field fractionation for the characterisation of gum arabic (Acacia sengal var senegal) and comparison with gel permeation chromatography. *Analytical Methods,* 5**,** 4047-4052.

ANG, S. 2009. *Hydrodynamic studies on polysaccharides and their interactions.* PhD, University of Nottingham.

ANG, S., KOGULANATHAN, J., MORRIS, G. A., KÖK, M. S., SHEWRY, P. R., TATHAM, A. S., ADAMS, G. G., ROWE, A. J. & HARDING, S. E. 2010. Structure and Heterogeneity of Gliadin: A Hydrodynamic Evaluation. *European Biophysics Journal with Biophysics Letters,* 39**,** 255-261.

ARAGON, S. R. 2011. Recent advances in macromolecular hydrodynamic modeling. *Methods,* 54**,** 101-114.

AUDIE, J. P., JANIN, A., PORCHET, N., COPIN, M. C., GOSSELIN, B. & AUBERT, J. P. 1993. Expression of Human Mucin Genes in Respiratory, Digestive and Reproductive Tracts Ascertained by in-situ Hybridization. *Journal of Histochemistry & Cytochemistry,* 41**,** 1479-1485.

AZIAH, A. & KOMATHI, C. 2009. Physicochemical and functional properties of peeled and unpeeled pumpkin flour. *Journal of Food Science,* 74**,** S328-S333.

BANSIL, R. & TURNER, B. S. 2006. Mucin structure, aggregation, physiological functions and biomedical applications. *Current Opinion in Colloid & Interface Science,* 11**,** 164-170.

BASSO, M., LUCIANO, R., FERRETTI, F., MURACA, M., PANETTA, F., BRACCI, F., OTTINO, S. & DIAMANTI, A. 2012. Association between celiac disease and primary lactase deficiency. *European Journal of Clinical Nutrition,* 66**,** 1364-1365.

BECKWITH, A. C., NIELSEN, H. C., WALL, J. S. & HUEBNER, F. R. 1966. Isolation and Characterization of a High-Molecular-Weight Protein from Wheat Gliadin. *Cereal Chemistry,* 43**,** 14.

BERG, J. M., TYMOCZKO, J. L., STRYER, L. & GATTO, G. J. 2012. *Biochemistry*, WH Freeman and Co.

BEWLEY, J. & REID, J. 1985. *Biochemistry of storage carbohydrates in green plants (pp. 289–304)*, New York: Academic Press.

BOLTE, G., OSMAN, A., MOTHES, T. & STERN, M. 1996. Peptic-tryptic digests of gliadin: contaminating trypsin but not pepsin interferes with gastrointestinal protein binding characteristics. *Clinica Chimica Acta,* 247**,** 59-70.

BREWER, A. K. & STRIEGEL, A. M. 2009. Particle size characterization by quadruple-detector hydrodynamic chromatography. *Analytical and Bioanalytical Chemistry,* 393**,** 295-302.

BUCHNER, P., COOPER, R. & WASSERMANN, A. 1961. 774. Influence of counter-ion fixation on molecular weight and shape of a polyelectrolyte. *Journal of the Chemical Society (Resumed)***,** 3974-3983.

BURCHARD, W. 1992. Static and dynamic light scattering approaches to structure determination of biopolymers. Royal Society of Chemistry, Cambridge, UK.

BURCHARD, W., SCHMIDT, M. & STOCKMAYER, W. H. 1980. Information on Polydispersity and Branching from Combined Quasi-Elastic and Intergrated Scattering. *Macromolecules,* 13**,** 1265-1272.

CAPUTO, I., BARONE, M. V., LEPRETTI, M., MARTUCCIELLO, S., NISTA, I., TRONCONE, R., AURICCHIO, S., SBLATTERO, D. & ESPOSITO, C. 2010. Celiac anti-tissue transglutaminase antibodies interfere with the uptake of alpha gliadin peptide 31–43 but not of peptide 57–68 by epithelial cells. *Biochimica et Biophysica Acta (BBA)-Molecular Basis of Disease,* 1802**,** 717-727.

CARLSTEDT, I., LINDGREN, H., SHEEHAN, J. K., ULMSTEN, U. & WINGERUP, L. 1983. Isolation and Characterization of Human Cervical-Mucus Glycoproteins. *Biochemical Journal,* 211**,** 13-22.

CHERNOVA, T., GUR'YANOV, O., BRACH, N., PAVLOV, A., POROKHOVINOVA, E., KUTUZOVA, S., CHEMIKOSOVA, S. & GORSHKOVA, T. 2007. Variability in the composition of tissue-specific galactan from flax fibers. *Russian Journal of Plant Physiology,* 54**,** 782-789.

CHOURPA, I., DUCEL, V., RICHARD, J., DUBOIS, P. & BOURY, F. 2006. Conformational Modifications of Alpha Gliadin and Globulin Proteins upon Complex Coacervates Formation with Gum Arabic as Studied by Raman Microspectroscopy. *Biomacromolecules,* 7**,** 2616-2623.

COHEN, J. & PRIEL, Z. 1989. Viscosity of dilute polyelectrolyte solutions: concentration dependence on sodium chloride, magnesium sulfate and lanthanum nitrate. *Macromolecules,* 22**,** 2356-2358.

COLE, J. L., LARY, J. W., MOODY, T. P. & LAUE, T. M. 2008. Analytical ultracentrifugation: sedimentation velocity and sedimentation equilibrium. *Methods in Cell Biology,* 84**,** 143-179.

CÖLFEN, H. & HARDING, S. E. 1997. MSTARA and MSTARI: Interactive PC Algorithms for Simple, Model Independent Evaluation of Sedimentation Equilibrium Data. *European Biophysics Journal with Biophysics Letters,* 25**,** 333-346.

CREETH, J. M., BHASKAR, R. K., HORTON, J. R., DAS, I., LOPEZVIDRIERO, M. T. & REID, L. 1977. Separation and Characterization of Bronchial Glycoproteins by Density-Gradient Methods. *Biochemical Journal,* 167**,** 557-569.

CREETH, J. M. & HARDING, S. E. 1982. Some Observations on a New Type of Point Average Molecular-Weight. *Journal of Biochemical and Biophysical Methods,* 7**,** 25-34.

DARE, R., MAGEE, J. & MATHISON, G. 1972. In-vitro studies on the bactericidal properties of natural and synthetic gastric juices. *Journal of Medical Microbiology,* 5**,** 395-406.

DAUS, S., PETZOLD-WELCKE, K., KÖTTERITZSCH, M., BAUMGAERTEL, A., SCHUBERT, U. S. & HEINZE, T. 2011. Homogeneous sulfation of xylan from different sources. *Macromolecular Materials and Engineering,* 296**,** 551-561.

DAVIES, J. R., HOVENBERG, H. W., LINDEN, C. J., HOWARD, R., RICHARDSON, P. S., SHEEHAN, J. K. & CARLSTEDT, I. 1996. Mucins in Airway Secretions from Healthy and Chronic Bronchitic Subjects. *Biochemical Journal,* 313**,** 431-439.

DE RITIS, G., OCCORSIO, P., AURICCHIO, S., GRAMENZI, F., MORISI, G. & SILANO, V. 1979. Toxicity of wheat flour proteins and protein-derived peptides for in vitro developing intestine from rat fetus. *Pediatric Research,* 13**,** 1255-1261.

DEACON, M., DAVIS, S., WHITE, R., NORDMAN, H., CARLSTEDT, I., ERRINGTON, N., ROWE, A. & HARDING, S. 1999. Are chitosan–mucin interactions specific to different regions of the stomach? Velocity ultracentrifugation offers a clue. *Carbohydrate Polymers,* 38**,** 235-238.

DEACON, M. P., DAVIS, S. S., WAITE, J. H. & HARDING, S. E. 1998. Structure and Mucoadhesion of Mussel Glue Protein in Dilute Solution. *Biochemistry,* 37**,** 14108-14112.

DEACON, M. P., MCGURK, S., ROBERTS, C. J., WILLIAMS, P. M., TENDLER, S. J. B., DAVIES, M. C., DAVIS, S. S. & HARDING, S. E. 2000. Atomic Force Microscopy of Gastric Mucin and Chitosan Mucoadhesive Systems. *Biochemical Journal,* 348**,** 557-563.

DEMELER, B. 2005. UltraScan: a comprehensive data analysis software package for analytical ultracentrifugation experiments. *Modern Analytical Ultracentrifugation: Techniques and Methods***,** 210-229.

DHAMI, R., HARDING, S. E., JONES, T., HUGHES, T., MITCHELL, J. R. & TO, K.-M. 1995. Physico-chemical studies on a commercial food-grade xanthan—I. Characterisation by sedimentation velocity, sedimentation equilibrium and viscometry. *Carbohydrate Polymers,* 27**,** 93-99.

DODD, S., PLACE, G. A., HALL, R. L. & HARDING, S. E. 1998. Hydrodynamic Properties of Mucins Secreted by Primary Cultures of Guinea-Pig Tracheal Epithelial Cells: Determination of Diffusion Coefficients by Analytical Ultracentrifugation and Kinetic Analysis of Mucus Gel Hydration and Dissolution. *European Biophysics Journal with Biophysics Letters,* 28**,** 38-47.

DOUBLIER, J.-L., GARNIER, C., RENARD, D. & SANCHEZ, C. 2000. Protein–polysaccharide interactions. *Current Opinion in Colloid & Interface Science,* 5**,** 202-214.

DUCEL, V., POULIQUEN, D., RICHARD, J. & BOURY, F. 2008. H-1 NMR Relaxation Studies of Protein-Polysaccharide Mixtures. *International Journal of Biological Macromolecules,* 43**,** 359-366.

DUCEL, V., RICHARD, J., POPINEAU, Y. & BOURY, F. 2004a. Adsorption Kinetics and Rheological Interfacial Properties of Plant Proteins at the Oil-Water Interface. *Biomacromolecules,* 5**,** 2088-2093.

DUCEL, V., RICHARD, J., POPINEAU, Y. & BOURY, F. 2005a. Rheological Interfacial Properties of Plant Protein-Arabic Gum Coacervates at the Oil-Water Interface. *Biomacromolecules,* 6**,** 790-796.

DUCEL, V., RICHARD, J., SAULNIER, P., POPINEAU, Y. & BOURY, F. 2004b. Evidence and Characterization of Complex Coacervates Containing Plant Proteins: Application to the Microencapsulation of Oil Droplets. *Colloids and Surfaces a-Physicochemical and Engineering Aspects,* 232**,** 239-247.

DUCEL, V., SAULNIER, P., RICHARD, J. & BOURY, F. 2005b. Plant Protein-Polysaccharide Interactions in Solutions: Application of Soft Particle Analysis and Light Scattering Measurements. *Colloids and Surfaces B-Biointerfaces,* 41**,** 95-102.

ELOFSSON, U., ELIASSON, A. C., WAHLGREN, M., LOOSVELD, A. M. A., COURTIN, C. M. & DELCOUR, J. A. 2000. Adsorption studies of interaction between water-extractable nonstarch polysaccharides and prolamins in cereals. *Cereal Chemistry,* 77**,** 679-684.

FDA 2013. Food Labeling; Gluten-Free Labeling of Foods. *78 FR 47154.* Federal Register.

FIEBRIG, I., HARDING, S. E., ROWE, A. J., HYMAN, S. C. & DAVIS, S. S. 1995. Transmission Electron Microscopy Studies on Pig Gastric Mucin and its Interactions with Chitosan. *Carbohydrate Polymers,* 28**,** 239-244.

FSA 2011. Guidance on the Composition and Labelling of Foodstuffs Suitable for People Intolerant to Gluten. Food Standards Agency.

FU, C. L., SHI, H. F. & LI, Q. 2006. A review on pharmacological activities and utilization technologies of pumpkin. *Plant Foods for Human Nutrition,* 61**,** 70-77.

FUJITA, H. 1962. *Mathematical Theory Of Sedimentation Analysis,* New York, Academic Press.

FUNAMI, T., NAKAUMA, M., NODA, S., ISHIHARA, S., ASAI, I., INOUCHI, N. & NISHINARI, K. 2008. Effects of some anionic polysaccharides on the gelatinization and retrogradation behaviors of wheat starch: Soybean-soluble polysaccharide and gum arabic. *Food Hydrocolloids,* 22**,** 1528-1540.

FURST, A. 1997. The XL-I analytical ultracentrifuge with Rayleigh interference optics. *European Biophysics Journal,* 25**,** 307-310.

GALLAGHER, E., GORMLEY, T. R. & ARENDT, E. K. 2004. Recent Advances in the Formulation of Gluten-Free Cereal-Based Products. *Trends in Food Science & Technology,* 15**,** 143-152.

GILLIS, R. B., ADAMS, G. G., HEINZE, T., NIKOLAJSKI, M., HARDING, S. E. & ROWE, A. J. 2013a. MultiSig: a new high-precision approach to the analysis of complex biomolecular systems. *European Biophysics Journal,* 42**,** 777-786.

GILLIS, R. B., ADAMS, G. G., WOLF, B., BERRY, M., BESONG, T., CORFIELD, A., KÖK, S. M., SIDEBOTTOM, R., LAFOND, D. & ROWE, A. J. 2013b. Molecular weight distribution analysis by ultracentrifugation: Adaptation of a new approach for mucins. *Carbohydrate Polymers,* 93**,** 178-183.

GOSSELL-WILLIAMS, M., LYTTLE, K., CLARKE, T., GARDNER, M. & SIMON, O. 2008. Supplementation with pumpkin seed oil improves plasma lipid profile and cardiovascular outcomes of female non-ovariectomized and ovariectomized Sprague-Dawley rats. *Phytother Res,* 22**,** 873-7.

GOYCOOLEA, F., MORRIS, E., RICHARDSON, R. & BELL, A. 1995. Solution rheology of mesquite gum in comparison with gum arabic. *Carbohydrate Polymers,* 27**,** 37-45.

GRALEN, N. 1944. *PhD Dissertation.* PhD, University of Uppsala, Sweden.

GREEN, P. H. & CELLIER, C. 2007. Celiac disease. *New England Journal of Medicine,* 357**,** 1731-1743.

GUERRIERI, N., CERLETTI, P. & SECUNDO, F. 2004. Gliadins and polysaccharides interaction. *SPECIAL PUBLICATION-ROYAL SOCIETY OF CHEMISTRY.* Royal Society of Chemistry; 1994.

HAGER, A.-S., ZANNINI, E. & ARENDT, E. 2012. Gluten-free Pasta—Advances in Research and Commercialization. *Cereal Foods World,* 57**,** 225-229.

HANEY, M. A. 1985a. The differential viscometer. I. A new approach to the measurement of specific viscosities of polymer solutions. *Journal of Applied Polymer Science,* 30**,** 3023-3036.

HANEY, M. A. 1985b. The differential viscometer. II. On-line viscosity detector for size-exclusion chromatography. *Journal of Applied Polymer Science,* 30**,** 3037-3049.

HARDING, S. E. 1997. The intrinsic viscosity of biological macromolecules. Progress in measurement, interpretation and application to structure in dilute solution. *Progress in Biophysics and Molecular Biology,* 68**,** 207-262.

HARDING, S. E. 2005. Challenges for the modern analytical ultracentrifuge analysis of polysaccharides. *Carbohydrate Research,* 340**,** 811-826.

HARDING, S. E., HORTON, J. C. & CÖLFEN, H. 1997. The ELLIPS suite of macromolecular conformation algorithms. *Eur Biophys J,* 25**,** 347-359.

HARDING, S. E. & JUMEL, K. 1998. Light scattering. *Current Protocols in Protein Science***,** 7.8. 1-7.8. 14.

HARDING, S. E., SCHUCK, P., ABDELHAMEED, A. S., ADAMS, G. G., KÖK, M. S. & MORRIS, G. A. 2011. Extended Fujita Approach to the Molecular Weight Distribution of Polysaccharides and Other Polymeric Systems. *Methods,* 54**,** 136-144.

HARDING, S. E., VÅRUM, K., STOKKE, B. R. T. & SMIDSRØD, O. 1991. Molecular weight determination of polysaccharides. *Advances in Carbohydrate Analysis,* 1**,** 63-144.

HARLOW, E. & LANE, D. 1988. *Antibodies: a laboratory manual*, Cold Spring Harbor Laboratory Cold Spring Harbor, NY.

HAYES, D. B., LAUE, T. & PHILO, J. 1995. SEDNTERP. University of New Hampshire, Durham.

HEINZE, T., NIKOLAJSKI, M., DAUS, S., BESONG, T., MICHAELIS, N., BERLIN, P., MORRIS, G. A., ROWE, A. J. & HARDING, S. E. 2011. Protein-like Oligomerization of Carbohydrates. *Angewandte Chemie International Edition,* 50**,** 8602-8604.

HROMÁDKOVÁ, Z., EBRINGEROVÁ, A. & MALOVÍKOVÁ, A. Year. The Structural, Molecular and Functional Properties of Lignin-Containing Beechwood Glucuronoxylan. *In:* Macromolecular symposia, 2005. Wiley Online Library, 19-26.

HROMÁDKOVÁ, Z., KOŠT'ÁLOVÁ, Z. & EBRINGEROVÁ, A. 2008. Comparison of conventional and ultrasound-assisted extraction of phenolics-rich heteroxylans from wheat bran. *Ultrasonics Sonochemistry,* 15**,** 1062-1068.

HROMÁDKOVÁ, Z., PAULSEN, B. S., POLOVKA, M., KOŠŤÁLOVÁ, Z. & EBRINGEROVÁ, A. 2012. Structural features of two heteroxylan polysaccharide fractions from wheat bran with anti-complementary and antioxidant activities. *Carbohydrate Polymers*.

HUGGINS, M. L. 1942. The viscosity of dilute solutions of long-chain molecules. IV. Dependence on concentration. *Journal of the American Chemical Society,* 64**,** 2716-2718.

HUGLIN, M., BRANDRUP, J. & IMMERGUT, E. 1989. *Polymer handbook*. Wiley, New York**,** 409.

IDRIS, O., WILLIAMS, P. & PHILLIPS, G. 1998. Characterisation of gum from *Acacia senegal* trees of different age and location using multidetection gel permeation chromatography. *Food Hydrocolloids,* 12**,** 379-388.

JOHNSTON, J. & OGSTON, A. 1946. A boundary anomaly found in the ultracentrifugal sedimentation of mixtures. *Transactions of the Faraday Society,* 42**,** 789-799.

JORDAN, N., NEWTON, J., PEARSON, J. & ALLEN, A. 1998. A Novel Method for the Visualization of the in-situ Mucus Layer in Rat and Man. *Clinical Science,* 95**,** 97-106.

JUMEL, K. 1994. *PhD Thesis.* University of Nottingham, UK.

JUMEL, K., BROWNE, P. & KENNEDY, J. 1992. The use of low angle laser light scattering with gel permeation chromatography for the molecular weight determination of biomolecules. *Laser Light Scattering in Biochemistry***,** 23-34.

KAPOOR, V. P., MILAS, M., TARAVEL, F. R. & RINAUDO, M. 1994. Rheological properties of seed galactomannan from *Cassia nodosa* buch.-hem. *Carbohydrate Polymers,* 25**,** 79-84.

KASARDA, D. D., OKITA, T. W., BERNARDIN, J. E., BAECKER, P. A., NIMMO, C. C., LEW, E., DIETLER, M. D. & GREENE, F. C. 1984. Nucleic acid (cDNA) and amino acid sequences of alpha-type gliadins from wheat (Triticum aestivum). *Proceedings of the National Academy of Sciences,* 81**,** 4712-4716.

KATZ, K. D., RASHTAK, S., LAHR, B. D., MELTON, L. J., KRAUSE, P. K., MAGGI, K., TALLEY, N. J. & MURRAY, J. A. 2011. Screening for celiac disease in a North American population: sequential serology and gastrointestinal symptoms. *The American Journal of Gastroenterology,* 106**,** 1333-1339.

KAVIMANDAN, A., SHARMA, M., VERMA, A. K., DAS, P., MISHRA, P., SINHA, S., MOHAN, A., SREENIVAS, V., DATTA GUPTA, S. & MAKHARIA, G. K. 2014. Prevalence of celiac disease in nutritional anemia at a tertiary care center. *Indian Journal of Gastroenterology : Official Journal of the Indian Society of Gastroenterology,* 33**,** 114-8.

KIMURA, S., GOHDA, T. & SAKURAI, Y. 2003. Characterization of Nidamental Mucin from Japanese Common Squid Todarodes pacificus. *Journal of the Tokyo University of Fisheries,* 89**,** 7-13.

KNOWLER, W. C., BARRETT-CONNOR, E., FOWLER, S. E., HAMMAN, R. F., LACHIN, J. M., WALKER, E. A. & NATHAN, D. M. 2002. Reduction in the incidence of type 2 diabetes with lifestyle intervention or metformin. *The New England Lournal of Medicine,* 346**,** 393.

KÖK, M., GILLIS, R., ANG, S., LAFOND, D., TATHAM, A., ADAMS, G. & HARDING, S. 2012. Can dietary fibre help provide safer food products for sufferers of gluten intolerance? A well-established biophysical probe may help towards providing an answer. *BMC Biophysics,* 5**,** 10.

KÖK, M. S., ABDELHAMEED, A. S., ANG, S., MORRIS, G. A. & HARDING, S. E. 2009. A Novel Global Hydrodynamic Analysis of the Molecular Flexibility of the Dietary Fibre Polysaccharide Konjac Glucomannan. *Food Hydrocolloids,* 23**,** 1910-1917.

KOŠŤÁLOVÁ, Z., HROMÁDKOVÁ, Z. & EBRINGEROVÁ, A. 2010. Isolation and characterization of pectic polysaccharides from the seeded fruit of oil pumpkin (*Cucurbita pepo* L. var. *Styriaca*). *Industrial Crops and Products,* 31**,** 370-377.

KRAEMER, E. O. 1938. Molecular weights of celluloses and cellulose derivates. *Industrial & Engineering Chemistry,* 30**,** 1200-1203.

LAMM, O. 1929. Die Differentialgleichung der Ultrazentrifugierung [The theory and method of ultra centrifuging]. *Z. Phys. Chem. A-Chem. T,* 143**,** 177-190.

LANTZ, R. K. & EISENBERG, R. B. 1978. Preservation of Acid-Phosphatase Activity in Medico-Legal Specimens. *Clinical Chemistry,* 24**,** 486-488.

LENZEN, S. 2008. The mechanisms of alloxan-and streptozotocin-induced diabetes. *Diabetologia,* 51**,** 216-226.

LEVINE, M. J., HERZBERG, M. C., LEVINE, M. S., ELLISON, S. A., STINSON, M. W., LI, H. C. & VANDYKE, T. 1978. Specificity of Salivary-Bacterial Interactions - Role of Terminal Sialic-acid Residues in Interaction of Salivary Glycoproteins with Streptococcus sanguis and Streptococcus mutans. *Infection and Immunity,* 19**,** 107-115.

LI, Q. H., FU, C. L., RUI, Y. K., HU, G. H. & CAI, T. Y. 2005. Effects of protein-bound polysaccharide isolated from pumpkin on insulin in diabetic rats. *Plant Foods for Human Nutrition,* 60**,** 13-16.

LIANG, L., PINIER, M., LEROUX, J.-C. & SUBIRADE, M. 2009. Interaction of alpha-Gliadin with Poly(HEMA-co-SS): Structural Characterization and Biological Implication. *Biopolymers,* 91**,** 169-178.

LIANG, L., PINIER, M., LEROUX, J.-C. & SUBIRADE, M. 2010. Interaction of α-gliadin with polyanions: Design considerations for sequestrants used in supportive treatment of celiac disease. *Biopolymers,* 93**,** 418-428.

LINLAUD, N., FERRER, E., CECILIA PUPPO, M. & FERRERO, C. 2011. Hydrocolloid Interaction with Water, Protein, and Starch in Wheat Dough. *Journal of Agricultural and Food Chemistry,* 59**,** 713-719.

MAGER, D. R., QIAO, J. & TURNER, J. 2012. Vitamin D and K status influences bone mineral density and bone accrual in children and adolescents with celiac disease. *European Journal of Clinical Nutrition,* 66**,** 488-495.

MAHENDRAN, T., WILLIAMS, P., PHILLIPS, G., AL-ASSAF, S. & BALDWIN, T. 2008. New Insights into the Structural Characteristics of the Arabinogalactan− Protein (AGP) Fraction of Gum Arabic. *Journal of Agricultural and Food Chemistry,* 56**,** 9269-9276.

MASUELLI, M. A. 2013. Hydrodynamic Properties of Whole Arabic Gum. *American Journal of Food Science and Technology,* 1**,** 60-66.

MAZUMDER, K. & YORK, W. S. 2010. Structural analysis of arabinoxylans isolated from ball-milled switchgrass biomass. *Carbohydrate Research,* 345**,** 2183-2193.

MEYER, F. A. 1983. Polymeric Structure of a High-Molecular-Weight Glycoprotein from Bovine Cervical-Mucus. *Biochemical Journal,* 215**,** 701-704.

MILAS, M., REED, W. F. & PRINTZ, S. 1996. Conformations and flexibility of native and re-natured xanthan in aqueous solutions. *International Journal of Biological Macromolecules,* 18**,** 211-221.

MITTAL, V., VÖLKEL, A. & CÖLFEN, H. 2010. Analytical ultracentrifugation of model nanoparticles: comparison of different analysis methods. *Macromolecular Bioscience,* 10**,** 754-762.

MOHSEN, S. M., YASEEN, A. A., AMMAR, A. M. & MOHAMMAD, A. A. 2010. Quality characteristics improvement of low-phenylalanine toast bread. *International Journal of Food Science and Technology,* 45**,** 2042-2051.

MORRIS, G. A., ADAMS, G. G. & HARDING, S. E. 2014. On hydrodynamic methods for the analysis of the sizes and shapes of polysaccharides in dilute solution: A short review. *Food Hydrocolloids*, 42**,** 318-334.

MORRIS, G. A., RALET, M.-C., BONNIN, E., THIBAULT, J.-F. & HARDING, S. E. 2010. Physical characterisation of the rhamnogalacturonan and homogalacturonan fractions of sugar beet (*Beta vulgaris*) pectin. *Carbohydrate Polymers,* 82**,** 1161-1167.

MUCCI, P., GRIGNAFFINI, G. F. & SIGHINOLFI, F. 1963. [The Preservative Action of EDTA on Leukocytes in vitro]. *Minerva Medica,* 54**,** 2277-80.

NADEEM, M. 2013. Screening for Coeliac Disease: Are We Good at It? *International Journal of Celiac Disease,* 1**,** 8-8.

NARAN, R., CHEN, G. & CARPITA, N. C. 2008. Novel rhamnogalacturonan I and arabinoxylan polysaccharides of flax seed mucilage. *Plant Physiology,* 148**,** 132-141.

NEWTON, K. P. & SINGER, S. A. Year. Celiac disease in children and adolescents: special considerations. *In:* Seminars in immunopathology, 2012. Springer, 479-496.

NIE, S.-P., WANG, C., CUI, S. W., WANG, Q., XIE, M.-Y. & PHILLIPS, G. O. 2013a. The core carbohydrate structure of Acacia seyal var. seyal (Gum arabic). *Food Hydrocolloids,* 32**,** 221-227.

NIE, S.-P., WANG, C., CUI, S. W., WANG, Q., XIE, M.-Y. & PHILLIPS, G. O. 2013b. A further amendment to the classical core structure of gum arabic (Acacia senegal). *Food Hydrocolloids,* 31**,** 42-48.

NIKOLAJSKI, M., ADAMS, G. G., GILLIS, R. B., BESONG, D. T., ROWE, A. J., HEINZE, T. & HARDING, S. E. 2014. Protein-like fully reversible tetramerisation and super-association of an aminocellulose. *Sci. Rep.,* 4.

NIKOLAJSKI, M., WOTSCHADLO, J., CLEMENT, J. H. & HEINZE, T. 2012. Amino-Functionalized Cellulose Nanoparticles: Preparation, Characterization, and Interactions with Living Cells. *Macromolecular Bioscience,* 12**,** 920-925.

NIKOLIĆ, G. S., CAKIĆ, M. D. & ILIĆ, L. A. 2001. Specific refractive index increments of inulin. *Journal of the Serbian Chemical Society,* 66**,** 397-401.

NISHIMURA, M., OHKAWARA, T., SATO, H., TAKEDA, H. & NISHIHIRA, J. 2014. Pumpkin seed oil extracted from Cucurbita maxima improves urinary disorder in human overactive bladder. *Journal of Traditional and Complementary Medicine,* 4**,** 72.

OLSSON, C., HÖRNELL, A., IVARSSON, A. & SYDNER, Y. M. 2008. The everyday life of adolescent coeliacs: issues of importance for compliance with the gluten-free diet. *Journal of Human Nutrition and Dietetics,* 21**,** 359-367.

ORTEGA, A. & GARCÍA DE LA TORRE, J. 2007. Equivalent radii and ratios of radii from solution properties as indicators of macromolecular conformation, shape, and flexibility. *Biomacromolecules,* 8**,** 2464-2475.

PAGANUZZI, A. S., ZUCCO, F., CARDELLI, M., DEANGELIS, I., MATTEI, R., PINO, A., ROCCA, E. & ZAMPAGLIONI, F. 1985. Cytotoxic Effects Of Wheat Gliadin-Derived Pepetides. *Toxicology,* 37**,** 225-232.

PAMIES, R., CIFRE, J. G. H., MARTÍNEZ, M. D. C. L. & DE LA TORRE, J. G. 2008. Determination of intrinsic viscosities of macromolecules and nanoparticles. Comparison of single-point and dilution procedures. *Colloid and Polymer Science,* 286**,** 1223-1231.

PEITZSCH, R. M., BURT, M. J. & REED, W. F. 1992. Evidence of partial draining for linear polyelectrolytes; heparin, chondroitin 6-sulfate, and poly (styrene sulfonate). *Macromolecules,* 25**,** 806-815.

PERKINS, S. J. 1986. Protein volumes and hydration effects. The calculations of partial specific volumes, neutron scattering matchpoints and 280-nm absorption coefficients for proteins and glycoproteins from amino acid sequences. *European Journal of Biochemistry / FEBS,* 157**,** 169-180.

PHILLIPS, G. O., TAKIGAMI, S. & TAKIGAMI, M. 1996. Hydration characteristics of the gum exudate from Acacia senegal. *Food Hydrocolloids,* 10**,** 11-19.

PINIER, M., FUHRMANN, G., GALIPEAU, H. J., RIVARD, N., MURRAY, J. A., DAVID, C. S., DRASAROVA, H., TUCKOVA, L., LEROUX, J.-C. & VERDU, E. F. 2012. The Copolymer P(HEMA-co-SS) Binds Gluten and Reduces Immune Response in Gluten-Sensitized Mice and Human Tissues. *Gastroenterology,* 142**,** 316-U223.

PINIER, M., VERDU, E. F., NASSER-EDDINE, M., DAVID, C. S., VEZINA, A., RIVARD, N. & LEROUX, J.-C. 2009. Polymeric Binders Suppress Gliadin-Induced Toxicity in the Intestinal Epithelium. *Gastroenterology,* 136**,** 288-298.

POZO-RUBIO, T., CAPILLA, A., MUJICO, J. R., DE PALMA, G., MARCOS, A., SANZ, Y., POLANCO, I., DOLORES GARCIA-NOVO, M., CASTILLEJO, G., RIBES-KONINCKX, C., VAREA, V., PALAU, F., ORTIGOSA, L., PENA-QUINTANA, L. & NOVA, E. 2013. Influence of breastfeeding versus formula feeding on lymphocyte subsets in infants at risk of coeliac disease: the PROFICEL study. *European Journal of Nutrition,* 52**,** 637-646.

PTITCHKINA, N. M., DANILOVA, I. A., DOXASTAKIS, G., KASAPIS, S. & MORRIS, E. R. 1994. Pumpkin pectin: gel formation at unusually low concentration. *Carbohydrate Polymers,* 23**,** 265-273.

PULLAN, R. D., THOMAS, G. A. O., RHODES, M., NEWCOMBE, R. G., WILLIAMS, G. T., ALLEN, A. & RHODES, J. 1994. Thickness of Adherent Mucus Gel on Colonic Mucosa in Humans and its Relevance to Colitis. *Gut,* 35**,** 353-359.

QASIM, M. A. & TAHA, M. 2013. Investigation of the mechanism of protein denaturation by guanidine hydrochloride-induced dissociation of inhibitor-protease complexes. *Protein Pept Lett,* 20**,** 187-91.

QI, W., FONG, C. & LAMPORT, D. T. 1991. Gum arabic glycoprotein is a twisted hairy rope : a new model based on o-galactosylhydroxyproline as the polysaccharide attachment site. *Plant Physiology,* 96**,** 848-55.

RENARD, D., GARNIER, C., LAPP, A., SCHMITT, C. & SANCHEZ, C. 2012. Structure of arabinogalactan-protein from Acacia gum: From porous ellipsoids to supramolecular architectures. *Carbohydrate Polymers,* 90**,** 322-332.

RENARD, D., LEPVRIER, E., GARNIER, C., ROBLIN, P., NIGEN, M. & SANCHEZ, C. 2014. Structure of glycoproteins from Acacia gum: An assembly of ring-like glycoproteins modules. *Carbohydrate Polymers,* 99**,** 736-747.

RICHARDS, E. G., TELLER, D. C. & SCHACHMAN, H. K. 1968. Ultracentrifuge studies with Rayleigh interference optics. II. Low-speed sedimentation equilibrium of homogeneous systems. *Biochemistry,* 7**,** 1054-1076.

RINAUDO, M., MILAS, M. & DUNG, P. L. 1993. Characterization of chitosan. Influence of ionic strength and degree of acetylation on chain expansion. *International Journal of Biological Macromolecules,* 15**,** 281-285.

RINDE, H. 1928. *Dissertation.* University of Uppsala, Sweden.

ROBERTSON, T. B. & GREAVES, J. 1911. On The Refractive Indices Of Solutions Of Certain Proteins V. Gliadin. *Journal of Biological Chemistry,* 9**,** 181-184.

ROWE, A. 1992. The concentration dependence of sedimentation. *In:* HARDING, S. E., ROWE, A. J. & HORTON, J. C. (eds.) *Analytical ultracentrifugation in biochemistry and polymer science.* Royal Society of Chemistry.

ROWE, A. J. 2011. Ultra-weak reversible protein-protein interactions. *Methods,* 54**,** 157-166.

RYAN, M. & GROSSMAN, S. 2011. Celiac disease: implications for patient management. *Gastroenterology Nursing,* 34**,** 225-228.

SAINSBURY, K., MULLAN, B. & SHARPE, L. 2012. Gluten free diet adherence in coeliac disease: The role of psychological symptoms in bridging the intention-behaviour gap. *Appetite*, 61,52-58.

SANCHEZ, C., SCHMITT, C., KOLODZIEJCZYK, E., LAPP, A., GAILLARD, C. & RENARD, D. 2008. The acacia gum arabinogalactan fraction is a thin oblate ellipsoid: a new model based on small-angle neutron scattering and ab initio calculation. *Biophysical Journal,* 94**,** 629-639.

SANCHEZ, H., OSELLA, C. & DE LA TORRE, M. 2002. Optimization of Gluten-Free Bread Prepared from Cornstarch, Rice Flour, and Cassava Starch. *Journal of Food Science,* 67**,** 416-419.

SANGHA, J. S., KHAN, W., JI, X., ZHANG, J., MILLS, A. A., CRITCHLEY, A. T. & PRITHIVIRAJ, B. 2011. Carrageenans, sulphated polysaccharides of red seaweeds, differentially affect Arabidopsis thaliana resistance to Trichoplusia ni (Cabbage Looper). *Plos One,* 6**,** e26834.

SCHUCK, P. 2000. Size-distribution analysis of macromolecules by sedimentation velocity ultracentrifugation and Lamm equation modeling. *Biophysical Journal,* 78**,** 1606-1619.

SCHUCK, P., GILLIS, R. B., BESONG, T. M., ALMUTAIRI, F., ADAMS, G. G., ROWE, A. J. & HARDING, S. E. 2014. SEDFIT–MSTAR: molecular weight and molecular weight distribution analysis of polymers by sedimentation equilibrium in the ultracentrifuge. *Analyst,* 139**,** 79-92.

SCHUCK, P. & ROSSMANITH, P. 2000. Determination of the sedimentation coefficient distribution by least-squares boundary modeling. *Biopolymers,* 54**,** 328-341.

SCHULER, V., LUSSI, A., KAGE, A. & SEEMANN, R. 2012. Glycan-binding specificities of Streptococcus mutans and Streptococcus sobrinus lectin-like adhesins. *Clinical Oral Investigations,* 16**,** 789-796.

SCHUPPAN, D., JUNKER, Y. & BARISANI, D. 2009. Celiac disease: from pathogenesis to novel therapies. *Gastroenterology,* 137**,** 1912-1933.

SEBASTIAN LASA, J., ZUBIAURRE, I. & OSCAR SOIFER, L. 2014. Risk Of Infertility In Patients With Celiac Disease: a meta-analysis of observational studies. *Arquivos de Gastroenterologia,* 51**,** 144-150.

SECUNDO, F. & GUERRIERI, N. 2005. ATR-FT/IR Study on the Interactions between Gliadins and Dextrin and Their Effects on Protein Secondarty Structure. *Journal of Agriculture & Food Chemistry,* 53**,** 1757-1764.

SEIFERT, A., HEINEVETTER, L., CÖLFEN, H. & HARDING, S. 1995. Characterization of gliadin-galactomannan incubation mixtures by analytical ultracentrifugation—Part I. Sedimentation velocity. *Carbohydrate Polymers,* 28**,** 325-332.

SERDYUK, I. N., ZACCAI, N. R. & ZACCAI, J. 2007. *Methods in Molecular Biophysics: Structure, Dynamics, Function*, Cambridge University Press.

SHAN, L., MOLBERG, Ø., PARROT, I., HAUSCH, F., FILIZ, F., GRAY, G. M., SOLLID, L. M. & KHOSLA, C. 2002. Structural basis for gluten intolerance in celiac sprue. *Science,* 297**,** 2275-2279.

SHEEHAN, J. K. & CARLSTEDT, I. 1984. Hydrodynamic Properties of Human Cervical-Mucus Glycoproteins in 6M-Guanidinium Chloride. *Biochemical Journal,* 217**,** 93-101.

SHEEHAN, J. K. & CARLSTEDT, I. 1987. Size Heterogeneity of Human Cervical Mucus Glycoproteins - Studies Performed with Rate-Zonal Centrifugation and Laser Light-Scattering. *Biochemical Journal,* 245**,** 757-762.

SHERBLOM, A. P. & CARRAWAY, K. L. 1980. A Complex of 2 Cell-Surface Glycoproteins from Ascites Mammary Adenocarcinoma Cells. *Journal of Biological Chemistry,* 255**,** 2051-2059.

SILANO, M., VINCENTINI, O., MUZZARELLI, R. A., MUZZARELLI, C. & DE VINCENZI, M. 2004. MP-Chitosan protects Caco-2 cells from toxic gliadin peptides. *Carbohydrate Polymers,* 58**,** 215-219.

SNARY, D., ALLEN, A. & PAIN, R. H. 1970. Structural Studies on Gastric Mucoproteins - Lowering of Molecular Weight after Reduction with 2-Mercaptoethanol. *Biochemical and Biophysical Research Communications,* 40**,** 844-851.

SOLLID, L. M. & KHOSLA, C. 2005. Future therapeutic options for celiac disease. *Nature Clinical Practice Gastroenterology & Hepatology,* 2**,** 140-147.

SOLOMON, O. & CIUTA, I. 1962. Determination of the intrinsic viscosity of polymer solutions by a simple determination of viscosity. *J Appl Polym Sci,* 6**,** 683-6.

SONG, Y., GAO, L., LI, L. & ZHENG, Q. 2010. Influence of gliadins on rheology of methylcellulose in 70% (v/v) aqueous ethanol. *Food Hydrocolloids,* 24**,** 98-104.

SPRAGG, S. P., HALSALL, H. B., FLEWETT, T. H. & BARCLAY, G. R. 1969. Thermal Polymerization of Orosomucoid. *Biochemical Journal,* 111**,** 345-352.

STEFANIAK, A. B., ABBAS VIRJI, M., HARVEY, C. J., SBARRA, D. C., DAY, G. A. & HOOVER, M. D. 2010. Influence of artificial gastric juice composition on bioaccessibility of cobalt-and tungsten-containing powders. *International Journal of Hygiene and Environmental Health,* 213**,** 107-115.

STEPHEN, A. M., PHILLIPS, G. O. & WILLIAMS, P. A. 2006. *Food Polysaccharides and their Applications*, CRC Press, Taylor & Francis.

STROUS, G. J. & DEKKER, J. 1992. Mucin-type glycoproteins. *Critical Reviews in Biochemistry and Molecular Biology,* 27**,** 57-92.

SZAFLARSKA-POPŁAWSKA, A. 2014. Review paper Coexistance of celiac disease and type 1 diabetes. *Przeglad Gastroenterologiczny,* 9**,** 11-17.

SZAJEWSKA, H., CHMIELEWSKA, A., PIEŚCIK-LECH, M., IVARSSON, A., KOLACEK, S., KOLETZKO, S., MEARIN, M., SHAMIR, R., AURICCHIO, R. & TRONCONE, R. 2012. Systematic review: early infant feeding and the prevention of coeliac disease. *Alimentary Pharmacology & Therapeutics,* 36**,** 607-618.

TAVALLAIE, R., TALEBPOUR, Z., AZAD, J. & SOUDI, M. R. 2011. Simultaneous determination of pyruvate and acetate levels in xanthan biopolymer by infrared spectroscopy: effect of spectral pre-processing for solid-state analysis. *Food Chemistry,* 124**,** 1124-1130.

THEISEN, A., JOHANN, C., DEACON, M. P. & HARDING, S. E. 2000. *Refractive increment data-book for polymer and biomolecular scientists*, Nottingham University Press.

THORNTON, D. J., SHEEHAN, J. K., LINDGREN, H. & CARLSTEDT, I. 1991. Mucus Glycoproteins from Cystic Fibrotic Sputum - Macromolecular Properties and Structural Architecture. *Biochemical Journal,* 276**,** 667-675.

VAN HOLDE, K. & BALDWIN, R. 1958. Rapid attainment of sedimentation equilibrium. *The Journal of Physical Chemistry,* 62**,** 734-743.

VAN HOLDE, K. E., JOHNSON, W. C. & HO, P. S. 2006. *Principles of physical biochemistry*, Prentice Hall

VERBEKEN, D., DIERCKX, S. & DEWETTINCK, K. 2003. Exudate gums: occurrence, production, and applications. *Applied Microbiology and Biotechnology,* 63**,** 10-21.

VINCENTINI, O., DE ANGELIS, I., IANNUCCELLI, R., SILANO, M., STAMMATI, A. & DE VINCENZI, M. 2005. Protective effects of mannan in Caco-2/TC7 cells treated with wheat-derived peptides. *Carbohydrate Polymers,* 62**,** 338-343.

WALES, M. & VAN HOLDE, K. 1954. The concentration dependence of the sedimentation constants of flexible macromolecules. *Journal of Polymer Science,* 14**,** 81-86.

WALLIA, A. & MOLITCH, M. E. 2014. Insulin therapy for type 2 diabetes mellitus. *JAMA,* 311**,** 2315-2325.

WEST, J., LOGAN, R., HILL, P., LLOYD, A., LEWIS, S., HUBBARD, R., READER, R., HOLMES, G. & KHAW, K. 2003. Seroprevalence, correlates, and characteristics of undetected coeliac disease in England. *Gut,* 52**,** 960-965.

WIERDSMA, N. J., VAN BOKHORST-DE VAN DER SCHUEREN, M. A. E., BERKENPAS, M., MULDER, C. J. J. & VAN BODEGRAVEN, A. A. 2013. Vitamin and Mineral Deficiencies Are Highly Prevalent in Newly Diagnosed Celiac Disease Patients. *Nutrients,* 5**,** 3975-3992.

WIESER, H., KONITZER, K. & KOEHLER, P. 2012. Celiac Disease—Multidisciplinary Approaches. *Cereal Foods World,* 57**,** 215-224.

WILLIAMS, M. A., FOSTER, T. J., MARTIN, D. R., NORTON, I. T., YOSHIMURA, M. & NISHINARI, K. 2000. A molecular description of the gelation mechanism of konjac mannan. *Biomacromolecules,* 1**,** 440-450.

WINKWORTH-SMITH, C. & FOSTER, T. J. 2013. General Overview of Biopolymers: Structure, Properties and Applications. *In:* THOMAS, S., DURAND, D., CHASSENIEUX, C. & JYOTISHKUMAR, P. (eds.) *Handbook of Biopolymer-Based Materials - From Blends and Coposites to Gels and Complex Networks.* Wiley-VCH.

WITTGREN, B., BORGSTRÖM, J., PICULELL, L. & WAHLUND, K. G. 1998. Conformational change and aggregation of κ-carrageenan studied by flow field-flow fractionation and multiangle light scattering. *Biopolymers,* 45**,** 85-96.

WOLFF, D., CZAPLAB, S., HEYER, A. G., RADOSTA, S., MISCHNICK, P. & SPRINGER, J. 2000. Globular shape of high molar mass inulin revealed by static light scattering and viscometry. *Polymer,* 41**,** 8009-8016.

WOYCHIK, J. H., DIMLER, R. J. & BOUNDY, J. A. 1961. Starch Gel Electrophoresis Of Wheat Gluten Proteins With Concentrated Urea. *Archives of Biochemistry and Biophysics,* 94**,** 477-&.

WU, A. M. & PIGMAN, W. 1977. Preparation and Characterization of Armadillo Submandibular Glycoproteins. *Biochemical Journal,* 161**,** 37-47.

XU, G. Q., FORSTNER, G. G. & FORSTNER, J. F. 1996. Interaction of Heparin with Synthetic Peptides Corresponding to the C-Terminal Domain of Intestinal Mucins. *Glycoconjugate Journal,* 13**,** 81-90.

YADAV, M., JAIN, S., TOMAR, R., PRASAD, G. & YADAV, H. 2010. Medicinal and biological potential of pumpkin: an updated review. *Nutrition Research Reviews,* 23**,** 184-190.

YOO, S. H., LEE, B. H., LEE, H., LEE, S., BAE, I. Y., LEE, H. G., FISHMAN, M. L., CHAU, H. K., SAVARY, B. J. & HOTCHKISS JR, A. T. 2012. Structural characteristics of pumpkin pectin extracted by microwave heating. *Journal of Food Science,* 77**,** C1169-C1173.

ZEMLJIČ, L. F., ČAKARA, D., MICHAELIS, N., HEINZE, T. & KLEINSCHEK, K. S. 2011. Protonation behavior of 6-deoxy-6-(2-aminoethyl) amino cellulose: a potentiometric titration study. *Cellulose,* 18**,** 33-43.

ZHAO, L., LI, L., LIU, G.-Q., LIU, X.-X. & LI, B. 2012. Effect of frozen storage on molecular weight, size distribution and conformation of gluten by SAXS and SEC-MALLS. *Molecules,* 17**,** 7169-7182.

Appendix 1: Literature search for sedimentation and weight average molar mass pairs for mucins

Mucin type	M_w (kDa)	$s_{20,w}$	Notes	Reference
HCM	9700	50.1	Extrapolation to s^0 not specified	Carlstedt et al. (1983)
PGM	9000	60	Extrapolation to s^0 not specified	Deacon et al. (1998)
Rat Ascites	650	14.9	Extrapolation to s^0 not specified	Sherblom & Carraway (1980)
HCM Whole HCM Subunits HCM T domains	10800 200 30	40.4 19.2 8.7	Extrapolation to s^0 not specified, GuHCl	Sheehan & Carlstedt (1984)
H Airway M	19000 29000 21000 20000	48.9 54.8 55.8 48.2	Extrapolation to s^0 not specified	Davies et al. (1996)
H Bronchial M	5100 7000 5800 3300 5100	16.1 20.8 17.6 17.8 15.6	Extrapolation to s^0 not specified, originally given as s_{25} values, corrected with SEDNTERP	Creeth et al. (1977)
Armadillo Submandibular Glycoproteins	78 31	1.5 1.8	Only 'S' quoted	Wu & Pigman (1977)
PGM	1850 110	16.7 4.4	Originally given as s_{25} values, corrected with SEDNTERP	Snary et al. (1970)
BCM	1640	65.8		Meyer (1983)
Guinea Pig Trachial Epithelial M	4700 3300 4500	28.5 28.5 35.5		Dodd et al. (1998)
H Cystic Fibrosis M	14700	47.1	GuHCl	Thornton et al. (1991)
Squid M	2600 2200	16.9 14.3		Kimura et al. (2003)

Key: B = Bovine, H = Human, P = Porcine
C = cervical, G = gastric, M = Mucin

Appendix 2: Published work

Schuck, P., Gillis, R. B., Besong, T. M. D., Almutairi, F., Adams, G. G., Rowe, A. J., Harding, S. E. (2014). SEDFIT-MSTAR: Molecular weight and molecular weight distribution analysis of polymers by sedimentation equilibrium in the ultracentrifuge. *Analyst*; 139 (1), 79-92.

Gillis, R. B., Adams, G. G., Heinze, T., Nikolajski, M., Harding, S. E., & Rowe, A. J. (2013). MultiSig: a new high-precision approach to the analysis of complex biomolecular systems. *European Biophysics Journal*, 42 (10), 777-786.

Gillis, R. B., Adams, G. G., Wolf, B., Berry, M., Besong, T. M. D., Corfield, A., Kok, M. S., Sidebottom, R., Lafond, D., Rowe, A. J., Harding, S. E. (2013). Molecular weight distribution analysis by ultracentrifugation: Adaptation of a new approach for mucins. *Carbohydrate Polymers*, 93 (1), 178-183.

Kök, S. M., Gillis, R. B., Ang, S., Lafond, D., Tatham, A., Adams, G. G., & Harding, S. E. (2012). Can dietary fibre help provide safer food products for sufferers of gluten intolerance? A well-established biophysical probe may help towards providing an answer. *BMC Biophysics*, 5 (1), 10.